Medical Express UAV Challenge

Design an Autonomous fuel-cell MAV System, consisting of a swash plate hybrid UAV, to win the Outback 2018 UAV Challenge

A. Imbrechts	4359283	J.A. Pietrak	4347293
S.J.M. Janssens	4352882	E.M. Raijmakers	4297032
T. Kim	4343433	S. Strübing	4176251
M.P. Klopsch	4274776	C.J. Sun	4368169
A.J. van Liere	4302842	D.C. van Wijngaarden	4351185

Final Report

Design Synthesis Exercise

TU Delft Delft University of Technology

Aerospace Engineering

July 4, 2017

Preface

This report was written during the course AE3200 Design Synthesis Exercise (DSE) taught at the Faculty of Aerospace Engineering, TU Delft, The Netherlands. The authors are Team 05 "Medical Express UAV Challenge" participating in the course during the Spring Semester of 2017. The purpose of the DSE is to provide the students with experience of the full design cycle of an aerospace engineering project over the course of 10 weeks with 10 students and serves as a final thesis for the successful completion of the BSc Aerospace Engineering.

We would like to thank all staff members at the Faculty of Aerospace Engineering as well as those from other faculties and outside the university, for their continued support and especially Bart Remes, Dries Visser and Matej Karasek for providing the team with the opportunity to work on this project. Finally we would like to thank our parents for their love and support.

Team 05
Delft, July 4, 2017

List of Abbreviations

ACMA Australian Communications and Media Authority

ADT Actuator Disk Theory

AFC Alkaline Fuel Cell

ATSB Australian Transport Safety Bureau

BEC Battery Eliminator Circuit

BEM Blade Element Method

CASA Civil Aviation Safety Authority

DC Direct Current

DL Disk Loading

DMFC Direct Methanol fuel cell

DoF Degrees of Freedom

DSE Design Synthesis Exercise

ESC Electronic Speed Controller

FBD Free Body Diagram

FC Fuel Cell

FMEA Failure Mode Effect Analysis

FM Figure of Merit

FTA Fault Tree Analysis

FTS Flight Termination System

IMU Inertial Measurement Unit

LLT Lifting Line Theory

MEUC Medical Express UAV Challenge

PCB Printed Circuit Board

PEMFC Proton Exchange Membrane Fuel Cell

PEM Proton Exchange Membrane Fuel Cell

PL Power Loading

RAMS Reliability, Availability, Maintainability and Safety

RC Radio-controlled (aircraft)

RPM Revolutions per Minute

SF Safety Factor

SLAM Simultaneous Localisation and Mapping

SoaC System on a Chip

SoC State-Of-Charge

Nomenclature

α	Angle of attack	[°]
α_{Hell}	Hellman constant	[-]
$\bar{c}$	Mean aerodynamic chord	[m]
$\bar{y}$	Spanwise location of the mean aerodynamic chord	[m]
$\ddot{\theta}$	Angular acceleration	rad/s
η	Efficiency	[-]
Γ	Dihedral angle	[°]
Λ	Sweep angle	[°]
λ	Taper ratio	[-]
μ	Dynamic viscosity	[m^2/s]
Ω	Revolutions per minute	[RPM]
ϕ	Local flow angle	[°]
ρ	Density	[kg/m^3]
$\mathbf{r}$	Arm vector	m
θ	Pitch attitude	[°]
θ_b	Collective blade pitch (blade angle + pitch angle)	[°]
A	Wing aspect ratio	[-]
a	Axial inflow	[-]
a_h	Horizontal acceleration	[m/s^2]
a_v	Vertical acceleration	[m/s^2]
b	Angular inflow	[-]
C_m	Moment coefficient	[-]
C_N	Normal force coefficient	[-]
C_Q	Torque coefficient	[-]
C_T	Tangential force coefficient	[-]
C_T	Thrust coefficient	[-]
$C_{D,0}$	Zero-lift drag coefficient	[-]
$C_{D,i}$	Inviscid lift-induced drag coefficient (or vortex drag or parasite drag)	[-]
$C_{D,v}$	Viscous drag coefficient	[-]
$C_{d_{\text{min}}}$	Aerofoil minimum drag coefficient	[-]
C_D	Drag coefficient	[-]
C_f	Skin friction coefficient	[-]
$C_{l,0}$	Aerofoil lift coefficient at minimum aerofoil drag	[-]
C_{L_c}	Canard lift coefficient	[-]
C_{L_c}	Lift coefficient of canard	[-]
C_L	Lift coefficient	[-]

D	Drag	[N]
E	Energy	[Wh]
e	Oswald efficiency factor	[-]
e_{H2}	Specific Energy of Hydrogen	[Wh/g]
F_h	Horizontal force	[N]
F_v	Vertical force	[N]
$f_{L/D}$	Fuselage length-to-diameter ratio parameter	[-]
f_{tc}	Thickness ratio parameter	[-]
f_M	Mach number parameter	[-]
F_{xb}	Body force in x direction	[N]
F_{yb}	Body force in y direction	[N]
g_0	Gravitational acceleration	[m/s]
h	Height	[m]
h_{ref}	Reference height	[m]
I_{yy}	Second moment of area around the y-axis	m^4
J	Potential Energy	[N]
k	Viscous factor	[-]
K_{c}	Correction factor accounting for parasite drag due to miscellaneous items)	[-]
L_{fus}	Length of the fuselage	[m]
M	Mach number	[-]
m	Mass	[kg]
M_{tot}	Total moment acting on UAV	[Nm
n	Rotational frequency of a propeller	[Hz]
P	Power	[W]
Q	Torque	[Nm]
q_∞	Dynamic pressure	[kgs/m]
S	Wing lifting surface area	[m^2]
SM	Stability margin	[%]
T	Thrust	[N]
t	Time	[s]
U	Voltage	[V]
V	Velocity	[m/s]
$v_{\text{Wi,h}}$	Wind speed at a non-reference altitude	[m/s]
$v_{\text{Wi,ref}}$	Wind speed at reference altitude	[m/s]
V_h	Horizontal speed	[m/s]
V_v	Vertical speed	[m/s]
V_{AS}	Airspeed	[m/s]

V_{GS}	Ground speed	[m/s]
$v_{wind_{max}}$	Maximum allowed wind velocity when standing	[m/s]
x_{wing}	Position of aerodynamic centre of wing	[m]
y_T	Vertical position of propellers	[m]

Executive Overview

Mission Overview
In an era where the need for humanitarian aid increases, the need for smart technology is dire. It is therefore why competitions such as the Medical Express UAV Challenge (MEUC), taking place in 2018 in Dalby Australia, were created. The challenge aims to create a cost effective and innovative solution to autonomously find people in remote areas and retrieve blood samples from them. This competition was the main source of requirements of this project. On top of that, the TU Delft also set some minimum requirements for this particular Design Synthesis Exercise. In addition to these initial stakeholders, the Royal Netherlands Navy showed interest in the design as well. Due to the fact that some requirements were contradictory with the requirements that were set by the MEUC, the choice to focus primarily on the MEUC was made. In the long-term future plans of this project, the design will continue to be developed and adapted to suit the requirements of the Navy. In conclusion, a mission need statement and project objective statement were set up in order to encapsulate the most essential needs for the mission and project.

Mission need statement: *Provide a fully autonomous UAV capable of medical sample retrieval within the operational range of more than 60 km, within 50 minutes or less, from a remote location on arbitrary terrain.*

Project objective statement: *Design a fully autonomous, fuel-cell powered, swash-plate propeller hybrid UAV by 10 students in 10 weeks with a system cost of €8,000 or less, capable of winning the Medical Express UAV Challenge 2018.*

The UAV will perform the flight according to a specific scenario: The UAV takes-off vertically from the base due to a sign issued through the ground station. It transitions to horizontal flight and flies to a target of which the route to the location is determined through a set of preset waypoints. It has to locate the target which can be within a range of 100 m from the reported location. After localisation of the landing zone, the UAV transitions to hover again and lands on the target. After a person has put in the payload (blood sample for the challenge), the UAV is armed again and takes-off to fly back to base with the payload. Only when the mission is completed and none of the requirements are violated, the system is said to have successfully performed its task.

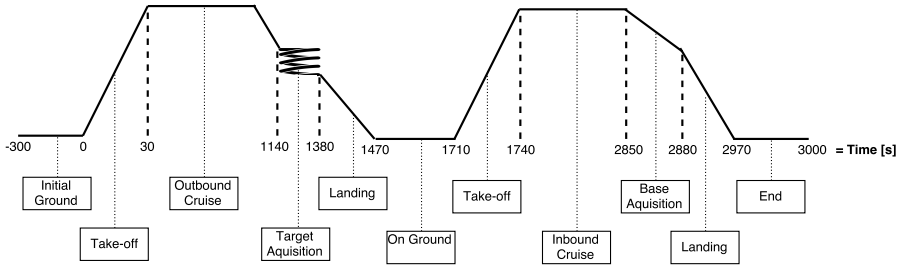

Figure 1: Graphical Mission Profile for Medical UAV Express

Requirements
The functions and requirements for the UAV system were derived during the starting phase of the design process for a UAV system capable of winning the Medical Express UAV Challenge 2018. From an extensive list of requirements, the following driving requirements were identified:

- **MEUC-UCTC-12** The UAV shall have a continuous datalink with the UAV controller at the basestation.
- **MEUC-NAVY-10** The UAV shall be capable of VTOL.
- **MEUC-TUD-02** The Medical Express UAV Challenge shall be completed in 50 min or less.
- **MEUC-TUD-06** The UAV shall be fully electrical.
- **MEUC-TUD-11** The maximum dimension of the UAV shall not be larger than 4 m.
- **MEUC-TUD-18** The UAV shall use a fuel-cell.
- **MEUC-TUD-20** The UAV shall be able to hover.
- **MEUC-TUD-21** The UAV shall feature a fixed wing.

Furthermore, as mentioned above, the navy requirements were deemed to be contradictory. Although the majority of the Navy requirements coincided with the initial requirements, as provided by the challenge committee and TU Delft, the requirements specified on the fuel system were conflicting. As it was found to be

unfeasible to design a fuel system that complied with both Navy and Challenge requirements, it was chosen to fully optimise this particular design for the MEUC. Future alterations on this design can be made to create a design that is also suited for Navy purposes.

Risk Management
Once the objective of the project was clear, a thorough risk assessment was executed. It was essential to perform the risk assessment in an early stage of the design, as to perform an accurate risk mitigation. Over 100 potential risks were identified and were categorised into: business, legal, operational, payload, and health related risks resulting mostly from mission requirements, stakeholder analysis and safety regulations. In addition, more technical categories such as subsystem specific risks and production risks aimed to foresee potential weaknesses of the design and itself, including damage and wear out that may happen over time of system usage. Each risk has a proposed mitigation plan that decreases its severity or probability of its occurrence. In effect of mitigation all critical risks were reduced in severity with the severest risk having a "High Priority" rank, which indicates they should be closely monitored into the future. Those risks are:

- **HSE-2:** Collision with operator, user or other people
- **Leg-1:** Not meeting air safety regulations
- **FC-1:** Running out of fuel

They are important for safety of operation and widely interconnected with the functionality of different subsystems, therefore they may have a bearing on the success of the mission.

Baseline Phase
One of the major goals of period before the Baseline Report was to create concepts using design option trees representing a range of valid design alternatives both at system and sub-system level and in a later process enable a qualitative trade-off and choice of the most promising option. The criteria taken into account for trade-off were: technological availability, complexity, mass, safety, cost, reliability and sustainability. The trade-offs were performed on subsystems of the UAV system, including: aerodynamic configurations, communication, primary and secondary power, flight control, target & obstacle acquisition, navigation, location determination and attitude determination. In result three system concepts were generated. The subsystem composition should not be considered as fully fixed and might be combined or exchanged between concepts.

Table 1: Overview of the three system concepts

Design Options	Concept 1	Concept 2	Concept 3
Aerodynamic Configuration	VTOL Flying Wing	Hybrid Helicopter	Tilt-Rotor
Communication	Direct Radio	Radio UAV	Satellite
Primary Power	PEMFC	AFC	DMFC
Secondary Power	FC Boost	Supercapacitors	Battery
Flight Control	ESC	Dedicated Surfaces	Thrust Vectoring
Target & Obstacle Acquisition	Radar	Lidar	Stereo Vision
Navigation Algorithm	SLAM	Real-time Avoidance	SLAM
Location Determination	GPS & Radar	GPS & Barometer	GPS & Laser
Attitude Determination	IMU	Magnetometer	Gyroscope

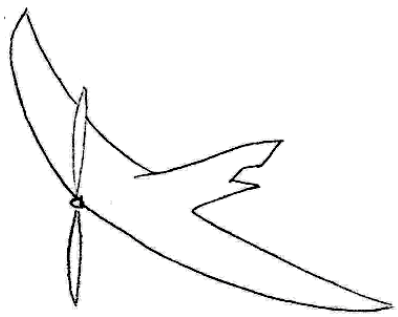

Figure 2: Aerodynamic Concept 1

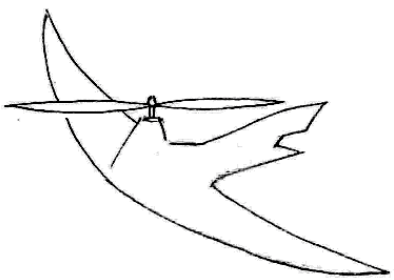

Figure 3: Aerodynamic Concept 2

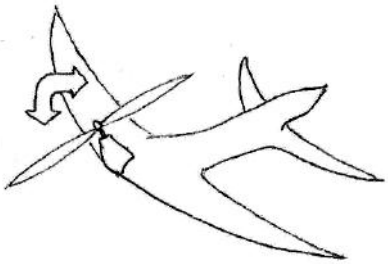

Figure 4: Aerodynamic Concept 3

Midterm Phase
During the midterm phase, a large emphasis was laid on the trade-offs between the design options that were

chosen in the baseline phase. Based on the power requirements from other subsystems, the power subsystem was sized and suitable options were selected to be incorporated in the power subsystem. It was concluded after the trade-off that a battery was going to be used for the flight termination system and as a secondary power source for the main UAV system. The fuel cell type to be used is the Proton Exchange Membrane Fuel Cell (PEMFC).
The aerodynamic configuration of the UAV resulted in a certain configuration layout. After a trade-off between a compound helicopter, flying wing and tilt rotor aircraft, the flying wing concept scored the most points and was thus the configuration upon which the final design was made. The preliminary planform design parameters for the flying wing concept is presented in table 2 and a planform sketch can be seen in fig. 5.

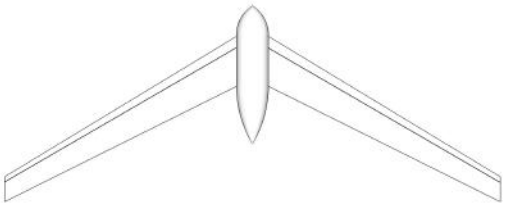

Figure 5: Flying Wing planform design.

Table 2: Design Parameters - Flying Wing

Parameter	Value	Parameter	Value
e	0.75	$\bar{c}$	0.2425 m
$C_{D,0}$	0.014	λ	0.5
m	7.76 kg	$V_{\text{endurance}}$	17.62 m/s
A	12.4	t_{max}	6.3 h
b	2.9 m	S	0.678 m^2
Λ	30°	W/S	112.17 N/m^2
P_{cruise}	445.3 W	$(L/D)_{\text{cruise}}$	10.62
P_{climb}	959.8 W	$C_{L_{\text{design}}}$	0.154
$C_{L_{\text{stall}}}$	2.00		

The different subsystems had to be integrated into one flying wing system. Since the wings were too small to fit in most of the subsystems, a fuselage was added to serve as a space to fit in the different subsystems. The system integration is visualised in fig. 6 and 7.

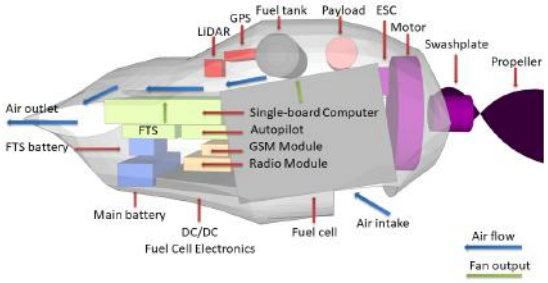

Figure 6: Internal layout

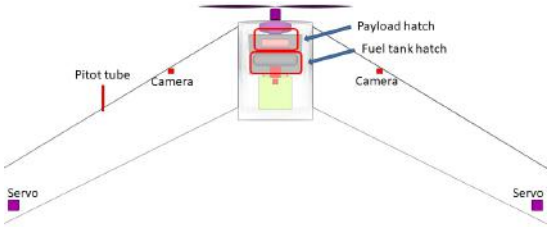

Figure 7: Top view layout

At this stage the final concept regarding all the different subsystems were chosen and a further detailed sizing of the chosen options was performed in the final phase towards the final review, where the finalised design for the mission is presented. This process is outlined in the following.

Final Phase
During the midterm project, a global design of the UAV was made. The final design further refined this design. Also, this phase put its main emphasis on the verification and validation aspect of the design. For the power, communications and the electronics subsystem, the final phase consisted of deciding on the final components. For the aerodynamics chapter however, a lower level trade-off had to be performed. As mentioned in the midterm phase, it was decided to use a flying wing configuration in the design. The flying wing however was further specified into three different design configurations variations. The considered design configurations are presented in fig. 8.

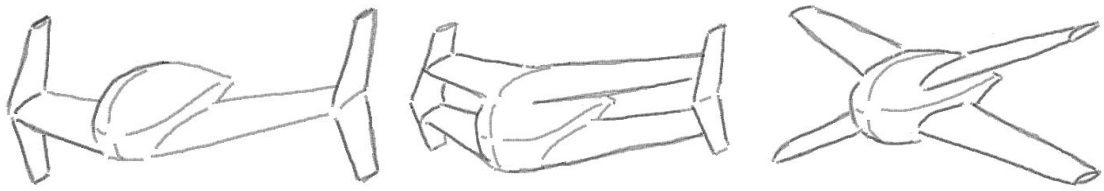

(a) Single Wing **(b)** Double Wing **(c)** X-Wing

Figure 8: Sketches of investigated configurations

Additionally to the subsystems that were mentioned above, a few subsystems were not touched upon until this phase. The two subsystems that were developed in this phase were the propulsion design and the fuselage design. Regarding the propulsion subsystem, 4 propellers were chosen to fulfil the thrust and stability requirements. One main propeller, two cruise propellers, and one yaw propeller was chosen, as depicted in fig. 9a. What can also be seen from this figure is that the fuselage design was designed in the shape of a teardrop, as this shape proved to be the most aerodynamically advantageous. The internal layout of the fuselage is depicted in fig. 9b.

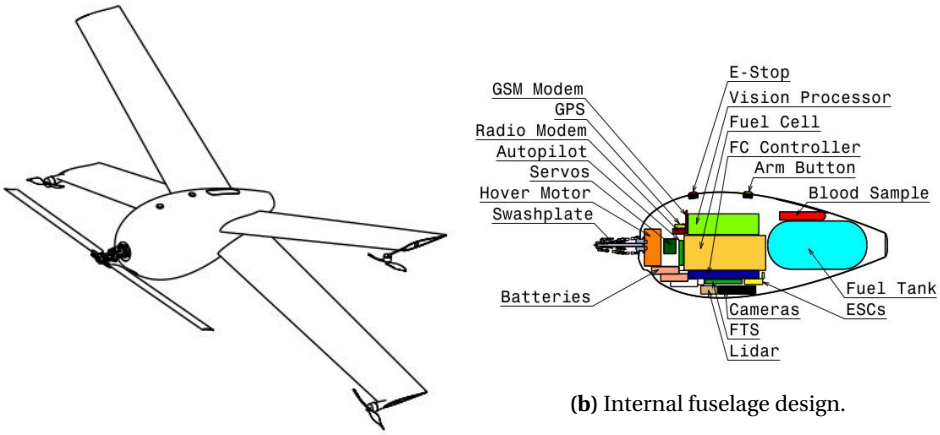

(a) Assembly isometric view.

(b) Internal fuselage design.

Figure 9: Final Layout

As can be seen, the design of the UAV consists of many subsystems. To create one integral system out of these systems is a complicated task. For once, most of the subsystems had a high dependency upon other subsystems. The relations between the subsystems are illustrated in fig. 10. The red box indicates the three subsystems that were most interlinked and thus wherein the highest iterative process took place.

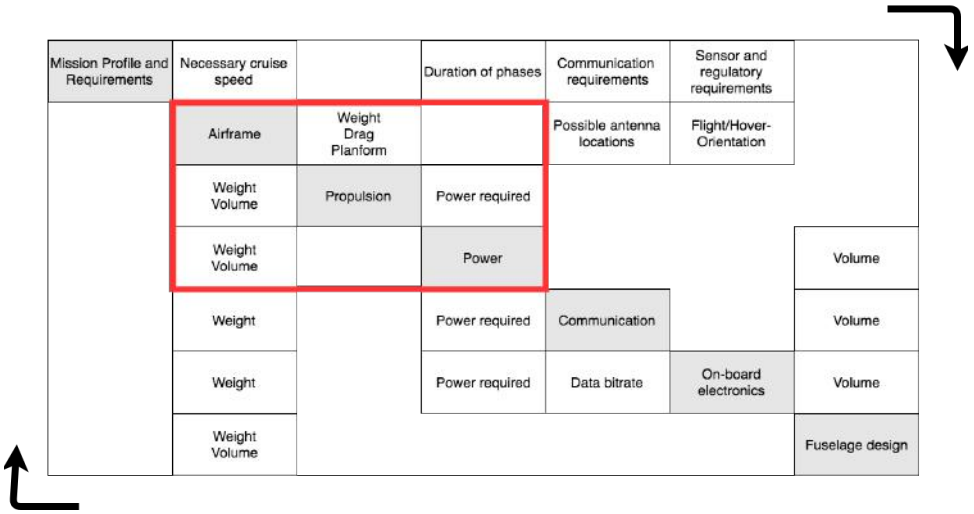

Figure 10: Design N^2-chart

Once the system was properly integrated, the final planform parameters and the budget of the final design could be created and are depicted in table 3 and table 4 respectively. The total in the budget table for the UAV system includes an additional 5% margin to account for missed components such as cables and such. The final design complies with almost all of the requirements that were identified. However, some requirements have not yet been fulfilled. One of the reasons why these requirements are still open is that further analysis has yet to be done in the next stage of the project to confirm the compliance of some requirements. However, as the requirements that are not complied with are not driving requirements, it can be said with confidence that the system will appeal to the stakeholders.

Table 3: Planform parameters and aerodynamic characteristics for the optimal (final) planform

Planform	
Surface area S	$0.6645\,\mathrm{m}^2$
Aspect ratio A	4.232
Taper ratio λ	0.8
Spanwidth b	1.576 m
Mean aero. chord $\bar{c}$	0.1989 m
Total mass m	8.454 kg
Systems m_{sys}	2.04 kg
Velocity V	27.7 m/s
Lift coef. C_L	0.3907
Lift-over-drag ratio L/D	9.866
Drag D	8.403 N
Drag coef. C_D	0.027 91
Zero-lift drag coef. $C_{D,0}$	0.018 68
Fuselage $(C_{D,0})_{\text{fus.}}$	0.0079
Wing $(C_{D,0})_{\text{wing}}$	0.0084
Interference $(C_{D,0})_{\text{interf.}}$	5.0×10^{-5}
Other $(C_{D,0})_{\text{other}}$	0.0019
Induced drag coef. $C_{D,\text{i}}$	0.009 173
Oswald factor. e	0.902
Viscous drag coef. $C_{D,\text{v}}$	5.9×10^{-5}
Stall velocity	14.31 m/s
Stall lift coef.	1.032
Endurance velocity	19.61 m/s
Endurance drag	9.749 N
Range velocity	26.24 m/s
Range L/D	9.950
Range drag	8.3322 N
Maximum velocity	34.2 m/s
Maximum drag	9.578 N

Table 4: Final Budget

Subsystem	**Mass [g]**	**Cost [€]**
Communication	162.4	216.15
Control System	468.6	1162.13
Swash-Plate	198.55	115.03
Motors and Propeller	822.7	385.03
Power	1824.3	19004.5
Structure	4151.2	115.13
Ground	2305.5	1267.63
Total	10769	23537

Finally, once the design of the UAV was created, thought was given about the logistics of the UAV. It was required for the UAV to be transportable for one person. Therefore, a casing solution was created for the UAV. To fit the UAV in a case, the system will be disassembled. The case dimensions and layout are illustrated in fig. 11 and fig. 12.

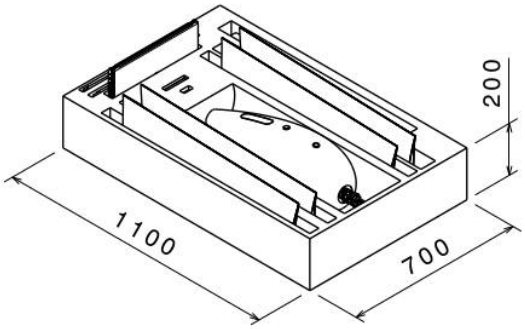

Figure 11: UAV casing dimensions.

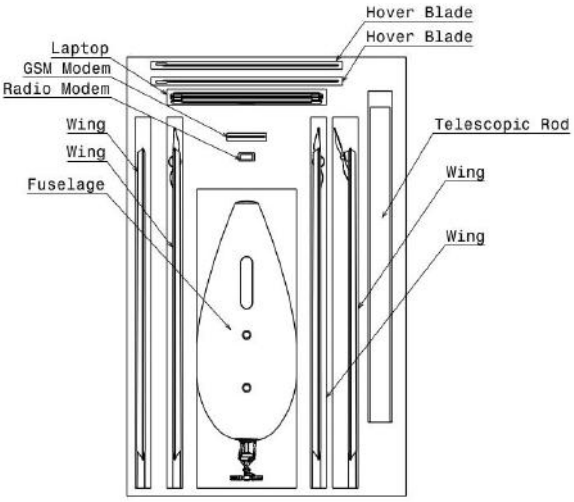

Figure 12: Disassembled UAV ready for transport.

Contents

1 Introduction

The past decades the potential of technological solutions has exploded, also the need for humanitarian aid is ever growing. Small Unmanned Aerial Vehicles (UAV) may bring a solution to this, it is therefore that the Medical Express UAV Challenge (MEUC) was created. This competition is open to everybody and aims to stimulate the design of cost efficient and innovative UAV's. This DSE project focuses on designing a fully autonomous, fuel-cell powered, swash-plate propeller hybrid UAV with 10 students in 10 weeks with a system cost of €8,000 or less, capable of winning the Medical Express UAV Challenge 2018. The MEUC competition is won when the UAV can autonomously take off, search for a target, land on it, take off again and return to base all within a given time span. Aside from the requirements imposed by the MEUC the TU Delft and the Royal Dutch Navy also added requirements which should be included in the design. This requires the UAV to include a fuel cell, swash plate and hybrid design.

This report will discuss how the UAV system is designed. It is the last in a series of three but can be read as a standalone document. The design process was structured by dividing the team into different sub-departments such as power, aerodynamics & structures, propeller & motor, electronics and communication. Other tasks which regard project planning, market and sustainability plans were distributed among the team members equally. Through this system the team has made an iteration method which involved all subsystems to come to an optimal design.

Chapter 2 opens the report with an analysis of all mission requirements, representations of system functionality together with an outline of the mission profile, wind conditions and the most important requirements. Chapter 3, discusses the most innovative and critical part of the UAV - the power subsystem. After this, chapter 4 discusses the aerodynamic configuration, aerofoil selection and fuselage aerodynamic analysis. The chapter that follows is chapter 5 which discusses the stability and control of the chosen configuration both in cruise flight and hover, during transition manoeuvres and while standing on the ground in windy conditions. Chapter 6 focuses on the aerodynamic design of all fours propellers, the choice of suitable motors and design of the swash plate. Structural issues are considered in chapter 7, the materials chosen for the main structural elements are presented along with their properties. The spar and wing skin are sized according to maximum allowable loads. Chapter 8, presents information on all electronic hardware. Data handling and autopilot critical functions, such as FTS, automated target acquisition or obstacle avoidance are discussed in this chapter as well. The next chapter, chapter 9, discusses the design of the communication subsystem, software and hardware, together with an analysis of the available data transfer options on the site of the competition. Chapter 10 presents all actions taken within systems engineering to integrate components of the UAV system within one coherent and optimised form. Applicable schematics, drawings and diagrams show final dimensions of the system and integration within the fuselage. This is followed by a summary of all budgets: mass, power, cost, etc. and a final check on requirements compliance and system feasibility. Altogether, an integrated system sensitivity analysis gives an indication of the most critical parameters that may influence the performance by having an impact on i.e. total weight, drag, power or flight performance. Chapter 10 also gives an outline of the production plan and a risk analysis summary. Chapter 11 summarises the business case analysis for the system, giving indication of market impact, business strategy, possible costs and profits. Sustainability considerations are discussed in chapter 11. RAMS analysis with Failure Mode Effect Analysis and similar methods, complementary HSE risk assessment and mitigation are discussed in chapter 12, along with the operations and logistics plan. Ultimately, the report is concluded in chapter 13 along with recommendations for the post DSE phase.

2
Mission Overview

This chapter gives an overview of the mission that the UAV needs to perform. The mission statement will be elaborated first in section 2.1 after which the functions of the missions will be identified in section 2.2. Furthermore, the requirements are analysed in section 2.3 and finally, the mission profile is studied in section 2.4.

2.1. Mission Statement

This project aims to design a UAV which is capable of winning the Medical Express UAV Challenge 2018. The challenge set up competition rules [4], of which requirements were deducted. On top of that, the TU Delft also set some minimum requirements for this particular DSE. The most notable ones are that the UAV must contain a swash-plate and should be fuel cell powered. The full list of requirements is presented in a compliance matrix in section 10.4. In addition to these initial stakeholders, the Royal Netherlands Navy showed interest in the design as well. Due to the fact that some requirements were contradictory with the requirements that were set by the UAV challenge, the choice to focus the design on the UAV challenge first was made. In the long-term future plans of this project, the design will be further developed and adapted to suit the requirements of the Navy. In conclusion, a mission need statement and project objective statement were setup in order to encapsulate the most essential needs for the mission and project.

Mission need statement: *Provide a fully autonomous UAV capable of medical sample retrieval within the operational range of more than 60 km, within 50 minutes or less, from a remote location on arbitrary terrain.*

Project objective statement: *Design a fully autonomous, fuel-cell powered, swash-plate propeller hybrid UAV by 10 students in 10 weeks with a system cost of €8,000 or less, capable of winning the Medical Express UAV Challenge 2018.*

2.2. Functional Analysis

In order to create a good design, one must understand what the system should be capable of. A helpful tool for gaining more understanding of the system, is to perform a functional analysis. The analysis is executed with the use of a functional flow block diagram (FFBD) and a functional breakdown structure (FBS).

The FFBD shows the systems functional flow in a time-sequenced, step-by-step flow diagram. It helps visualising the functions the system must perform in a logical order. The functional flow block diagram is developed in a series of levels. Functions of the first level are broad and general as can be seen in fig. 2.1. They are then expanded into more detailed and specific second level functions which can themselves be expanded into third or even fourth level functions, which are found infig. 2.2. Colours are used to help visualise the relation between functions of different level. The dotted lines indicate the transition between the levels.
The FBS is a diagram in which the different functions of the system are ranked hierarchically in an AND tree. This means that the functions of lower levels add up to form the basis for functions on higher levels as indicated through the different connections in between the functions. Functions that were discussed in the FFBD are also included in the FBS. The FBS gives another view on the system and creates the opportunity to identify functions that are time independent, and could thus not be implemented in the FFBD. The FBS for the Medical Express UAV is shown in fig. 2.3.

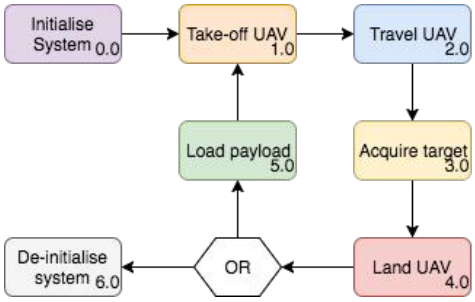

Figure 2.1: Top Level of the Functional Flow Block Diagram

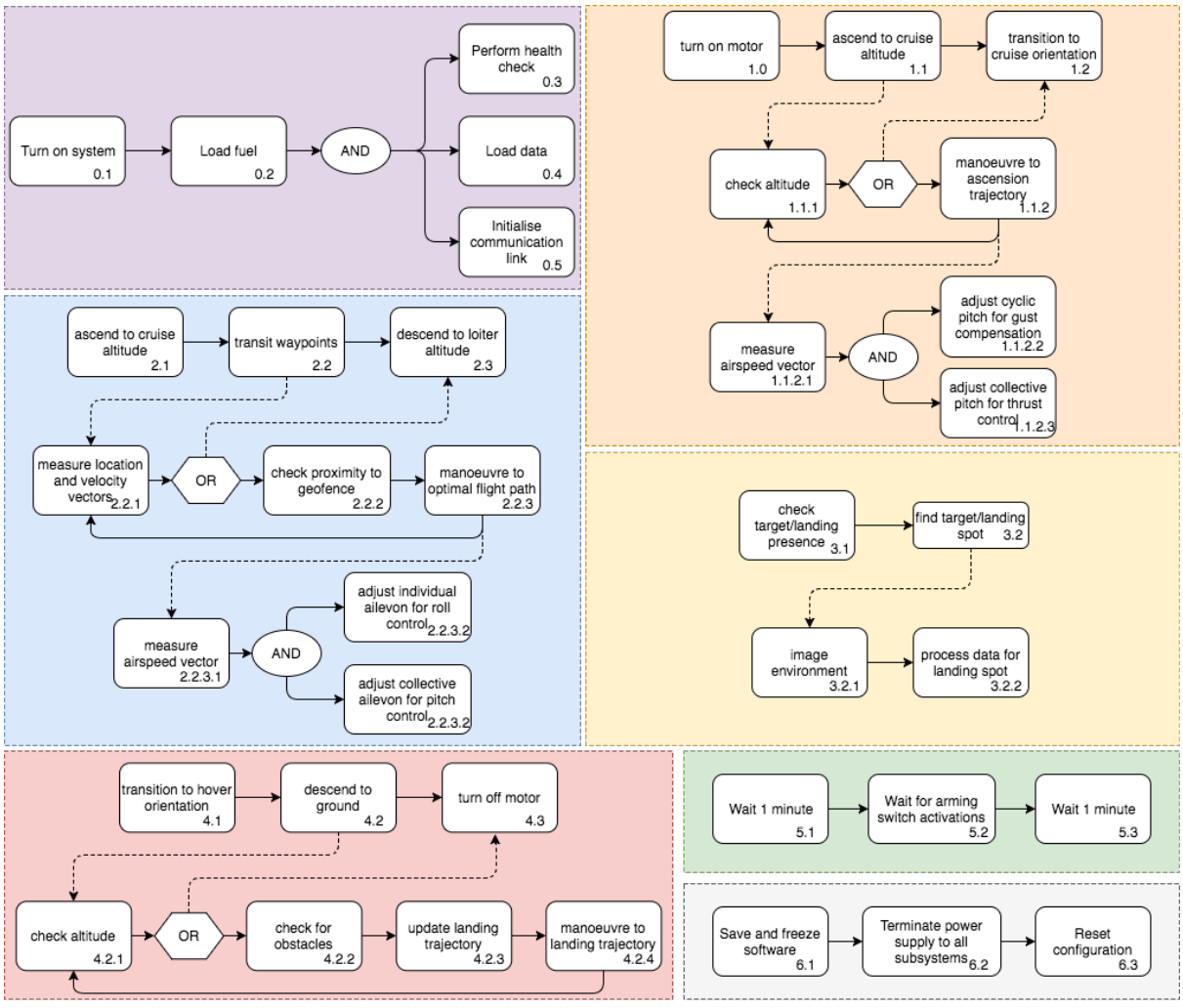

Figure 2.2: Lower Levels of the Functional Flow Block Diagram

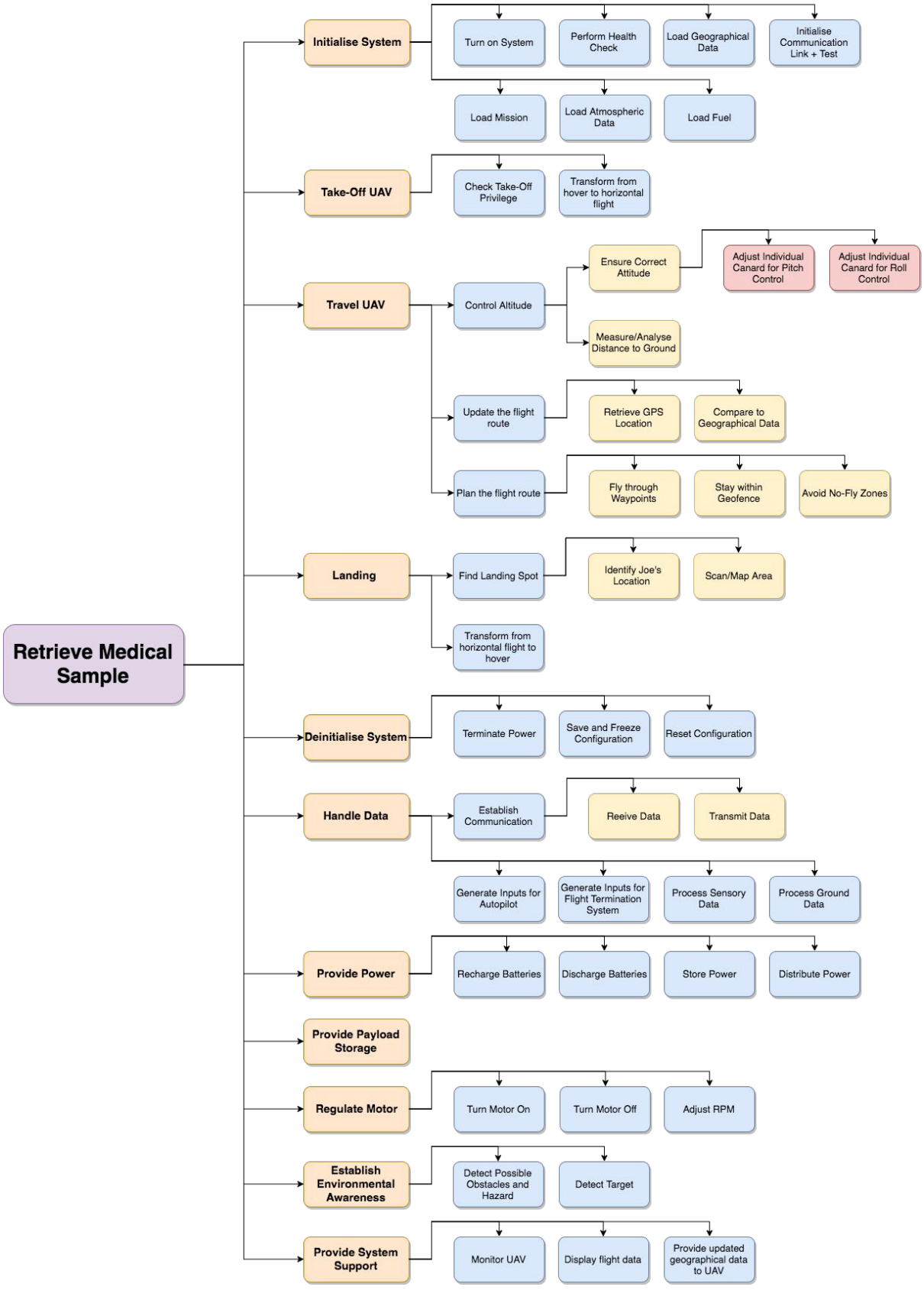

Figure 2.3: Functional Breakdown Structure

2.3. Requirements

Now that the functions have been analysed, the requirements can be properly identified. Three major stakeholder are involved in the requirement generation, as mentioned in section 2.1, which are the Challenge Com-

mittee, TU Delft and the Royal Netherlands Navy. The full requirements list is given in section 10.4. After identification of the requirements, the key requirements are marked so that special attention can be given to them during the design process. During this process certain requirements will turn out to be driving or even killer requirements. The definitions of key, driving and killer requirements are as follows [12]:

- **Key requirement:** A requirement of special importance to our customers or a requirement known or expected to present a risk item.
- **Driving requirement:** A requirement that drives the design more than usual.
- **Killer requirement:** A requirement which drives the design to an unacceptable extent.

Table 2.1 lists the requirements that were identified as key, driving and killer requirements. The driving requirements were identified in the early stage of the design process as they impacted the feasible design options significantly. Throughout the project, killer requirements have been identified. The main killer requirements stem from the addition of the Navy as a stakeholder. The majority of the Navy requirements coincided with the initial requirements, as provided by the challenge committee and TU Delft. However, several requirements were contradictory to the initial requirements. The identified killer requirements (MEUC-NAVY-05 and MEUC-NAVY-17), are requirements that are requirements on the fuel system. As it was found to be unfeasible to design a fuel system that complied with both Navy and Challenge requirements, it was chosen to fully optimise this particular design for the Outback Challenge. Alterations to this design can be made to create a design that is also suited for Navy purposes.

Table 2.1: Table identifying the key, driving and killer requirements

Requirement type	Identifiers
Key requirements	MEUC-TUD-02, MEUC-TUD-03, MEUC-TUD-05, MEUC-TUD-07, MEUC-TUD-08, MEUC-TUD-09, MEUC-TUD-10, MEUC-TUD-18, MEUC-TUD-19, MEUC-TUD-20, MEUC-TUD-22, MEUC-UCTC-12, MEUC-UCTC-13
Driving requirements	MEUC-NAVY-10, MEUC-TUD-02, MEUC-TUD-06, MEUC-TUD-11, MEUC-TUD-18, MEUC-TUD-20, MEUC-TUD-21, MEUC-UCTC-12
Killer requirements	MEUC-NAVY-05, MEUC-NAVY-17

2.4. Mission profile

Section 2.4 discusses the mission profile. The requirements relevant to the mission profile are:

- **MEUC-TUD-02** The Medical Express UAV Challenge shall be completed in 50 min or less.
- **MEUC-TUD-07** The UAV shall have a range of 60 km.
- **MEUC-CASA-02** The UAV shall not fly above 1500 ft AGL (Above Ground Level) during the entire mission.
- **MEUC-Sys-TUD-01-02** The UAV shall be able to fly in wind conditions of average wind speed up to 25 kts measured over a 10 minute time span.

The mission profile for the UAV is presented in fig. 2.4. The horizontal axis shows elapsed time. The vertical axis represents an indication of the altitude of the UAV.

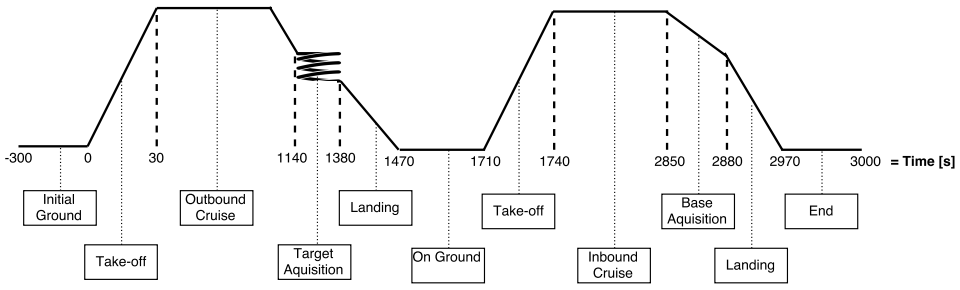

Figure 2.4: Graphical Mission Profile for Medical UAV Express

The cruising times are derived from the MEUC-TUD-02 mission time requirement. This requirement states a total mission duration of 50 minutes (3000 s), excluding the initial ground phase. First the segment duration of all non-cruising flight phases is estimated. The cruise time is determined by subtracting the total estimated time of all non-cruising segments from the maximum allowed mission flight time. This results in a total cruising time of 39 minutes for the inward and outward journey. A safety margin of 30 s is taken into account in the

mission profile. From the approximated cruising times and the MEUC-TUD-07 range requirement, the ground speed for cruise is calculated to be 27.0 m/s by dividing the cruise range by the cruise time.
The most critical wind speed at minimum allowed cruise level, decided to be 45 m, is calculated using the wind power law eq. (2.1) [21, p. 55]. The wind profile power law can be used to estimate the wind at altitudes $v_{\text{Wi,h}}$ up to 2000 m. For the wind calculation, the wind speed measured at ground level $v_{\text{Wi,ref}}$ is used as reference. The Hellman constant, α_{Hell}, is an empirical derived constant for which 1/7 is used for the mission analysis for neutral atmosphere conditions [35, p. 864-865]. The height of the reference wind measurement, h_{ref}, is assumed to be at a standard height of 10 m. Two wind conditions are considered: the average wind in September in Dalby (7 kts)[1], which will determine the design cruise speed and the worst case scenario (25 kts wind) which will determine the maximum speed the UAV should be able to fly at. Two wind direction cases were considered: a constant cross-wind and a head-wind outward journey followed by a tail-wind inward journey flown at a constant airspeed. The required airspeed of the first scenario is computed using eq. (2.2) and the second scenario by solving eq. (2.3) for the true airspeed. fig. 2.5 illustrates these two cases. One can see that the head and tail wind case is always the one requiring the highest airspeed and it is therefore the one taken to design the cruise and maximal airspeed. Furthermore, it creates considerable discrepancies between the outward and inward journey cruise time. The maximum airspeed of these two cases is then taken for the cruise

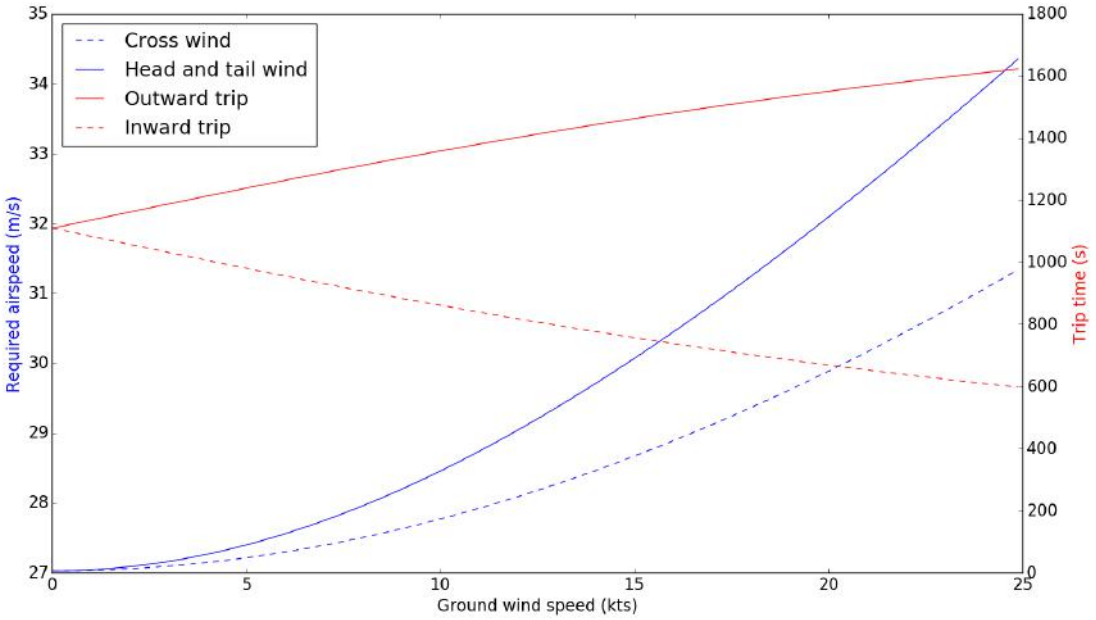

Figure 2.5: Influence of the wind on the required airspeed and influence of the wind on the inward and outward cruise time for the head and tail wind scenario

speed and for the maximum speed.

$$v_{\text{Wi,h}} = v_{\text{Wi,ref}} \left(\frac{h}{h_{\text{ref}}} \right)^{\alpha_{\text{Hell}}} \tag{2.1}$$

$$V_{AS} = \sqrt{V_{GS}^2 + v_{\text{Wi,h}}^2} \tag{2.2}$$

$$(V_{AS} + v_{\text{Wi,h}})(2 \cdot 18.5 \cdot 60 - (30 \cdot 10^3 / (V_{AS} - v_{\text{Wi,h}}))) + (V_{AS} - v_{\text{Wi,h}})(30 \cdot 10^3 / (V_{AS} - v_{\text{Wi,h}})) = 60 \cdot 10^3 \tag{2.3}$$

Using the reference data described before, the wind speed at 45 m is calculated to be equal to 4.4 m/s for the average case and 15.7 m/s for the worst case. This results in a cruise speed of 27.7 m/s and a maximum speed of 34.2 m/s.

[1] URL `http://www.bom.gov.au/climate/averages/tables/cw_041522.shtml` [cited 20 June 2017]

3

Power Design

The power system must be able to provide sufficient power during any flight condition the UAV might encounter. A thorough design of this system is therefore essential. In the following chapter this will be done. First, a brief overview of the operation principles of main power system will be given. Next, the approach and methodology will be outlined as explained, followed by the presentation and analysis of the design solution. Verification and validation possibilities will be discussed afterwards, before ending the chapter with the conclusion and especially recommendations for the further design.

3.1. Overview

In this section a brief overview of the power design will be given. The design of power system of the UAV system has to comply with the following list of requirements, especially using a fuel cell as primary power source according to MEUC-TUD-18. As this technology defines the design in a way that everything will be built around possible fuel cells, this section shall introduce the reader briefly into this technology and its application. As the FTS has to have a separate power source according to MEUC-Sys-UCTC-03-14-Power-05, a battery capable of powering it will be chosen, however not discussed in detail. The focus of this chapter lies on the main power source.

Requirements:

- **MEUC-TUD-06** The UAV shall be fully electric only.
- **MEUC-TUD-10** The UAV system including fuel and payload shall not be heavier than 15 kg.
- **MEUC-TUD-18** The UAV shall use a fuel-cell.
- **MEUC-TUD-20** The UAV shall be able to hover.
- **MEUC-Sys-TUD-18-15-Power-01** The fuel cell products shall not contaminate the environment.
- **MEUC-Sys-TUD-18-15-Power-02** The fuel cell shall be capable of providing power throughout the whole mission duration.
- **MEUC-Sys-UCTC-03-14-Power-05** The FTS shall have a separate power supply in addition to the fuel cell.

When designing a fuel cell system, first the type of fuel cell has to be chosen according to the needed application. For this design a Proton Exchange Membrane fuel cell (PEM) has been chosen for its wide availability and overall good specific power and especially power density. For more information on other types of fuel cells and the choice for a PEM, please see [19].

The basic operation of a PEM fuel cell is extremely simple. Hydrogen and oxygen are combined in a reaction to form water. This can usually be observed in the exothermic combustion reaction:

$$2H_2 + O_2 \rightarrow 2H_2O + \text{Energy} \tag{3.1}$$

However, in the case of a fuel cell the hydrogen is not burnt in the literal meaning and thus not only heat is being produced but also electrical energy. This is due to the fact that the hydrogen on the so-called anode side and oxygen, or usually ambient air, on the cathode side are separated by the electrolyte membrane which only allows the transfer of positive hydrogen ions. Therefore, in order to form a complete water molecule the electrons of the hydrogen have to find another way from the anode to the cathode. This way takes them through the load circuit, thus creating an electric current through the systems that need to powered. This process is illustrated in fig. 3.1a.

Fuel cells typically only have a mediocre specific power as can be seen in table 3.1, however combined with a suitable tank and the high specific energy of hydrogen of 39.7 Wh/g, this can lead to systems with a specific energy of more than 300 Wh/kg. This exceeds the specific energy of most batteries, for reference see table 3.2, and thus promises longer flight times than a battery system with equivalent mass. As every Watt of the fuel

[1] URL `https://goo.gl/Unb329` [cited 26 June 2017]
[2] URL `https://goo.gl/VLwkij` [cited 26 June 2017]

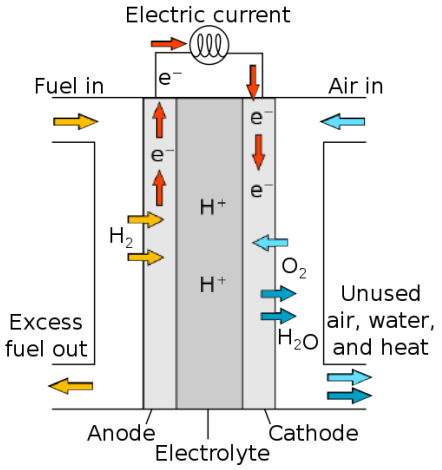

(a) A single PEM Fuel Cell[1]

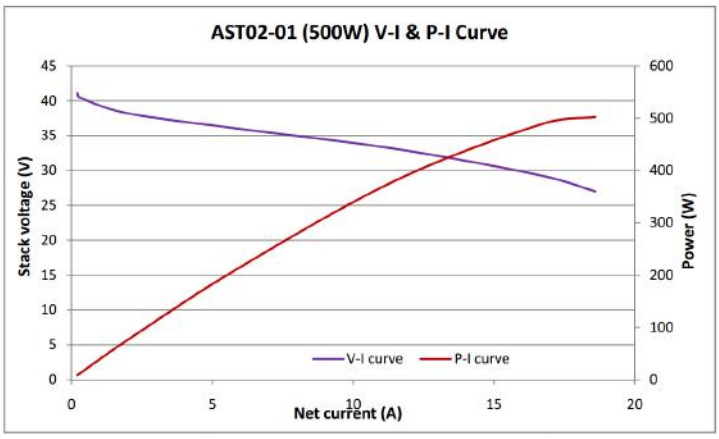

(b) Example of the characteristic electrical curves of a fuel cell stack - here with the A-500 AEROSTAK rated at 500 W by HES[2]

Figure 3.1: Basic Operating Principles of Fuel Cells:
Figure 3.1a shows the basic chemical reaction: A fuel cell is powered by the supply of hydrogen on the anode side and oxygen from the ambient air on the cathode side separated by an electrolyte membrane. This membrane only allows a transfer of the hydrogen protons from the anode side to the cathode side to form water, the electron of the hydrogen molecule cannot pass. They have to go the long way through the load circuit. This is the used electric current.
Figure 3.1b shows an example of the characteristic V-I and P-I curves of a fuel cell stack. These curves can be optimised for the application and change with every stack and are thus for illustrating purposes only. It can clearly be seen that the voltage of the stack is not constant, making a DC/DC converter necessary to achieve a constant voltage.

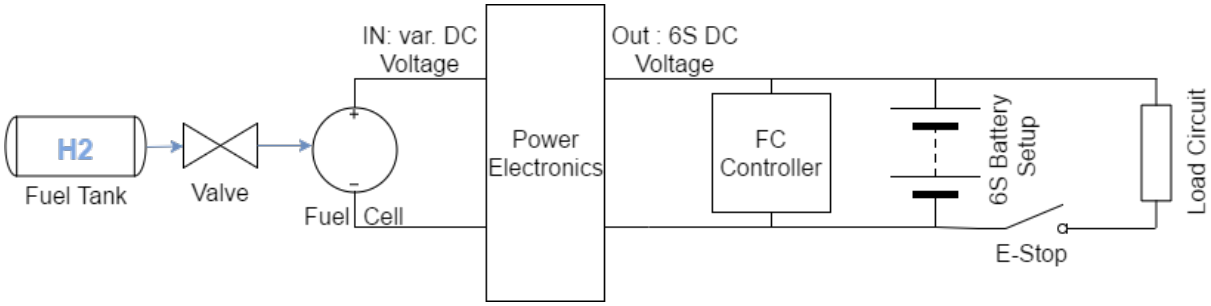

Figure 3.2: Outline of the power system illustrating energy flow and circuit configuration. Fuel cells themselves have a mediocre specific power, but combined with a suitable storage solution they have very good specific energies. In combination with batteries to overcome peak power phases exceeding the rated power of the fuel cell, this system may promise longer flight times than an equivalent battery system.

cell is relatively heavy, the fuel cell should not be oversized and should only be able to deliver a power around the average mission power it is intended for, in such a way that the maximum potential of the fuel cell is used. As the mission includes phases above average power, e.g. take-off, the missing power can be delivered by an auxiliary power system specifically designed for this task. Depending on the duration of these high power phases, the most lightweight solution for this secondary power system may consists of supercapacitors for very short high power bursts or batteries for longer power addition.
These two power systems have to integrated with each other. A battery, as the traditional secondary power source, delivers a near constant DC voltage. The output voltage of the fuel cell however varies with the power setpoint. Generally, with increasing the output power, the stack voltage drops. This is illustrated in fig. 3.1b. As the voltage alone also determines the efficiency of the fuel cell, the efficiency generally drops as well with increasing power. Due to the varying output voltage a piece of power electronics, more specifically a DC/DC converter, is needed that transforms the variable to a constant DC voltage that matches the voltage of the auxiliary power source. These can be combined then in parallel in such a way that the battery delivers additional current, and thus power when more power is needed than the fuel cell can deliver. This is shown in the outline of the power system design for this project in fig. 3.2. It may be noticed that a 6S battery, thus an array of six battery cells in series, is specified in the diagram. This is due to the fact that this is the voltage requirement by the main power consumers, the motors, as will be explained later.

Table 3.1: Fuel Cell Database - Unfortunately, only two manufacturers offer weight-optimised high performance PEM fuel cell stacks in the power region below 5 kW. Due to the significant difference in specific power, it is expected that for most mission profiles, an Intelligent Energy fuel cell will be chosen.

Manufacturer	Rated Power [W]	Weight incl. Controller [g]	Specific Power [W/g]
HES Energy Systems	200	650	0.31
HES Energy Systems	500	1400	0.36
HES Energy Systems	1000	2250	0.44
HES Energy Systems	tailor 200 W - 3kW	approx. following m = 1.97 P + 317.35	varying
Intelligent Energy	650	750	0.87
Intelligent Energy	1600	1300	1.23

3.2. Methodology

After having outlined the operational and design principles of the main power system, this section will describe the process of designing the main power system. This is done by introducing the approach, followed by important parameters and assumptions used in the logic of the design tool. This section will end with short remarks on the limitation of the design tool.

As the Medical Express UAV challenge will be held in September 2018, the possibility to use experimental components or products that are still in development has been discarded. Instead, the power system shall consist of products that are currently available on the market or in the last stage of development and early customer access. For this purpose databases of all the main elements, namely PEM fuel cells, batteries, super capacitors and hydrogen gas tanks, were created. The entries of these databases can be found in tables 3.1, 3.2, 3.3, and 3.4 respectively.
These databases are used in the design optimisation of the power system. For this purpose a simple tool was developed. In the following the logic, circumstances and assumptions of the program will be explained. The logic including the main formulas used can be seen also in fig. 3.3. The formulas include basic principles of physics as well as fuel cell specific formulas. The fuel cell specific formulas can also be found in [23].

Code Logic

1. **Inputs**:
   - Mission Profile:
     The power system still has to be able to provide enough power and carry sufficient energy to fulfil the mission in the worst possible conditions. Thus, the mission profile provides the power requirements during and the duration of each of the flight phases. This mission profile changes with each design iteration.
   - Databases:
     These contain the different options and specifications for fuel cells, batteries, supercapacitors, and hydrogen gas tanks as can be seen in figures 3.1, 3.2, 3.3, and 3.4 respectively.
2. **Parameters:**
   - Efficiency:
     These include the assumed average efficiency for the motors including controller as well as for the

[3] URL https://goo.gl/xEP5eJ [cited 26 June 2017]
[4] URL https://goo.gl/Q3GZSw [cited 26 June 2017]
[5] URL https://goo.gl/1gi4Ao [cited 26 June 2017]
[6] URL https://www.e-cigarette-forum.com/forum/attachments/img_4999-png.649531 [cited 26 June 2017]
[7] URL https://goo.gl/BpZotF [cited 26 June 2017]
[8] URL http://lygte-info.dk/review/batteries2012/A123%2026650%202500mAh%20(Green)%20UK.html [cited 26 June 2017]
[9] URL https://goo.gl/4b3Eob [cited 26 June 2017]
[10] URL https://goo.gl/w8GHPE [cited 26 June 2017]
[11] URL https://goo.gl/n1XfKR [cited 26 June 2017]
[12] URL https://goo.gl/JW84Ct [cited 26 June 2017]
[13] URL https://www.rcgroups.com/forums/showthread.php?2612591-Graphene-Test-Results [cited 26 June 2017]
[14] URL https://hobbyking.com/en_us/graphene-600mah-1s-w-jst-syp.html [cited 26 June 2017]
[15] URL https://hobbyking.com/en_us/graphene-750mah-1s-w-jst-syp.html [cited 26 June 2017]
[16] URL https://hobbyking.com/en_us/graphene-950mah-1s-65c-w-jst-syp.html [cited 26 June 2017]
[17] URL https://goo.gl/XT5MZ8 [cited 26 June 2017]
[18] URL https://goo.gl/AA96Tk [cited 26 June 2017]
[19] URL https://goo.gl/VTExMW [cited 26 June 2017]

Table 3.2: Battery Database - These batteries were assembled as not only specifications by the manufacturer were present but also test data. Some batteries are listed several times in the list, but with different currents as the effective capacity changes with the discharge speed. The lists consists of various chemistries of lithium ion and lithium polymer batteries as these are the most suitable batteries for this application.

Name & Discharge Rate	Power [W]	Energy [Wh]	Weight [g]	Sp. Power [W/kg]	Sp. Energy [Wh/kg]	Voltage min. [V]
Sony US18650VTC5[3] @ 30A	84	7	44.1	1904.76	158.73	2.8
Sanyo NCR20650A[4] @ 30A	84	8.4	55.1	1524.50	152.45	2.8
Sanyo NCR20700A[5] @ 40A	110	8.5	60.1	1830.28	141.43	2.75
Samsung INR21700-30T[6] @ 50A	140	8.6	68.1	2055.80	126.28	2.8
Samsung INR21700-30T[6] @ 60A	168	7.7	68.1	2466.96	113.07	2.8
BestFire IMR26650[7] @ 30A	84	9.5	86.4	972.22	109.95	2.8
A123 26650[8] @ 50A	125	6.60	76.9	1625.49	85.81	2.5
A123 26650[8] @ 60A	150	6.02	76.9	1950.59	78.26	2.5
iJoy 40A 4200mAh 26650[9] @ 30A	84	13.20	92	913.04	143.424	2.8
Aosibo IMR18650[10] @ 20A	56	8.16	44.6	1255.61	182.96	2.8
Aosibo IMR18650[10] @ 30A	84	7.63	44.6	1883.41	170.96	2.8
Venom FPV 50C[11] @ 60A	540	17.43	160	3375	108.94	9
Turnigy Graphene 65C[12]	810	17.30	188	4308.51	92.04	9
Turnigy Graphene 1300mAh[13]	780	17	176	4431.82	96.59	12
Turnigy Graphene 600mAh[14]	78.45	1.31	15	4308.5	87.44	3
Turnigy Graphene 750mAh[15]	99.37	1.66	19	4308.5	87.44	3
Turnigy Graphene 950mAh[16]	130.75	2.19	25	4308.5	87.44	3
INR18650-35E[17] @ 1A	2.8	12.17	48.6	57.61	250.35	2.8
INR18650-35E[17] @ 5A	14	11.16	48.6	288.07	229.59	2.8
INR18650-35E[17] @ 10A	28	10.33	48.6	576.13	212.55	2.8
NCR18650GA[18] @ 5A	14	11.04	47.4	295.36	232.97	2.8
NCR18650GA[17] @ 10A	28	10.2	47.4	590.72	215.19	2.8
LG 18650 MJ1[19] @5A	14	10.82	47	297.89	230.234	2.8
LG 18650 MJ1[19] @7A	19.6	10.5	47	417.02	223.40	2.8

Table 3.3: Supercapacitor Database - Two manufacturer produce high performance supercapacitors, Maxwell and Skeleton Technologies. Supercapacitors made by Skeleton Techn perform generally better with regard to specific power and about similar with regard to energy density. However, a single component is also typically heavier than one of Maxwell.

Manufacturer	Model	Power [W]	Energy [Wh]	Weight [g]	Specific Power [W/g]	Specific Energy [Wh/kg]
Maxwell	BCAP3400 P285 K04	7280	3.848	520	14	7.4
Maxwell	BCAP0310 P270 T10	840	0.312	60	14	5.2
Maxwell	BCAP0350 E270 T11	570	0.354	60	9.5	5.9
Maxwell	BCAP1500 P270 K04	3920	1.512	280	14	5.4
Maxwell	BCAP2000 P270 K04	5040	2.016	360	14	5.6
Skeleton Tech	SCA0500	4532	0.5665	103	44	5.5
Skeleton Tech	SCA0750	6210	0.8418	138	45	6.1
Skeleton Tech	SCA1200	10191	1.3509	237	43	5.7
Skeleton Tech	SCA1800	12760	2.0416	319	40	6.4
Skeleton Tech	SCA3200	16995	3.605	515	33	7
Skeleton Tech	SCHE0320	2899.2	0.3584	64	45.3	5.6
Skeleton Tech	SCHE0500	3318.7	0.5621	77	43.1	7.3
Skeleton Tech	SCHE0900	6021	1.0125	135	44.6	7.5
Skeleton Tech	SCHE1300	7506	1.476	180	41.7	8.2
Skeleton Tech	SCHE2800	12529.1	3.1759	349	35.9	9.1
Skeleton Tech	SCHE3500	10140	3.939	390	26	10.1

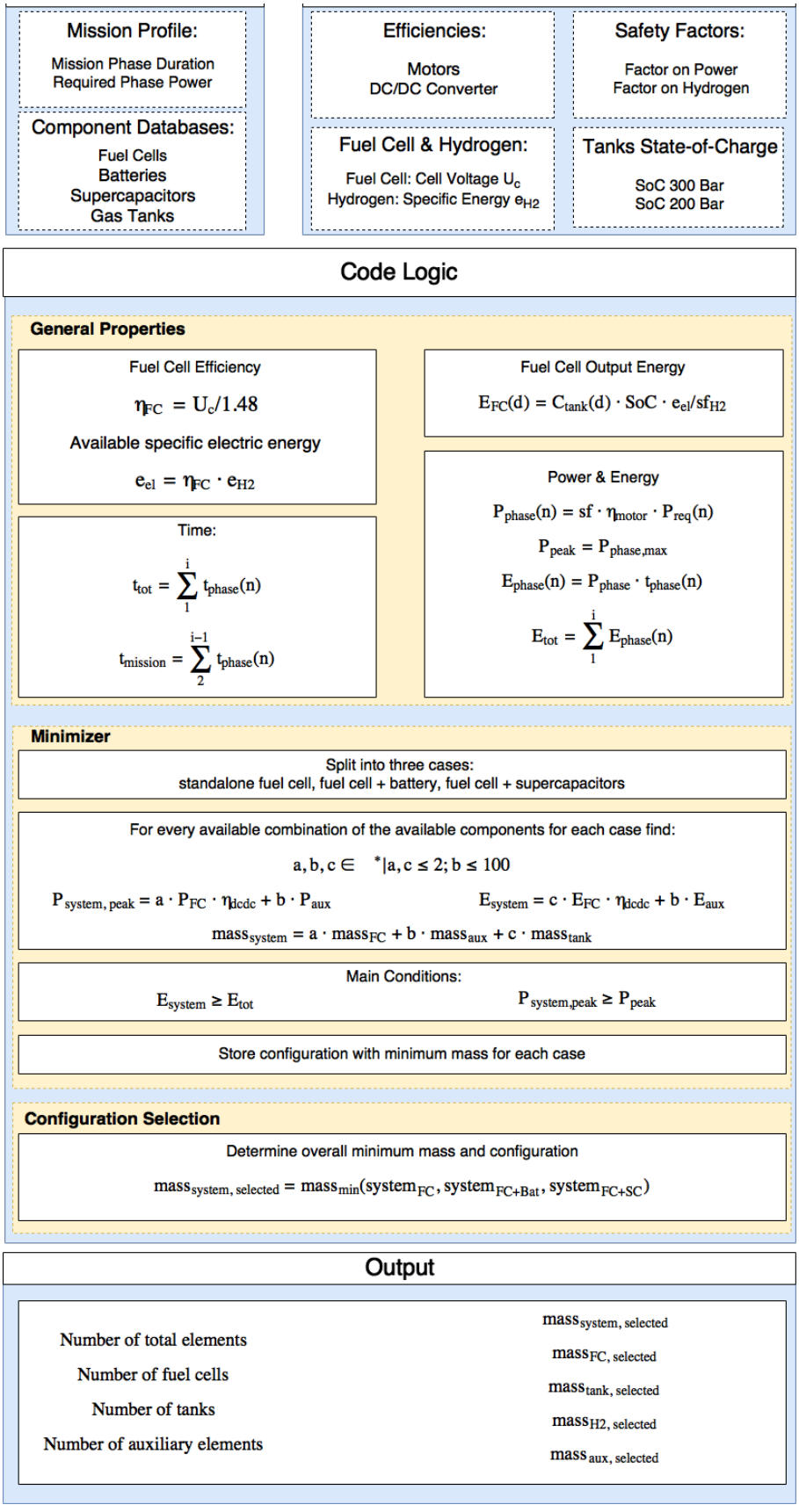

Figure 3.3: Tool for the design of the main power source including the main equations

Table 3.4: Gas Tank Database - The two fuel manufacturers also distribute lightweight tanks from numerous manufacturers in varying sizes. Generally, the gravimetric efficiency increases with increasing tank volume. Intelligent Energy also offers tanks for military applications with a decreased safety factor. These tanks should thus be even lighter than the ones displayed here.

Distr.	Name	Pressure [bar]	Water Vol. [L]	H2 Vol. [std. L]	Empty Mass [kg]	H2 Cap. [g]	Gravimetric Eff. [%]
HES	LC 0.5-30 A1	300	0.5	150	0.825	13.2	1.60
HES	LC 1.6 - 20 A1	200	1.6	320	1.275	28.2	2.21
HES	LC 1.1-30 A	300	1.1	330	1.175	29.1	2.47
HES	LC 2.0 - 20 A1	200	2	400	1.655	35.2	2.13
HES	LC 2.1 - 20 A1	200	2.1	420	1.475	37.0	2.51
HES	LC 2.2 - 20 A1	200	2.2	440	1.685	38.7	2.30
I.E.	Type IV 1.5	300	1.5	450	1.01	39.6	3.92
I.E.	Type III 1.5	300	1.5	450	1.06	39.6	3.74
HES	LC 2.4 - 20 A1	200	2.4	480	1.715	42.3	2.46
HES	LC 2.5 - 20 A1	200	2.5	500	1.725	44.0	2.55
HES	e.2.0	300	2	600	1.575	52.8	3.35
HES	LC 2.17 - 30 A	300	2.17	651	1.875	57.3	3.06
HES	e.3.0	300	3	900	1.975	79.3	4.01
HES	LC 3.1 - 30 A	300	3.1	930	2.175	81.9	3.77
HES	LC 4.0 - 30 A1	300	4	1200	2.975	105.7	3.55
HES	LC 4.7 - 30 A	300	4.7	1410	3.175	124.2	3.91
I.E.	IE 6L	300	6	1800	2.85	158.5	5.56
I.E.	IE 6.8L	300	6.8	2040	2.94	179.7	6.11

DC/DC converter. For the DC/DC converter, an average efficiency of 90% was assumed while for the motors the average efficiency of the hover motor was determined to be 83% and applied to all motors.

- Safety Factors:
  There are several safety factors applied. The main safety factor is applied to the required power imported in the mission profile, and adds 20% of safety margin. The second safety factor is applied to the hydrogen capacity of the tanks, which is applied for several reasons. It might be that not 100% of the hydrogen stored in the tank are accessible. Furthermore, the fuel cell might consume slightly more hydrogen than anticipated. Thus, a 10% safety factor is added here.
- Tanks maximum state-of-charge (SoC):
  Depending on the tank system pressure, it might not be possible to fill the tank completely with the possibilities that are offered in the surrounding area of the place of operation. The nearest automotive hydrogen gas station is about 1000 km away from Dalby in Sydney. As industrial gas cylinders filled with hydrogen at 200 bar are readily available throughout most of the world, it is always possible to fill a 200 bar tank to near 100 %. 300 bar cylinders are unfortunately not offered regularly in Australia. However, with some planning it is possible to have 300 bar industrial cylinders shipped to Australia, e.g. by the Linde Group.
- Fuel Cell & Hydrogen Parameters:
  The voltage of one individual cell of the fuel cell stack determines its efficiency and varies with the power set point. At 100% power the voltage is lower than at lower set points. Thus, an average voltage has to be assumed and was chosen to be 0.65 V in accordance to literature [23].

  The specific energy of hydrogen determines the maximum energy stored in hydrogen that can be carried in a given tank. This value is 39.7 Wh/g.

3. **General Mission Properties:**

- Fuel Cell Properties:
  First the fuel cell efficiency is calculated using the cell voltage. Next, this efficiency is used to find the effective electrical specific energy of hydrogen. Finally, with this result and the safety factor on hydrogen and the SoC of the tanks, the effective energy capacity of each tank is calculated.
- Power and Energy required:
  Using the efficiency and safety factor, the actual required power for each mission phase is calculated as well as the peak power during the mission. From this and the duration of each respective phase, the consumed energy is calculated.

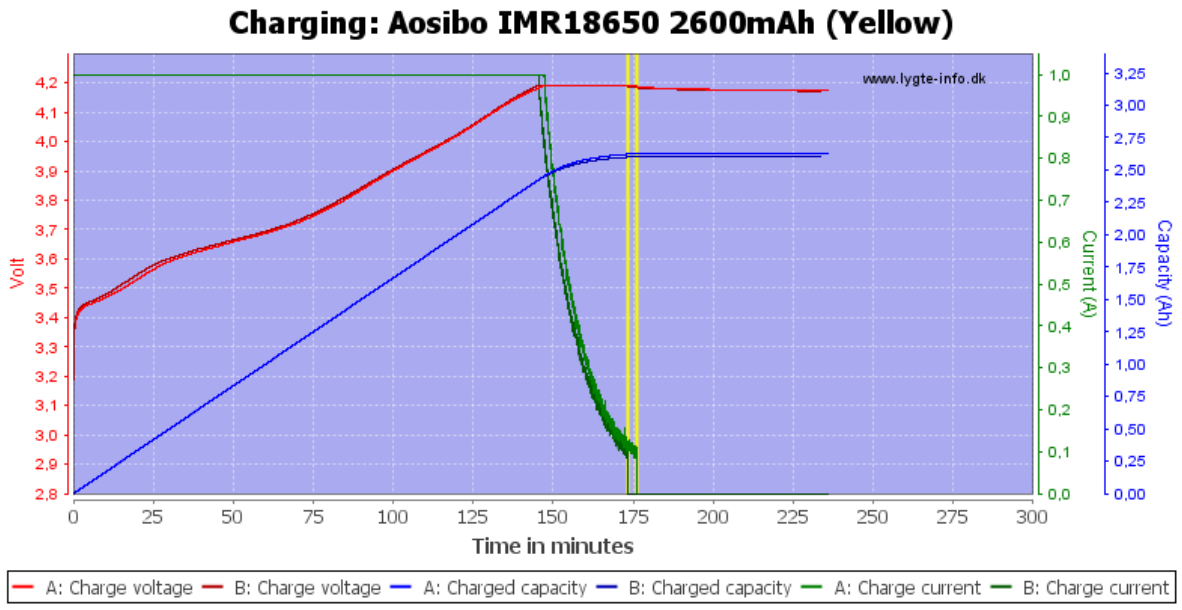

Figure 3.4: Charge curve for the Aosibo IMR18650 2600mAh battery[20]

4. **Weight Minimizer:**
   - Three different cases are computed: a standalone fuel cell system or a fuel cell combined with an auxiliary power source, namely batteries or supercapacitors.
   - For each of these cases it combines up to two fuel cells with up to two tanks and, if applicable, up to 100 batteries/supercapacitors of the same type with each other to form a system.
   - Of the systems that are able to provide at least the peak power, carry enough energy for the mission and are also able to deliver this energy, the lightest system is saved for each case. For the cases with auxiliary power, it is determined if the second power source needs to be recharged during the mission by excess power from the fuel cell.
5. **System Selection:**
   Of the three cases, standalone fuel cell, and the fuel cell combinations with battery or supercapacitor, the lightest version is saved and the properties given out.

The design tool is not without flaws. The two main limitations of the program are both connected to the case where recharging of the auxiliary power source is necessary during flight, be it with batteries or supercapacitors.
First, while the tool recognises that recharging is necessary, it does not check if there is sufficient power available from the fuel cell during low power phases to charge the auxiliary power source sufficiently before the next high power phase. This has to be checked for the output design. However, as the available fuel cell power is usually close to the average power and thus a multiple of the low power phases, it is quite certain that there is sufficient power available. There was no incident during the iteration process where this was not the case. Furthermore, this check can be easily implemented in the tool for a coming version.
The second limitation is similar but connected to the auxiliary power source. While there might be sufficient power available to recharge from the fuel cell, there are limitations on how fast a supercapacitor but even more a battery can be recharged. This has to be checked as well. An implementation in the code is more complicated as a charge curve is different for each individual supercapacitor/battery and is not linear. For example, batteries typically have a fast constant current recharge phase up to around 80% SoC, and transition then into a slow constant voltage charge phase. An example of this can be seen in fig. 3.4.
If a charge limitation of 80% SoC is implemented, this check can be done easily by the program as well as long as the charge curve is known as the charge progresses linearly in this phase. However, it might not give the very lightest solution anymore, as it effectively uses only 80% of the the capacity of the battery once partially discharged during the flight.

[20] URL `https://goo.gl/pCkKSt` [cited 26 June 2017]

Table 3.5: Mission profile for the design of the power system - This mission includes the worst case scenario with 25 kts wind conditions and is not based on the average wind conditions.

Mission Phase	Duration [s]	Propulsion Power [W]	Communication Power [W]	Electronics Power [W]
Initial Ground	300	0	5	8
Take-off	30	957.41	5	74
Outbound Cruise	1110	488	5	41
Target Aquisition	240	258	5	59
Landing	90	568.12	5	92
On ground	240	0	5	8
Take-off	30	957.41	5	74
Inbound Cruise	1110	488	5	41
Base Aquisiton	30	258	5	59
Landing	90	568.12	5	92
End	10	0	5	8

Table 3.6: Power System Setup including their main properties. Additionally to these components also a charger for the auxiliary power is needed.

Main Power	Type	Name	#	Mass [g]	Properties	Size [mm]	Cost/p. [€]
Primary	Fuel Cell incl. Contr.	I.E. AC64	1	750	P = 650 W	84 x 196 x 198 170 x 65 x 20	~13000
Auxiliary	LiMn-Battery	Aosibo 2600mAh	12	44.6	P = 84 W, E >7.6 Wh	⌀18.3 x 65.3	8.00
Storage	Gas Tank	I.E. Type IV 300 Bar	1	1010	1.5 L Vol. 450 std.L. ~39.6 g H_2	⌀116 x 238	n/a
FTS Power	Li-Ion-Battery	EagleTac 750mAh	2	19.7	P <6 W, E >2.5 Wh	⌀14.3 x 51.2	4.50

3.3. System Solution & Analysis

After implementing the tool in the process of the design iterations, a solution has emerged at the end of the process. This solution is based on the mission profile that can be found in table 3.5. In this section the components will be listed and the performance of the system during the mission will be discussed.

The solution given consists of fuel cell manufactured by Intelligent Energy with a rated power of 650 W and its controller in combination with a type IV 300 bar storage tank capable of storing 1.5 water liters of pressurized hydrogen gas. The auxiliary power source consists of a LiMn-battery bank with two branches in parallel and each branch consisting of 6 cells in series. Furthermore a high current charger is needed in order to be able recharge the batteries during flight. This should be designed in-house in the detailed design. In addition a battery capable of powering the FTS system has been selected. These main components can also be found in table 3.6 and displayed in fig. 3.5.

Analysing the system behaviour during the flight conditions for both the worst case wind conditions (25 kts) and the average wind conditions (7 kts) and ensure that this is a valid solution, shows some remarkable differences. In fig. 3.6, the remaining battery energy and hydrogen stored during both mission conditions are displayed.
The battery energy plot in fig. 3.6a will be analysed first. Both missions show the same first two phases, on the ground and take-off, as expected. Then the energy curves deviate. For the worst wind conditions, the battery will be discharged at a high rate during cruise while for the average wind conditions this is not the case. Due to this, the batteries need to be recharged during the mission time for the worst case scenario, in the loiter phases and on the ground when picking up the medical sample, while for the average case they do not. In fact, with the average wind conditions the battery charge would be enough to fly the mission two times and still have about 25 Wh worth of energy left, assuming hydrogen would be refuelled. The worst case condition ends with almost no energy left in the batteries at the end of one mission.

[21] URL `http://lygte-info.dk/review/batteries2012/Aosibo%20IMR18650%202600mAh%20%28Yellow%29%20UK.html` [cited 26 June 2017]

(a) Fuel Cell, Controller, Tank ©*Intelligent Energy*
CENSORED DUE TO NDA RESTRICTIONS

(b) Selected Battery Cell Aosibo[21]

Figure 3.5: Essential Components of the Main Power System
Figure 3.5a shows the fuel cell, fuel cell controller, and storage tank as seen from bottom left to top right. On the fuel cell front the casing with the circular fan outlet is clearly visible. The fan sucks both cooling as well as reactant air through the fuel cell stack and is controlled by the controller PCB. The effectiveness of this solution has to be investigated and maybe modified for the use in the mission conditions. In the back the storage tank is displayed. Attached to it, in red, is the hydrogen pressure regulator. Two outlets can be seen. The big one is the sensor measuring the tank capacity. This is connected to the controller. The smaller one is the hydrogen outlet that will be connected to the fuel cell inlet.
Figure 3.5b shows two of the selected LiMn battery cells. These have a capacity of 2600mAh and a high discharge rate.

These circumstances cause the used hydrogen consumption to differ as well for both conditions. This is illustrated in fig. 3.6b. The additional energy necessary to recharge the batteries during the worst wind conditions has to be generated from the hydrogen stored in the tank. As the hydrogen consumption during the worst case features a constant slope, this implies that the fuel runs at a constant maximum set point which is true and can be seen in fig. 3.7. The consumption during average conditions varies with the fuel cell set point. However, at the end of both missions there is still hydrogen left in the tanks.

From the analysis of the remaining energy and energy consumption within the system, the next step is to illustrate the power consumption during the mission. This is done in fig. 3.7 using the worst case wind conditions. Noticeable is that the fuel cell runs at 100% set point after its start up on the ground until the end of the mission. Furthermore, the graph should be examined closely. The fuel cell power still has to be transformed by the power electronics and thus 10% of that are lost. Furthermore, one might think that the total power is simply the sum of fuel cell power and battery power, after taking the efficiency of the DC/DC converter into account. This is however not always the case, since the total power also accounts for the power needed to recharge the batteries. Therefore, it is only the case when the batteries are being discharged. When the the batteries are being charged, the fuel cell power after the DC/DC converter and total power required are effectively the same and the power needed to maintain the flight condition could be determined by adding the now negative battery power to the total power required.

Concluding, a valid solution for the power system has been found, capable of flying the MEUC in the worst possible wind conditions. For an application with no landing and take-off in between and ideal conditions with no wind the following performance characteristics can be reached:

- **Max. Endurance:** > 1.5 h at 19.61 m/s
- **Max. Range:** > 145 km at 27.7 m/s
- **Continuous Hovering:** > 40 min
- **Maximum Speed:** > 55.7 m/s (200 km/h) at 1154 W

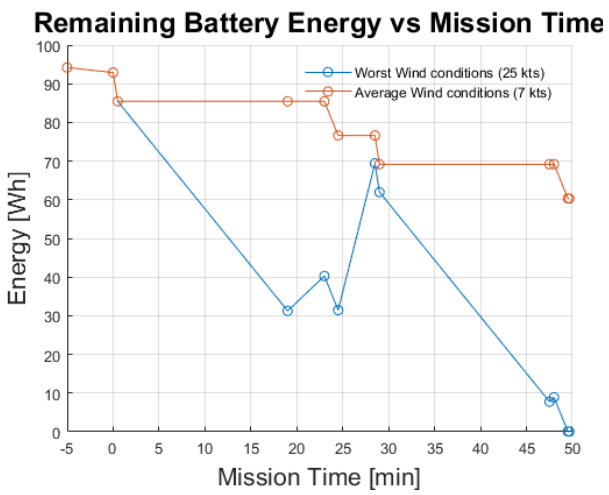

(a) Remaining energy contained in the battery.

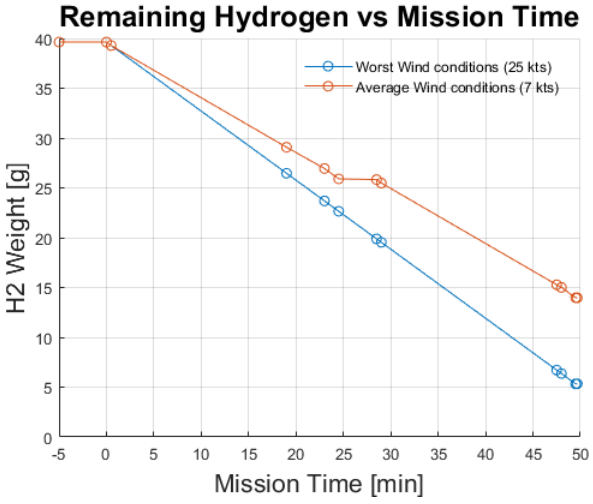

(b) Remaining hydrogen mass contained in the tank.

Figure 3.6: The energy remaining in the system over the mission displayed by means of remaining energy in the battery and the remaining hydrogen in the tank for the worst and average wind conditions. It can be seen that both batteries and tank are oversized for the average conditions, but are needed for the worst wind conditions. The batteries even have to be recharged during low power phases for the worst wind conditions causing the fuel cell to constantly run at maximum power.

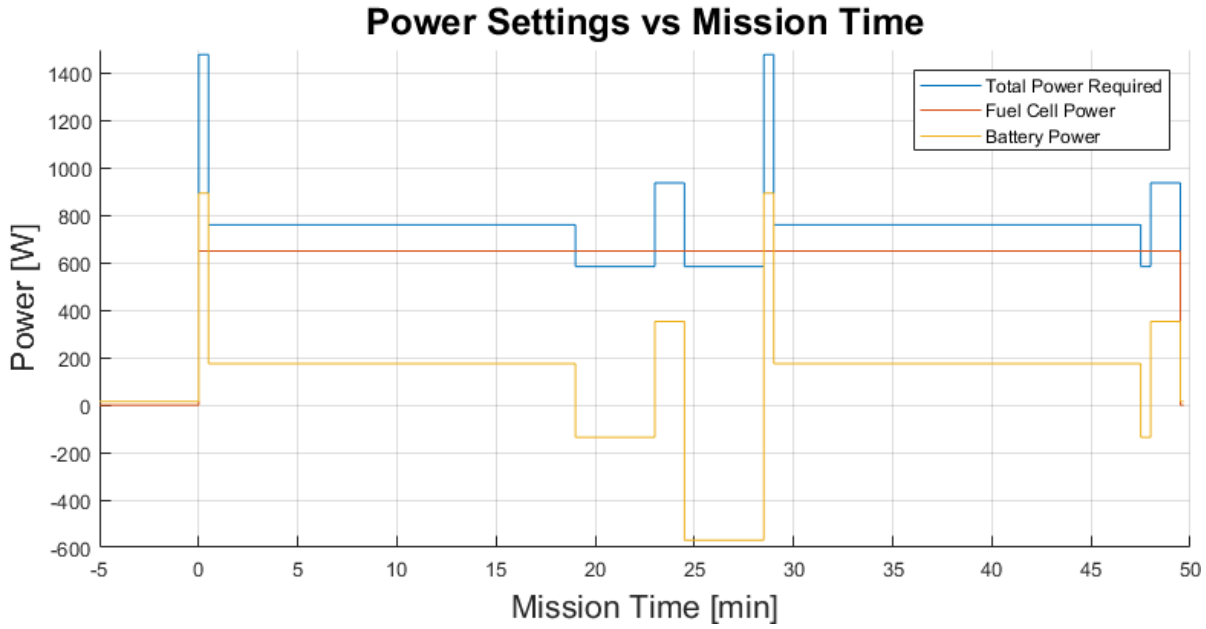

Figure 3.7: Power setting of the flight during worst case wind conditions

As the required cruise power is higher than the power the fuel cell can deliver, the only phases when the battery can be recharged are low power loiter phases during target acquisition and on the ground. Due to the limited time, the fuel cell will run at 100% set point from the moment of take-off at the base until touchdown at the same location. A negative battery power indicates the power with which the battery will be recharged. Note: The fuel cell power still has to be transformed by the DC/DC converter and has thus to be multiplied by the efficiency of 90%.

3.4. Verification & Validation

In this section, the verification and validation strategy for the power system and its main individual components and the sizing tool that was created will be discussed.

As the power system is assembled mostly out of products available on the market there is no verification or validation of the specifications given by the manufacturers possible without buying the product and testing it. This is especially true for the fuel cell as the manufacturer is hesitant to release detailed specifications beyond the basic dimensions and power rating. Thus validating tests regarding the efficiency and actual power performance have to be conducted. For batteries however, some manufacturers claim properties that do not hold up against a sanity check. For example, a discharge rating of 150C while featuring at the same time a wire no thicker than 1 mm. As this would clearly not work or in the worst case start a fire, it was thus decided to only allow batteries to the design that can be verified by results of discharge tests already conducted. The results for the selected batteries can be found in fig. 3.8. As can be seen batteries vary in their capacity and energy content depending on the discharge rate. This was taken into account during the design and is thus considered to be validated.

As the program is self-developed and based on databases of existing components only and not on a mathematical or physical model, there is no verification method available. This also becomes clear, when examining fig. 3.9. It is apparent that the output, the power system mass, does not follow any relation that could be verified but jumps in discrete steps when different design options or components are selected, as expected. It can thus not be guaranteed that the output is always the most optimal solution. Instead verification is done by checking if the given output is a valid solution. That is, if the system selected by the tool is actually capable of fulfilling the mission. This check has been conducted and outlined in the previous section.

3.5. Conclusion & Recommendations

In this chapter the design of the power system has been explained. A suitable power system has been found both for the main power system as well as the FTS power system. The proper function of the design tool and the battery performance have been verified.

However, there is still room to improve the design further. The parameters that have been assumed should be validated in tests. Especially, the fuel cell should be tested thoroughly. As there is no information provided by the manufacturer about the behaviour of this piece of equipment at different power set points, the average cell voltage and with it the average efficiency had to assumed. These test can be used to further refine the design. This would allow the safety margin, which is in this stage 20% and an additional 10% on efficiency, to further be reduced and could lead to weight savings of 100g or more for the same power requirements, see section 10.3. This alone could lead to a snowball effect saving more weight and power. After a detailed design with aerodynamic refinements, it is estimated that it should be possible for the fuel cell system to reach a weight of around 2100 g.

Furthermore, the biggest problems that arise during the design of a fuel cell stack concern the cooling and the water management inside the cell. According to the manufacturer there is no test data available, therefore these cases have to investigated during tests after purchase of the fuel cell.
Concerning the cooling, the stack temperature is controlled with a feedback loop keeping the stack between 15 and 50°C using only the cooling fan speed. It has to be ensured that this range can be achieved for both low and high expected temperatures as well as during hovering and fast forward flight.
The membrane of the fuel cell should neither be too dry on both anode and cathode side nor to humid, or flooded. This is called water management. A flooding in the fuel cell lowers the reaction rate and thus the power output. A dry and thus overheating fuel cell stack can cause the membranes to crack and thus causing permanent damage to the fuel cell. Again experiments have to conducted in both cold and hot conditions, low and high relative humidity, at low and high airspeeds.
It addition it may be necessary to carry out a catalyst cleaning cycle which involves shutting off the air supply for a few seconds after a certain interval. This could be done on the ground before taking off or during flight in low power phases where the batteries can provide sufficient power. The exact interval after which this is necessary, needs to be tested as well for a refined design.

Moreover, there has to be a suitable refuelling option. First, it should be decided how hydrogen refuelling is principally done. There are two suitable options: Standard refuelling using a receptacle or implementing a

[22] URL `https://goo.gl/E8jREh` [cited 26 June 2017]

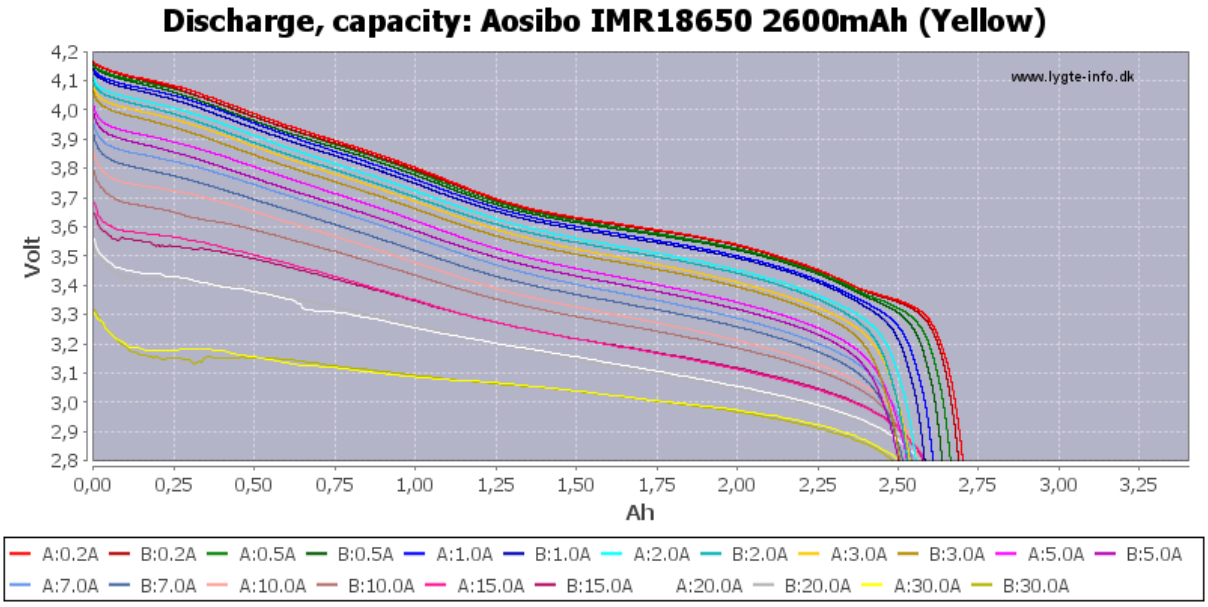

(a) Variation of capacity of the selected battery cells depending on the discharge rate

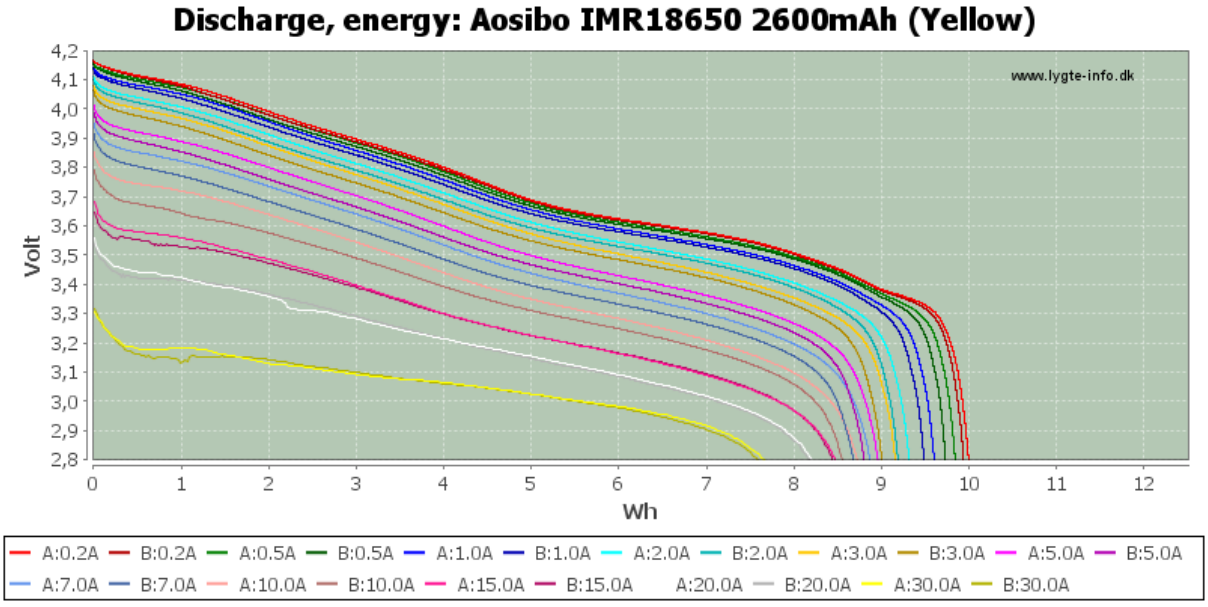

(b) Variation of energy content of the selected battery cells depending on the discharge rate

Figure 3.8: Validation of battery performance by evaluating existing discharge curves for the selected battery cell. As can be observed battery properties can vary with the discharge current and thus power drawn from them. This has to be accounted for in the design.[22]

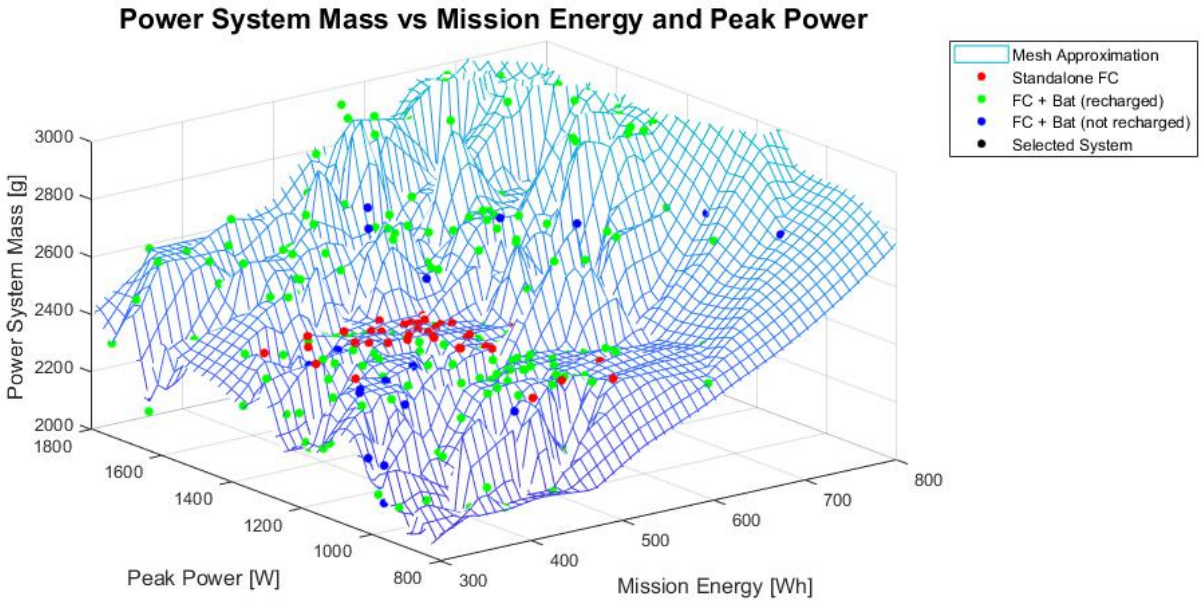

Figure 3.9: A surface plot illustrating the output of the power design tool depending on the total energy required during the mission and the peak power required, also showing the selected design option. This plot contains 500 data points that are generated on random inputs and approximated by a mesh. As can be seen the output follows no fixed relation but jumps in discrete steps. This causes the mesh to be inaccurate as half of the points lie beneath it, including the selected solution. However this, together with the check that the picked solution is in fact a valid solution capable of fulfilling the mission, is seen as verification that the solution found is at least close to the optimal, if not the optimal.

swapping option of the tank for a second. The later allows the refuelling of the empty tank while the second one enables the UAV to already fly another mission. In this case the battery pack has to be swapped as well if missions are being flown in bad weather conditions.
Next, there are three principal options on how to transfer hydrogen into the tanks. The first two base on the same principle of using standard industrial gas cylinders to refuel. One using a sufficiently large gas cylinder directly connected with fittings to the refuelled tank ensuring by the size of the industrial cylinder that the pressure drop is minimised and thus still a high state of charge of the tank can be achieved. The other option is using a compressor to boost the pressure to the pressure needed in the tank. This is the more expensive version but also the more professional one, a 100% SoC can always be achieved. It also allows the cylinders to be of a lower nominal pressure than the tank, reducing the cost for these. The third option is a large storage tank of higher pressure that allows several fuelling cycles, for example, using a 700 bar tank whose pressure is regulated to the 300 bar of the UAV tank by a pressure regulator. A disadvantage is that only about 57% of the capacity of this storage tank is usable as it does not feature a boost function. This tank can be taken to a regular hydrogen gas station to be filled when needed.

In the case of an application as specified by the Royal Netherlands Navy, there are several more recommendations to make.
First, the resistance to salt water splashes of the PEM has to be investigated, and in case this turns to be fatal for it, design considerations to avoid water entry into the fuel cell have to be found. Secondly, as the mission intended by the Navy is an endurance mission and not a range mission like the MEUC, there will be a major redesign. As the airspeeds are lower, there should be an aerodynamic redesign. However, in the case that is not happening, there are still options to consider. As the mission of the Navy is generally of lower power, beside take-off and landing, the storage and auxiliary power combination can be reconsidered. As the batteries would not be used during cruise, they can be significantly reduced and the weight saving be used to implement a bigger tank. Another option would be to swap the high power batteries for batteries of the same weight with a high capacity. This could then be used to continuously contribute power while letting the fuel cell run at the optimal efficiency point except during peak power phases and extending the flight time this way. This would be the cheapest version on short and mid-term prospective. Only for long-time use would swapping the tank maybe become cheaper. All in all, fuel cells seem to be the ideal power source for long endurance missions if the question of salt water effects on the PEM can be solved.

4

Aerodynamic design

Before the wing planform can be optimised, the wing configuration has to be known. This configuration is determinant for the UAV's aerodynamic characteristics. In this chapter, configurations are analysed and a final configuration is chosen. The overview of the configuration that are considered and the performance analysis methodology is given in section 4.1. As the calculations are highly dependent on drag and the calculation of it is not straightforward, the drag is thoroughly elaborated on in section 4.2. Section 4.3 will discuss several geometric input parameters needed for the drag analysis, where-after the actual drag model will be explained in section 4.4. The trade-off is executed and presented in section 4.5. In the end, section 4.6 will provide verification on the created analysis tool.

4.1. Overview

4.1.1. Configurations

Three wing configurations are assessed for performance within compliance of the mission requirements:

- **Single wing**:
  The single wing (or monoplane) configuration is a fixed-wing configuration where a single wing is mounted midway up the fuselage. A schematic of the single wing configuration is presented in fig. 4.1:

Figure 4.1: Schematic of single wing configuration

  This configuration theoretically has the highest efficiency and lowest drag of any wing configuration, mainly due to its minimisation of interference drag. However, the requirements MEUC-NAVY-10 and MEUC-Sys-TUD-01-02, require that the UAV must stay upright when subjected to the maximum wind force. Therefore double winglets are attached to offer the necessary contact points.

- **Double wing**:
  The double wing, biplane or boxed wing configuration is a fixed wing configuration where two main wings are stacked in an unstaggered fashion. The top and bottom wing are mounted to the fuselage. The wingtips of both main wings are connected to form a closed box wing. A schematic of the double wing configuration is presented in fig. 4.2:

Figure 4.2: Schematic of double wing configuration

Biplanes, in general, permit lighter wing structures, lower wing loading and a smaller span for a specific wing surface area. Consequently, due to the reduced roll inertia and roll damping, biplanes offer an improved manoeuvrability. In addition, closed wings achieve minimal induced drag by potentially eliminating wing-tip vortices and their accompanying drag component. However, interference drag is an issue, limiting the configuration's performance. The pure-boxed-wing standing stability contact points are defined by the wing spacing, which is equivalent to the fuselage height. If this distance found not to be sufficient in order to fulfil standing stability, wingtips are added, as with the single wing.

- **X-wing**:
  The X-wing configuration is, a non-closed double wing configuration, with both main wings under an equal and opposite dihedral angle. The single wing configuration is as presented in fig. 4.3:

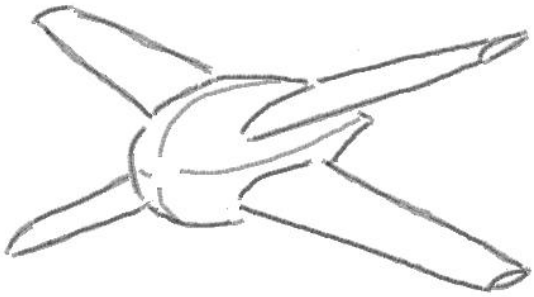

Figure 4.3: Schematic of X-wing configuration

The primary reason for the X-wing's presence in the list of design options is its excellent standing stability. No addition of extra surfaces is required to fulfil the wind-induced requirement. This absence of extra surfaces decreases the total drag, hence increasing performance. The lift generated, however, is subjected to the same dihedral angle as the wings are. Therefore more lift is necessary to counteract a given gravitational force, which increases the lift-induced drag.

4.1.2. Methodology

Two of the most common mission parameters are range and endurance:

- Range, i.e., the maximum amount of distance the UAV can fly with its on-board energy repository. Range is the primary mission objective, and its optimisation induces the optimal design in terms of power system. The flight condition corresponding to maximum range is a maximal lift-over-drag ratio, i.e., $(C_L/C_D)_{\max} = (L/D)_{\max}$.
- Endurance, i.e., the maximum length of time the UAV can spend in cruising flight. Loitering is done at endurance speed and requires minimum flight power available P_a (and equivalently, power required P_r).This is fulfilled for $\sqrt{C_D/C_L^3}$.

The primary mission objective is range, but endurance should be considered for the loiter phase of the mission. A pure optimisation for range would potentially yield a heavy aircraft with large lift and drag values. As lift is required to keep the aircraft airborne, and therefore cannot be considered for optimisation, drag should be minimised to yield both a high lift-over-drag ratio (L/D), while keeping the magnitude low. Minimal drag induces a small and light power system, which allows for a light aircraft.

4.2. Drag Determination

The aerodynamic drag D can be expressed in the non-dimensional drag coefficient C_D, dynamic pressure q_∞, and total wing surface area S, as shown in eq. (4.1). C_D can be expressed as the sum of the zero-lift drag coefficient or parasite drag)$C_{D,0}$, the inviscid lift-induced drag coefficient $C_{D,\mathrm{i}}$ (i.e., vortex drag), and the viscous drag coefficient $C_{D,\mathrm{v}}$ due to lift as shown in eq. (4.2). The analysis of all three drag contributors will be considered separately.

$$D = C_D q_\infty S, \qquad \text{where } q_\infty = \frac{\rho_\infty V_\infty^2}{2} \tag{4.1}$$

$$C_D = C_{D,0} + C_{D,\mathrm{i}} + C_{D,\mathrm{v}} \tag{4.2}$$

4.2.1. Zero-lift drag coefficient

The zero-lift drag coefficient $C_{D,0}$ is the drag coefficient of the UAV when no lift is generated. Zero lift drag, $C_{D,0}$ is composed of the following aerodynamic drag components:

- Skin friction drag resulting from viscous shearing stresses over the wetted surface;
- Pressure drag (or form drag) resulting from the integrated effect of the static pressure acting normal to the wetted area, resolved in the drag direction;
- Interference drag resulting from the proximity of two bodies;
- Profile drag, which is the sum of the skin friction and the pressure drag for a two-dimensional airfoil.

Due to the inherent complexity of aerodynamic simulations, calculating the parasite drag as a summation of the components listed above, is difficult. Hence, $C_{D,0}$ is not defined as the summation of these aerodynamic drag components, but rather as the difference between the total drag coefficient and the induced drag, eq. (4.3).

$$C_{D,0} = C_D - \left(C_{D,\mathrm{i}} + C_{D,\mathrm{v}}\right) \tag{4.3}$$

The "build-up technique" is used to approximate $C_{D,0}$, where it is calculated as a function of the aerodynamic surface shape and Reynolds number Re [32]. It is the summation of the following different components, multiplied by a safety factor:

- **Fuselage**:
  The zero-lift drag coefficient of a fuselage $\left(C_{D,0}\right)_{\text{fus.}}$ is determined from eq. (4.4):

$$\left(C_{D,0}\right)_{\text{fus.}} = C_{\mathrm{f}} f_{L/D} f_M \frac{S_{\text{wet}_{\text{fus.}}}}{S} \tag{4.4}$$

  where:

  - C_{f}: skin friction coefficient based on the Prandtl relationship.

$$\begin{aligned} (C_{\mathrm{f}})_{\text{lami.}} &= \frac{1.327}{\sqrt{Re}} \\ (C_{\mathrm{f}})_{\text{turb.}} &= \frac{0.455}{\left[\log_{10}(Re)\right]^{2.58}} \end{aligned} \tag{4.5}$$

    Laminar flow may be assumed for $Re < 200\,000$, and turbulent flow may be assumed for $Re > 4\,000\,000$[32];
  - $f_{L/D}$: fuselage length-to-diameter ratio, based on the fuselage length L_{fus} and equivalent diameter D_{fus} (not to be confused with drag D)

$$f_{L/D} = 1 + \frac{60}{(L/D)^3} + 0.0025\left(\frac{L}{D}\right) \tag{4.6}$$

  - f_M: Mach number parameter

$$f_M = 1 - 0.08M^{1.45} \tag{4.7}$$

  - $S_{\text{wet}_{\text{fus}}}$: wetted area, i.e., the actual surface area of the material in contact with the air; the area on which pressure and shear stresses are acting.

- **Wing**:
  The aircraft wing is treated as a lifting surface, for which eq. (4.8) holds:

$$\left(C_{D,0}\right)_{\text{wing}} = C_{\mathrm{f}} f_{\text{tc}_{\text{wing}}} \left(\frac{S_{\text{wet}_{\text{wing}}}}{S}\right) \left(\frac{C_{d_{\text{min}_{\text{wing}}}}}{0.004}\right)^{0.4} \tag{4.8}$$

  where:

- f_{tc}: thickness ratio parameter, based on the maximum thickness over chord ratio $(t/c)_{max}$ of the aerofoil;

$$f_{tc} = 1 + 2.7\left(\frac{t}{c}\right)_{max} + 100\left(\frac{t}{c}\right)^4_{max} \tag{4.9}$$

- S_{wet} is the approximation of the lifting wetted surface area by the surface area of a box enclosing the lifting surface;
- $C_{d_{min}}$: minimum drag coefficient of the aerofoil;

- **Wing interference**:
  Wing interference accounts for additional drag caused by the proximity of multiple bodies, i.e., the areas where the wing joins the fuselage and the points where the wing is connected to wingtip devices. This drag can be approximated from known interference-section drag ratios $D_{interf.}/D_{section}$ [17], where the section is the wing. Note that these ratios are known for tailplanes, due to the unconventional nature of the tailless aircraft, these values have been deemed to give an accurate representation.

  - The single wing with winglets is approximated by a tail with winglets;
  - The boxed wing is approximated by two superposed tails with winglets positioned such that the winglets connect to form the box;
  - The X-wing is approximated by two superposed tails under an equal but opposite dihedral angle Γ;

  Following eq. (4.10), table 4.5 shows the results for the interference drag ratio.

$$\frac{(C_{D,0})_{interf.}}{(C_{D,0})_{wing}} = \frac{D_{interf.}}{D_{wing}} \tag{4.10}$$

- **Other Drag**:
  Additional drag is generated by the air-cooling system, due to momentum lost by air passing through the power plant installation, and other systems (such as, e.g., pitot tube, surface roughness, leakage, rivets and bolts, etc.). This drag is approximated by a 10 % fraction of the total $C_{D,0}$ summed over the components[32]. Equation (4.11) shows the calculation of this zero lift drag contribution, where $C_{D,0}$ is the summed aircraft zero-lift drag coefficient.

$$(C_{D,0})_{rest} = 0.1\,(C_{D,0})_{sum} \tag{4.11}$$

It can be concluded that the summed zero-lift drag coefficient $(C_{D,0})_{sum}$ is equal to eq. (4.12):

$$(C_{D,0})_{sum} = (C_{D,0})_{fus} + n_{wing}(C_{D,0})_{wing} + n_{vt}(C_{D,0})_{vert} + (C_{D,0})_{interf.} + (C_{D,0})_{rest} \tag{4.12}$$

The safety factor K_c that accounts for the other items that produce drag (e.g., external sensors and antennas, landing rods, a non-streamlined fuselage), as in eq. (4.13), where $K_c = 1.2$[32].

$$C_{D,0} = K_c\,(C_{D,0})_{sum} \tag{4.13}$$

4.2.2. Lift-induced drag

The inviscid lift-induced drag coefficient $C_{D,i}$ is determined from eq. (4.14), a function of lift coefficient C_L, aspect ratio A, and the Oswald efficiency factor e. C_L and e will be discussed below:

$$C_{D,i} = \frac{C_L^2}{\pi A e_{np.}} \tag{4.14}$$

- **Lift coefficient**:
  $C_{D,i}$'s lift-induced nature is reflected in the dependency on C_L, where $C_{D,i} \propto C_L^2$. When the aircraft is in equilibrium, the generated lift L is equal in magnitude and opposite in direction to the aircraft weight W, i.e., $\mathbf{L} = -\mathbf{W} = -m\mathbf{g_0}$ and $L = mg_0 = C_L q_\infty S\cos(\Gamma)\cos^2(\Lambda)$, where Γ and Λ are the wing dihedral and sweep angles, respectively. Accordingly, the aircraft lift coefficient C_L is determined from eq. (4.15):

$$C_L = \frac{mg_0}{q_\infty S\cos(\Gamma)\cos^2(\Lambda)} \tag{4.15}$$

- **Oswald efficiency factor**:
  As the to-be-analysed configurations sport non-planar wing lay-outs, a correction factor $K_{\text{np.}}$ is applied to the familiar planar factor e, resulting in a non-planar factor $e_{\text{np.}}$. The application of $K_{np.}$ follows eq. (4.16)[26]:

$$e_{\text{np.}} = \left(1 + \frac{2}{K_{\text{np.}}} \frac{h}{b}\right)^2 e \tag{4.16}$$

  Herein, h/b is the height-over-span ratio of the non-planar configuration. $K_{\text{np.}}$ and e are discussed below:

  - The correction factor $K_{\text{np.}}$ is derived from the vortex lattice method, where an optimal wing loading (i.e., optimally twisted) is assumed. The configurational factors are listed in table 4.6.
  - The planar Oswald efficiency factor e is estimated from Schaufele's diagram [26] (see fig. 4.4), where the relation of e to a wing's aspect ratio A and $C_{D,0}$ is displayed.
    It is important to keep in mind that the estimations based on Schaufele's diagram have a 12 % error margin, and only accounts for aspect ratio in terms of wing parameters. On the diagram one can see that all the curves have the same vertical intercept, and there is a linear correlation between $C_{D,0}$ and the slope of the curves.

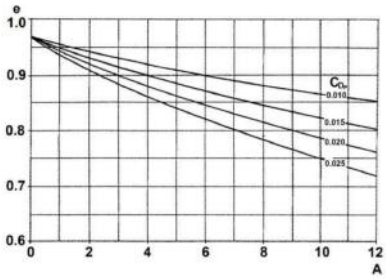

Figure 4.4: Oswald efficiency factor as a function of CD0 and aspect ratio

  From the diagram, a linear correlation between $C_{D,0}$ and $\frac{\mathrm{d}A}{\mathrm{d}e}$ is observed, as shown in eq. (4.17):

$$e = 0.97 - (0.712 C_{D,0} + 0.0028) A \tag{4.17}$$

  This correlation is assumed to be valid for $C_{D,0}$ beyond those shown in the diagram.
  The values for e lead to a 12 % error margin. However, this was deemed reasonable.

4.2.3. Viscous drag

The viscous drag due to lift is the drag due to the integrated effect of the static pressure acting normal to the wetted surface, resolved in the drag direction [37]. The viscous drag calculation for both aerofoil and wing is as displayed in eq. (4.18). It varies with the lift coefficient and some constants.

$$C_{D,\text{v}} = k\left(C_L - C_{l,0}\right)^2 \tag{4.18}$$

Accordingly, the values of k and $C_{l,0}$ are found by fitting a quadratic polynomial of the form $C_d = C_{d,0} + k\left(C_l - C_{l,0}\right)^2 = (k)\, C_l^2 + \left(-2kC_{l,0}\right) C_l + \left(C_{d,0} + C_{l,0}^2\right)$ to the $(C_d - C_l)$-plot of a specific aerofoil. Note that these values are valid only for a specific Reynolds number. This method is only valid for application on aerofoil data corresponding to the linear segment of the $C_l - \alpha$-plot.

4.3. Geometry

The drag analysis requires a significant number of geometric parameters. The optimisation is conducted over a subset of key parameters; the other parameters will be assumed. In this section, an elaboration on these parameters is presented.

4.3.1. Fuselage

The fuselage is modelled as the assembly of three basic shapes: half a sphere and a cone connected by a cylinder of radius equal to the sphere, as shown in fig. 4.5:
An optional eccentricity, defined as the fuselage width over height ratio, i.e. $e_{\text{fus.}} = w_{\text{fus.}}/h_{\text{fus.}}$, can be applied if required. The dimensions and weight are determined as follows:

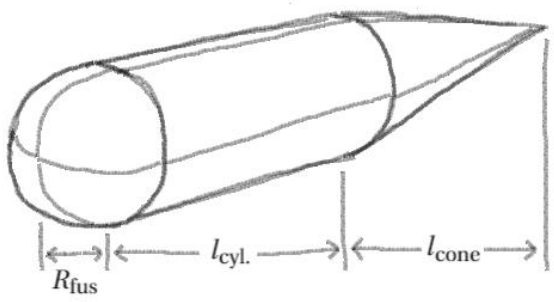

Figure 4.5: Approximation of the fuselage

- Due to the utilisation of these basic shapes, the wetted surface area $S_{\text{fus.}}$ and volume $V_{\text{fus.}}$ is easily calculated using eq. (4.19):

$$\begin{aligned} S_{\text{fus.}} &= e_{\text{fus.}} \pi R_{\text{fus.}} \left(2R_{\text{fus}} + 2l_{\text{cyl.}} + \sqrt{l_{\text{cone}}^2 + R_{\text{fus.}}^2} \right) \\ V_{\text{fus.}} &= e_{\text{fus.}} \pi R_{\text{fus.}}^2 \left(\frac{2}{3} R_{\text{fus.}} + l_{\text{cyl.}} + \frac{1}{3} l_{\text{cone}} \right) \end{aligned} \tag{4.19}$$

- The weight of the empty fuselage consists of only the skin weight. Hence, $W_{\text{fus.}}$ follows directly, as per eq. (4.20):

$$W_{\text{fus.}} = S_{\text{fus.}} t_{\text{skin}} \rho_{\text{skin}} \tag{4.20}$$

4.3.2. Wing

The wing is assumed to be trapezoidally shaped. These tapered wings are structurally strong, easy to build, and stimulate an elliptical spanwise lift distribution, as per Prandtl's lifting-line theory.
A trapezoidal wing is fully defined by the surface area S, aspect ratio A, taper ratio λ, and sweep angle Λ. From this, the other wing planform parameters can be deduced, following eq. (4.21):

$$\begin{aligned} b &= \sqrt{SA} & \bar{c} &= \frac{2}{3} \frac{1+\lambda+\lambda^2}{1+\lambda} c_{\text{r}} \\ c_{\text{r}} &= \frac{2b}{A(1+\lambda)} & \bar{y} &= \frac{b}{6} \frac{1+2\lambda}{1+\lambda} \end{aligned} \tag{4.21}$$

Note that the sweep angle Λ is not present in eq. (4.21). Hence, Λ is considered a secondary planform parameters, and will not be used as an optimisation parameter. The determination of the wing dimensions follows directly from the planform and the aerofoil, but the weight also accounts for the spar, which carries the handling and operational loads.

- The wetted surface area of the wing S_{wing} and the volume V_{wing} are determined from eq. (4.22):

$$S_{\text{wing}} = \frac{S_{\text{af.}}}{c} S \qquad V_{\text{wing}} = \frac{c_{\text{af.}}}{c} S \tag{4.22}$$

- The wing is not a hollow structure like the fuselage is; it is strengthened by a carbon-fibre spar and filled with foam for vibrational damping. Accordingly, the weight of the wing contains the skin weight $W_{\text{wing,skin}}$, the foam weight $W_{\text{wing,foam}}$, and the spar weight $W_{\text{wing,spar}}$. That is,

$$\begin{aligned} W_{\text{wing}} &= W_{\text{wing,skin}} + W_{\text{wing,skin}} + W_{\text{wing,skin}} \\ &= S_{\text{wing}} t_{\text{skin}} \rho_{\text{skin}} + V_{\text{wing}} \rho_{\text{foam}} + V_{\text{spar}} \rho_{\text{spar}} \end{aligned} \tag{4.23}$$

4.3.3. Configurations

Now that the drag model and the corresponding geometric calculations are explained, the configurational setup is presented. Note that if angular planform parameters (i.e., Λ and Γ) are not explicitly specified, they are set to zero.

- **Single wing**:
  The single wing configuration (fig. 4.1) is approximated by:
  - A single fuselage;

- A single lifting wing with spar;
- Two non-lifting wings at the wingtips of the lifting wing, not strengthened by a spar.

- **Double wing**:
  The double configuration (fig. 4.2) is approximated by:
  - A single fuselage;
  - Two lifting wings with spars;
  - Two non-lifting wings at the wingtips of the lifting wing, not strengthened by a spar.

- **X-wing**:
  The single wing configuration (fig. 4.3) is approximated by:
  - A single fuselage;
  - Two lifting wings with spars, where both wings are subjected to an opposite but equal dihedral angle.

4.4. Drag model

The drag tool is created to calculate the drag with different inputs. A schematic of the data flow within the drag model is displayed in fig. 4.6.

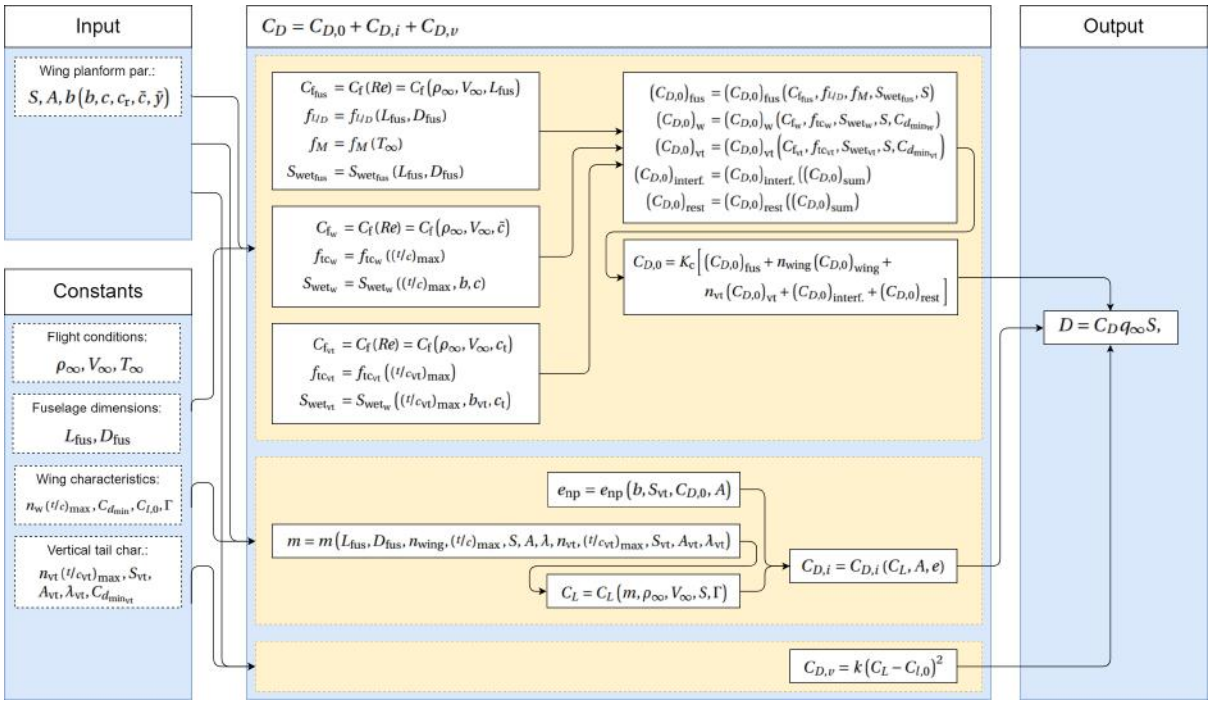

Figure 4.6: Schematic of the aerodynamic tool, indicating the variable and constant inputs; the transformation equations and dependencies; and the output.

Both variable and constant inputs are required to perform the analysis:

- The variable inputs consist of:
  - **Base input**:
    The fuel cell and system mass, i.e., $m_{\text{on-board}} = m_{fc} + m_{sys.}$
  - **Optimisation inputs**:
    The parameters over which the optimisation is performed and are considered the primary wing planform parameters (i.e., wing surface area S, aspect ratio A, and taper ratio λ).
- The definitions of the "constant" inputs follows in the subsequent subsections.

4.4.1. Fuselage

An initial estimate is made for the fuselage dimensions, as displayed in table 4.1. From preliminary computational flow dynamic simulations, it was determined that the flow would be 32 % turbulent and 68 % laminar.

Table 4.1: Fuselage input values

Fuselage	
Radius $R_{\text{fus.}}$	0.128 m
Cylindrical segment length $l_{\text{cyl.}}$	0.0930 m
Conical segment length l_{cone}	0.373 m
Length	0.594 m
Equivalent diameter	0.256 m

4.4.2. Aerofoil

Due to the heavy reliance of both geometric and aerodynamic properties on the aerofoil, it should be selected with care regarding its performance characteristics. The aerofoil selection procedure is comprised of five steps:

1. Trade-off criteria are established, as shown in table 4.2.

   - High weight, (16–20) %: mostly drag related parameters, which influence the overall efficiency of the wing most.
   - Medium weight, 12 %: parameters which mostly include lift and thus weight characteristics. These have lower priority since weight has less effect on the efficiency than drag.
   - Low weight, (4–8) %: parameters related to angle of attack, still important but not the most influential.

2. A suitable planform is assumed to perform the airfoil selection analysis. This planform defines the mean aerodynamic chord $\bar{c}$, and therefore the Reynolds number Re. The planform is assumed as in table 4.3.

Table 4.2: Trade-off criteria weight factors

Trade-off criteria	Preference	Weight
C_l at $\alpha = 0$	High	8 %
$\left\lvert \frac{dC_l}{d\alpha} \right\rvert$ at $\alpha > \alpha_{\text{stall}}$	Low	4 %
α at $C_l = 0$	Low	12 %
$C_{l_{\max}}$	High	12 %
α at $C_{l_{\max}}$	High	4 %
C_D of wing	Low	20 %
$(C_l/C_d)_{\max}$	High	16 %
C_l at $(C_l/C_d)_{\max}$	Low	12 %
$(t/c)_{\max}$	High	12 %

Table 4.3: Planform used for aerofoil selection

Planform	
Surface Area S	1.543 m^2
Aspect ratio A	5.714
Spanwidth b	2.969 m
Taper ratio λ	0.8
Mean aerodynamic chord $\bar{c}$	0.522 m
Reynolds number Re	9.46×10^5

3. Suitable aerofoils are selected. The German website Aerodesign[1] was used as reference to choose suitable candidates for the aerofoil trade-off.
4. The aerofoils are analysed with XFLR5™[34]. This program is based on XFOIL, which has proven to be valid in the design of the MIT Daedalus [2]. XFLR5™requires the following inputs:

   - The aerofoil shape, encoded in an accompanying `.dat`-file;
   - The range of angles of attack α over which the analysis is done. This range should include the angle of attack of zero lift $\alpha_{C_l=0}$ and the stall angle of attack α_{stall}, hence including $\alpha_{C_{l_{\max}}}$. These lower and upper bounds are chosen such that the operational range of the aerofoil is captured and all data required for the trade-off is available.
   - The Reynolds number Re follows directly from the pre-assumed planform, i.e., table 4.3.
   - The mach number M is set to zero, as compressibility effects are assumed negligible on account of the low airspeeds.

5. The program is run for all the aerofoils to produce $(C_l - C_d)$, $(C_l - \alpha)$, and $(C_l/C_d - \alpha)$-graphs. This data is then used to perform the trade-off.

Since numerical values were used, the aerofoils were ranked based on performance for each of the criteria. Every aerofoil is given a number from 1–7 (found in brackets behind the data in table 4.4). This rank, indicating performance, will then be multiplied by the weight of the criteria column, and then divided by 7 to yield a

[1] URL `https://www.aerodesign.de/english/profile/profile_s.htm` [cited 22 June 2017]
[2] URL `http://web.mit.edu/aeroastro/news/magazine/aeroastro-no3/2006drela.html` [cited 15 May 2017]

maximum score of 100 %. The aerofoil with the highest sum will then be selected for the design; highlighted in green in table 4.4.

Table 4.4: Aerofoil trade-off

Trade-off criteria	MH60	MH61	MH62	MH64	MH45	HS 3.0/8.0B	HS520
C_l at $\alpha = 0$ [-]	0.07852 (3)	0.02227 (1)	0.0826 (4.5)	0.08563 (6)	0.0717 (2)	0.172 (7)	0.0826 (4.5)
$\left\|\frac{dC_l}{d\alpha}\right\|$ at $\alpha > \alpha_{stall}$ [-]	low (7)	high (0)	low (7)	high (0)	low (7)	high (0)	low (7)
α at $C_l = 0$ [°]	-0.74 (3)	-0.215 (1)	-0.78 (4)	-0.81 (5)	-0.669 (2)	-1.642 (7)	-0.892 (6)
$C_{l_{max}}$ [-]	1.346 (6)	0.965 (1)	1.18 (4)	1.015 (2)	1.32 (5)	1.13 (3)	1.39 (7)
α at $C_{l_{max}}$ [°]	14 (7)	8.5 (1)	11 (4)	9 (2)	13 (5)	9.7 (3)	13.8 (6)
C_D of wing [-]	0.010158 (4)	0.010385 (3)	0.010011 (6)	0.009774 (7)	0.010096 (5)	0.011167 (1)	0.010682 (2)
$(C_l/C_d)_{max}$ [-]	97.5 (5)	94.5 (3)	94 (2)	88 (1)	94.6 (4)	109 (7)	99.3 (6)
C_l at $(C_l/C_d)_{max}$ [-]	0.795 (2)	0.58 (7)	0.729 (5)	0.59 (6)	0.78 (4)	0.83 (1)	0.785 (3)
$(t/c)_{max}$ [%]	10.08 (6)	10.26 (7)	9.3 (4)	8.59 (2)	9.85 (5)	8 (1)	8.84 (3)
Sum	63.4 %	44.6 %	62.3 %	56.0 %	60.0 %	49.1 %	64.6 %

Finally, HS520 came out as the best performer as the aerofoil for the design. Its shape is depicted in fig. 4.7.

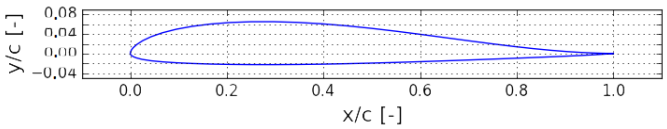

Figure 4.7: HS520 - Aerofoil shape

The HS520 aerofoil is specifically designed for swept tailless aircraft having low aspect ratio and/or low sweep angle. It has a small reflex at the tail which is common for a flying wing design. The HS-family of aerofoils is a popular choice for swept wings that should operate at relative low Reynolds numbers ($Re < 500\,000$) due to the low drag that these aerofoils generate[1]. The above criteria suit the design in general and justify the selection of this aerofoil. Note that in the design process the thickness of the required spar will be taken into account for the sizing of the airfoil in order to make it structurally feasible. This only affects the dimensions and thus the C_L rather than the airfoil characteristics. The stall lift coefficient $C_{L_{max}}$ is determined from the product of the two-dimensional maximum lift coefficient C_l and a transformation factor, as in eq. (4.24).

$$C_{L_{max}} = \frac{C_{l_{max}}}{1 + \frac{C_{l_{max}}}{\pi Ae}} \tag{4.24}$$

4.4.3. Structure & Materials

The materials used for the wing structure are carbon-fibre for the wing spar, S Glass-fibre composite was chosen for the wing skin and the internal structure will be filled with a PE-LD foam. The justification for the choice of these specific materials together with their properties are explained in section 7.2. As justified in section 7.3, the thickness of the wing skin is set to the 1 mm minimum manufacturable thickness for S Glass-fibre composite material. The spar was designed as a box to have similar area moment of inertia along both of its principal axes. The critical loading case was considered to be the handling one where forces up to 270 N can be exerted on the tip of the spar. The geometrical dimensions and location of the spar that should withstand that critical loading case is given in section 7.3.

4.4.4. Winglets

The size of the winglets is determined by the UAV's fulfilment of the standing stability. That is, the winglets are sized such a that standing stability is guaranteed. Herein, standing stability is defined as equilibrium when subjected to maximum wind force. The root chord of the winglet $(c_r)_w$ is defined by the tip chord c_t of the wing, i.e., $(c_r)_w = c_t$. Furthermore, the winglet taper ratio λ_w is assumed to be 0.2, as this minimises the surface area (and therefore the parasite drag generated), while still offering the necessary contact points. A schematic of the UAV under maximum wind load is displayed in fig. 4.8:

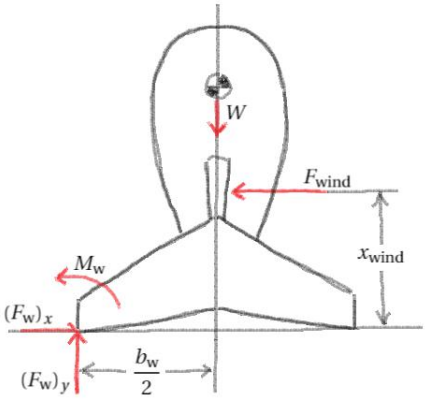

Figure 4.8: Standing stability free-body diagram

The accompanying equilibrium equation is displayed in eq. (4.25):

$$\begin{aligned} F_x = 0 &: (F_w)_x - F_{wind} = 0 \\ F_y = 0 &: (F_w)_y - W = 0 \\ M_w = 0 &: x_{wind} F_{wind} - W \frac{b_w}{2} = 0 \end{aligned} \tag{4.25}$$

where:

$$\begin{aligned} F_{wind} &= C_{D_{wind}} q_{wind} S \\ W &= m g_0 = (m_{basic} + m_w) g_0 \\ m_w &= n_w S_w m_{spec.} = n_w S_w \left(c_{af.} \rho_{skin} + S_{af.} \rho_{foam}\right) \\ S_w &= b_w \left(c_{avg.}\right)_w = b_w \frac{1+\lambda_w}{2} (c_r)_w = b_w \frac{1+\lambda}{2} \lambda c_r \end{aligned} \tag{4.26}$$

The location of the centre of wind on the body x-axis, x_{wind}, is assumed to be equal to the mean aerodynamic chord $\bar{c}$. Furthermore, $C_{D_{wind}}$ is assumed to be equal to 1.3[3].
Rewriting to known values and simplifying yields the polynomial in eq. (4.27):

$$\left(n_w \frac{1+\lambda_w}{2} c_t m_{spec.}\right) b_w^2 + \left(m_{basic}\right) b_w + \left(-2 x_{wind} \frac{F_{wind}}{g_0}\right) = 0 \tag{4.27}$$

Solving eq. (4.27) yield the winglet span b_w for which the UAV fully satisfies standing stability.

4.4.5. Configurations

Definitions of inputs specific to the three configurations are listed below:

- **Zero-lift drag coefficient**:
  - The configurational wing-interference drag ratios $D_{interf.}/D_{section}$, derived from eq. (4.10), are as in table 4.5:

Table 4.5: Total interference drag

Configuration	$(C_{D,0})_{interf.}/(C_{D,0})_w$
Single wing	0.04
Boxed wing	0.08
X-wing	0.06

- **Lift-induced drag**:
  - The correction factor $K_{np.}$, derived from the vortex lattice method, are as in table 4.6:
- **Geometry**:
  - Planform parameters not defined by the three optimisation parameters (i.e., wing surface area S, aspect ratio A, and taper ratio λ) are listed in table 4.7:

[3] URL `https://www.grc.nasa.gov/www/k-12/airplane/shaped.html` [cited 04 Jule 2017]

Table 4.6: Induced drag correction factor [22]

Configuration	K_{np}
Single wing	2.13
Double wing	1.92
X-wing	2.61

Table 4.7: Planform parameters (not determined by optimisation) [22]

Configuration	Γ	Λ
Single wing	0.0°	30°
Double wing	0.0°	30°
X-wing	20°	30°

– For the X-wing, standing stability is satisfied on account of the dihedral angle Γ applied to both wings. Therefore, no winglets are present on this configuration.

4.4.6. Constraints

- Requirement MEUC-TUD-11 stipulates a maximum spanwidth of the UAV. However, requirement MEUC-TUD-14 has a larger impact on the maximal spanwidth of the UAV, as structural integrity should be taken into account for determination of disassembly locations. Hence, a maximum spanwidth of 3.0 m is set for optimisation.
- The root chord of the planform is constrained to be 22 cm at minimum. This constraint results from the maximum t/c of the aerofoil HS520 which is 8.82 %. For a 22 cm root chord, the thickness would be 1.94 cm. This is the minimum thickness the spar should have at the root to provide structural integrity as explained in section 7.3.

4.5. Configuration trade-off

The configurational trade-off is performed based on the trade-off criteria presented in table 4.8.

Table 4.8: Trade-off criteria weight factors

Trade-off criteria	Preference	Weight
Feasibility	High	25 %
Drag D	Low	25 %
Lift-over-drag ratio L/D	High	20 %
Wind force F_{wind}	Low	20 %
Mass m	Low	10 %

Since the winglets are sized such that standing stability is fulfilled, which is different for each configuration, and, consequently, a basis for comparison. This winglet sizing has a direct correlation with the first criterion, i.e., feasibility. It was found that the single wing would require winglets of 0.8068 m. These dimensions are of significant size relative to usual winglet size and this configuration is therefore deemed impractical and rated unfeasible. The next criteria (i.e., drag D, lift-over-drag ratio L/D, wind force F_{wind}, and mass m) are ordered according to significance. Herein, wind force is the force that the UAV has to be able to react to whilst in hover. Every configuration ranked according to their performance relative to the criteria and given a number from 1–3 (found in brackets behind the data in table 4.9). This performance indicating rank is multiplied by the weight of the criteria column, and then divided by 3 to yield a maximum score of 100 %. The aerofoil with the highest sum will then be selected for the design; highlighted in green in table 4.9.

Criteria	Single wing	Double wing	X-wing
Feasibility [-]	Low (1)	High (2.5)	High (2.5)
Drag D [N]	7.981 (3)	8.922 (1)	8.403 (2)
Lift-over-drag ratio L/D [-]	11.37 (3)	8.937 (1)	9.866 (2)
Wind force F_{wind} [N]	80.01 (1)	42.35 (2.5)	45.55 (2.5)
Mass m [kg]	9.254 (1)	8.131 (2.5)	8.454 (2.5)
Sum	60.00 %	63.33 %	76.67 %

Table 4.9: Aerodynamic configuration trade-off table

The complete set of data from which the trade-off performance is extracted is found in table 4.10. Furthermore, the $(D-V)$-plots, indicating the variation of the drag with velocity, for all three configurations are displayed in figures 4.9, 4.10, and 4.11.

Table 4.10: Comparison of the optimised planform parameters and aerodynamic characteristics for each of the three configurations.

Configuration	Single wing	Double wing	X-wing
Planform			
Surface area S	0.5484 m^2	0.5806 m^2	0.6645 m^2
Aspect ratio A	3.484	3.677	4.232
Taper ratio λ	0.8	0.8	0.8
Spanwidth b	1.382 m	1.461 m	1.576 m
Mean aero. chord $\bar{c}$	0.3984 m	0.1995 m	0.1989 m
Wind force F_{wind}	80.01 N	42.35 N	45.55 N
Winglet span b_{w}	0.8068 m	0.3120 m	-
Total mass m	9.254 kg	8.131 kg	8.454 kg
Systems m_{sys}	2.04 kg	2.04 kg	2.04 kg
Velocity V	27.7 m/s	27.7 m/s	27.7 m/s
Lift coef. C_L	0.4870	0.4041	0.3907
Lift-over-drag ratio L/D	11.37	8.937	9.866
Drag D	7.981 N	8.922 N	8.403 N
Drag coef. C_D	0.032 12	0.033 92	0.027 91
Zero-lift drag coef. $C_{D,0}$	0.021 64	0.018 77	0.018 68
Fuselage $(C_{D,0})_{\text{fus.}}$	0.0096	0.0091	0.0079
Wing $(C_{D,0})_{\text{wing}}$	0.0053	0.0084	0.0084
Vertical surfaces $(C_{D,0})_{\text{vert.}}$	0.0046	0.0014	–
Interference $(C_{D,0})_{\text{interf.}}$	2.1×10^{-5}	6.7×10^{-5}	5.0×10^{-5}
Other $(C_{D,0})_{\text{other}}$	0.0022	0.0022	0.0019
Induced drag coef. $C_{D,\text{i}}$	0.009 980	0.012 18	0.009 173
Planar Oswald factor e	2.17	1.16	1.25
Non-planar Oswald factor $e_{\text{np.}}$	0.906	0.903	0.902
Viscous drag coef. $C_{D,\text{v}}$	3.23×10^{-4}	9.6×10^{-5}	5.9×10^{-5}
Stall velocity	16.33 m/s	15.13 m/s	14.31 m/s
Stall lift coef.	1.051	1.017	1.032
Endurance velocity	19.90 m/s	20.21 m/s	19.61 m/s
Endurance drag	9.168 N	10.3243 N	9.749 N
Range velocity	25.86 m/s	26.56 m/s	26.24 m/s
Range L/D	11.47	8.962	9.950
Range drag	7.910 N	8.897 N	8.3322 N
Maximum velocity	34.2 m/s	34.2 m/s	34.2 m/s
Maximum drag	9.162 N	9.934 N	9.578 N

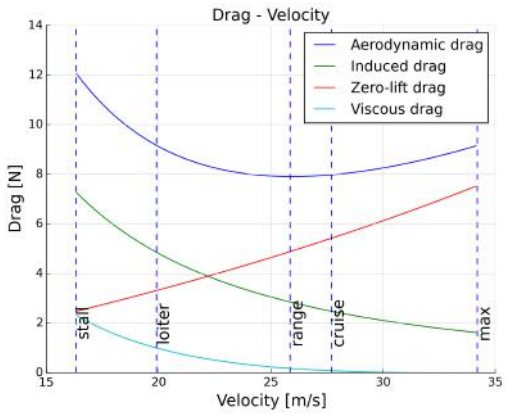

Figure 4.9: Single wing: $(D-V)$-graph

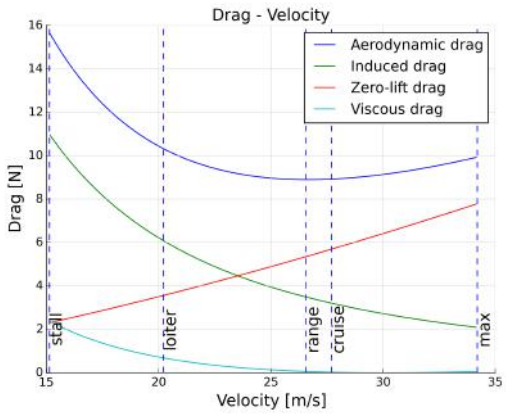

Figure 4.10: Double wing: $(D-V)$-graph

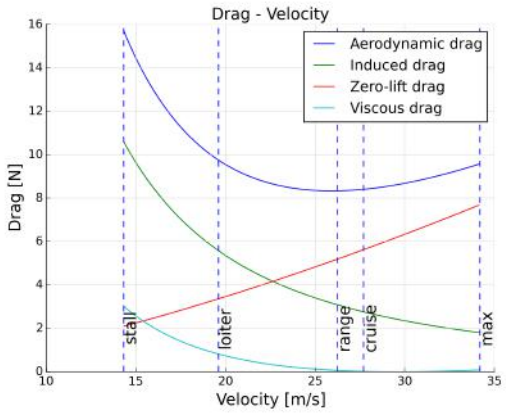

Figure 4.11: X-wing: $(D-V)$-graph

4.6. Verification & Validation

The aerodynamic tool that optimises the planform as described above produces results that have to be verified. This means that one has to check the correctness of the analytic calculation procedures applied within the tool. The tool is dependent on an accurate estimation of the drag of the aerodynamic design. Drag coefficient C_D is estimated using a model (described in section 4.4) which is based upon a build-up technique. It adds up the following components:

- Parasitic drag coefficient $C_{D,0}$ of the several components of the design;
- Lift induced drag $C_{D,i}$;
- Viscous drag $C_{D,v}$.

An approach is needed to verify the analytic formulas for those three different components as implemented within the tool. As was already explained in section 4.4, the formulas are dependent on planform parameters. This means that the verification of the tool shall be performed on a predefined aerodynamic design. This can be different from the optimised final design, but it is chosen like this in order to check the validity of the applied formulas before usage on optimising the design. The design used to perform the verification has the following characteristics:

- A single wing configuration with geometrical parameters as explained in table 4.11;
- Two winglets on the sides, which are modelled as vertical tails with geometrical parameters as explained in table 4.12.

Table 4.11: Wing planfrom parameters of verification model

Wing Planform	
Surface area S	1.543 m^2
Spanwidth b	2.969 m
Aspect Ratio A	5.714
Taper Ratio λ	0.8
Mean aerodynamic chord $\bar{c}$	0.522 m
Aerofoil	MH62
Reynolds number Re	9.46×10^5
Flight altitude h	450 m
Flight velocity V	28 m/s

Table 4.12: Winglet parameters of verification model

Winglet Planform	
Surface area S	0.106 m^2
Spanwidth b	0.23 m
Aspect ratio A	0.498
Taper ratio λ	1.0
Mean aerodynamic chord $\bar{c}$	0.462 m
Aerofoil	NACA0010
Reynolds number Re	8.37×10^5

For the purpose of verification, the above described model was simulated in XFLR5™[34] and can be seen in fig. 4.12. This is a software package which is open source and widely used to simulate aerodynamic performance of planforms build of a certain aerofoil. For its simulations, lifting line theory, vortex lattice methods and 3D-panel methods could be used. The advantages and disadvantages of the different methods can be found in [27]. In general XFLR5™is applicable to wings operating at low Reynolds numbers and that have low to moderate sweep. The verification model is a straight wing that is operating at relative low Reynolds number. This should be suitable for analysing using the software. The results that came out of the tool for the different $C_{D,0}$s are compared to the results of the simulation for verification. However, XFLR5™is not capable of accurately modelling a fuselage body. Therefore, a different approach is used for verifying the fuselage which

is explained more into detail below. The induced and viscous drag coefficients are verified by comparing the outcome of the tool for the drag coefficient C_D at the design lift coefficient with the value read from the drag polar graph simulated through XFLR5 ™for the same lift coefficient.

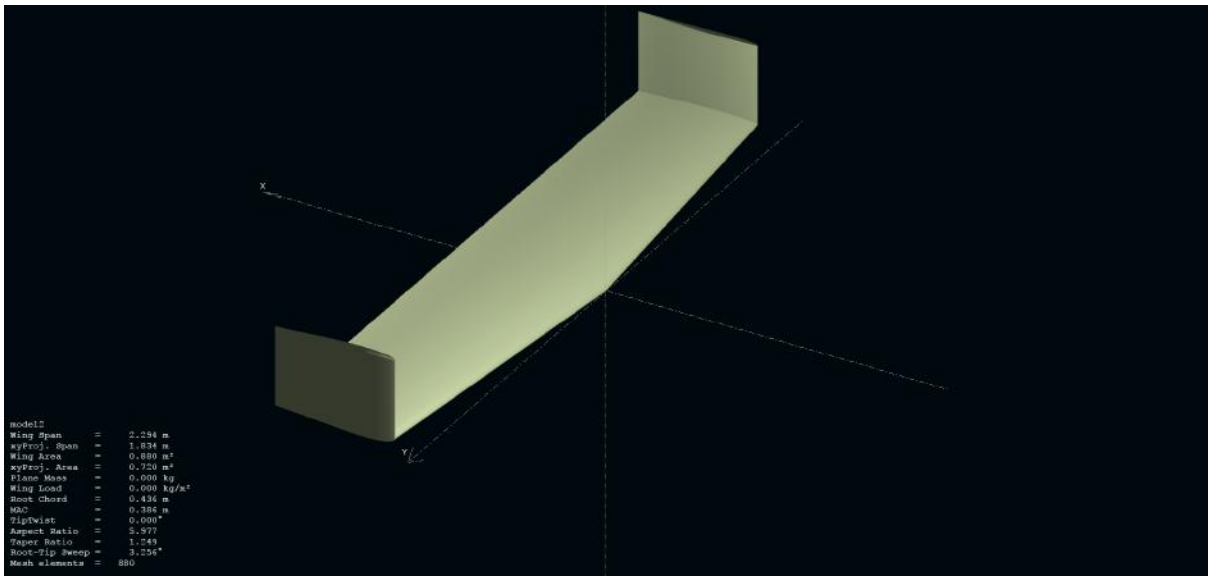

Figure 4.12: Verification model

- **Fuselage**:
  The fuselage is verified and validated by comparing the implemented fuselage drag model with values calculated by a Young model and real test data provided by literature [39]. The comparison of the data with the Young model and the test data is given in table 4.13.

Table 4.13: Fuselage verification and validation data [39]

			$C_{D,0_{fus}}$			Error model	
$\frac{RE}{10^6}$	l/d	T.P.	Measured	Young method	Model	Measurement	Young method
2.04	5	0.6 L_{fus}	0.0022	0.00236	0.00318	44.58%	34.78%
3.06	5	0.52 L_{fus}	0.0022	0.00244	0.00321	45.86%	31.51%
2.09	5	0.22 L_{fus}	0.00435	0.00409	0.00485	11.56%	18.65%
3.135	5	0.17 L_{fus}	0.00415	0.00388	0.00470	13.33%	21.22%
2.075	5	0.33 L_{fus}	0.00364	0.00361	0.00437	20.07%	21.07%
3.11	5	0.28 L_{fus}	0.00359	0.00351	0.00423	17.93%	20.62%
2.05	5	0.15 L_{fus}	0.0044	0.00437	0.00518	17.83%	18.64%
3.07	5	0.1 L_{fus}	0.00421	0.00414	0.00502	19.31%	21.33%
0.84	4.95	0.1 L_{fus}	0.0053	0.0053	0.00648	22.33%	22.33%
1.173	6.67	0.1 L_{fus}	0.0045	0.0047	0.00491	9.15%	4.50%

  From the table it can be concluded that the model used in the aerodynamic tool overestimates the fuselage drag in a range of 9.15% to 45.86% with respect to given test data. Comparing the model using calculations made using the Young model gives smaller discrepancy, but still positive. As the verification and validation of the fuselage model gives positive discrepancies on the drag coefficient, the aerodynamic tool can be used to estimate the fuselage drag with a positive safety margin. The location of the transition point of the airflow over the fuselage is verified using a k - epsilon CFD model in cruise conditions. The velocity map over the fuselage can be seen in fig. 4.13. From fig. 4.13 it can be concluded that the stream over the fuselage will transfer from laminar to turbulent at 68% of the total fuselage length. Therefore the aerodynamic tool used a 68% laminar friction coefficient and a 32% turbulent friction coefficient for the fuselage drag calculation.

- **Zero lift drag coefficient $C_{D,0}$ and Drag coefficient C_D**
  The $C_{D,0}$ and total C_D results of the model are compared to the simulation results for verification purposes in table 4.14.

  From the table above (table 4.14), it is shown that the tool estimates the $C_{D,0}$ of the wing with -15% dif-

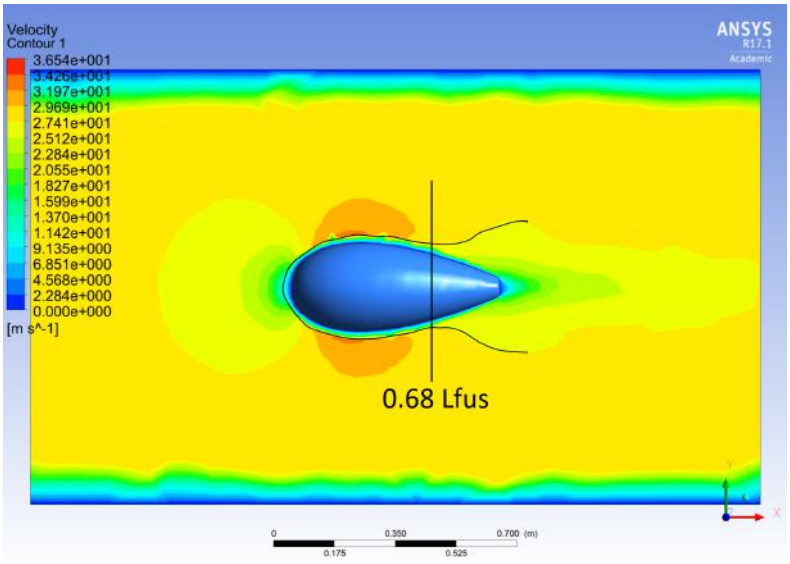

Figure 4.13: Velocity map over fuselage at V_{cruise} = 27.7 m/s produced using a k - epsilon CFD model

Table 4.14: Verification of the $C_{D,0}$ and total C_D results

XFLR5™Results	Tool Results	Percentage Difference w.r.t. XFLR5™Results
Single Wing		
0.00535	0.004542	−15.1 %
Single Winglet		
0.00034	0.000339	−0.43 %
Total model C_D		
0.00897	0.009371	4.46 %

ference with respect to the simulated value by XFLR5™$\left(\frac{\text{<Tool Value> - <XFLR5 Value>}}{\text{<XFLR5 Value>}} \cdot 100\right)$. The minus means that it is an underestimation. The $C_{D,0}$ of the winglet is estimated accurately by the model, since the difference is only -0.43%. The verification of the $C_{D,0}$ calculation of the fuselage was shown in the item above. However, the differences in the $C_{D,0}$ values are not of significant importance. This is due to the fact that total model C_D is estimated with a difference of 4.46 %. As a result, the total drag is slightly overestimated by the tool. This surprisingly overestimation is due to the contingency factor of 4% that was considered to account for other drag generating components. The design team came to the conclusion that the tool is capable of estimating the drag within a 5% accuracy which is sufficient enough for this design stage. This verifies the use of the aerodynamic tool.

4.7. Conclusions & Recommendations

Eventually, an X-wing configuration will be used, mostly due to its outstanding standing stability. The disadvantages of the angled wings are countered and overcome by not requiring winglets to fulfil standing stability. The velocity of 26.24 m/s, at which a maximum range can be accomplished, is close to the cruise velocity of 27.70 m/s, which indicates a successful optimisation.

Structural analysis was not taken into account parametrically, and thus involved the manual input of dimensions for the spar and skin. Implementation of structural analysis would significantly improve the accuracy of the model. Furthermore, an approximation for fuselage sizing would benefit the drag analysis, as both are completely decoupled at the moment.

5
Stability & Control

This chapter discusses the stability of the UAV in its different flight phases. In section 5.1, the hover stability is discussed. Section 5.2 is about longitudinal stability after transition to horizontal flight. The section also includes an analysis of the transitions. Section 5.3 discusses how the control in pitch, yaw and roll is tackled.

5.1. Hover and Landing Stability

For hover and landing stability, an important effect that has to be considered is that of an external torque. Due to conservation of angular momentum, the UAV will not change its orientation, unless disturbed.

- Gust will act as a disturbance and will therefore cause the UAV to rotate around its center of gravity. The average gust duration is found to be 5 seconds[1]. A gust force will cause the UAV to rotate perpendicular to both the center-of-gravity to center-of-wind distance vector $\mathbf{r}_{\text{c.g.}-\text{wind}}$ and the wind force vector $\mathbf{F}_{\text{wind}}$, as in eq. (5.1):

$$\mathbf{Q}_{\text{wind}} = \mathbf{r}_{\text{c.g.}-\text{wind}} \times \mathbf{F}_{\text{wind}} \tag{5.1}$$

  Herein, the wind force is determined from eq. (4.26).
  If the wind force is parallel to the yaw-axis (i.e., $\mathbf{F}_{\text{wind}} \parallel \mathbf{z}$) as in fig. 5.1, the gust induces a pitching moment.
- The torque caused by the propeller induces a rolling moment. This moment is countered by the torque propeller, which causes an equal moment in the opposite direction. This is discussed in section 5.3.3.

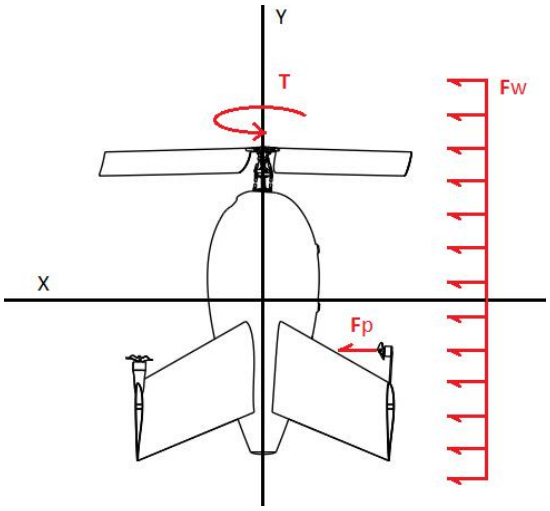

Figure 5.1: FBD of load situation in hover

The moment due to the gust is not compensated. By using eq. (5.2), the angle that the UAV is shifted by is calculated to be 42 degrees by performing a double of $\ddot{\theta}$.

$$Q_{\text{wind}} = r_{\text{c.g.}-\text{wind}} F_{\text{wind}} = I_{yy}\ddot{\theta} \tag{5.2}$$

As can be seen in the FBD (fig. 5.2), this disturbance will easily be compensated by gravity, if the blades are pitched for thrust vectoring (fig. 5.3) [1].

[1] URL `https://www.eol.ucar.edu/weather/weather_fl/gust.html` [cited 23 June 2017]

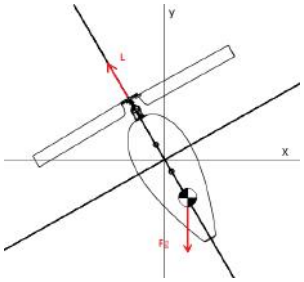

Figure 5.2: FBD after gusts

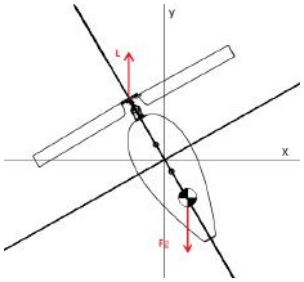

Figure 5.3: FBD after thrust vectoring

During take-off and landing, the ground effect should be considered. In the case of a conventional helicopter the ground or fountain effect can increase lift. However, this is only the case when the UAV is close to the ground. Since the mission will not benefit from the ground effect, take-off should be executed as fast as possible. For landing, the ground effect should be avoided, since it could give unexpected inputs to the autopilot which can jeopardise the mission. It is therefore crucial to investigate the ground clearance needed in order to land safely when a prototype is built.

5.2. Flight Stability

In this section, the stability of the UAV is analysed in detail. Section 5.2.1 investigates whether the UAV can be designed such that it can have steady flight, then the static and dynamic stability characteristics are investigated in section 5.2.2. The transition manoeuvres from cruise to hover and from hover to cruise are investigated in section 5.2.3 and section 5.2.4 respectively. The lateral stability characteristics are shown in section 5.2.5 and finally the standing stability of the UAV in windy conditions is investigated in section 5.2.6

5.2.1. Steady flight

Before investigating static stability, an analysis has to be done to make sure the UAV can sustain a pitch moment of zero at all air speeds and such that it can maintain in steady flight throughout the entire mission profile.
In order to perform this analysis, several assumptions had to be made:

- Steady flight, i.e.,
  - Thrust **T** is equal and opposite in direction to drag **D**, i.e., $\mathbf{T} = \mathbf{D}$;
  - Lift **L** is equal and opposite direction to weight **W**, i.e., $\mathbf{L} = \mathbf{L}_{wing} + \mathbf{L}_c = \mathbf{W}$;
  - The sum of the moments about any point is equal to zero, i.e., $\sum \mathbf{M} = 0$.
- Negligible canard moment and drag
- Canard produces no downwash therefore the free stream velocity of the canard is the same as that of the wings
- Negligible fuselage moment and lift
- The aerodynamic centre of the canard is at the front of the fuselage.

In this section, the propeller used for hover and take off is called the canard, as the propeller blades will be placed in a horizontal orientation to act as an effective control surface. The moment of the canard has been considered negligible due to the fact that the moment created by the lift of the canard is much more relevant and bigger in magnitude.
A free body diagram was produced to analyse which forces would be acting on the UAV and is shown in fig. 5.4. The diagram also represents the sign conventions that are used in this section.

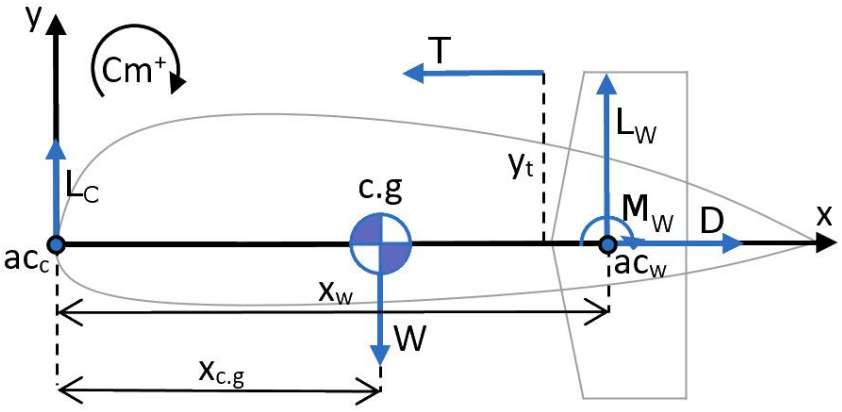

Figure 5.4: Free body diagram of the UAV

By summing the moments about the centre of gravity, the total moment M_{tot} is calculated using eq. (5.3), which can be then be expanded into eq. (5.4).

$$M_{\text{tot}} = M_{\text{wing}} + L_{\text{wing}}(x_{\text{c.g.}} - x_{\text{wing}}) - T y_T + L_{\text{c}} x_{\text{c.g.}} \tag{5.3}$$

$$M_{\text{tot}} = C_m q S_{\text{wing}} \bar{c} + C_L q S_{\text{wing}}(x_{\text{c.g.}} - x_{\text{wing}}) - C_D q S_{\text{wing}} y_T + C_{L_{\text{c}}} q S_{\text{c}} x_{\text{c.g.}} \tag{5.4}$$

By setting M_{tot} to zero, for a given geometric configuration and C_L, it is possible to find the required canard lift coefficient to keep the aircraft steady, using eq. (5.5)

$$C_{L_{\text{c}}} = -\frac{C_m \bar{c} + C_L(x_{\text{c.g.}} - x_{\text{wing}}) - C_D y_T}{\frac{S_{\text{c}}}{S}(x_{\text{c.g.}})} \tag{5.5}$$

A program was written to go through all possible variations of x_{wing} and Λ, and for each combination, $x_{\text{c.g.}}$ was calculated. For the range of velocities the UAV is expected to fly at, it went through all possibles values for the C_L of the wing, found the accompanying $C_{L_{\text{c}}}$ for which the total moment is zero and checked if the lift generated would be equal to the weight. An additional check was made whether the bottom of the fuselage would not touch the ground when standing on its wingtips. As an output, it would provide all the geometrical combinations for which steady flight would be possible.
The inputs to the program are all values calculated from the aerodynamic tool described in chapter 4 as well as the individual masses of the motors and the predicted centre of gravity position of the fuselage with all its internal components.
A diagram of how the program works is shown in fig. 5.5.

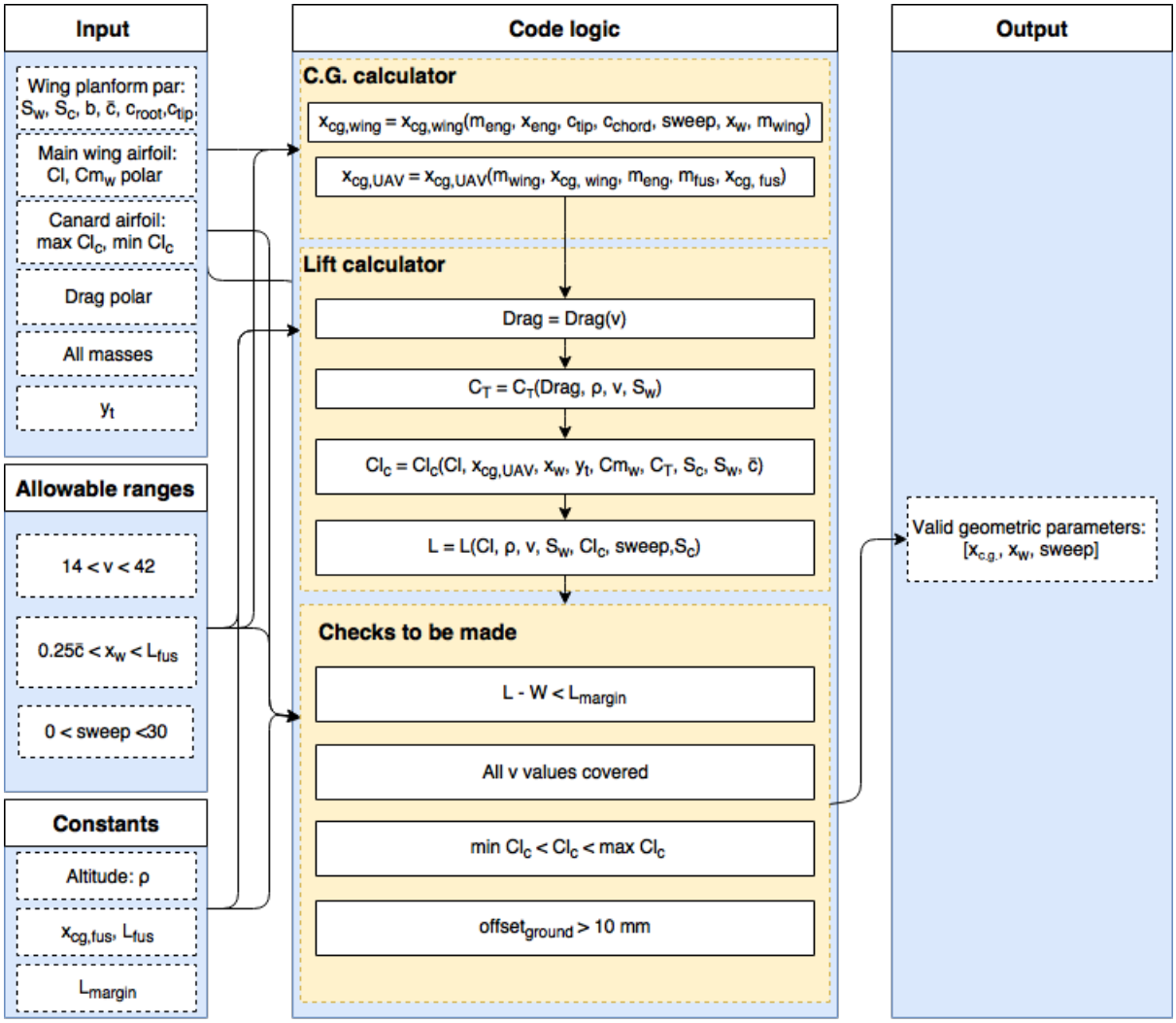

Figure 5.5: Steady flight code flow diagram

The range of values for the velocity were chosen with the lowest velocity set as the stall velocity and the highest velocity being the top speed. A maximum leading edge sweep angle of 30 degrees was set as a limit since any sweep angle beyond that would mean that the aircraft would not be able to fly within the desired velocity regime. The location of the aerodynamic centre of the wing was set to range between the entire length of the fuselage.

The centre of gravity of the UAV was estimated using the following method:

- The position of the fuselage centre of gravity was estimated in CATIA to be at 0.272 m from the front of the fuselage. It is assumed that this position could vary by ±1 cm if the position of certain internal components were to be adjusted.
- The propellers were placed below the axis of symmetry at the wingtips to ensure that they would be able to create the largest possible pitching moment and to ensure that they would also be able to create an effective yawing moment.
- The single propeller required for torque was placed at 30 % of the tip chord.
- The location of the centre of gravity of the wing structure was estimated to be at half of the wingspan and at 30 % of the chord length. Then the mass of the motors was also added to the wing to provide the total centre of gravity of the wing. This is seen in eq. (5.9).
- An estimate for the location of the aerodynamic centre of the wing was made by calculating the span wise position of the point using eq. (4.21) and its chord wise position at approximately $0.25\bar{c}$ from the leading edge. From this, the point of the leading edge connection was deduced. This is shown in eq. (5.6)
- Taking into account the location of the leading edge, the location of the centre of gravity of the total wing section was determined based on the location of the centre of gravity of the wing structure, as well as the

location of the two cruise motors, as well as the motor on one side of the wing that will be used to provide the counter-torque during the hover phase. The equation is shown in eq. (5.9)

- The final centre of gravity of the UAV is then calculated taking into account all the relevant masses and distances, as shown in section 5.2.1

$$x_{\text{L.E.}} = x_{\text{wing}} - \bar{Y}\tan(\Lambda_{\text{L.E.}}) - 0.25\bar{c} \quad (5.6) \qquad x_{\text{motor}} = x_{\text{L.E.}} + y_T \tan(\Lambda_{\text{L.E.}}) \quad (5.7)$$

$$x_{\text{motor}_{\text{side}}} = x_{\text{L.E.}} + \frac{b}{2}\tan(\Lambda_{\text{L.E.}}) + 0.3c_{\text{r}} \quad (5.8) \qquad x_{\text{c.g.}_{\text{wing}}} = x_{\text{L.E.}} + \frac{b}{4}\tan(\Lambda_{\text{L.E.}}) + 0.3\frac{1+\lambda}{2}c_{\text{r}} \quad (5.9)$$

$$x_{\text{c.g.}} = \frac{\left(m_{\text{wing}} + m_{\text{motor}} + m_{\text{motor}_{\text{side}}}\right) x_{\text{c.g.}_{\text{wing}}} + m_{\text{fus.}} x_{\text{fus.}}}{m_{\text{wing}} + m_{\text{motor}} m_{\text{motor}_{\text{side}}} + m_{\text{fus.}}}$$

Due to the low amount of taper, it has been assumed that the sweep angle at the leading edge of the wing is the same as the sweep at the quarter chord point.
The offset that the bottom of the fuselage had with the ground was checked using the following formula:

$$\text{offset}_{\text{ground}} = x_{\text{L.E.}} + \frac{b}{2}\tan(\Lambda_{\text{L.E.}}) + c_{\text{t}} - L_{\text{fus.}}$$

The stability margin (S.M) of the UAV was calculated while assuming that the neutral point of the UAV is at the aerodynamic centre of the wing. The formula used was:

$$SM = 100\frac{x_{\text{c.g.}} - x_{\text{wing}}}{\bar{c}} \quad (5.10)$$

By observing the combinations of geometrical parameters that were produced by the program as an output, the following parameters were chosen based on the low sweep angle and also due to the relatively lower stability margin that reduces the use of the canard:

Table 5.1: Geometrical parameters

x_{wing} (m)	y_T (m)	$x_{\text{c.g.}}$ (m)	$\Lambda_{L.E}$ (°)	$S.M$ (%)	offset_{ground} (mm)
0.4	-0.28	0.341	11	29.64	18

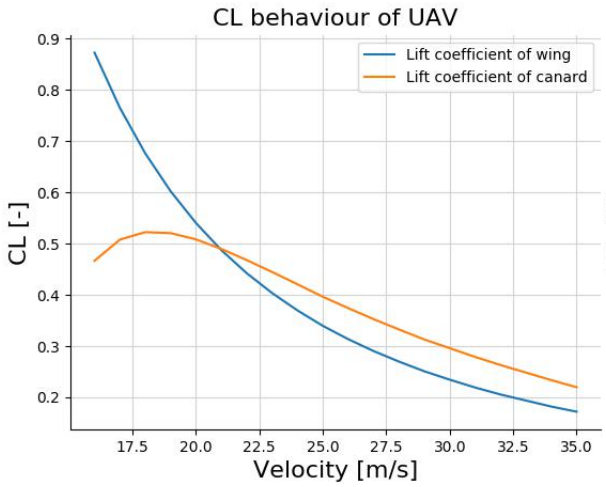

Figure 5.6: Lift required for steady flight

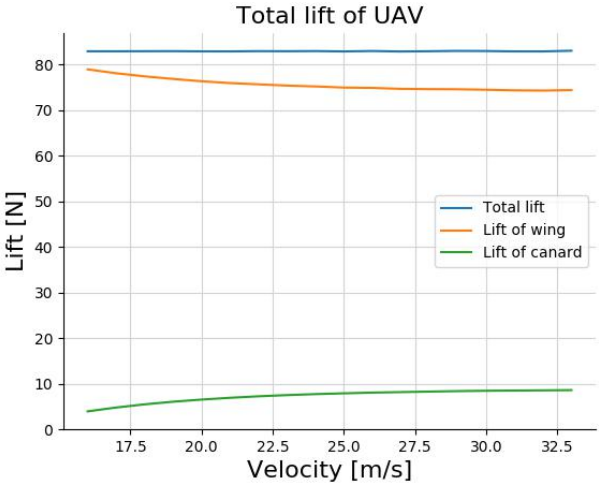

Figure 5.7: C_L required for steady flight

The aerodynamic design was designed using a sweep angle of 30 degrees to account for the fact that there would eventually be sweep added to the wing profile as shown in chapter 4. With a 11 degree of sweep, the aerodynamic planform will be capable of producing sufficient lift. It is also observed that contrary to the stall speed of 16 m/s that was concluded in chapter 4, a minimum flying speed of 14 m/s has been deduced. This is because at all speeds, the canard is producing positive lift.
The fuselage clearance from the ground at the moment is 18 mm. This is risky since it is expected that the wing will bend slightly when it hits the ground, so it is also expected that extra material will be required at the

trailing edge of the tip wingtips to increase the clearance and prevent any damage being done to the fuselage as well as its components.
A sensitivity analysis was performed to be able to see the effect of slight changes in locations of $x_{c.g.}$, y_T and x_{wing} on whether the UAV is still able to maintain steady flight. These slight changes are expected due to manufacturing accuracy, the effect of accidents on and off ground, as well as differences in calculations of the $x_{c.g.}$ and x_{wing} and real locations. It is also known already that the c.g. position will shift due to fuel being consumed as well as due to the introduction of a blood sample during the middle of the mission.
The mass of the fuel represents less than 1% of the total mass and is located close to the centre of gravity, thus the shift will not be considerable. The same applies to the mass of the blood sample that will be introduced. The sensitivity analysis is presented below and analysed for $x_{\text{c.g.}}$, y_T, x_{wing}, Λ, and Drag. It is important to note that in this analysis the geometric parameters are assumed to be independent of each other, when they are actually highly interconnected. For example, shifting the position of x_{wing} would naturally shift $x_{\text{c.g.}}$ also.

Table 5.2: $x_{\text{c.g.}}$ sensitivity analysis [x_{wing} = 0.4, y_T = -0.28, Λ = 11]

$x_{\textbf{c.g.}}[m]$	CL_{max}	CL_{min}	$CL_{c_{max}}$	$CL_{c_{min}}$	$V_{max}[m/s]$	$V_{min}[m/s]$
0.32	0.359	0.167	0.704	0.354	33	24
0.34	0.901	0.200	0.566	0.261	33	16
0.36	0.947	0.187	0.215	-0.010	33	16

Table 5.3: y_T sensitivity analysis [x_{wing} = 0.4, $x_{\text{c.g.}}$ = 0.34, Λ = 11]

$y_T[m]$	CL_{max}	CL_{min}	$CL_{c_{max}}$	$CL_{c_{min}}$	$V_{max}[m/s]$	$V_{min}[m/s]$
-0.28	0.901	0.200	0.566	0.261	33	16
-0.24	0.887	0.175	0.687	0.257	33	16
-0.2	0.606	0.195	0.740	0.315	33	19

Table 5.4: x_{wing} sensitivity analysis [$x_{\text{c.g.}}$ = 0.34, y_T = -0.28, Λ = 11]

$x_{\textbf{wing}}[m]$	CL_{max}	CL_{min}	$CL_{c_{max}}$	$CL_{c_{min}}$	$V_{max}[m/s]$	$V_{min}[m/s]$
0.38	0.950	0.211	0.211	-0.040	33	16
0.4	0.901	0.200	0.566	0.261	33	16
0.42	0.396	0.190	0.705	0.374	33	23

Table 5.5: Λ sensitivity analysis [$x_{\text{c.g.}}$ = 0.34, y_T = -0.28, x_{wing} = 0.4]

Λ [°]	CL_{max}	CL_{min}	$CL_{c_{max}}$	$CL_{c_{min}}$	$V_{max}[m/s]$	$V_{min}[m/s]$
9	0.891	0.197	0.551	0.256	33	16
11	0.901	0.200	0.566	0.261	33	16
13	0.912	0.203	0.583	0.266	33	16

Table 5.6: Drag sensitivity analysis [$x_{\text{c.g.}}$ = 0.34, x_{wing} = 0.4, y_T = -0.28, Λ = 11]

Change in drag [%]	CL_{max}	CL_{min}	$CL_{c_{max}}$	$CL_{c_{min}}$	$V_{max}[m/s]$	$V_{min}[m/s]$
+ 10	0.911	0.201	0.496	0.241	33	16
0	0.901	0.200	0.566	0.261	33	16
-10	0.891	0.198	0.639	0.279	33	16

Several conclusions can be made about how the steady flight characteristics of the UAV will change if certain parameters end up changing.

- $x_{\text{c.g.}}$ When it shifts forward, the operational velocity regime decreases drastically as the minimum flying speed increases. It also causes the canard to have to operate at higher lift coefficients. The main wing produces less lift, while the canard produces more. Shifting it forward also means that the minimum flying speed increases, thus decreasing the operational velocity range. If possible, it will be highly beneficial to try and move the centre of gravity of the UAV as rearward as possible. This also means that any sort of payload bay should be placed at the backwards section of the fuselage.

- y_T With the vertical location of the cruise propellers, they are already at their maximum distance from the UAV's axis of symmetry however when bringing it closer to the axis of symmetry, the UAV becomes more reliant on the canard for lift and eventually it is incapable of flying at low speeds. Therefore it would be beneficial to keep the propellers where they are.
- x_{wing} With the aerodynamic centre of the wing, bringing it closer to the front of the UAV will cause the wing to produce more lift, and thus reduce the lift of the canard. There would also only be a small increase in the minimum flying speed of the UAV. Moving the wing's more rearwards would not be beneficial.
- Λ It is only beneficial to decrease the sweep angle if possible, however this highly depends on having the trailing edge of the wingtips have contact with the ground.
- D An increase in drag will increase the lift of the main wings and a decrease in drag will decrease the lift of the main wings. If possible it would be preferable to reduce drag when considering all the other subsystems however this would increase the dependence on the canard and possibly cause it to stall, and thus increase the minimum flying speed.

The sensitivity analysis has also acted as a verification of the behaviour of the program. It is verified that the program acts logically to the behaviour that is expected of it.

5.2.2. Static and dynamic stability

Once the UAV geometric parameters have been chosen and the UAV is proven to be able to fly in steady conditions, static and dynamic stability should be investigated. In order to do so, a model of the pitch behaviour of the UAV was developed. Assumptions were made in the making of the model:

- Aerodynamic effects due to the rotation of the UAV are negligible
- The moment inertia of the UAV is that of one cylinder and two plates
- Canard moment and drag are negligible
- Fuselage moment and lift are negligible
- The aerodynamic effects of thrust on the wings is negligible
- Aerodynamic effects such as hysteresis are assumed not to happen

The functioning of the model is illustrated in fig. 5.8. The model was verified using known basic behaviours of flying wings, for example (more tests were performed on the model):

- A centre of mass ahead of the aerodynamic centre results in a stable UAV, as expected[15]
- A centre of mass behind the aerodynamic centre results in an unstable UAV, as expected[15]
- Increased thrust results in higher speed and/or climb rate, as expected
- Decreased thrust results in lower speed and/or a descent rate, as expected

Additional data should however be used in the future to improve the accuracy of the model and get rid of the most influential assumptions. For example:

- Measuring the drag, moment and lift of the entire UAV in a wind tunnel test. These results would greatly improve the drag, lift and moment model.
- Measuring the moment of inertia. It would help improve the accuracy of the dynamic behaviour of the UAV.
- Measuring the aerodynamic forces created by the pitch rotation of the UAV. It would improve the accuracy of the model during fast manoeuvres.

The model is first used to investigate the static longitudinal stability of the UAV. In order to do so, the UAV is started in quasi steady flight, i.e. with canard lift coefficient resulting in $M_{\text{tot}} = 0$ and a power setting such that $T = D$. The settings are not set to their exact values and the discrepancies act as disturbances. The resulting behaviour of the UAV can be seen in fig. 5.9. One can see that the UAV is statically stable: an increase of the angle of attack results in a pitch down moment of the UAV and a decrease of angle of attack results in a pitch up moment. However, it is also quite clear that, while the UAV is statically stable, it is not dynamically stable: the oscillation caused by the alternation of pitch up and pitch down moments grows fast.
In order to keep the UAV stable despite its dynamic instability, the autopilot uses the sensor readings to get $\dot{\theta}$ (using the gyroscope) and γ (using for example the pitot tube and an altimeter) and determines the C_{L_c} and power setting that will stabilise the UAV. The canard is used to damp the oscillations and the power setting is used to bring the vertical speed down to 0, which is equivalent to bringing γ to 0. The commands, function of θ and γ, are shown in eq. (5.11) and eq. (5.12) as used in the simulation. An example of stabilisation is shown in fig. 5.10, by starting with a steadily flying UAV and then suddenly increasing the airspeed of 1 m/s at $t = 0$ s.

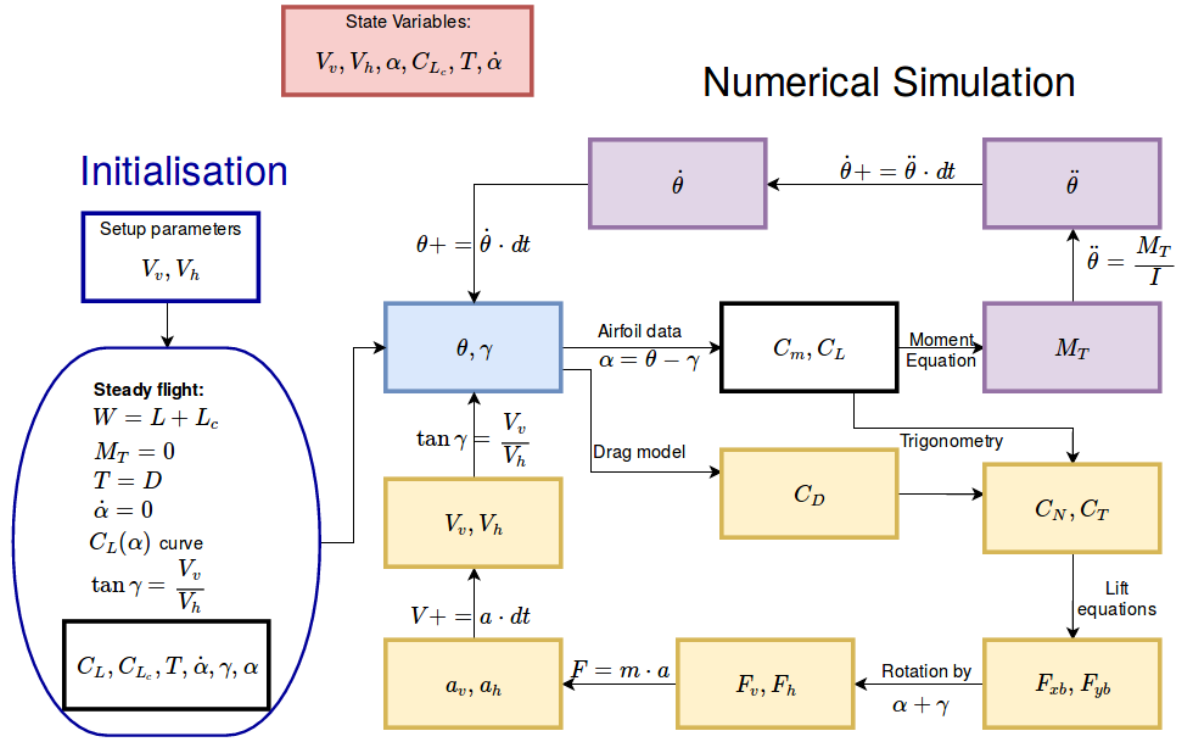

Figure 5.8: Functioning of the pitch behaviour model

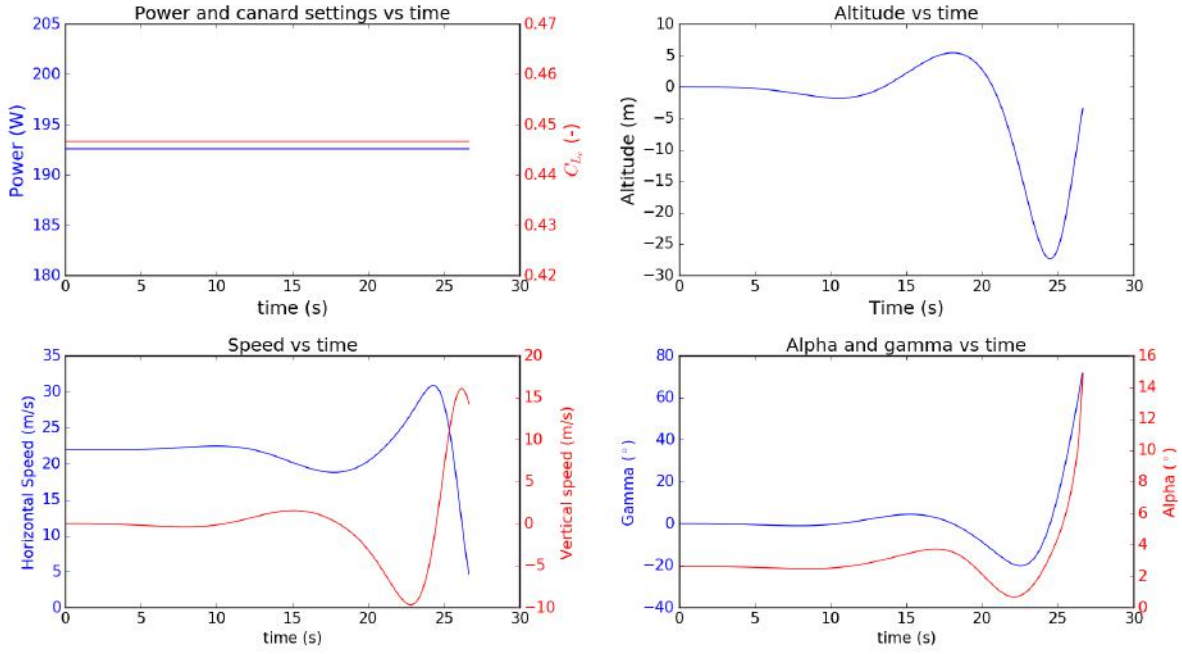

Figure 5.9: Behaviour of the UAV without active stabilisation. One can see that the UAV is statically stable but also strongly dynamically unstable, as the pitch up and pitch down oscillations grow at a fast rate. Therefore, an active stabilisation strategy is required to fly the UAV.

One can see that the autopilot successfully manages to bring back the UAV to a steady state in roughly 5 s and without large changes in altitude. Further improvements to the tuning of k_1, k_2 and k_3 would result in a faster stabilisation.

$$P_{t_{i+1}} = P_{t_i} - (k_1\gamma + k_2\dot{\gamma})dt \tag{5.11}$$

$$C_{L_c,t_{i+1}} = C_{L_c,t_i} - (k_3\dot{\theta})dt \tag{5.12}$$

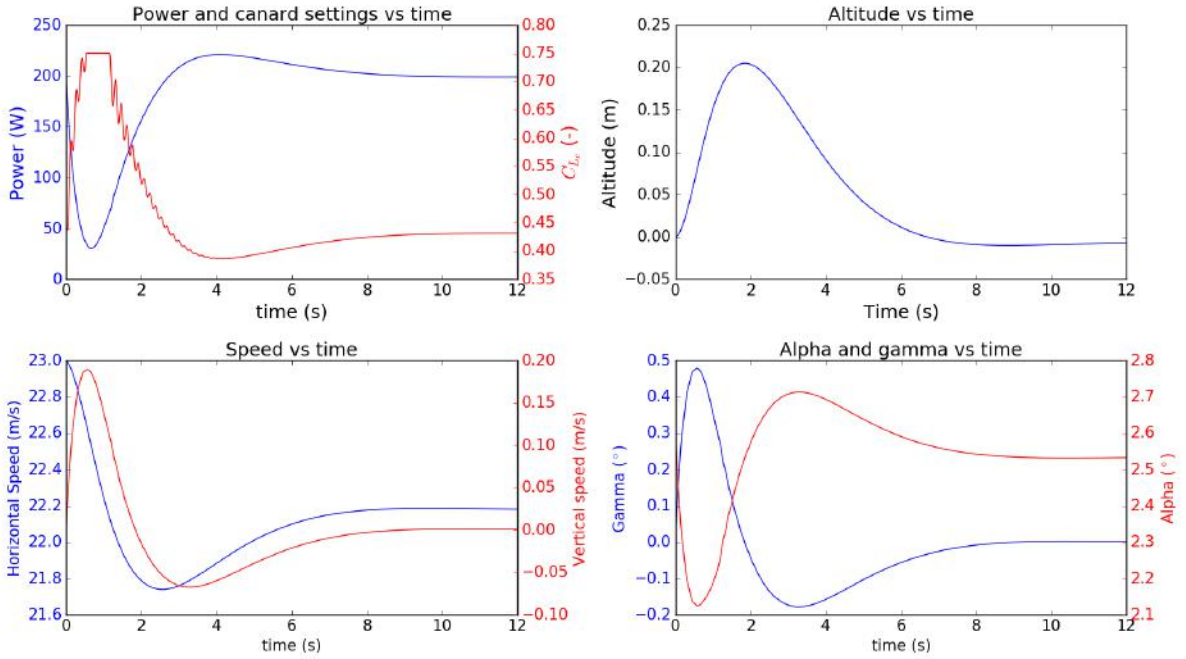

Figure 5.10: Autopilot stabilisation of the UAV, after a sudden increase of airspeed of 1 m/s. The stabilisation algorithm uses readings from the IMU together with the power and canard setting to damp oscillations and bring the vertical speed to zero. The current tuning ($k_1 = 100$, $k_2 = 300$, $k_3 = 2000$) manages to stabilise the UAV in roughly 5 s.

5.2.3. Forward to hover transition

The transition from forward flight to hover is performed by pulling up at high speed (above 31 m/s), as shown in fig. 5.11. The high speed is required to have enough energy to be able to pull up without stalling. The pull up is initiated by increasing the thrust and the lift of the canard. Once the pull up has been initiated, the thrust and the lift of the canard is set to zero to avoid a further increase of the angle of attack which would result in the wing stalling and inertia finishes the transition. The canard is finally used to stop the rotation of the UAV. The manoeuvre results in a vertical UAV ($\theta \approx 90°$) 30 m above the beginning of manoeuvre with practically no horizontal velocity and an upward velocity of 7 m/s, as can be seen in fig. 5.11. This vertical velocity can be used to help the hover motor to rapidly start the hover propeller. Once the hover propeller has fully started, the transition is successful. The maximal acceleration encountered during this manoeuvre is 3.4 g.

5.2.4. Hover to forward flight transition

The transition from hover to forward flight is done in several steps. First, the swash-plate is used to create a moment to flip the UAV upside down and start a nosedive. The hover motor is then stopped and the propeller transforms into the canard wing. The UAV is then left free falling to gain some speed, as shown in fig. 5.12. The cruise propellers can not be turned on at this point since the strong pitch up moment they would create can not be compensated (the airspeed is too low for the aerodynamic moments to have an effect) and would result in a spinning UAV. As soon as the airspeed is above 10 m/s, the cruise propellers are turned on and the lift of the canard is reduced to prevent a too strong pitch up moment. The UAV starts pulling up. As soon as the vertical velocity reaches 0 m/s, the power and canard settings are set to the steady flight settings corresponding to the current airspeed and the active stabilisation described in section 5.2.2 is turned on. This results in a stabilised forward flying UAV and therefore a successful transition. The transition requires an altitude of 45 m and takes about 6s. The maximal acceleration encountered during this manoeuvre is 2.6g.

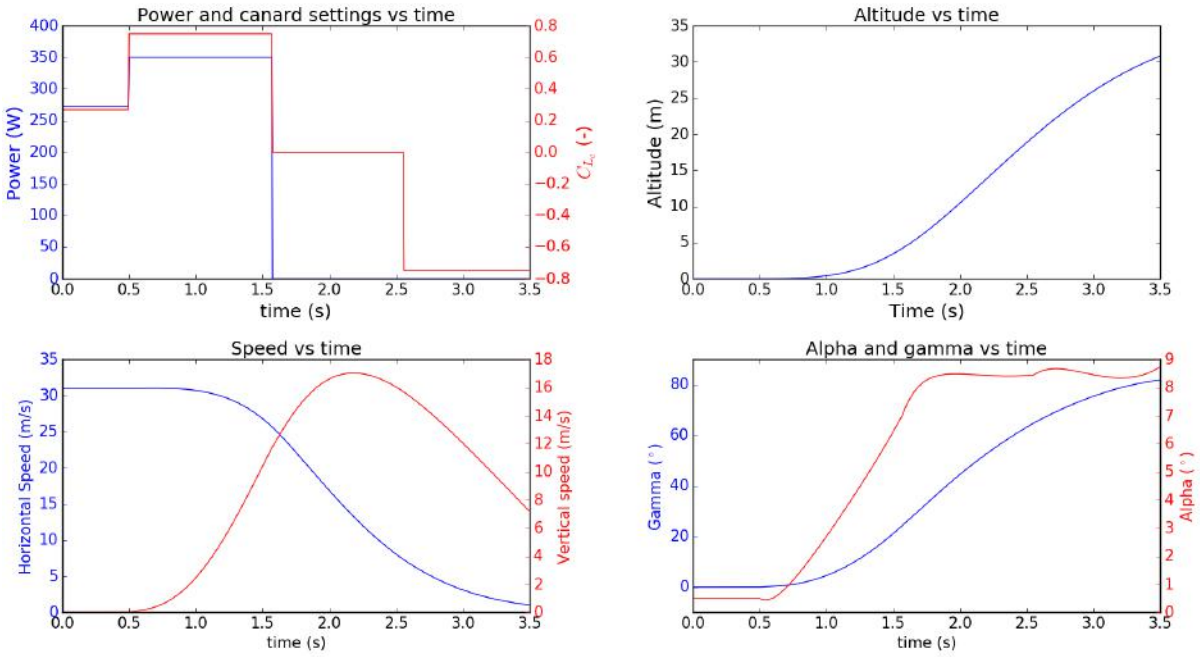

Figure 5.11: Transition from forward flight to hover. The transition has to be operated at high speed to be able to complete the pull up without stalling. The pull up is initialised and stopped by the canard and the power settings. The manoeuvre takes 3.5 s and results in an altitude increase of 30 m and a peak acceleration of 3.4 g.

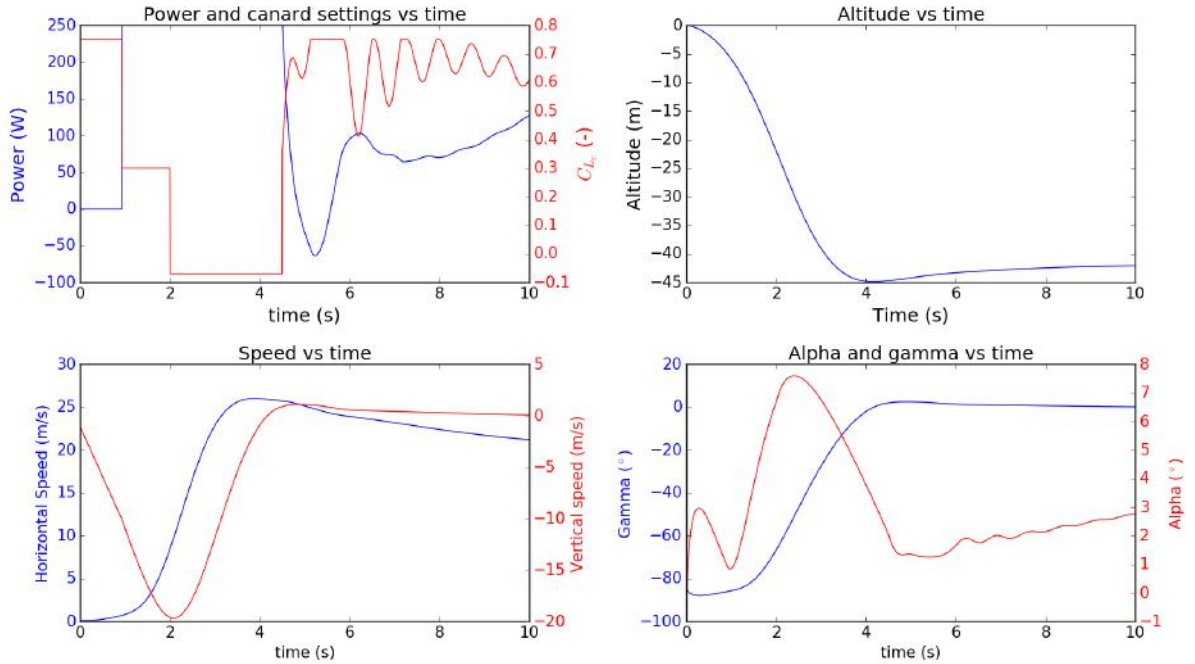

Figure 5.12: Transition from nosedive to forward flight. The UAV is first left free falling, then cruise motors are turned on to pitch up and finally active stabilisation is used to stabilise the UAV. The manoeuvre takes about 6 s and results in an altitude drop of 45 m and a peak acceleration of 2.6 g.

5.2.5. Lateral stability

A lateral stability analysis was performed using XFLR5. The analysis was performed by investigating the aircraft's behaviour at its cruise speed and α when it would encounter sideslip. It is important to note that for this subsection alone, the axis system shown in fig. 5.13 and notation is used. eq. (5.13) and eq. (5.14) represents the moment around the Z_B and X_B axis respectively.

$$C_n = \frac{N}{\frac{1}{2}\rho V^2 Sb} \tag{5.13}$$

$$C_l = \frac{L}{\frac{1}{2}\rho V^2 Sb} \tag{5.14}$$

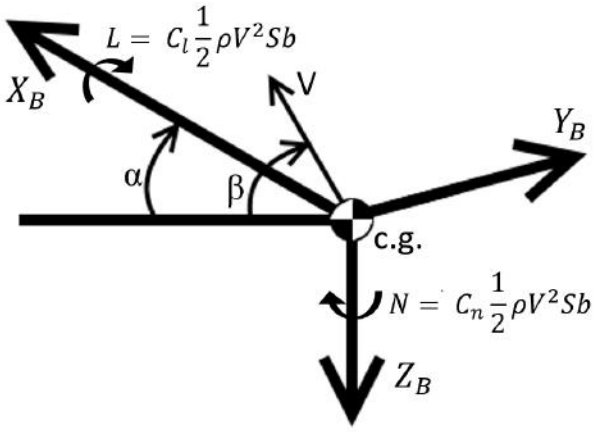

Figure 5.13: Lateral stability axis system

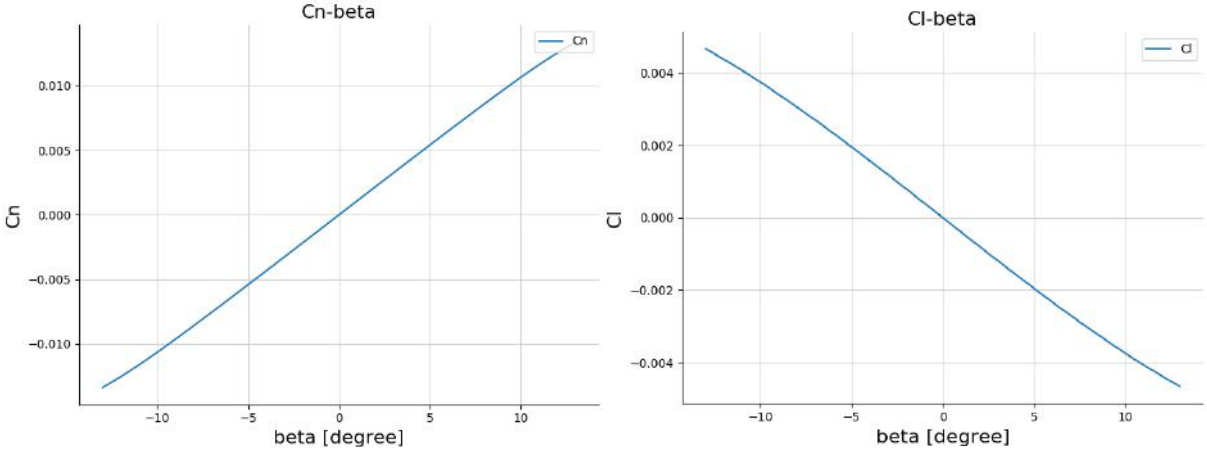

(a) C_n-β relation shows a positive slope, thus stable relationship.

(b) C_l-β relation shows a negative slope, thus stable relationship.

Figure 5.14: Lateral stability diagrams

From fig. 5.14a it can be seen that the slope of the curve, thus C_{n_β} is positive. This indicates that in the event that the UAV encounters side slip, it will rotate itself to a state where there is no sideslip. From fig. 5.14b it can be seen that the slope, C_{l_β} is negative. Thus for example, in the event that the UAV is encountering sideslip coming from its right side, it will cause the UAV to roll to the left due to the difference in α that the wings are experiencing. In the case of sideslip, the UAV is exhibiting stable lateral characteristics.

5.2.6. Standing stability

In terms of landing stability when encountering wind forces, using equation eq. (4.25) and data about the centre of lift and centre of gravity. The maximum wind speed that the UAV could withstand when standing was calculated assuming a C_D of 2. to account for the fact that large amounts of drag can be created by the profile of the UAV, and using eq. (5.15) and eq. (5.16):

$$F_{wind}(L_{fus} - x_{\text{wing}}) = W\frac{b}{2}sin(\Gamma) \tag{5.15}$$

$$v_{wind_{max}} = \sqrt{\frac{4F_{wind}}{C_D \rho S \cos\Gamma}} = 17.6 m/s \tag{5.16}$$

If the wind speed is to be above 24.82 m/s, then the UAV will be at risk of falling over.

5.3. Control

In this chapter the control surfaces for the UAV are discussed. section 5.3.1 will discuss the pitch control, section 5.3.2 the yaw control and finally roll control is discussed in section 5.3.3.

5.3.1. Pitch Control

In cruise, longitudinal stability is secured by the swash plate which is able to control the pitch angle of the propellers so they can be used as canards. The canard is also used for the pitch control. Adjusting the collective blade pitch causes the UAV to be able to climb or descent. It is observed that the canard reaches a maximum C_L of 0.53 in its operational velocity range when it has a stall C_L of approximately 0.75, as seen in section 5.2.1 Therefore at all velocities it will be capable of providing pitch control when necessary.

5.3.2. Yaw Control

Yaw control is important in cruise since the drone is operated in a gusty environment. In the worst case the drone could be hit by a gust of 15.4 $\frac{m}{s}$ from the side. Comparing this to the vector of the cruise speed of 28 $\frac{m}{s}$ this creates a vector with side slip angle β as shown in eq. (5.17). When the gust is gone the UAV will have to return to its original position quickly. In this slipped position the moment created by putting one propeller at full throttle and the other at zero is modelled in eq. (5.18), eq. (5.19) and fig. 5.15. Using the rate of roll rate equation eq. (5.19) the amount of yaw angle which can be created in one second by putting one engine at full trust and the other at half can be modelled. This is shown in fig. 5.16

$$\beta = \frac{V_w}{V_c} = 28.8^\circ \tag{5.17}$$

$$M_{yaw} = T_l cos(\beta) d_l - T_r cos(\beta) d_r \tag{5.18}$$

$$T = \ddot{\theta} I_{zz} \tag{5.19}$$

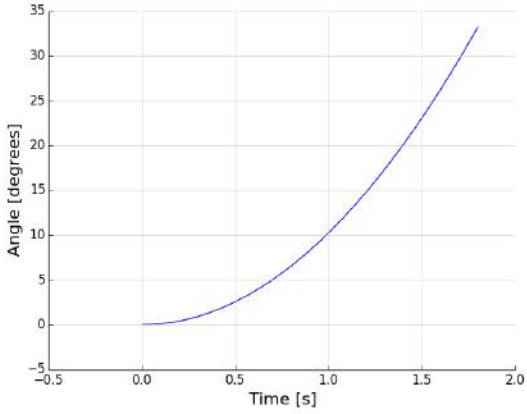

Figure 5.15: Returning from Gust

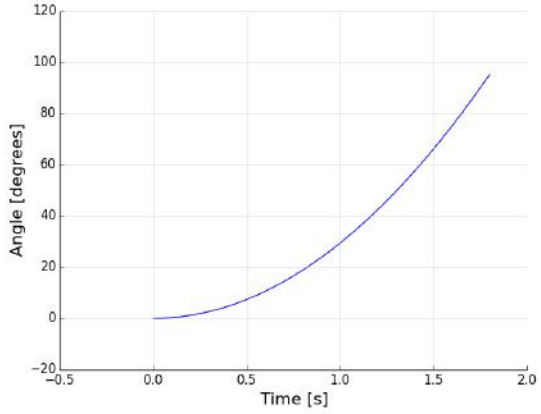

Figure 5.16: Yaw Angle over Time

5.3.3. Roll Control

For roll control two situations have been considered being hover and cruise. In hover the roll control should be able to keep the UAV from turning due to its torque. The effects of the wind are assumed to be negligible because the symmetric dihedral of the UAV. The torque produced by the rotor is 2.76 Nm, iterations with the help of [31] showed that ailerons only where not sufficient to counteract this torque. Therefore an off the shelve propeller will be placed at the wing tip which will provide the required 3.28 N of thrust. In cruise the possibility was investigated to use to canard as the roll control by pitching the blades in opposite direction. Using the criterion for roll rate was set to be 60 degrees in 1.3 seconds [31]. The moment caused by the canard is modelled by eq. (5.20). The lift coefficients which are used correspond to the canard having one blade at 1.7 degrees, which is needed to maintain the pitch control, and the other at 4.7 degrees. When using the equation for rate of roll rate eq. (5.21) it can be seen that with only using the canard a desired roll rate is achievable as shown in fig. 5.17. Therefore no extra ailerons are needed.

$$M_a = (L_l - L_r) d_b \tag{5.20}$$

$$\text{Rate of Roll Rate} = \frac{M_a}{I_x x} \tag{5.21}$$

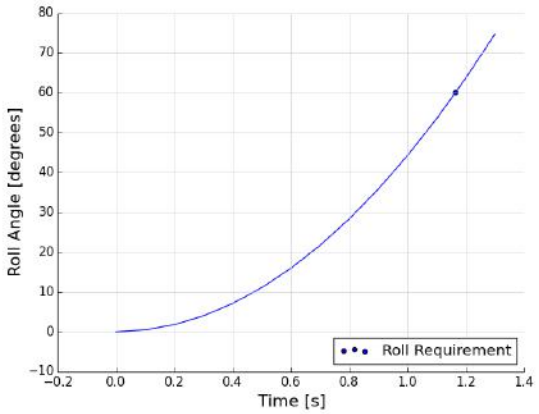

Figure 5.17: Roll Angle over Time

5.4. Conclusions & Recommendations

In conclusion the position of the wing has been determined such that steady flight can be achieved at all velocities in the velocity regime. The aerodynamic centre of the wing has been placed at 0.4 m from the front of the fuselage, with 11 degrees of leading edge sweep to ensure that the fuselage makes no contact with the ground. Furthermore, it can be said that the UAV is able to recover from gusts in the hover phase.

A model was made to analyse the dynamic behaviour of the UAV. It showed that the UAV is statically stable but strongly dynamically unstable. Fortunately, the model also proved that simple algorithms using sensor readings could rapidly stabilise the UAV, even starting from a disturbed state, as shown in section 5.2.2. The forward flight to hover transition was then investigated in section 5.2.3. The simulation outputted a manoeuvre duration of 3.5 s, an altitude increase of 30 m and a peak acceleration of 3.4 g. The hover to forward flight transition was also investigated in section 5.2.4. The simulation outputted a manoeuvre duration of 6 s, an altitude drop of 45 m and a peak acceleration of 2.6 g.

While the model provides good estimations for the behaviour of the UAV, it could be greatly improved by reducing the number of assumptions and by using wind tunnel data instead of the currently used drag, lift and moment model. The inaccuracy of these models greatly affect the simulations and a wind tunnel would be a relatively easy way to improve the accuracy of the simulations. Furthermore, more complex stabilisation algorithms, taking into account the accuracy of the IMU readings should also developed to solve the problems caused by the dynamic instability of the UAV. Also, experiments should be performed to determine how to flip the UAV upside down during the hover to forward flight transition. Finally, the consequences in terms of aerodynamic effects and time of the start-up and shut-down of the hover propeller should be investigated.

It has been calculated that the aircraft will be able to withstand a wind speed of 24.82 m/s in standing configuration before the UAV will be at risk of falling over.

The aircraft has also deemed to be laterally stable. In terms of control surfaces the propellers are used for yaw control, the canard surface is used for pitch and roll control.

A last recommendation for this section is to perform actual tests with a model in order to validate our models. This could be done by measuring the actual roll rates and angles and check these with our calculations.

6
Propulsion

This chapter describes the iterative process and decisions that were made during the design of the cruise, hover and torque propellers. First an explanation of the propeller configuration is provided. This is followed by a brief summary of the theories necessary to understand and perform the design of the propellers. These theories are the basis of the software developed and used for the design. Their limitations and the method of verification are outline in the following section. After outlining the design an aerofoil selection was performed. Section 6.4 and section 6.9 discuss the performance of the obtained final propeller designs and the choices of compatible motors. Finally a conclusion is drawn and recommendations are made, which can be found in section 6.11 and provide suggestions for further improvement of the design.

6.1. Propeller Configuration

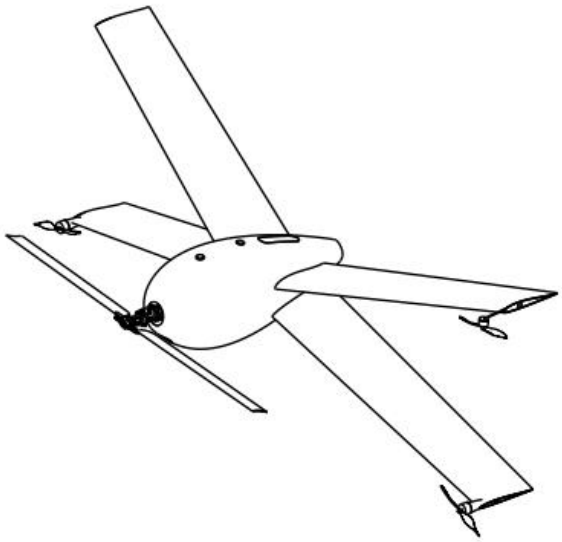

Figure 6.1: Isometric view of the UAV showing the four propellers

Figure 6.1 shows the chosen configuration for the propulsion system. The configuration consists of 4 propellers in total: one hover propeller with a swashplate located in front of the aircraft, two fixed pitch cruise propellers attached to the two bottom wings and one propeller used during hover to counter-act the torque of the main hover rotor located on the right top wing. The main reason behind the selected setup is to split the functionality of the propellers between the cruise and hover phase, that require very different propeller designs for efficient operation. With separate propellers higher efficiency at lower power consumption can be achieved. The cruise propellers can function at higher RPM with a decreased blade radius and the hover propeller can have more advantageous geometry and rotate at slower, optimal velocity. The weight of the motors can be decreased as high RPM, low torque motors are generally lighter than low RPM, high torque motors and also more commercially available. A drawback of this configuration is the need for four different motors of three different types. Nevertheless, with this configuration, the motors do not have to work at very different operating points and it is therefore possible to select them such that they operate at a high efficiency point, reducing the electric power required for propulsion. Furthermore, to harvest maximum efficiency of the hover propeller, the swashplate allows for 100 degrees of rotation, which will place the hover blades horizontally during cruise flight. This allows them to be used as canard lifting surface that help with the control and stability of the UAV and decreases the drag produced by the hover propeller during horizontal flight significantly. Considerations about the stability of the UAV and the torque control can be found in chapter 5.
The cruise propellers will be placed at the tips of the bottom wings. They will have a fixed pitch and orientation. For maximum efficiency they are placed as far as possible from the hover propeller and fuselage such that they

will receive maximum undisturbed flow. This also improves the yaw control that can be achieved with them, which is outlined in chapter 5. Further it allows the UAV to pitch up more quickly and recover from a diving manoeuvre.
An added benefit found from chapter 5 was that placing the propellers at the bottom meant that the aerodynamic centre would move behind the centre of gravity, thus reducing the amount of sweep that would be required to stand on the ground. Another major benefit of having the centre of gravity ahead of the aerodynamic centre is that it makes the UAV statically stable[15], which results in the UAV being less dependent on the canard making it more effective as a control surface. Lastly this means that the distance between the canard and the main wing can be maximised thus interference between the two will be minimised.
Finally, the torque propeller will be placed on the top-right wing of the UAV, facing in direction normal to the wing surface, attached to an extension rod that will move its wake away from the wing surface. It will be activated only in hover to counteract the torque of the hover propeller. In cruise it shall be locked in feather position to minimise the produced drag.
All propellers are mounted in a standard puller configuration mainly due to the high sweep of the UAV planform and the need for ground clearance upon landing, which needs to be in the range of 10 - 20 cm for landing on grass.

6.2. Theoretical Background

To achieve the best possible design and most accurate results for each of the four propellers it was decided to apply three different aerodynamic theories. Lifting Line Theory (LLT) is based on the discrete vortex sheet distribution over the rotor blade, while Blade Element Momentum Theory (BEM) uses momentum conservation and force balance to estimate the thrust and torque of a propeller. They are both used to determine the dimensions of the propellers at the required level of thrust (determined by the total drag of the aerodynamic configuration). Both approaches have some limitations, which can be avoided by using both of them at the same time in an iterative setup. Next to that Actuator Disk Theory (ADT) is used to verify the sizing of the hover propeller. ADT is usually applied during the initial sizing of helicopter rotors, which is why it is not effective for the cruise propeller design. The following section discusses how the theories were applied to obtain all four propeller designs.

6.2.1. Lifting Line Theory

The Prandtl Lifting Line Theory is a computational model of the aerodynamics of a propeller that treats the blades as a number of 2D sections. A detailed explanation can be found in [24]. The method attempts to find the velocity induced by the vortical wake of the blades, then find the induced angle of attack along the length of the blade. With the induced angle of attack, the lift on each of the sections can be determined and by integrating along the propeller blade the total lift can be found. Because the induced velocity is initially unknown this method is iterative and generally performed by computers. To use the lifting line theory effectively the effects of the wake on the blade and then blade on the wake are attempted to be taken into account. This allows some 3D effects to be calculated but because small disturbances are assumed it fails to model the strong 3D effects near the root and tip of the blade.
XROTOR [10] is a software that uses the lifting line theory. It tries to find a propeller design with minimum induced losses. It specifically uses the Graded Momentum Formulation, which relies on the Betz-Prandtl tip loss fudge factor which assumes that the rotor has a low advance ratio, generally less than 0.5, which is applicable to our design case.It further assumes that the disk loading is relatively low and hence the wake contraction and the wake self-deformation are small. The advantage of this theory is its computational economy.
XROTOR was chosen as it has been used at the Faculty of Aerospace Engineering at TU Delft and also in hobby applications and proven sufficiently accurate in propeller design. It was developed by Mark Drela of MIT.
XROTOR takes as input airfoil data, in which the $C_l - \alpha$ curve is approximated as linear and the $C_l - C_d$ drag polar is assumed quadratic. Then the flight altitude is set and the density and speed of sound is calculated using the International Standard Atmosphere. Following this, a design point can be specified. In order to do this a tip radius, a hub radius, RPM, desired thrust and C_l are entered. The hub radius is the radius in which the propeller is connected to the motor shaft and no airfoil will be present. This was assumed to be 1 cm during the design, which is in alignment with propellers of this size currently on the market. The desired thrust is received from the aerodynamics group and is the cruise drag divided by two as two propellers will be used for cruise. The tip radius and RPM are provided by the Blade Element Momentum Theory, explained in the following. The C_l values is the value at which C_l divided by C_d is maximum for the aerofoil. This design point allows maximum efficiency of the propeller design. However, in order to comply with dimensional limitations outlined later, the design C_l be lowered which will result in a larger chord.
One disadvantage of XROTOR is that it cannot be used for the design of the hover propeller due to the fact that the Lifting Line Theory doesn't converge at low airflow velocities. For the hover design a custom software was

developed outlined later in the chapter.

6.2.2. Blade Element Momentum Theory

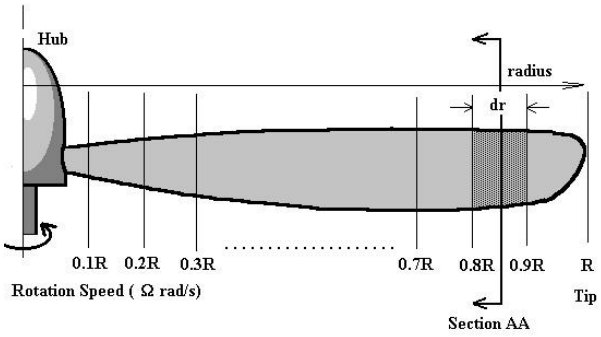

Figure 6.2: Blade Sectioning[1]

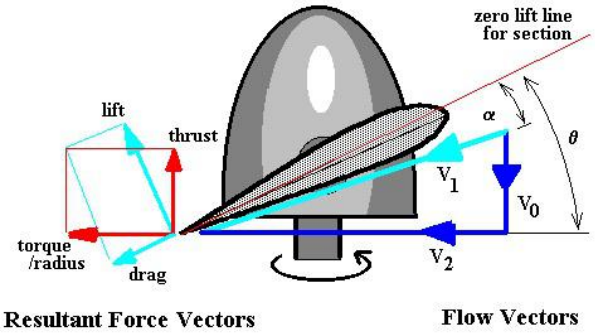

Figure 6.3: Force balance at each propeller section[1]

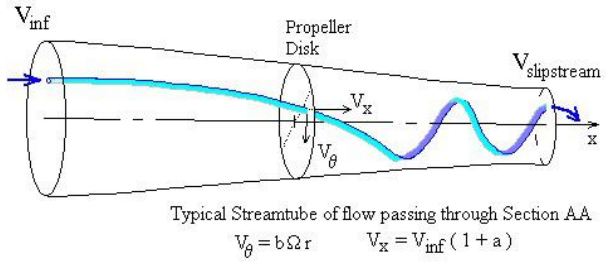

Figure 6.4: Streamtube model used for Actuator Disk Theory[1]

Complementary to XROTOR, which is based on the Lifting Line Theory, a program was written to implement Blade Element Momentum (BEM) Theory and cross-verify the results of XROTOR. The method is applied in two different ways. First, it is used to start the iteration and roughly estimate a design point established on the lowest power required from the range of possible combinations of propeller's diameter, chord length and geometric hub-to-tip and pitch angles and operational RPM. Those results are later fed to the XROTOR to refine the blade geometry - chord distribution, pitch and twist. Secondly, to verify the results of the iterations, a distribution of thrust and torque across the blade can be plotted. This method has a range of limitations i.a. it is not accounting for 3D effects that lead to theoretical efficiency error in range 5-10%[2]. Next, the chord is assumed to be constant throughout the length of the blade and geometric twist is assumed to be linear. Another limitation observed during analysis is the lack of the convergence of the solutions at conditions close to stall of the blade segment. Additional conditions had to be implemented to improve the accuracy of solution. Some sources [25] suggest different approach to ensure the convergence, yet they require use of very advanced algorithms that combine empirical (e.g. Glauert's method) and analytic solution regions. Finally, throughout analysis of the blade with fine mesh, which usually improves convergence, is also computationally expensive and hence time-consuming. Application of more efficient, low level programming language would be advisable for further development. Beside its limitations, BEM enables for assessment of blade efficiency in a range of operational conditions and realising the progress of propeller blade stall, which helps to pin down a design point and investigate the sensitivity of that point to i.e. changing RPM, pitch or flight velocity.
To estimate thrust T and torque Q and basing on that efficiency η and shaft power P_{in} required following equations are applied:

$$V_0 = V_{\text{inf}}(1+a) \tag{6.1}$$

$$V_2 = \Omega(1-b)dr \tag{6.2}$$

$$V_1 = \sqrt{V_0^2 + V_2^2} \tag{6.3}$$

$$\phi = \tan(V_0/V_2)^{-1} \tag{6.4}$$

$$\alpha = \theta_b - \phi \quad (C_d, C_l) = f(\alpha) \tag{6.5}$$

$$\Delta T = \frac{1}{2}\rho V_1^2 c N_b (C_l cos(\phi) - C_d sin(\phi)) \tag{6.6}$$

$$\Delta Q = \frac{1}{2}\rho V_1^2 c N_b (C_l sin(\phi) + C_d cos(\phi))dr \tag{6.7}$$

$$\Delta T = 4\rho\pi r V_{\text{inf}}^2 a(1+a)dr \tag{6.8}$$

$$\Delta Q = 2\rho\pi r^3 V_{\text{inf}}^2 b(1+a)\Omega dr \tag{6.9}$$

$$T = \sum \Delta T \tag{6.10}$$

[1] URL `https://goo.gl/yd3vDD` [cited 25 June 2017]
[2] URL `https://community.dur.ac.uk/g.l.ingram/download/wind_turbine_design.pdf` [cited 25 June 2017]

$$Q = \sum \Delta Q \tag{6.11}$$

$$n = \frac{\Omega}{2\pi 60} \tag{6.12}$$

$$C_T = \frac{T}{\rho n^2 D^4} \tag{6.13}$$

$$C_Q = \frac{Q}{\rho n^2 D^5} \tag{6.14}$$

$$J = \frac{V_{\text{inf}}}{nD} \tag{6.15}$$

$$\eta = \frac{J}{2\pi}\frac{C_T}{C_Q} \tag{6.16}$$

$$P_{in} = Q\Omega \tag{6.17}$$

$$P_{out} = T V_{\text{inf}} \tag{6.18}$$

BEM approach is built upon iterative calculations of the axial a and angular b components of velocity at each of the two-dimensional blade sections. As for simple 2D aerofoil, the force balance is applied to each section to estimate lift and drag (see eqs. (6.6) and (6.7)) and as a result thrust and torque can be obtained, which are then multiplied by amount of blades N_b. At the same time thrust and torque components can be calculated from axial and angular momentum conservation (Bernoulli's law) within the stream tube boundary swept out by the blades of the propeller, see fig. 6.4. Equations eqs. (6.9) and (6.10) can be applied, which together with equations eqs. (6.1) and (6.2) create a system of 6 non-linear equations to solve for 4 unknowns: a, b, T, Q. In the numerical solution of the problem, inflow components a, b are first guessed and then ΔT and ΔQ are calculated with the force balance. Then, the new a, b are re-calculated with momentum conservation. This procedure is repeated until convergence is reached. A more detailed overview of the BEM Calculator code used is represented on the Flow Diagram, fig. 6.5. The overall process involves two more functions: a functions

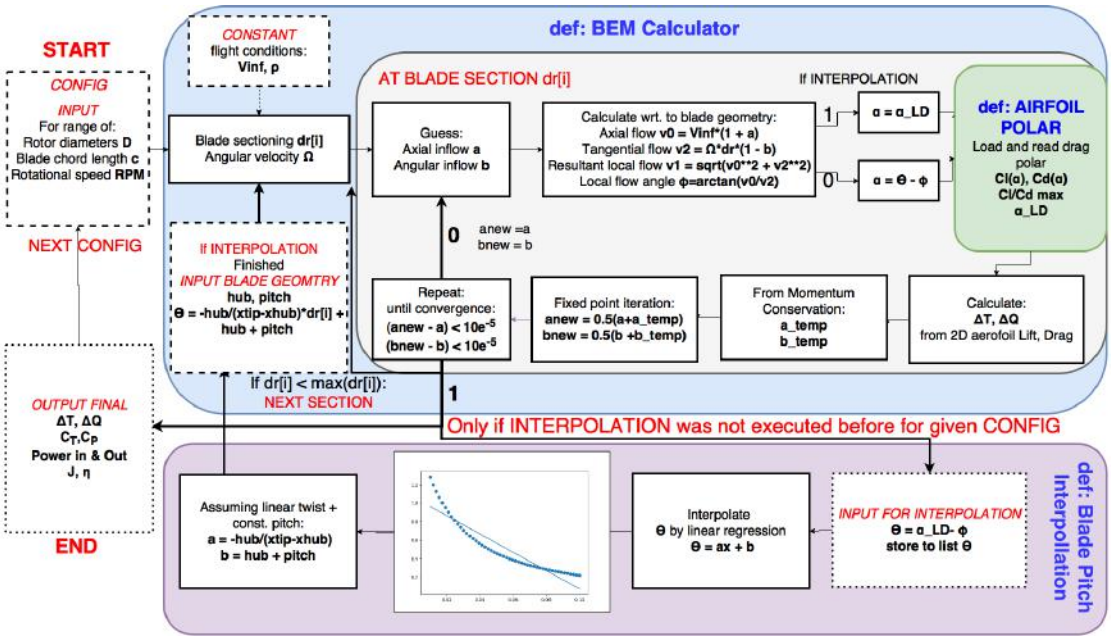

Figure 6.5: BEM Calculator code flow diagram

that reads the aerofoil polar to obtain the C_l, C_d components based on the local angle of attack and another functions that re-evaluates the aerofoil geometry. The purpose of the Blade Pitch Interpolation function is to sort out ill-conditioned propeller geometries leading to stall at the majority of the blade length. It assumes linear (thus not ideal) total blade pitch, which is a combination of geometric blade twist and constant pitch. It considerably improves the results, as can be seen on figs. 6.6 and 6.7.

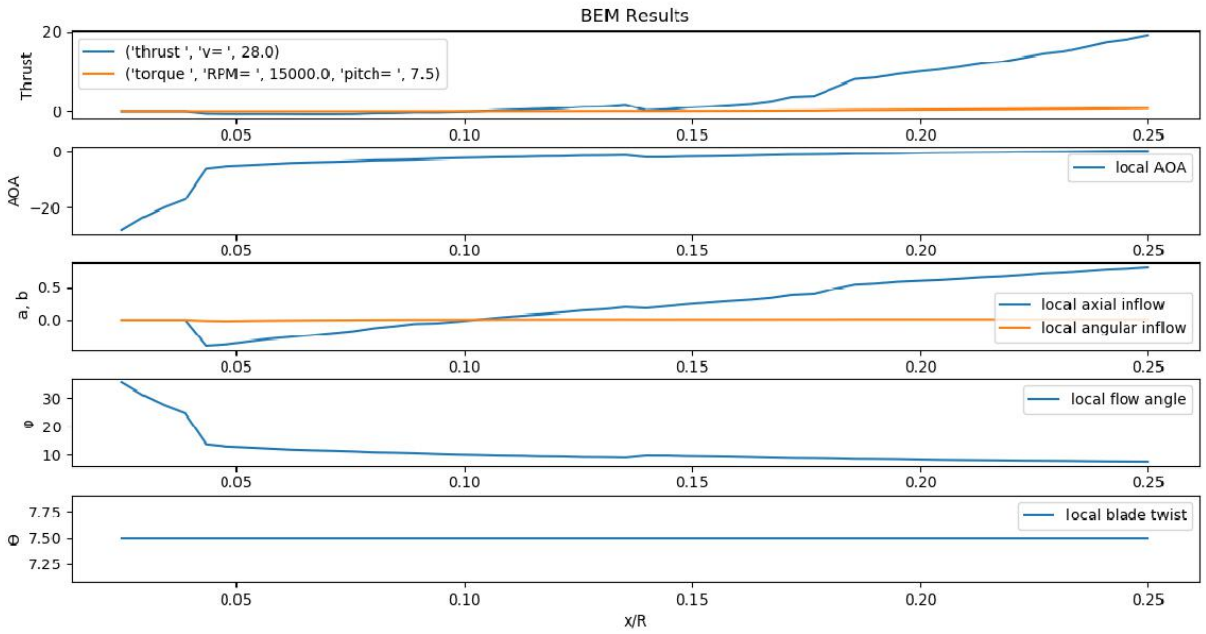

Figure 6.7: Ill-conditioned result leading to stall propagating from blade tip.

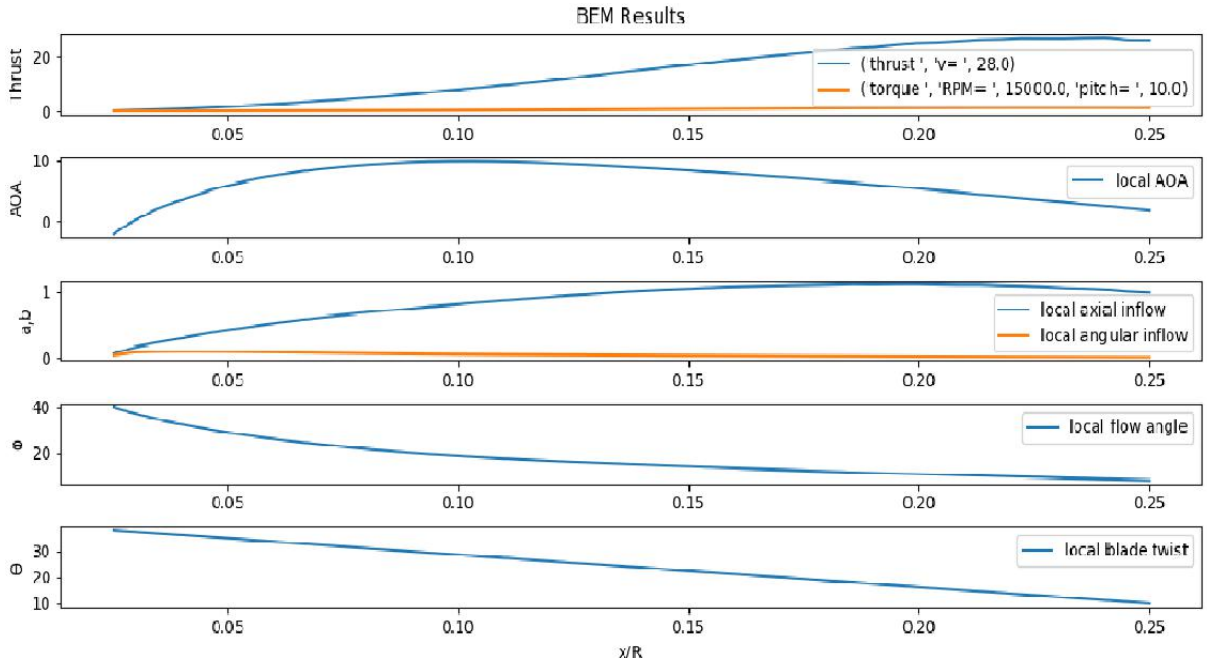

Figure 6.6: Improved blade geometry not leading to stall.

The design points are then chosen based on the minimum power required for the amount of thrust the propeller has to produce. The results are fed into XROTOR which refines blade geometry and the solutions are compared. The results of successive iterations are presented in table 6.1. Figure 6.8 presents an example output of the optimisation algorithm for minimum power required at required thrust below 5N for a range of geometric inputs: diameters between 0.1-1m, chord lengths between 0.1-0.006m, and RPM from 20000 to 1000. Blue dots are all valid configurations, while red ones represent the minimum power design points. One see observe a decreasing trend in relation between power and design of a propeller, which corresponds generally high RPM-small diameter designs.

6.2.3. Verification and Validation

Table 6.1 presents the comparison of the results obtained with two different approaches. The difference in blade geometry is visible as chord and blade pitch change across the blade of the propeller, yet the final results sums up to comparable values for thrust, torque and efficiency. This is due to the fact that XROTOR

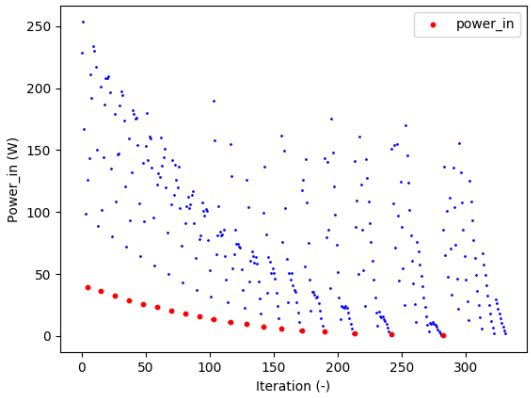

Figure 6.8: Power optimisation code output.

re-distributes the chord length and applies a suitable blade twist to that, while BEM code assumes the blade to be of constant width. Thanks to refining in XROTOR the chord decreases, efficinenct usually increases For the results of hover propeller sizing please refer to the section below with Actuated Disk method explained.

Table 6.1: Blade Element Momentum and Lifting Line Theory results comparison.

	1			2			3		
	BEM	**LL**	**Error**	**BEM**	**LL**	**Error**	**BEM**	**LL**	**Error**
R [m]	0.10	0.10	-	0.089	0.089	-	0.09	0.09	-
RPM	7000.00	7000.00	-	10000.00	10000.00	-	15000.00	15000.00	-
c_{avg} **[m]**	0.030	0.018	-71%	0.020	0.018	-9%	0.0130	0.0124	-5%
T [N]	3.93	3.93	0%	4.48	4.55	2%	4.15	4.20	1%
Q [Nm]	0.18	0.18	1%	0.14	0.14	-2%	0.09	0.09	0%
P_{in} **[W]**	132.47	134.00	1%	150.98	149.00	-1%	143.94	142.00	-1%
Efficiency	0.82	0.81	-2%	0.82	0.85	3%	0.80	0.82	2%
hub angle [deg]	55.50	50.63	-4.87	51.25	54.31	3.06	50.00	54.33	4.33
pitch angle [deg]	16.77	29.32	12.55	14.50	18.53	4.03	10.30	13.85	3.55

6.2.4. Actuator Disk Theory

$$P_{id} = T\sqrt{\frac{T}{2A\rho}} \tag{6.19}$$

$$FM = \frac{P_{id}}{P_{meas}} \tag{6.20}$$

$$DL = \frac{T}{A} \tag{6.21}$$

$$PL = \frac{mass}{P_{meas}} \tag{6.22}$$

Actuator Disk theory or momentum theory is based on momentum conservation in the streamtube spanned by rotor blades, similar to the application of Bernoulli's law in BEM. ADT is widely used in helicopter design to perform the initial sizing of the rotor blades and often provides a statistical relation between helicopter mass, power and disk area through Disk Loading (DL)-Power Loading (PL) relation (see similarity with aerodynamic W/S, T/W diagrams). The literature[3][8] suggests that the figure of merit, which describes the propeller theoretical max efficiency for an efficient RC size propeller should be approximately 0.6, which should be a good indicator for the propeller design accuracy.

6.3. Constraints and Limitations

In the following section some of the constraints and limitations of the used methods are outlined. Further limitations concerning manufacturing are discussed.

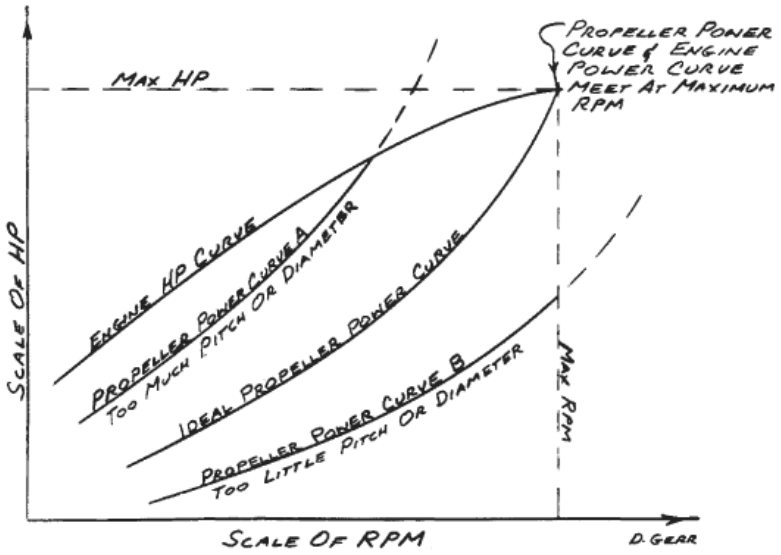

Figure 6.9: Propeller power curve indicating the influence of different design parameters[3]

6.3.1. RPM

Rate of rotation of a propeller blade is an essential parameter influencing blades design. For large propellers RPM is usually limited by a critical Mach number achievable at the tips of the rotor. Due to higher tangential velocity the tips are experiencing drag divergence before the central sections do. The general trend is that the propeller's diameter is decreasing with an increasing RPM. The problem is a trade-off between the propeller's diameter, the pitch and the velocity of rotation such that all sections of the blade are operating at their maximal achievable lift-over-drag ratio. It is theoretically possible to find an optimal configuration that would result in ideal power curve fig. 6.9, yet due to 3D interactions and non-linear aerodynamic effects taking place at the propeller blade it is a numerically very difficult problem and some approximations have to be made. During analysis of different geometric configurations, it was discovered that at an operational speed of approx. 28 m/s, with approx. 3.5-4.5N of required thrust, there are two main groups of propellers presenting a high efficiency performance: the large diameters ($0.3m < D < 0.8m$) with corresponding high chord length and RPM up to 5000, and the small diameters (0.1-0.2m) with an operational RPM around 15000 or more. For taking a design point, the second group of propellers is a more preferable choice. The reasoning behind it is decreased structural weight of the propeller and a more lightweight motor thanks to the lower required torque.

6.3.2. Dimensional Limitations

Minimum Chord A group manufacturing a UAV at MIT limited their minimum chord to 6 mm as it was not possible to manufacture an airfoil with a chord smaller than this [36]. Another method to determine a minimum chord is by analysing and limiting the local Reynolds number along the propeller chord. Low Reynolds numbers, typically lower than 50,000 are difficult to analyse numerically as the viscous forces in the flow become important. Another important factor is efficiency which tends to increase with the Reynolds Number [9]. The minimum chord can be calculated by solving the Reynolds number equation for the chord. The chord then depends on the speed, in this case the speed of the rotor at different radius locations. The speed is dependent on the RPM and the propeller radius. Once the RPM range and propeller radius range have been defined, the minimum chord can be calculated. This can also be done dynamically when testing different combinations during the optimisation process. Using a radius of 0.5 m and an RPM of 3000, the minimum chord should be for example 5.98 mm at the tip.

Aspect Ratio Propeller blade aspect ratio can be approximated by a eq. (6.23):

$$AR = \frac{R}{c_{avg}} \tag{6.23}$$

Equation (6.23) gives a good indication of blade slenderness. It is also an important design parameter that enables for verification of the design with respect to the standard dimensions used for propellers of similar applications. Different internet sources on RC application propellers indicate that an optimal AR is usually in

[3] URL `http://web.mit.edu/drela/Public/web/qprop/motorprop.pdf` [cited 23 June 2017]

range of 6 to 8[4,5]. At the same time helicopter design theory indicated that helicopter propeller AR should be in the range of 14 to 20[3]. Those values are taken as a safety check and as an indication of a good design.

6.4. Propeller Selection

The following section discusses the choice of the design parameters for all four propellers mounted at the UAV system. The results were obtained and verified with the use of XROTOR and BEM.

6.4.1. Cruise

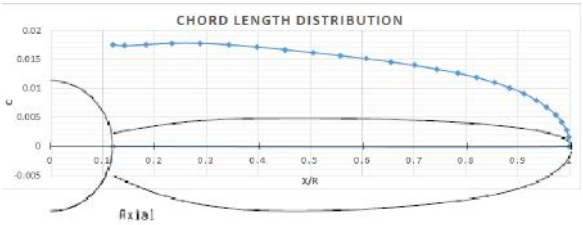

Table 6.2: Cruise propeller chord length distribution

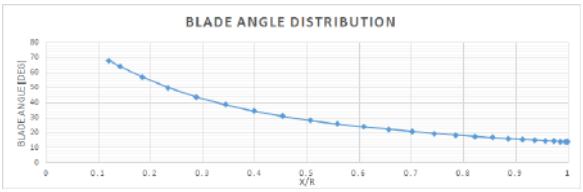

Table 6.3: Cruise propeller blade angle distribution

Cruise Propeller Design	
Aerofoil	CLARK-Y
R [m]	0.085
RPM	15000
c_{avg} [m]	0.017
T [N]	4.20
Q [Nm]	0.09
P_{in}[W]	142
η	0.82
hub angle [°]	54.335
pitch angle [°]	13.851
AR	6.54

Table 6.4: Cruise propeller parameters

The final iteration on the cruise propeller design resulted in the parameters presented in table table 6.4. The propeller of 0.085m, including a 12% hub radius, will have two blades with a rather high geometric blade twist angle of approximately 54° at the hub, decreasing in a quasi-quadratic manner to the tip where the angle will be approximately 14°. Table 6.2 presents the geometric chord distribution overlapped with the XROTOR plot of the actual blade geometry. The aerofoil used for cruise propeller is CLARKY-Y with a high camber and a C_L at maximum L/D of 0.9505 (more explanation on the aerofoil choice can be found insection 6.6.1. The propeller operates at a constant orientation and RPM of 15000 in cruise flight. Two units of that type are going to be mounted at the lower wings' wingtips, providing 8.4N of thrust in total at the expense of 284W of power in cruise flight at a velocity of 27.7 m/s. Further characteristics of the propeller investigated with XROTOR presented on fig. 6.10 reveal good distribution of the blade efficiency across the length, operating at values above 0.8 at 80% of the blade length with C_l values ranging from 0.9505 to 0.4 at the tip.

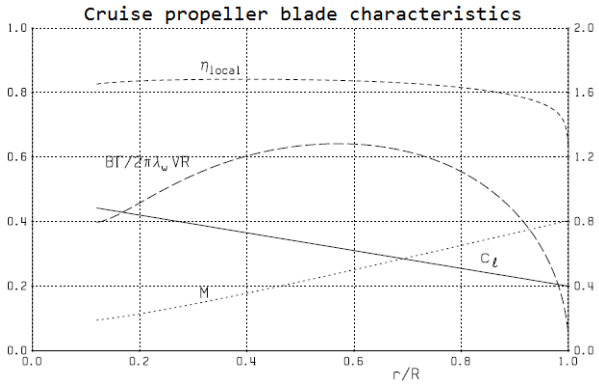

Figure 6.10: Blade lift, mach number and efficiency distribution.

[4] URL https://www.recreationalflying.com/tutorials/groundschool/propeller.html [cited 25 June 2017]
[5] URL http://dc-rc.org/pdf/Model%20Propellers%20Article.pdf [cited 25 June 2017]

6.5. Hover

Table 6.5: Hover propeller design parameters

Hover Propeller Design	
Aerofoil	NACA 0012
R [m]	0.44
RPM	3000
c_{const} [m]	0.06
T take-off [N]	98.83
Q [Nm]	2.76
P_{in} [W]	957.41
η	0.82
hub angle [°]	0
pitch angle [°]	6.86
AR	7.33

The hover propeller has two straight, untwisted blades with an applied constant pitch of approximately 6.5° in hover, achieved by a deflection of the swashplate. It uses the symmetric NACA-0012 aerofoil. Such a design allows the propeller to be used as a canard surface, fixed in the horizontal position, without generating negative lift, stalling or additional pitching moment, which could negatively affect the UAV's stability. In cruise the propeller is expected to produce around 8 N of extra lift. A straight blade has the additional advantage of being easy to produce. The propeller will be rotating at a rather low RPM of 3000 revolutions per minute and will produce almost 100 N of thrust during take-off, which will allow to reach 45 meters altitude - the minimum for the transition manoeuvre in 6 seconds or less from the moment engine had been started. Using the Actuated Disk Theory, power loading, disk loading and the figure of merit of the propeller can be calculated:

$$DL = 2.849 \quad lb/ft^2$$
$$PL = 32.806 \quad lb/hp$$
$$P_{id} = 630.4 \quad W$$
$$FM = 0.6584$$

The resulting FM of 0.6584 is within the reasonable limit for the small-scale propeller and indicates good propeller efficiency. Aspect Ratio of the propeller is smaller than indicated by the helicopter design theory values of 14 to 20, yet this can be explained by UAV mass being incomparably smaller than one of the full-sized helicopter. Blades of aspect ratio higher than 10 would be too thin to be manufactured. Unfortunately, due to the limitations of both XROTOR and BEM calculator (close to zero flight velocity leads to divergence of the results and ill-conditioned analysis), it is not possible to perform a reliable investigation of hover propeller's performance with these software. Wind-tunnel testing or CFD analysis would be advisable to enable its performance assessment with increased accuracy.

6.5.1. Torque Propeller

In contrast to the design of the cruise and the hover propeller, the torque propeller is not tailored to the particular UAV. The torque propeller is used in short manoeuvres only, which means that the efficiency is not a strict requirement for the propeller selection. Therefore, off-the-shelve propellers would suffice. The main purpose of this roll propeller is to counteract the torque that is produced by the hover propeller during hover flight. Additionally it may provide yaw control in hover manoeuvre. Therefore, the main selection requirement is the required thrust. The selected hover propeller produces a torque of 2.76 Nm. As the wing span of the aerofoil is 0.84 m, which was determined in chapter 4. Therefore, the propeller needs to produce a minimum of 3.29 N thrust. The propeller will be mounted on the top left wingtip of the UAV facing in direction normal to the wing surface, such that produced thrust will be exactly at 90° with the moment arm and maximum torque will be produced. Extension rod may be necessary to place the propeller behind the edge of the wing and thus avoid creating swirl flow hitting the wing directly beneath it. This creates additional bending moment on the wing, so the structural design of torque propeller mount should be carefully considered. With this requirement, the Aerostar carbon fibre propeller is selected as the roll propeller. In combination with this propeller, a suitable motor was selected. The selected motor and its properties are given in section 6.9. The properties of the propeller and motor combination are listed in fig. 6.12.

Figure 6.11: Roll propeller[6]

Figure 6.12: Roll propeller/motor characteristics

Property	Value
R [m]	0.076
RPM	15160
T [N]	4.51
P_{in} [W]	125.4
η [G/W]	3.7

6.6. Aerofoil Selection

In the aerofoil selection procedure different aerofoils are selected for the cruise and hover. As tailored designs are made for both the cruise propeller and the hover propeller, aerofoils should be selected for the specific purpose of these propellers. For the torque propeller however, an off-the-shelf propeller is chosen. Therefore, no specific aerofoil selection has taken place for the chosen propeller.

6.6.1. Cruise

For the cruise propeller, four different aerofoils are considered to be used in the design of the propeller. The four aerofoils selected present good properties for the cruise propeller purposes [2]. In addition to that, the aerofoil of the DelftaCopter [38], the MA409, is also investigated and considered for the design. The selected aerofoils are presented in fig. 6.13:

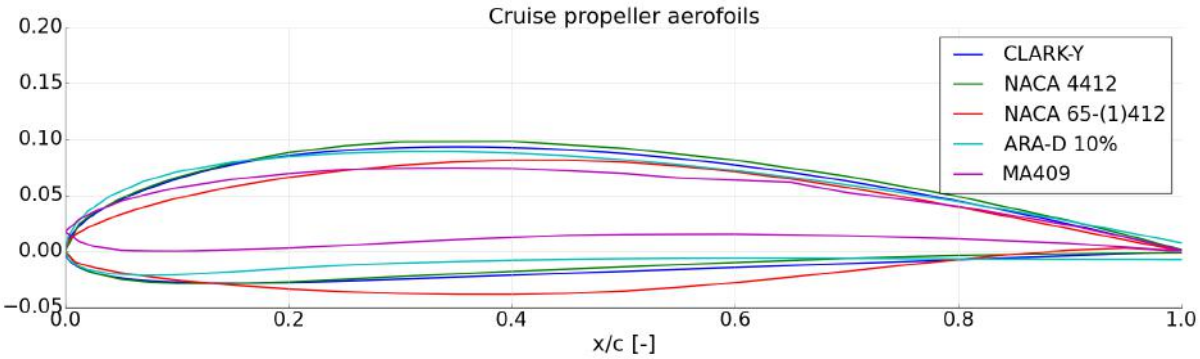

Figure 6.13: Cruise propeller aerofoils selected for analysis

For the five selected aerofoils, a power analysis was executed to determine which aerofoil has the best performance characteristics under cruise condition. The characteristics are determined at the average airspeed of the UAV, 27.7 m/s. The propeller setup for which, each of the aerofoils was investigated had the same properties: rotational speed of 15000 RPM, 2 blades, thrust of 4.2 N and a diameter of 0.170 m. In table 6.6, the power comparison for each aerofoil is presented. The aerofoil with the lowest power required is the CLARK-Y, which is chosen to be incorporated in the cruise propeller design.

Table 6.6: Cruise aerofoil selection

Aerofoil	ARA-D 10%	Clark-Y	NACA4412	NACA 65-(1)412	MA409
Power [W]	146	142	160	168	173

6.6.2. Hover

Furthermore, the hover propeller aerofoil was chosen. Again for this purpose, four different aerofoils are selected. The hover aerofoil has additional requirement that it must comply with, since the aerofoil should be symmetrical. This requirement stems from the fact that the propeller will be used as a canard during cruise flight. For an asymmetrical aerofoil in this formation, one aerofoil would orientated such that it has negative camber. This is a result of the limitations of the swash-plate. For the aerofoil selection, a variety of the maximum thickness locations and t/c ratios were included such that there is diversity in the selection. The selected aerofoils are listed in fig. 6.14:

[6] URL `https://hobbyking.com/en_us/aerostar-carbon-fiber-propeller-6x4-1pcs.html` [cited 22 June 2017]

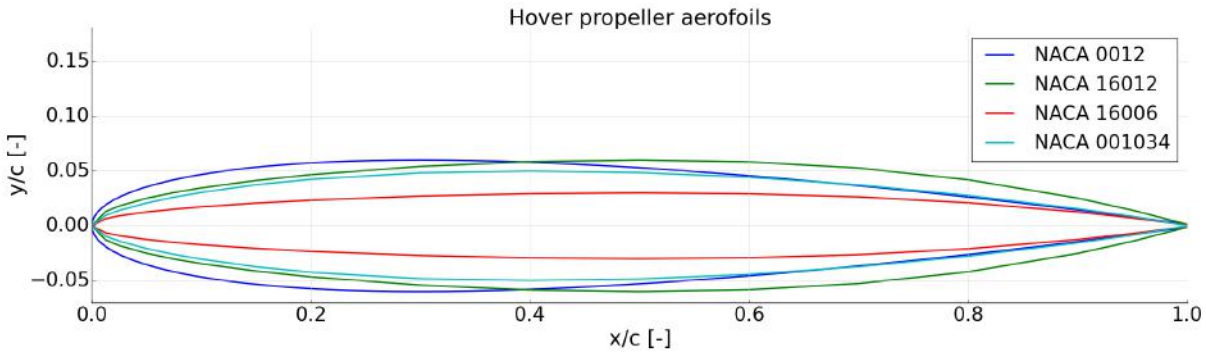

Figure 6.14: Hover propeller aerofoils selected for analysis

Again, a similar power comparison is performed as was for cruise, but with an air velocity of zero. The results are indicated in table 6.7. The aerofoil with the lowest power required is the NACA 0012 and will be used in the final hover propeller design.

Table 6.7: Hover Aerofoil Selection

Aerofoil	NACA 0012	NACA 16012	NACA 16006	NACA 001034
Power [W]	868.41	1070.72	1084.19	1038.30

6.7. Noise Profile

Another characteristics of the cruise propeller investigated with XROTOR is its noise profile. The resultant instantaneous sound pressure is plotted against the distance from the source of sound. The designed propellers are very silent. As can be seen in fig. 6.15 the noise heard on the ground with the UAV flying at 40 m above at 27.7 m/s would not exceed 47dB for one propeller. For two propellers 3dB have to be added[7], so the sound heard would be 50dB, which is comparable to the average noise level in a quiet room, even below the loudness of human speech heard from the distance of 1 to 2 meters. fig. 6.16 shows a two-dimensional representation of the noise produced by the propeller. Here the contour lines present the regions experiencing the same noise exposure with values in decibels marked at the edges.

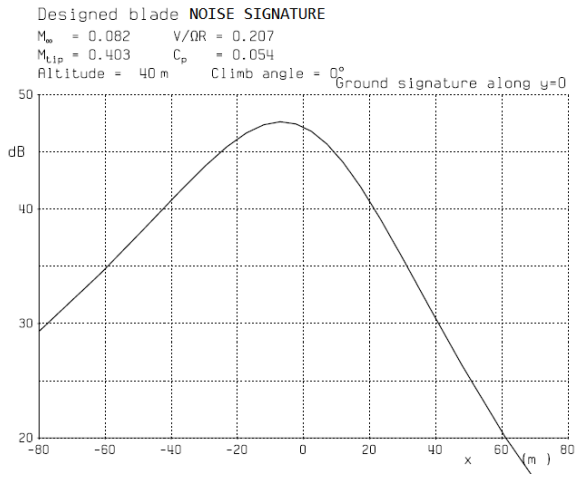

Figure 6.15: Cruise propeller noise profile heard on the ground with the UAV moving overhead at cruise speed of 27.7 m/s at 40 m altitude to the right

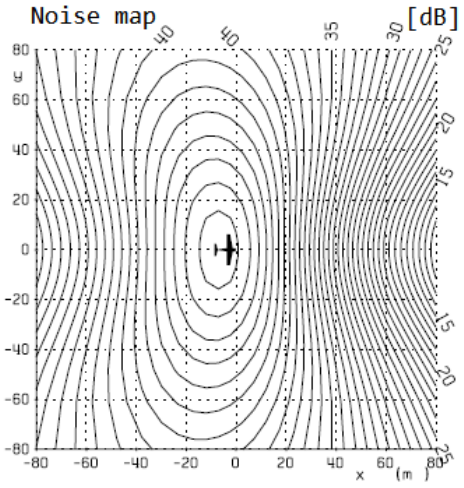

Figure 6.16: 2D propeller noise map showing the sound heard at location x, y = 0, 0 with the UAV moving to the right

6.8. Performance Analysis

Cruise is the most critical phase of the UAV mission, hence it is important to analyse its performance under changing flight conditions. To achieve that BEM calculator was used for the cruise propeller configuration

[7] URL `http://hep.physics.indiana.edu/~rickv/Multiple_sources.html` [cited 26 June 2017]

under range of variable flight speeds. This gives a good indicator of chosen design efficiency even if assumed cruise speed has to be changed, or UAV experiences a gust of wind changing its relative airspeed. The results are presented below:

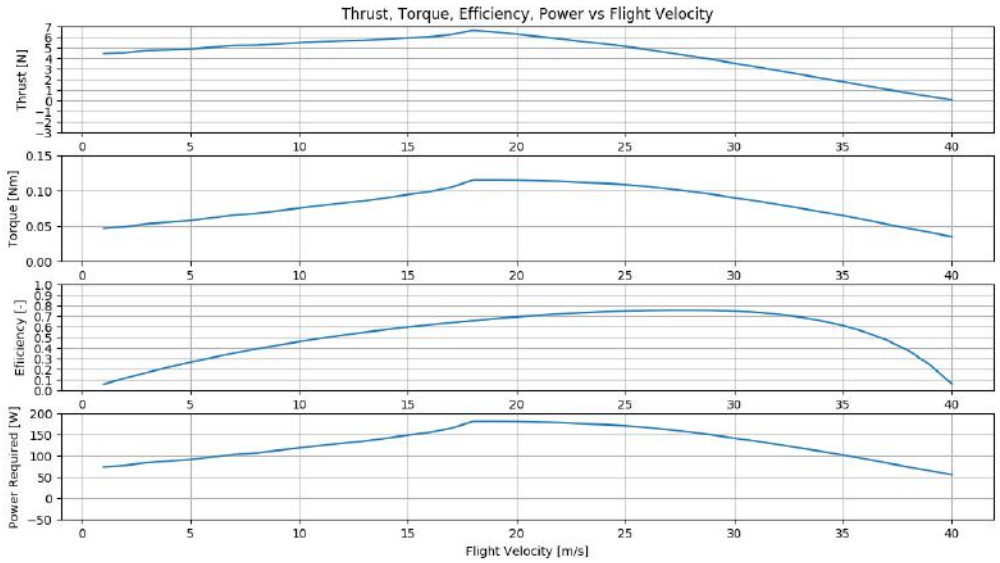

Figure 6.17: Performance graphs for the cruise propeller

It can be seen that the best performance of the propeller can be achieved at cruise velocity around 27.7m/s, but at the same additional thrust can be produced at cost of increase in power input. At maximum 2.5N of thrust can be produced for 40 Watts extra of power at velocity around 18m/s. That can be preferable when flying against strong headwind or when needed to accelerate the UAV quickly. The propulsion system has a maximum operational speed of approx. 41m/s at that RPM/pitch setup, thus flying at velocities above 35m/s should be avoided. There is a visible kink in the graph appearing below 20m/s, it is caused by problems with convergence of the solution at highly twisted sections of the blade. Increasing the resolution even further does not solve the problem. As discussed in section 6.11 additional solutions need to be implemented in the code to guarantee BEM convergence at all points.

6.9. Motor Selection

Propellers have 3 major requirements on the motors: shaft power, torque and frequency of rotation. These three parameters are related by eq. (6.17). High torque motors unfortunately requires a large moment arm and therefore a considerable rotor diameter. Because of this, high torque, slow rotating motors are heavy and low torque, fast rotating motors are lightweight. Gearboxes are often used to increase the torque of brushless motors. However, the vibrations they create disturb the IMU and it was therefore decided not to use them. The efficiency of a given motor is a function on the operating point, as illustrated in fig. 6.18. Efficiency has to be kept as high as possible for mostly two reasons:

- A motor with a higher efficiency results in energy and power savings and is therefore less demanding on the power subsystem.
- A lower efficiency results in greater amounts of heat generated. This extra heat might cause overheating problems and will require a more sophisticated cooling system.

Therefore, it is important to select a motor that will operate in its high efficiency region. Unfortunately, very few manufacturers provide data about the relations between efficiency, torque and frequency of rotation of their motors. Because of this, only two motors could be compared for the hover motor.

6.9.1. Hover motor

Two motors are investigated: the U-10 Plus and the MN5212[9,10]. The MN5212 is lightweight (249 g), works at high RPM (above 7500 RPM) but is inefficient (73% at operating point). The U-10 Plus is heavy (511 g) but works at lower RPM (above 3000 RPM), is more powerful and is more efficient (83% at operating point). It

[9] URL `http://store-en.tmotor.com/goods.php?id=364` [cited 26 June 2017]
[10] URL `http://store-en.tmotor.com/goods.php?id=378` [cited 26 June 2017]

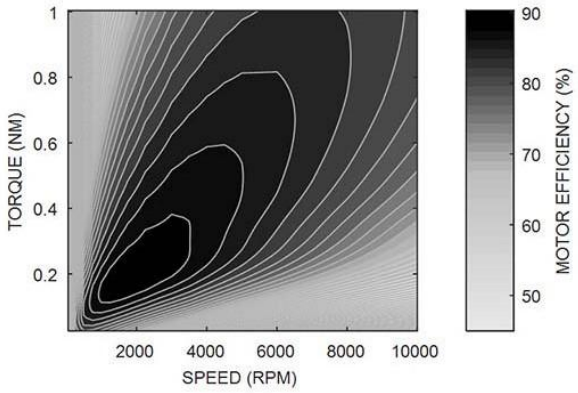

Figure 6.18: Example of a typical efficiency map of a brushless motor[8]

was decided to go with the heavier version for several reasons: the higher efficiency results in a lower power system mass, easier cooling, the extra power allows for faster and heavier take-offs, and the slower rotational frequency improves the propeller performances. The selected motor is shown in fig. 6.19.

6.9.2. Cruise motor

Since the cruise propellers rotate at much higher rotational frequencies, their torque is much smaller and these motors can be lightweight. The T-Motor F80 KV1900[11] was chosen because of its low weight (42 g) and its ability to deliver the required shaft power (244 W). Further specifications of the motor are unfortunately not available and tests will have to be performed to determine its actual performances. The selected motor is shown in fig. 6.20

Figure 6.19: The hover motor (U-10 Plus)[9]

Figure 6.20: The cruise motor (F80 KV1900)[11]

Figure 6.21: The torque motor (MT1806)[12]

6.9.3. Torque motor

For the torque propeller, a similar high RPM, low torque motor was chosen. The factor of major importance in the selection process was it's weight. MT1806 weights only 18g and is suitable to operate with 5 to 7 inches diameters propellers [12]. It is expected to deliver required 4.51 Newtons of thrust while operating at rotational speed of 15160RPM. The motor is depicted on fig. 6.21 and more information regarding its specifications can be found in table 10.3.

6.10. Swashplate Integration

Requirement MEUC-TUD-19 states that the system shall include a swashplate. The swashplate is integrated in the hover propeller and its deflection enables pitch and roll control (the third axis of rotation - yaw angle is controlled by a small torque propeller during hover and by differential thrust of the cruise propellers during cruise). On top of that, the swashplate has to allow for a large blade pitch deflection of at least 100° to put the

[11] URL `http://store-en.tmotor.com/goods.php?id=314` [cited 26 June 2017]
[12] URL `https://www.emaxmodel.com/emax-multicopter-motor-mt1806.html`

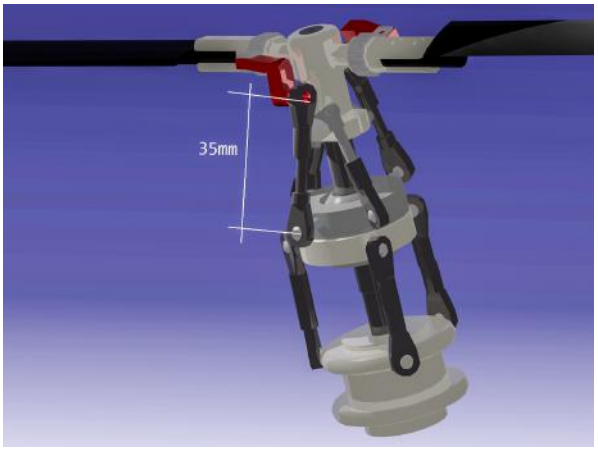

Figure 6.22: Swashplate in hover position

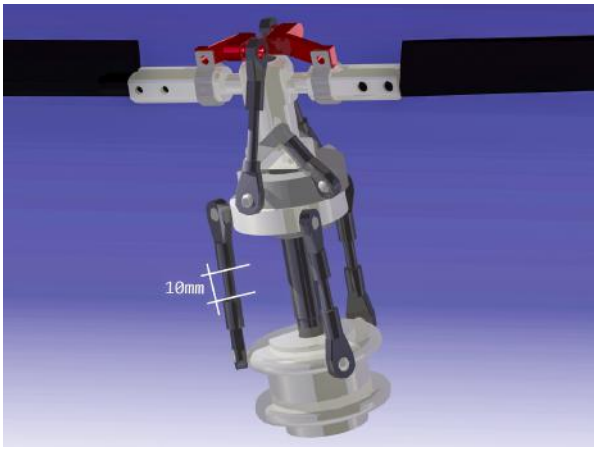

Figure 6.23: Swashplate in cruise position

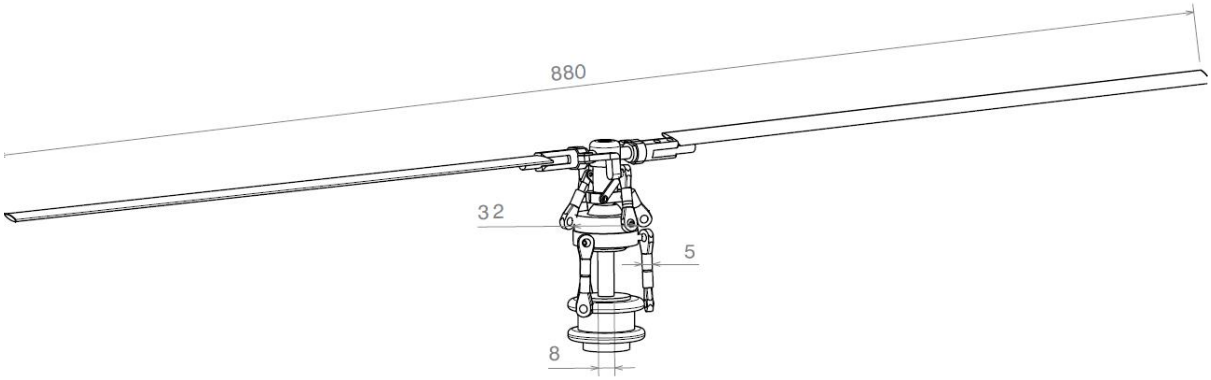

Figure 6.24: Swashplate CAD drawing

hover propeller in canard position during cruise (90° flip). An additional margin of 5° deflection in the fully vertical and fully horizontal position has to be possible, so that the blade can then serve as a control surface. The swashplate design presented in figs. 6.22 and 6.23 is a modified existing swashplate for a helicopter that has an increased range of rotation, as the original design enabled only a maximum of 80° rotation. The general principle of operation is the same as for every helicopter swashplate, the deflection of the blade is achieved by extension or contraction of servos attached to the swashplate (for the motor specification see section 8.3). Unequal vertical movement of the servos tilts the swashplate and through rigid linkages translates this to blade rotation movement. To achieve such a high pitch change some custom-made connections between the blade hub and the actuator attached to the rotating plate have to be made. This part is marked in red on the CAD renders above and its dimensions can be found in fig. 6.25. The sizing was based on the measurements taken from the CAD assembly with a scaled swashplate design and the actual size of the hover rotor blades, yet it shall be mentioned that depending on the choice of off-shelf parts used for mechanism assembly, the dimensions may change slightly. Things like minimum manufacturable thickness of the linkage heads, or distance of ball joints from the rotating plate can influence the design. In its final form the swashplate should be analysed in terms of the structural strength and build in such a way that its weight is minimised for the required loads. The extension (kinematics) of actuators causing rotation of the hub over range of angles should be possibly linear, such that control over the swashplate is easy to predict and implement in the autopilot. In the presented working case, the connector's dimensions can be seen in the drawing in fig. 6.25, the connector rods have a length of 35 mm and 95° blade pitch is achieved with a 10 mm extension of the actuators.

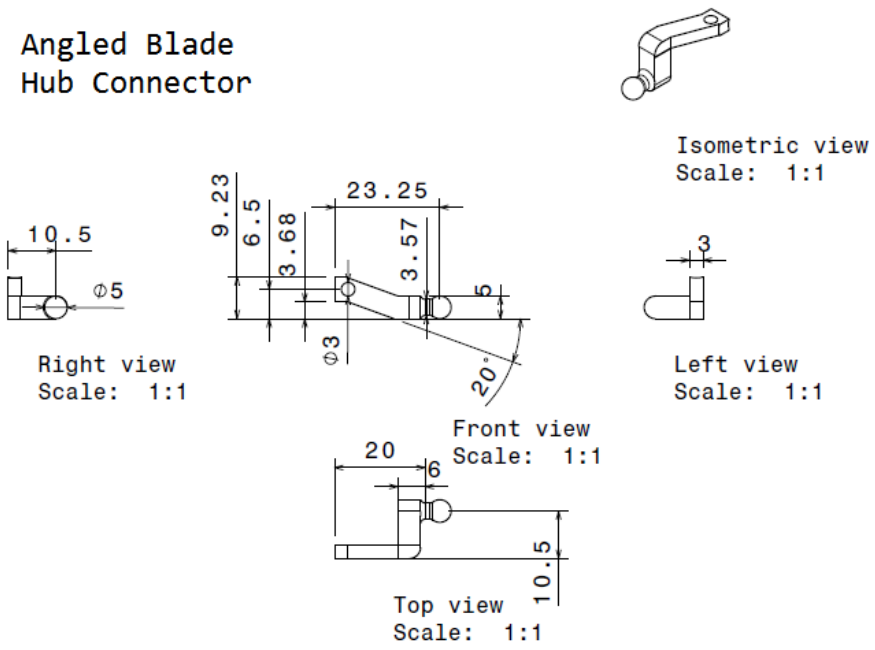

Figure 6.25: Custom-made blade hub attachment part dimensioned drawing

6.11. Conclusion & Recommendations

The motor selection for the cruise and hover propellers was based on the propellers' requirements for torque and rotational speed. The U-10 Plus was, despite its large weight (511 g), selected as the hover motor thanks to its good efficiency (83%) and high torque at low RPM. The specifications of the motor are unfortunately quite limited and testing the motor's performances should be performed in the later stages. The T-Motor F80 KV1900 was selected as the cruise propeller because of its low weight (42 g) and high power output (above 1 kWe). Unfortunately, no information is available about the efficiency of this motor. It is therefore recommended to test the cruise motor's performances in the future. Should the motor offer poor performances (for example low efficiency), a revision of the cruise motor selection should be performed.

For future development of the propeller design, there is a range of possible improvements that could be applied to achieve higher accuracy of the results. First of all, any of the tools used for analysis did not account for the unsteady 3D effects taking place at the rotor blades. Due to the complexity of these phenomena the best results can be obtained with wind tunnel testing and/or advanced CFD analysis. Secondly, aerofoil selection could be further extended, which should also include a complementary detailed drag polar database for a wide range of angles of attack. At highly twisted sections of the propeller blade, flow can reach very high (both positive and negative) values of angle of attack, which exceed the range of data available and lead to problems with the convergence of the solution. This leads to another problem observed with both LLT and BEM tools that do not necessarily converge for all ranges of flow velocities. Usually at very high RPM and high local flow angles, Blade Element Theory in the form it was applied, tend not to reach the desirable accuracy while iterating over inflow values. On the other LLT did not converge for high required thrusts.
LLT generated invalid solutions when the forward flight velocity was set close to zero, or zero, such as in the hover condition. That made the design of the hover propeller particularly difficult. There are methods [25] suggesting a guaranteed convergence by parametrisation of the problem, which simplifies the set of two non-linear equations to just one function of local inflow angle. The method further introduces different regions of solution set, where analytic and numerical methods have to be combined. This approach is out of scope of this analysis, yet presents a promising improvement to solution method. Finally, the BEM calculator that was written in Python takes a significant amount of time to iterate over some sections of the propeller blades, when the flow angle is high or changes rapidly (again a problem of convergence), which makes the whole optimisation process extremely time-consuming. It would be highly advisable to use low-level computational language to deal with at least some of the more computationally heavy parts of the calculations and to optimise the algorithms used by improving the search for suitable geometry solutions.

To reduce the drag of the torque propeller during cruise it should be investigated whether using a one-bladed propeller would be worth it. One bladed propellers can trail in the airflow and in theory produce less drag than

two bladed designs. However to produce the same amount of thrust the surface will have to be larger and/or the RPM higher.

7

Structural analysis

This chapter illustrates how the internal structure of the UAV has been investigated. The discussion is limited to the analysis of the internal wing structure. That structure is build out of a spar running through the wing planform from the root to the tip, a composite skin for the outer shell of the wing and a foam to fill up the empty spaces inside the wing structure.
The discussion on the wing loading for the main wings is given in section 7.1. It will be discussed for several different flight conditions. After that, the most critical one will be chosen to analyse the structural integrity of the spar within the structure, assuming that most of the bending loads are carried by the spar. The skin will be carrying the torsional loading which is negligibly small as will be discussed in section 7.1 as well as part of the shear force loading. The results of the spar analysis will be discussed in section 7.3. Material selection is an important step as well. Materials with sufficient strength properties should be chosen such that a certain level of structural integrity is reached.

7.1. Wing Loading Diagrams

The different flight conditions have a different loading scenario on the wing of the UAV. It is necessary to have an understanding of the effects of the different loading scenarios on the structure of the UAV. In this way a suitable choice for the critical loading case can be made for which the structural design can be sized. The following subsections will each describe a different loading scenario for the wing. In each of them the wing is modelled by its spar with a fixed connection at the fuselage intersection. The UAV is used in a few different conditions throughout its mission time such as: handling for transportation, hover, cruise flight, standing on the ground and landing at the moment of touch down. Standing on the ground is not taken into account because landing at the moment of impact has the same forces but just larger due to impact of the UAV with the ground. During the hover phase, the thrust is exerted upon the fuselage structure and it is expected that the wings are not loaded heavily. Either way, the loading during hover will definitely be lower than the loading during cruise. Hover is discarded from the list and no longer investigated. The three remaining flight conditions (Cruise flight, Landing at the moment of impact and Handling) will be discussed in the following subsections. Not only the external loading diagrams will be given, but also the internal diagrams. Those are the bending, shear force, normal force and torque diagrams.

7.1.1. Sign convention

Without a well defined sign convention and axis system, it is impossible for other people to follow the generated diagrams and understand the information that they include. Forces and moment are vector quantities. That means that they have a direction and sign. The direction is given with respect to the predefined axis system and the sign will be according to the agreed sign convention. fig. 7.1, fig. 7.2 and fig. 7.3 represents the chosen axis system that will be used throughout the chapter for defining forces and moments. When a force is acting in the direction of the axis, then it will be considered a positive force. In terms of moments, the right hand rule will be utilised.

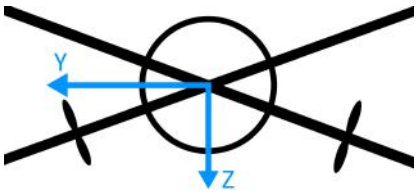

Figure 7.1: Sign convention y-z plane

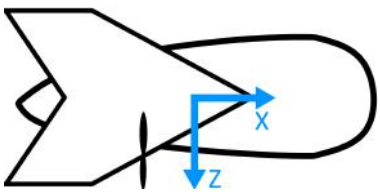

Figure 7.2: Sign convention x-z plane

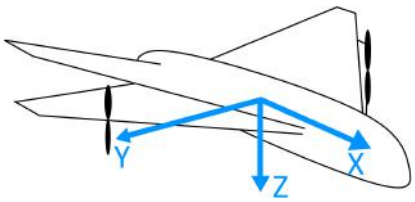

Figure 7.3: Isometric view

7.1.2. Cruise Flight

During cruise the swashplate of the hover propeller is used to turn the blades into a position where the Hover propeller can be used as an extra lifting surface (canard surface) and as control surface (elevons). On the two bottom wings, there are cruise propellers providing thrust as well as forming extra weight components.

Both wings will experience a lift, drag and moment distribution due to the pressure distribution over the wing planform. The structural weight distribution of the wing has to be taken into account as well.

There are four different half wings that are connected to the fuselage with a fixed connection. However, those four wings are in fact two pairs of wings with the same structural lay-out/external loading, the bottom half wings with the cruise motors and the top half wings without. The wing loading diagrams will be shown for one half wing with cruise propeller and one half wing without cruise propeller. The two other half wings are symmetric to one of those two.
The Free Body Diagram (FBD) of half a wing (applicable to both types) can be seen in fig. 7.4. For the wing without cruise prop, the value for weight and thrust of the cruise propeller should be considered zero.

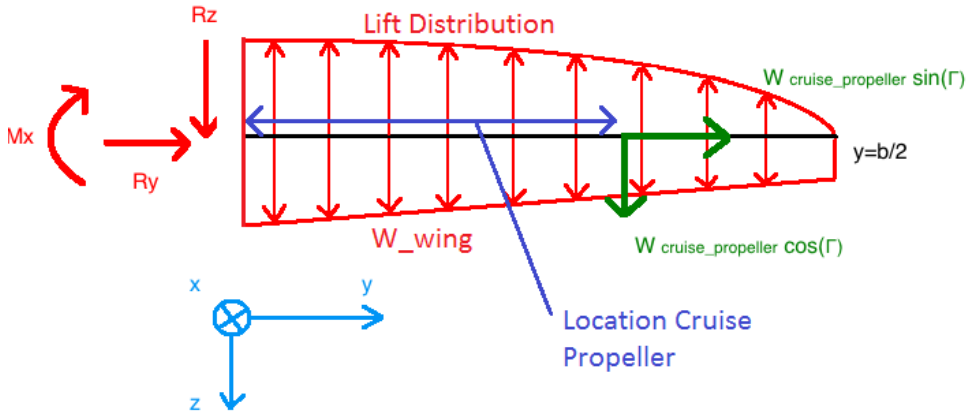

(a) External loading scenario (FBD/y-z-plane)

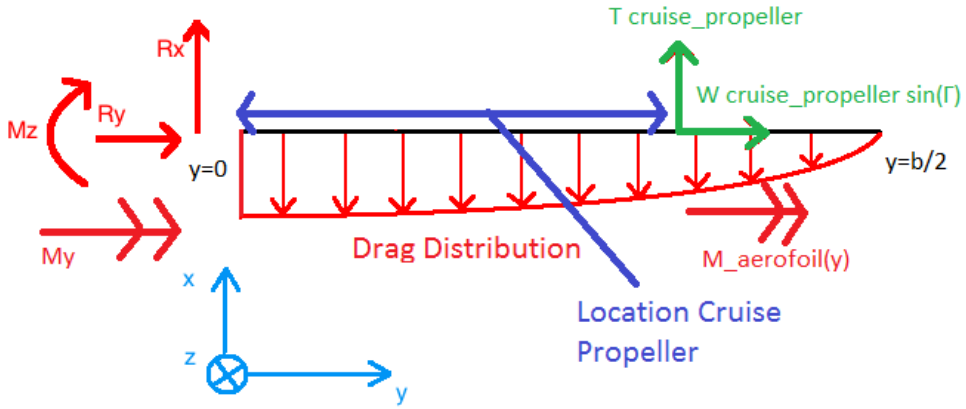

(b) External loading scenario (FBD/x-y-plane)

Figure 7.4: FBD of a quarter wing during cruise flight

The lift, drag and moment distribution acting upon the wing planform during the cruise phase should be known. It was decided to simulate these distributions using the wing and plane analysis function of the open source software XFLR5 [34]. The final design was modelled within this software without including the fuselage body because the software is not capable of dealing with complex and relative large bodies. The model as used within the software can be seen in fig. 7.5. The lift distribution is multiplied with 5.5 which is the design load factor. That is the maximum load factor encountered during flight times a safety factor of 1.5 which is widely used within structural design. The maximum load factor of 3.67 is achieved during the transition phases as explained in chapter 5.

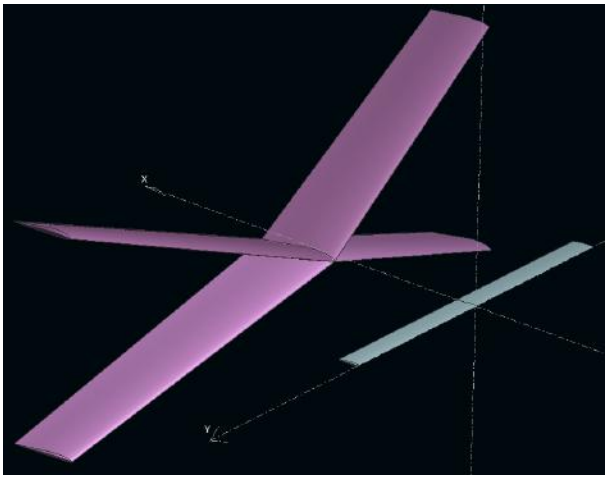

Figure 7.5: Final design XFLR5 model

The above shown planform was analysed at the cruise velocity of 27.7 $\frac{m}{s}$ and at an altitude of 380 m above sea level. The distribution should be generated for the cruise angle of attack α_{cruise}. This α_{cruise} is determined using the design lift coefficient of the aerofoil $C_{l,\text{des}}$ which is equal to 0.3907. Analysing the $C_l - \alpha$-plot of the HS520-aerofoil generated for the correct Reynolds number of $3.6E^5$. At a C_l equal to $C_{l,\text{des}}$, the α_{cruise} becomes 2.3 °.
Now that the external loads are known, the internal loading diagrams for the two types of half wings can be constructed using the following methodology based on the theory explained in chapter 7 of [16]:

- **Calculate the reaction forces at the fuselage connection**
  This can be done by solving the equilibrium equations (eq. (7.1)) around the fixed connection point at the fuselage intersection.

$$\sum F_x = 0, \sum F_y = 0, \sum F_z = 0, \sum M_x = 0, \sum M_y = 0 \quad \text{and} \quad \sum M_z = 0 \tag{7.1}$$

  The distributed loads are having an arbitrary character and will have to be represented by their respective resultant force at a specific location along the length of the distributed load. The resultant of a distributed load over a length L can be calculated by using eq. (7.2) and the location of that resultant force from the left end of the distribution can be found using eq. (7.3). $W(x)$ is the distribution function of the load and x is the variable along the width of the distributed load.

$$F_{res} = \int_L w(x)dx \tag{7.2}$$

$$\bar{x} = \frac{\int_L x w(x)dx}{\int_L w(x)dx} \tag{7.3}$$

- **Using the method of sections, determine the internal loading diagrams** The method of sections, cuts the structural member (spar in the case of this UAV) at a certain location along the length of the member. Then either the remaining part of the member to the left or to the right of the cut is used for analysis. In this case always the left part is taken because the cut will run from left to right over the length of the member to find the internal loads at different locations along the length of the member. At the cut all the internal forces and moments are drawn in their positive direction. By applying again the equilibrium equations eq. (7.1) to the left remaining section, the values of the internal loads are determined at the location of the cut. By cutting at several locations along the length of the beam, it is possible to construct the internal loading diagrams of both type of wings. These diagrams can be found in fig. 7.6 and fig. 7.7.

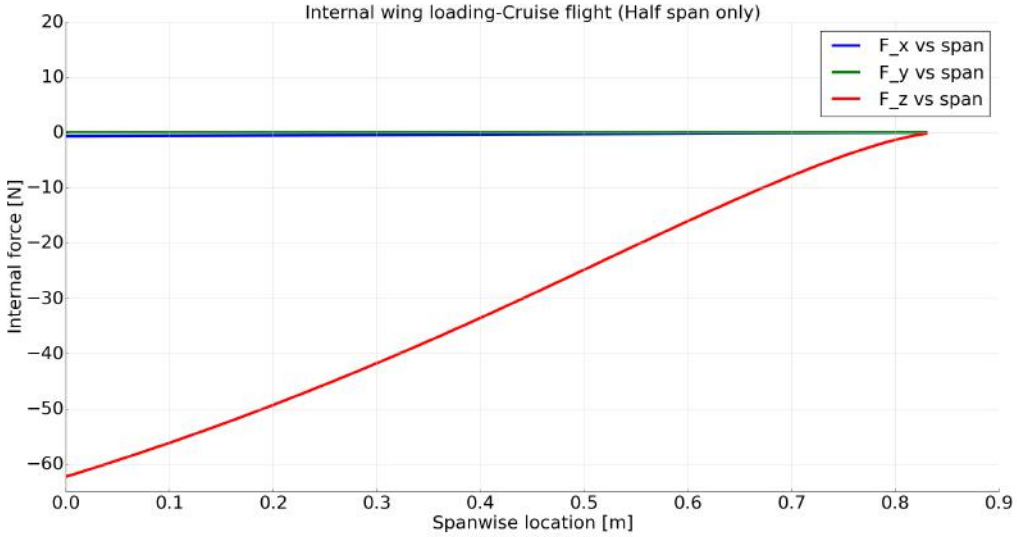

(a) Internal forces for the wing without the cruise propeller: The F_y distribution is zero everywhere because there are no normal forces in the wing without the cruise propeller. F_x distribution is rather small because it only includes the drag distribution which is significantly lower than the lift and structural weight distributions. That is why the F_z distribution is the largest one of the three.

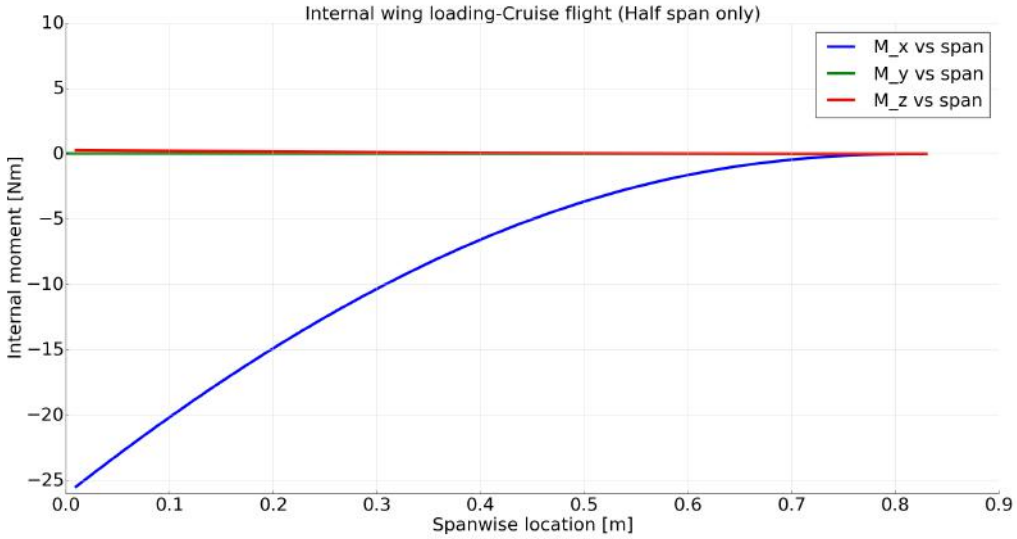

(b) Internal moments for the wing without the cruise propeller: The M_x distribution is the largest. This is again due to the lift and structural weight distribution. M_z distribution is again small due to the fact that it is only dependent on the drag distribution. The M_y distribution is the internal torque distribution along the span of the wing. It is solely due to the aerofoil pitching moment, no other torques are exerted upon the wing. As can be seen in the figure, the torsional loading is negligibly small.

Figure 7.6: Internal load diagrams for the wing without cruise propeller

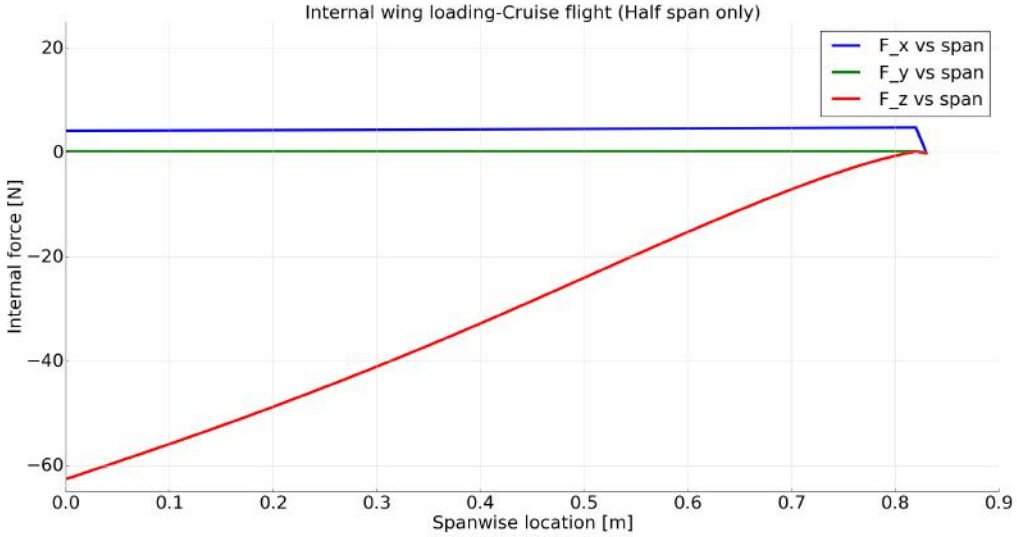

(a) Internal forces for the wing with the cruise propeller: The difference in this figure compared to fig. 7.6a is in the F_x distribution. In the end the jump indicated the effect of the thrust component of the cruise propeller. Since the weight of the cruise propeller is rather small, the other two distributions are quite similar to the case of no cruise propeller

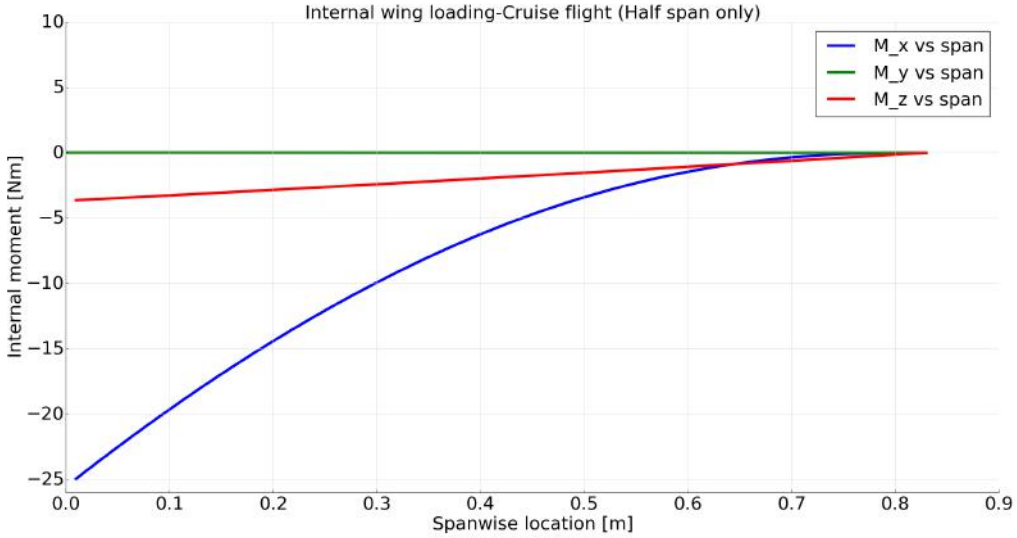

(b) Internal moments for the wing with the cruise propeller: The torsional loading is again negligible. The M_x distribution is similar as for the wing without the cruise propeller for the same reason of negligible cruise propeller weight. The M_x distribution is bigger due to the thrust of the cruise propeller

Figure 7.7: Internal load diagrams for the wing with cruise propeller

7.2. Material choice

For the UAV there were 5 components for which materials had to be chosen. The wing skin, wing spar, wing filler material, fuselage skin, and fuselage internal structure. For the wing spar and fuselage internal structure, carbon fibre was chosen to be the most optimal material due to its high structural stiffness as well as low weight. For the wing skin , an S Glass-fibre composite was chosen due to the fact that it's radio transparent, it's resistant to salt water, and also due to its attractive structural properties. For the wing filler material, PE-LD foam was chosen to be the best material primarily on the fact that its biodegradable and has a relatively low density. This foam is intend to damp the vibrations of the wing. The materials were picked from the CES EduPack [13]. The material properties are summarised in table 7.1.

Table 7.1: Material Properties

Property	S Glass fibre + Epoxy resin	PE-LD foam	PEEK + Carbon fibre
Density [kg/m3]	1840	16	1550
Young's modulus [GPa]	19	0.00025	56.1
Compressive strength [MPa]	301	0.01	363
Yield strength [MPa]	457	0.01	460
Tensile strength [MPa]	457	0.26	460
CO2 footprint [kg/kg]	5.41	4.86	21.1
Price [EUR/kg]	17.9	2.39	96.5

7.3. Stress analysis

The wing was optimised in the following manner. It is assumed that the skin will only be loaded in torsion, however due to the near negligible amounts of torsional moment that were identified in section 7.1.2, the skin thickness has been set at the minimum manufacturable thickness which is assumed to be 1 mm think.
The loading during flight was not deemed to be the most critical loading case as a maximum moment at the root was identified to be 25 Nm in section 7.1.2. This would be the approximate equivalent of a 3 kg load at the wingtips, which would mean that if two people were to try and lift the UAV at the wingtips, the wings would break. Two additional loading cases were identified to be the most critical loading cases. The spar is expected to be critically loaded in bending around both the x and y axis due to ground handling and landing on ground respectively. It can be found that a male in the age range of 20-30 would be able to exert a pulling force of 413 N [6], this is of course an extremely large force however it provides an idea of how large the ground handling loads could potentially be. In terms of forces when it lands on ground, in the case of the Delftacopter, it was forced into the ground from a height of 20 cm. When just assuming a drop of a 5kg object from a height of 20 cm and a wing deflection of 10 mm, this would be an average impact force of 980 N. These are all potentially much larger than the loads expected during flight.
Taking this into account, the following approach was taken to sizing the spar. Using the material properties in table 7.1, the spar was sized according to the mass that was allocated to it in the design for a compromise between maximum strength during handling and landing. This was done using the software "Autodesk Inventor". The result of this optimisation was a spar with the following dimensions. It was designed as a box with 2mm wall thickness, with the width linearly varying from 44 mm wide at the root chord to 10 mm at the tip chord. At all points along the span, the spar is centred at 30% of the chord for maximum height. It was designed as a box to maximise the spar's area moment of inertia in both axes. One note to make is that for all loading cases, a 1.5 safety factor is present.

7.3.1. Handling case

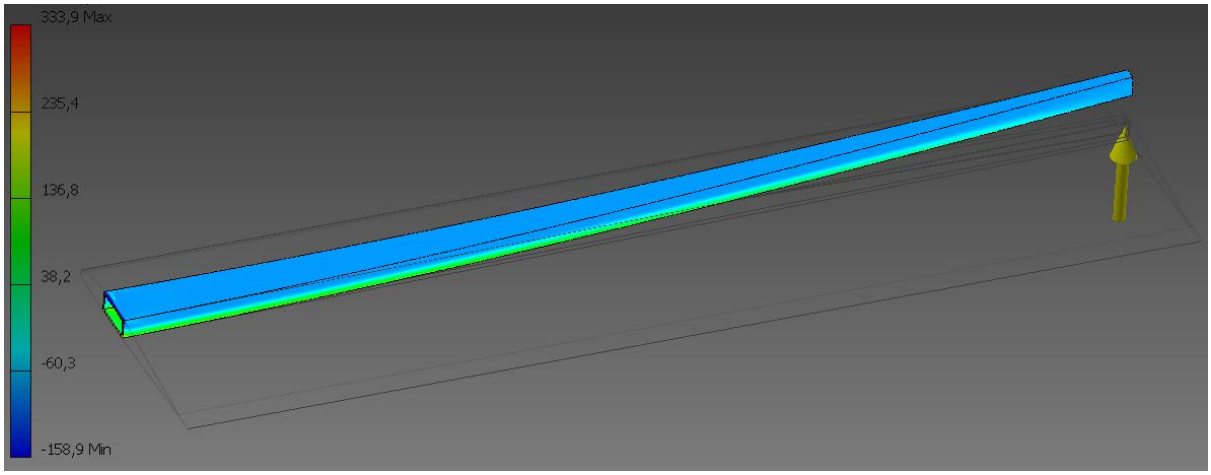

(a) 1st Principal Stress [MPa] - The maximum stress is simulated to be 333.9 MPa in tension situated at the root.

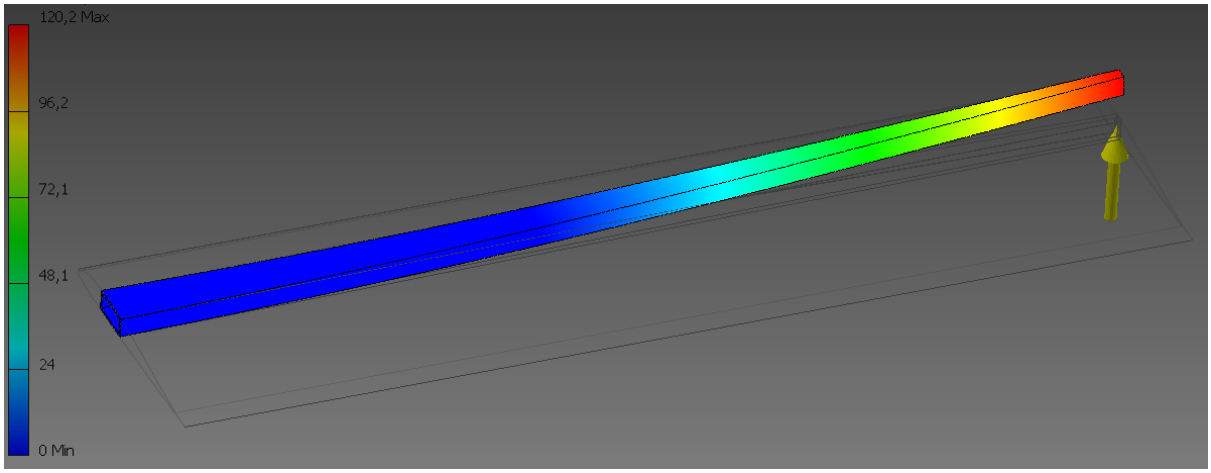

(b) Displacement [mm] - The spar is simulated to have a maximum deflection of just over 12 cm at the wing tip.

Figure 7.8: Spar Stress Analysis for a handling force of 270 N at the wing tip with a fixed constraint at the root. The maximum handling forces should not exceed 270 N on the wing tip.

It was identified that a handling load of 270 N would cause failure of the spar. This force of 270 N at the wingtip is still below the pulling force that a human could potentially exert however 270 N is considered to be large enough such that the wing's will not break during handling on ground. A "Handle with care" sign will still be added somewhere on the UAV to highlight the fact that it should still be handled carefully.

7.3.2. Landing case

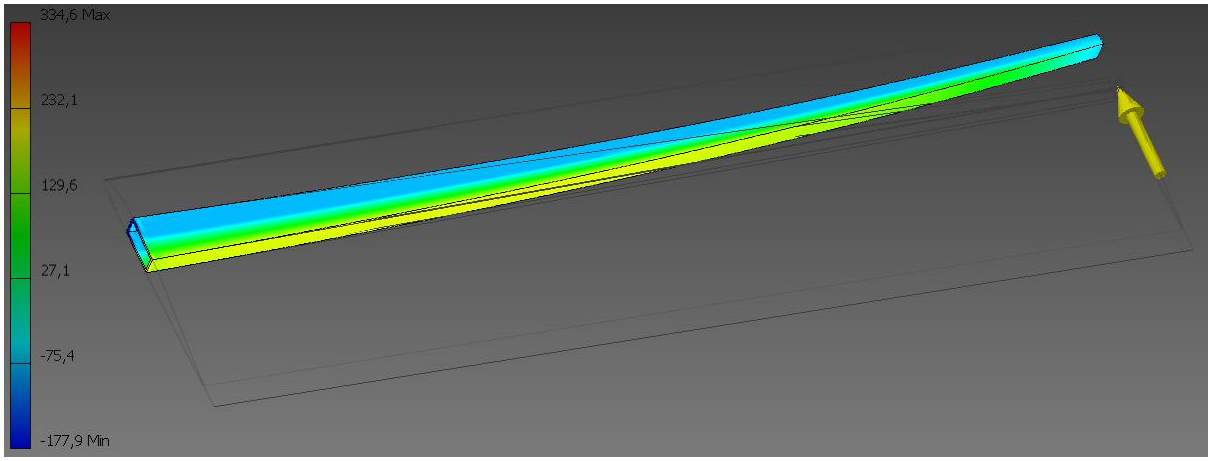

(a) 1st Principal Stress [MPa] - The maximum stress is simulated to be 334.6 MPa in tension situated at the root.

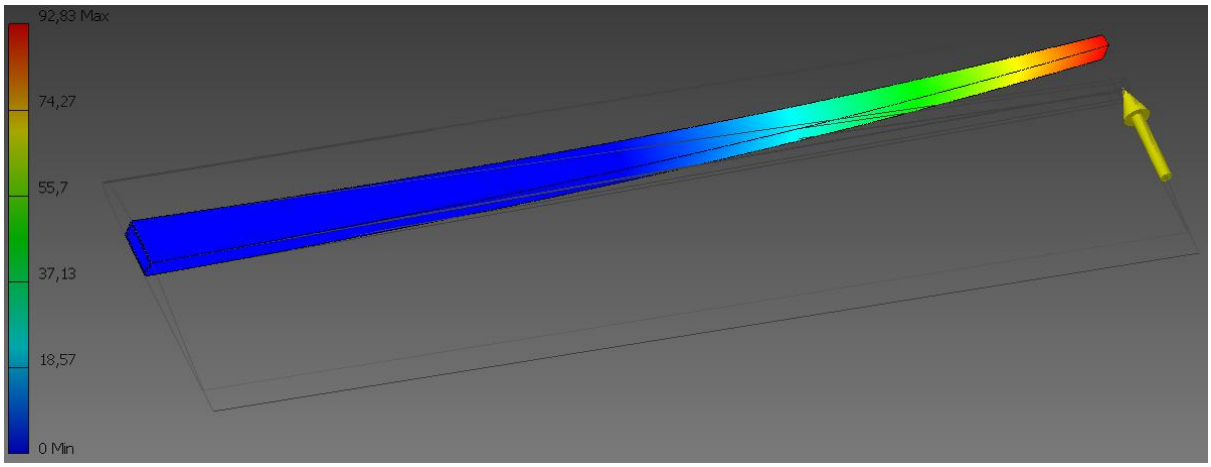

(b) Displacement [mm] - The spar is simulated to have a maximum deflection of about 9.3 cm at the wing tip.

Figure 7.9: Spar Stress Analysis for a landing force of 500 N at the wing tip with a fixed constraint at the root.

A maximum landing force at the wingtips would lead to failure of the wing spar however this would cause a wingtip deflection of 9.3 cm which would cause the fuselage to have impact with the ground. Therefore the maximum height at which the UAV could be dropped from was calculated by assuming the maximum allowed tip deflection would be 10 mm. This would mean that at maximum deflection, there would still be a 8 mm margin between the bottom of the fuselage and the ground. It is assumed that all the potential energy the UAV has at its maximum drop height is dissipated by the spar over its allowed deflection.

$$PE = mgh \tag{7.4}$$

$$F_{impact} = \frac{1}{4}\frac{PE}{d} \tag{7.5}$$

Using equations eq. (7.4) and eq. (7.5) it can be calculated that when purely relying on the spar, the UAV can be dropped from 2.6 cm. It is important however to acknowledge that during the landing, the skin will represent a large area moment of inertia, therefore it is expected that the UAV should be able to be dropped from a higher height without having the fuselage touch the ground.

7.4. Inventor verification

The program "Autodesk Inventor" was verified with hand calculations by means of a simple loading case. In this case, a loading case is created of a cantilever beam with a fixed connection on one side. The cross sectional profile is that of a rectangle. The beam has dimensions of width 12 mm, height 20 mm, and length 1 m. The deflection at the tip was calculated using eq. (7.7). The material properties of the PEEK/Carbon fiber composite from table 7.1 are used. It is assumed that a tip load of 100 N is applied.

$$I = \frac{bh^3}{12} = 8000mm^4 \tag{7.6}$$

$$\delta = \frac{PL^3}{3EI} = \frac{100 * 1^3}{3 * 56.1 * 10^9 * 8000 * 10^{-12}} = 0.0743m \tag{7.7}$$

When the same parameters are used in the Inventor software, a tip deflection of 74.16 mm is calculated. The loading case is shown in eq. (7.7). This represents a 0.19 % difference and this difference is deemed small enough so it can be said that the software is verified.

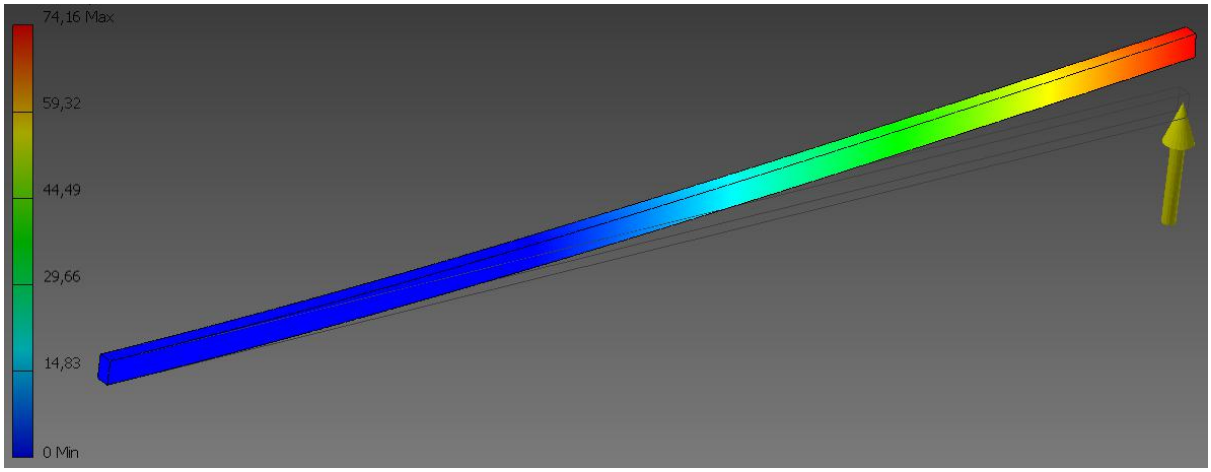

Figure 7.10: Inventor Deflection Verification [mm]

7.5. Conclusions & Recommendations

The wing was simplified to be a spar and the spar was sized according to the mass that was allocated to it as the maximum stresses were deemed to not be representative of what the maximum loads would be. This resulted in a spar that would be able to withstand a maximum tensile stress of 334.6 MPa, a maximum handling load at the wingtips of 270 N at the wingtip, and a maximum drop height of 2.6 cm when ensuring the bottom of the fuselage doesn't make contact with the ground. There are many points that can be continued with going into the Post DSE phase. Once a complete FEM model can be made that also takes into account the loading of the skin, then a more accurate estimation can be made for the maximum handing, and landing loads/height. This could also lead to further structural optimisation. It would also be recommended to investigate further a material for the spar that has a higher stiffness, as this would allow the UAV to be dropped from a higher height. The material choice is currently limited to the database in the CES EduPack as all material properties are provided however it is expected that there will be more materials available that are more beneficial. Furthermore the fuselage skeleton has to be designed such that the fuselage and all of its components could survive a landing from the maximum calculated height. Further the connection between the wings and fuselage have to be designed in detail so there is strength and ease of detachability. A further analysis has to be done with the wing skin at the trailing edge wingtip to check at what force they would fracture or crack, as this would add another limit to what height the UAV could be dropped from. Another investigation could be performed upon connecting the upper and lower wing tips on both sides. This would reduce tip vortexes which results in more lift and less drag. If designed properly, they could result in less structural weight for the wings. Finally an investigation has to be made of how the structures handles vibrations as the propellers will all cause vibrations throughout the structure, and this could cause problems with other subsystems that are sensitive to vibrations.

8 Electronics

This chapter outlines the design of the electronics that aid the UAV fulfil the mission. A number of components have been chosen and, together, they create a complete system that can be purchased, assembled, and tested in the next stage of the design. First, in section 8.1, the requirements concerning the electronics will be outlined, together with background information for the decisions made. This is then followed by the selection of the components and assembly in a system, ensuring that all components are powered correctly and can communicate with each other as intended. Many components require software to function and software is vital for the success of the mission, therefore the software design is outlined next. Lastly the chapter is concluded and recommendations for the next design phases are made.

8.1. Requirements & Background Information

Many of the requirements that the UAV needs to fulfil require electronics for example to control the flight, communicate with the ground station and autonomously detect the landing target.
As per requirement MEUC-TUD-03 the UAV shall be able to fly with Type 2 Autonomy and complete a mission. Type 2 Autonomy is defined by the Medical Express UAV Challenge rules as full autonomy without human interference. In order to achieve this the UAV needs to posses an Autopilot system, a number of sensors and a System on a Chip (SoaC) to detect obstacles and a landing target. Requirement MEUC-UCTC-02 demands that the UAV features a Flight Termination System (FTS). Requirement MEUC-TUD-05 dictates the use of the open source software Paparazzi UAV for flight termination and the autopilot. According to MEUC-TUD-18, the UAV shall feature a fuel-cell to provide power, which has already been selected and designed in chapter 3. Further requirement MEUC-UCTC-12 dictates that the UAV should have a continuous datalink to the ground station. There are a number of other requirements that apply to the electronics of the UAV, which can be found in table 10.9, table 10.10, table 10.11 and table 10.12.
The autopilot needs data about the position and attitude of the UAV to control it and fly its mission. To determine the absolute and relative attitude a 9 Degrees of Freedom (DoF) Inertial Measurement Unit (IMU), consisting of a 3-axis Gyroscope, a 3-axis accelerometer and a 3-axis Magnetometer was chosen. For location determination a GPS receiver will be used. The GSM module in the communication system can be added for additional accuracy and reduced startup time of the GPS. The GPS can also give a rough altitude estimation above sea level. The autopilot will feature a barometer, which can be used to estimate the altitude above ground and combined with the GPS for increased accuracy. To avoid obstacles during flight, specifically during the Loiter phase and to detect the Landing Target and land smoothly, it was decided that the UAV should feature cameras in the visible spectrum. Because the UAV transitions from hover to forward flight and back one camera will have to be placed on the bottom of the UAV facing towards the ground in forward flight and one on the back of the UAV facing downward during hover. To determine the altitude accurately during the landing phase a LIDAR (Light Detection And Ranging) sensor was chosen. This sensor will be in the back of the UAV and facing downward during hover. To process the images taken by the cameras an SoaC is required on-board the UAV. The SoaC needs to run image recognition algorithms and output control commands to the Autopilot.
The other electric components depend on the different subsystems and are described in the relevant chapter. The power system can be found in chapter 3. Information about the motors and actuators can be found in chapter 6. The communication system and its electronics are described in detail in chapter 9. In the following section the component selection of the other electronics is outlined.

8.2. Component Selection

This section outlines the selection of electronic components required to make the UAV fly and allow it to fulfil its mission.
Due to the requirement to use Paparazzi UAV for the FTS and Autopilot the choice of hardware was limited to compatible autopilot boards. The currently newest autopilot board compatible with Paparazzi UAV is the Chimera/v1.00[1], which offers faster double precision computation compared to other currently avail-

[1] URL `http://wiki.paparazziuav.org/wiki/Chimera/v1.00` [cited 25 June 2017]

able boards. Additionally it features a 9 DoF IMU, a barometer, a differential pressure sensor for a pitot tube and micro SD card data logging. This means these components do not have to be purchased separately and do not have to be assembled, which saves money and time. The Chimera/v1.00 is shown in fig. 8.1.

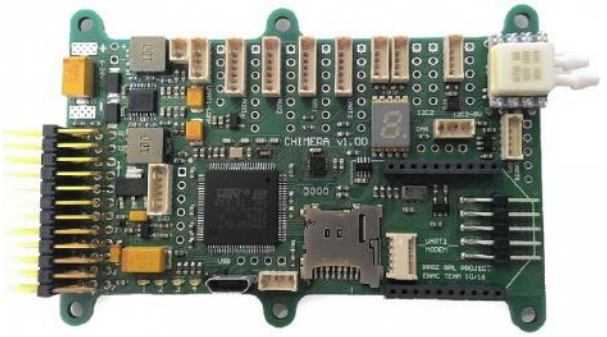

Figure 8.1: Autopilot and FTS: Chimera/v1.00[2]

In addition to the autopilot and FTS, a SoaC is needed. Nowadays there are a number of small, low power systems available that are specifically designed for image processing in mobile applications. NVIDIA has a long history of offering good products for this purpose. The newest SoaC available is the NVIDIA Tegra TX2[3]. Its predecessor, the Tegra TK1 was used in the DelftaCopter. The newest version features GPU-accelerated parallel processing capabilities and is available as the NVIDIA Jetson TX2 Development Kit for a reduced price when used for educational uses. It has a number of inputs and outputs, which are ideal to connect it to the cameras, the LIDAR and the autopilot. The NVIDIA Jetson TX2 Development Kit is shown in fig. 8.2. The Tegra TX2 requires a 19 V power supply therefore a DC/DC converter has to be purchased as well. A low-cost option is the Texas Instruments TPSB4259RKGT.

Figure 8.2: Soac: NVIDIA Jetson TX2 Development Kit[4]

The two cameras need to have a sufficiently high resolution, so that object and the landing target can be identified from a distance of 40 m or more. Other important factors to consider are the frame rate, the sensitivity, focal length, field of view, colour depth and colour mode. For Machine Vision, Global Shutter is usually preferred as it results in less disturbance to the images compared to Rolling Shutter and makes processing the images easier. Generally, monochrome images capture more information that colour images and are easier to process. However, since the landing target will likely be coloured and since a coloured video stream is more suitable, a colour camera was chosen. A suitable camera model is the Chameleon3 3.2 MP Color USB3 Vision with a Sony IMX265 sensor[5]. This camera features global shutter and a resolution sufficiently high to detect details on ground while having a good quality video for the livestream and later for media publications. The resolution of 3.2 MP was chosen as it was still affordable and is sufficient. Global shutter cameras can go up in price very quickly with resolution. A good explanation of global versus rolling shutter can be found in [6] and

[2] URL `https://drotek.com/shop/en/home/832-chimera-paparazzi-flight-controller.html` [cited 26 June 2017]
[3] URL `https://developer.nvidia.com/embedded-computing` [cited 26 June 2017]
[4] URL `http://a.co/9UCf7r2` [cited 26 June 2017]
[5] URL `https://goo.gl/K1JfYQ` [cited 26 June 2017]
[6] URL `https://www.ptgrey.com/KB/10028` [cited 3 July 2017]

[7]. The difference between the two is also shown in fig. 8.4. Rolling Shutter causes a significant distortion of the image at fast movements, which makes the processing of images more difficult. As the UAV will be travelling quickly Global Shutter is desirable. The ground resolution of the camera can be calculated[8] with the camera sensor size (1/1.8"), altitude (40 m), resolution (2048 x 1536 pixel) and lens size (10 mm). This results in a ground resolution of 8.93 x 6.61 cm per pixel. This results in 4.7 x 8.9 pixels for the Landing Target during Loiter. The chosen camera can be seen in fig. 8.3.

Figure 8.3: Camera: Chameleon3 3.2 MP Color USB3 Vision (Sony IMX265)[9]

Figure 8.4: A comparison of Global Shutter (left) to Rolling Shutter, showing the distortion caused by Rolling Shutter[7]

The LIDAR sensor selected for altitude determination is the LIDAR-Lite v3[10]. It's a low-cost 40 m range laser sensor with a resolution of +/- 2.5 cm. The sensor can be seen in fig. 8.5.

Figure 8.5: Altitude Sensor: LIDAR-Lite v3[11]

To determine the location of the UAV, a GPS sensor was selected. The GPS sensor is supposed to have an accuracy of 4.9 m or less, sufficient channels to determine the location quickly and a high refresh rate of 10 Hz or more as the UAV will be travelling up to 34.2 m/s. A good choice is the SparkFun Venus GPS with SMA Connector[12]. In addition, a GPS antenna is required. A compatible antenna is the Antenna GPS Embedded

[7] URL https://www.youtube.com/watch?v=dNVtMmLlnoE [cited 3 July 2017]
[8] URL http://canberrauav.org.au/guide/system-requirements/ [cited 3 July 2017]
[9] URL https://eu.ptgrey.com/support/downloads/10578 [cited 26 June 2017]
[10] URL https://www.sparkfun.com/products/14032 [cited 26 June 2017]
[11] URL https://www.sparkfun.com/products/14032 [cited 26 June 2017]
[12] URL https://www.sparkfun.com/products/11058 [cited 26 June 2017]

SMA[13]. This particular GPS system has a refresh rate of up to 20 Hz and an accuracy up to 2.5 m. The GPS system can be seen in fig. 8.6.

Figure 8.6: Location Sensor: SparkFun Venus GPS and Antenna GPS Embedded SMA[14]

Other components needed include a RGB LED, E-stop switch, arm switch and cables. The final selection of electronics components can be found in table 10.3. The voltage, power consumption, prices, size and mass of all components are listed there.

8.3. Hardware Setup

Now that the electronic components in the UAV system are chosen, special attention should be given to the connections between these components. In order to establish a clear overview of the interconnection, hardware block diagram and the electrical block diagram are created.

The hardware block diagram represents a tool that gives an overview of all the hardware components of the system, including ground system. The colours in the diagram represent the categories to which different components belong, as indicated in the legend. The arrows indicate the mechanical or electrical interaction that the components have between each other. The black arrows indicate a electrical interaction between the components whereas a red, dotted arrow indicates a mechanical relationship. All the electrical relations can be found in fig. 8.8. All other mechanical connections have properties as discussed in chapters 3, 5 and 6.
The ground station consists of a computer to which the GSM modem and the radio transceiver are connected.

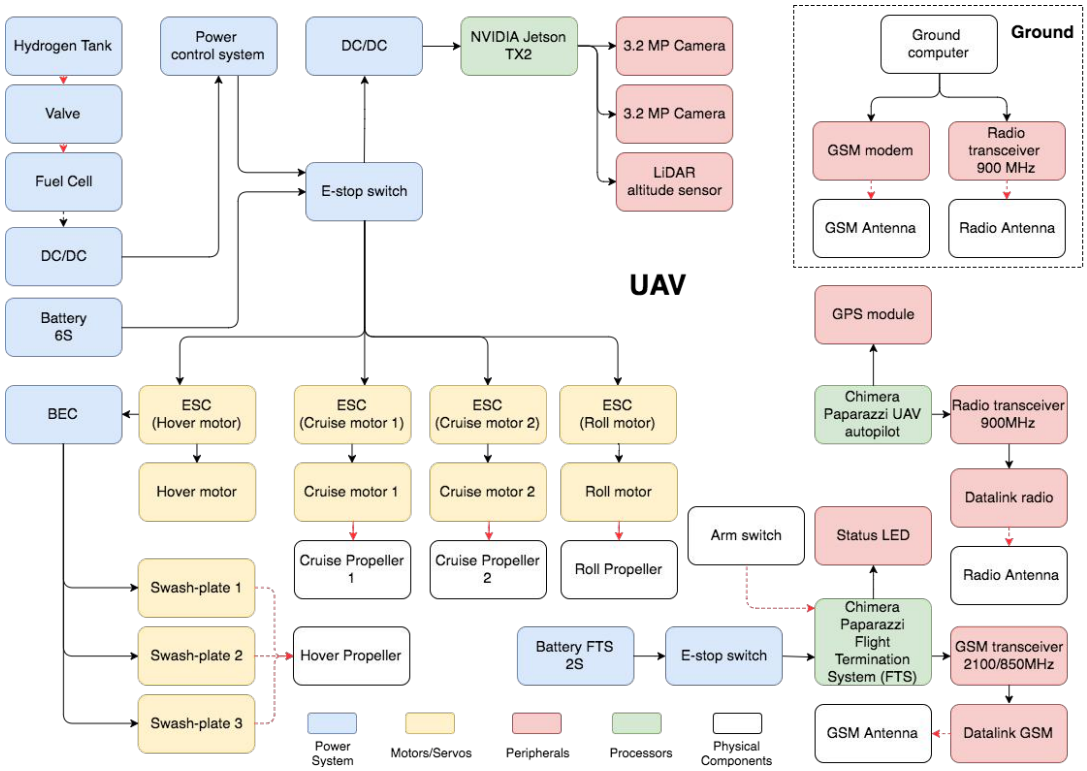

Figure 8.7: Hardware Block Diagram

[13] URL `https://www.sparkfun.com/products/177` [cited 26 June 2017]
[14] URL `https://www.sparkfun.com/products/177` [cited 26 June 2017]

The electrical block diagram, which can be seen in fig. 8.8, shows how power is distributed in the UAV system and the ground station. Further the voltages and power consumption of the different components are shown.

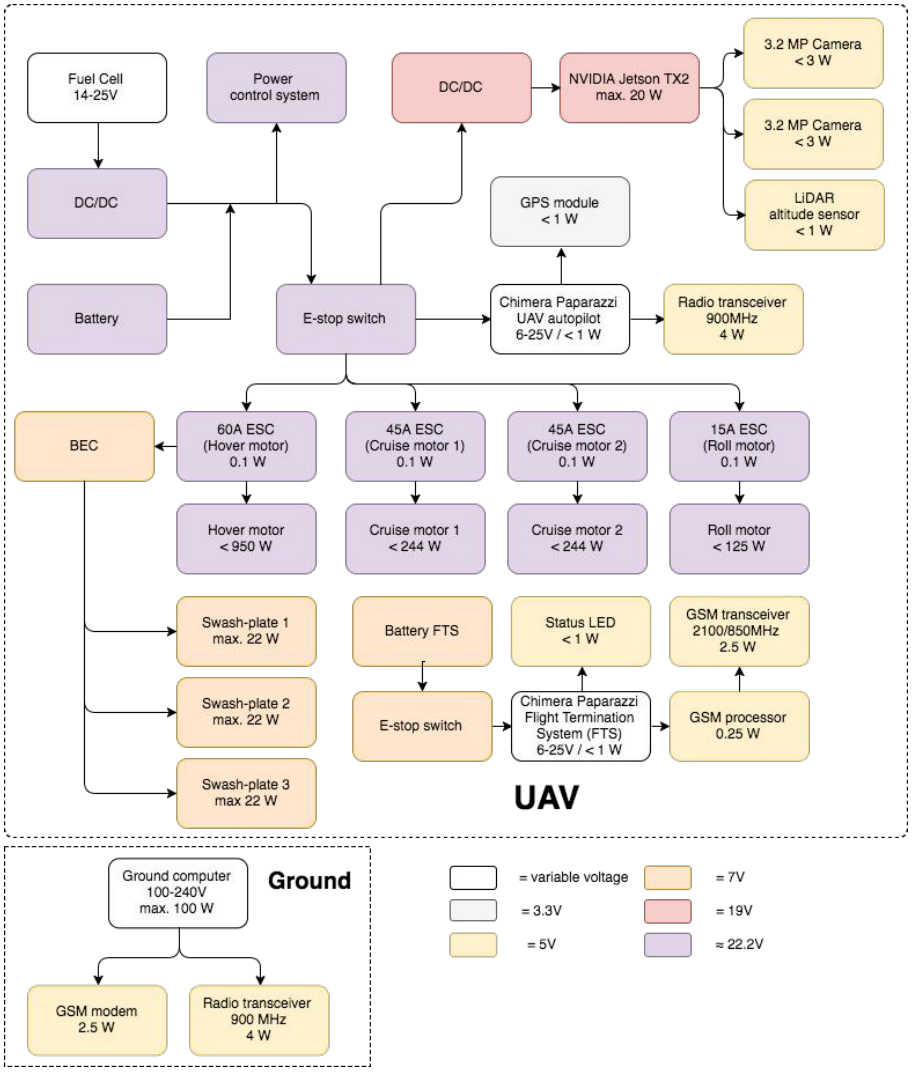

Figure 8.8: Electrical Block Diagram

The ground station computer is powered by regular household current but can also be powered by battery or with a generator. The ground communication system is then powered by the computer through its outputs. The UAV is powered by the fuel cell and two arrays of 6 cell (6S) batteries. The FTS needs to have a separate power supply and it therefore is powered by a 2 cell (2S) battery. The fuel cell provides a variable voltage between 14 to 25 V, but because many systems require a constant voltage, a DC/DC converter is needed to convert the output voltage to a constant 22.2 V (6S). The 6S batteries are connected in parallel to the fuel cell and provide additional power for power intensive phases such as take-off and landing. These batteries can be recharged by the fuel cell if needed. Directly behind the power supply is a mechanical E-stop switch, which is located on top of the UAV and when pressed, cuts all power to all systems. The autopilot, another DC/DC converter and the Electronic Speed Controllers (ESC) are connected to the power system through the E-stop switch. The DC/DC converter converts the 22.2 V provided by the power system to 19 V required by the SoaC. The SoaC then powers the two cameras and the LIDAR altitude sensor through its outputs. The autopilot can work with voltages from 6 - 25 V but in this case is powered by 22.2 V. The autopilot has its own voltage converters on the PCB, which power the radio transceiver and the GPS module. The ESCs work on the 22.2 V provided to them and power all 4 motors and control their speed. The ESC powering the hover motor has a Battery Eliminator Circuit (BEC) included, which is used to power the three swashplate servos. The BEC converts the 22.2 V to 7 V, which is ideal for the servos. Lastly, the FTS is powered by the 2S rechargeable battery mentioned previously. This battery will have to be swapped/recharged after every flight. The E-stop switch will also cut the power between the 2S battery and the FTS, as the GSM is connected to the FTS and needs to be switched off. The FTS is powered by 7 V and also has its own voltage converters, which power the

GSM processor and transceiver and the status LED, both running on 5V. The UAV features in total six different voltages and three power sources.

8.4. Data Handling

Not only do the components have a mechanical or electrical relationship, but also exchange data between each other. To ensure a complete understanding of the system and ensure smooth interactions, a data handling block diagram can be created. Data exchange takes place between components inside the UAV, but external data transmission also takes place. The data handling within the system is illustrated in fig. 8.9, and the external data handling in fig. 8.10.

The arrows in the fig. 8.9 represent the data and command flows. Elaboration on these arrows is given below:

1. Attitude Data
2. Pressure Data
3. Location Data
4. Optical Data
5. Camera Images
6. LiDAR Images
7. Heading, Speed and Altitude
8. Telemetry
9. Current Actuator Setting
10. Required Actuator Setting
11. Current Power System Setting
12. Required Power System Setting
13. Current Speed Setting
14. Required Speed Setting
15. Arm Switch Setting
16. LED Setting
17. Electronic Speed Setting in case of FTS
18. Actuator Setting in case of FTS
19. Switch-off Signal in case of FTS
20. Battery Charge State
21. Tank Charge State
22. Required Valve Setting
23. Power Setting
24. Fuel Cell Status

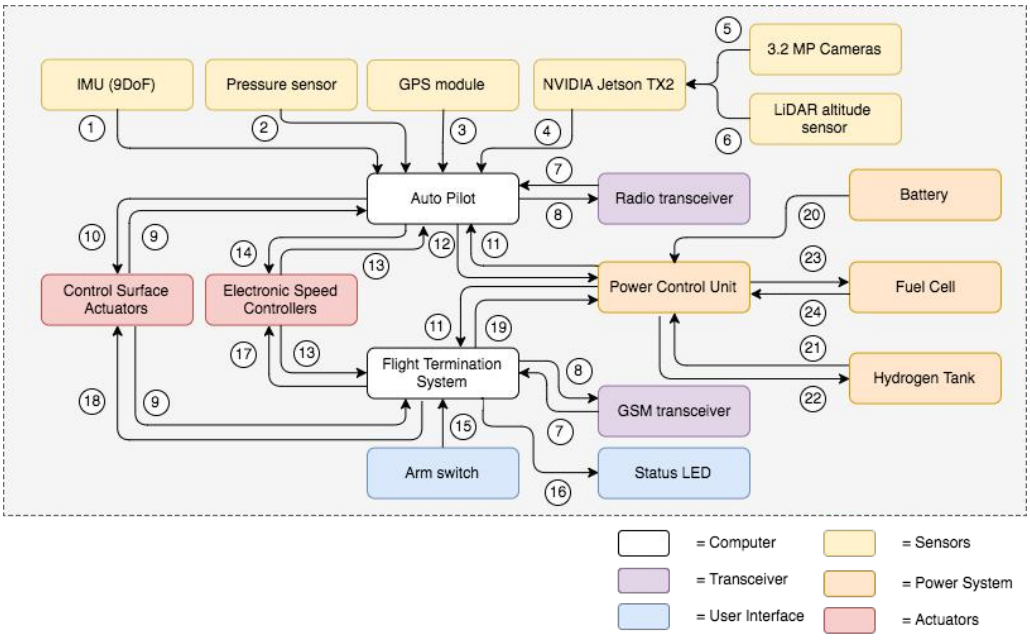

Figure 8.9: Data Handling Block Diagram

A similar diagram, fig. 8.10 is created for the data and command flow from the UAV to external computers. The arrows in the UAV that do have loose ends indicate the relation towards the internal data exchange, which was already elaborated on in the data handling block diagram. The data and command flows that flow between systems are indicated with dotted arrows and elaborated below:

1. Heading, Speed and Altitude
2. Dynamic No-Fly Zone
3. Flight Termination Command

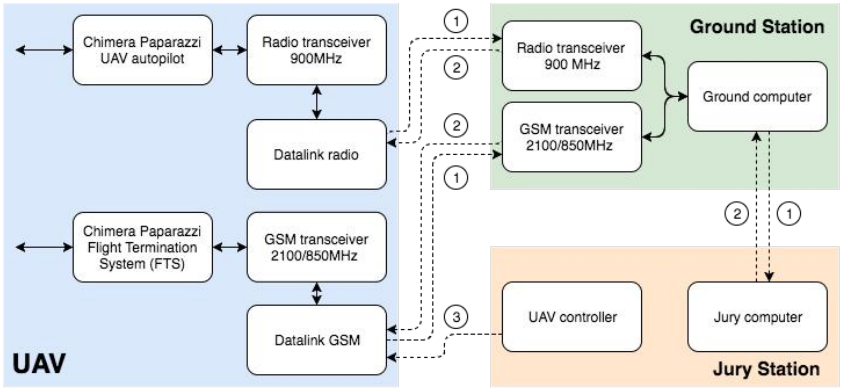

Figure 8.10: Communication Flow Diagram

8.5. Software

Most electronic components require software to function. As the electronic system of the UAV is custom, custom software will have to be developed but pre-existing software can be utilised, where available. Requirement MEUC-TUD-05 dictates the use of the open source software Paparazzi UAV [30] for flight termination, real time re-planning and autopilot design.
The UAV has a number of processors on which the software will run. The three major ones are the autopilot, the FTS and the SoaC. An overview of the processors and software design can be found in fig. 8.11. The software design will be outlined in detail in the following subsections.

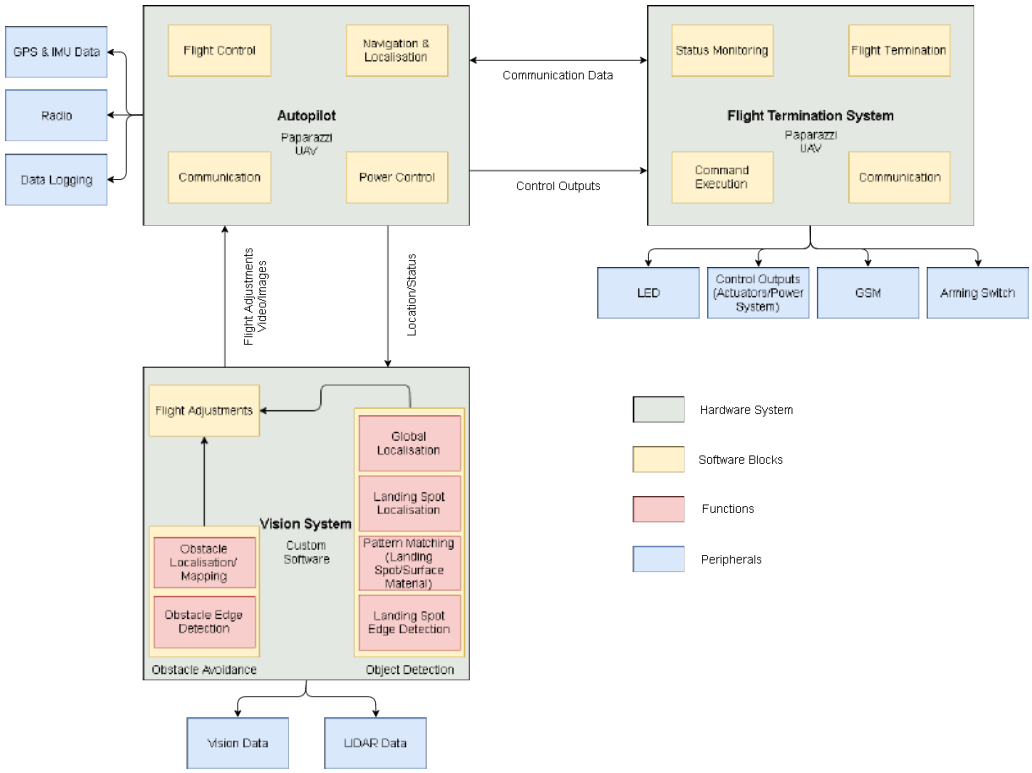

Figure 8.11: Software Block Diagram

8.5.1. Autopilot

The autopilot (Chimera/v1.00) will run Paparazzi UAV for Flight Control, Navigation and Localisation. Paparazzi UAV is an open source software suite that is designed for autonomous flying of UAVs. Paparazzi can

accept data from many different sensors and output commands to the actuators and ESCs of the UAV to control it. It can keep the UAV stable in the air, process position data and perform flight planning and execution. In order to do this, the autopilot will receive data from the GPS system, the 9 DoF IMU, the barometer and the pitot tube. Furthermore, the autopilot is directly connected to the radio transceiver and will have to send and receive signals to and from it. The autopilot is also responsible for Data Logging as it includes a micro SD card reader. It should log data such as the position, speed and health of the system. The autopilot will be connected to the SoaC, which will process the camera and LIDAR data. The autopilot will have to send the current location and attitude as well as the system status to the SoaC so that it can use it in the processing. The SoaC will in return send Flight Path Adjustments to the autopilot that it will have to incorporate in the Flight Planning and Execution. This is especially the case during loiter, when the UAV has to discover the landing target and during the landing phase as the SoaC will be seeing the target and measuring the altitude and trying to stay on target. The SoaC will also be sending video and images to the autopilot that it will have to forward to the radio or the FTS. The autopilot will also be connected to the FTS for two reasons. All of the control commands that the autopilot generates are sent through the FTS to the actuators so that the FTS can perform error checking and overwrite them if something is wrong. Further, the FTS is connected to the GSM module so the autopilot and the FTS will be communicating with each other the data that is being sent and received by the GSM. During normal flight operation this will be for example the video and images as the GSM is expected to be faster than the radio and also data such as the location, speed and health status.
A number of custom functions that also allow power control and communication as well as data exchange between the SoaC and the FTS with the Autopilot will have to be written.

8.5.2. Flight Termination System (FTS)

The Flight Termination System (Chimera/v1.00) will also run Paparazzi UAV just like the autopilot. The FTS however will perform significantly less computations and more error checking and signal forwarding. The FTS will be connected to the autopilot and receive control outputs that should be forwarded to the actuators and the ESCs. The FTS is also connected to the GSM transceiver and will send the data it receives from the autopilot through it, such as location, speed, status and video or images. The FTS will forward data it receives from the GSM to the autopilot if needed. Lastly the FTS is connected to the arming switch, the status LED and all the actuators, ESCs and the power system.
Flight Termination can also be triggered by a command send over the communication system either through the radio and then forwarded from the autopilot to the FTS or through the GSM and then directly executed by the FTS.

8.5.3. System on a Chip (SoaC)

The SoaC (NVIDIA Jetson TX2) will use a Linux distribution with custom software. Its input will the vision data received from the two cameras on the UAV and the altitude from the LIDAR. It will mainly be active during the loiter and landing phase as it will have to identify obstacles and the landing target and compute flight adjustments to ensure a safe landing. The SoaC will send these flight adjustments as well as video or images to the autopilot, which then incorporates the adjustments in the flight planning and execution and forwards the video to the communication system to send it to the ground station. The SoaC will also receive location and status data from the autopilot. It will use this information to determine which function to execute and to compute the location of objects globally. It should be investigated whether the available bandwidth to the Autopilot and the FTS is sufficient to forward Video. Alternatively the SoaC could receive its own direct connection to the GSM and Radio to bypass the Autopilot and FTS.
OpenCV (Open Source Computer Vision Library) [20] is a powerful open source library that supports a number of programming languages and operating systems and provides algorithms designed for real-time computer vision applications. OpenCV is commonly used on embedded systems or SoaCs such as the NVIDIA Tegra TX2 that was chosen for the UAV. OpenCV is intended to use to assist in the Object Detection, Obstacle Avoidance and Landing Spot Detection as it includes algorithms for Edge Detection, Object Localisation and Pattern matching and is optimised to consume as little computational resources and power as possible.

Obstacle Avoidance

During take-off, loiter and landing the SoaC is triggered by the autopilot to perform Obstacle Avoidance. The obstacle detection performed is relatively simple as the UAV takes off and lands near vertically and in areas where it can be assumed that the ground is acceptable for landing. This is because the UAV is placed in its take-off spot by a person, who can choose a suitable location with little to no obstacles. The UAV will land on a Landing Target placed on the ground by a person, who should also ensure that the area is clear and somewhat even. During the Loiter phase the UAV will stay above 40 m over the ground, where the obstacles

will only consist of trees in rare cases and possibly built up structures. Even though the likelihood of obstacles is small, for additional safety Obstacle Recognition and Avoidance algorithms are performed. During take-off the camera on the bottom of the UAV will be facing horizontally and in the direction that the UAV is intending to fly, therefore its images can be used. During landing, the situation is similar and the same camera can be used. During loiter, this camera is facing towards the ground and slightly forward, which will allow it to be used to determine objects underneath and slightly in front of the UAV.
The images received by the camera will first be pre-processed to bring out more details, then an Edge detection algorithm will process them. A popular method is Canny edge detection, which looks for discontinuities in the images. Once the object have been identified they need to be localised relative to the UAV. It is possible to determine a rough position of objects from 2D images by analysing the direction of lines and the size of objects. Further as the UAV is moving the images will change with time and objects move in them and visible from different viewpoints. Once the obstacles are identified and localised, it can be determined whether they are in the path of the UAV or not. In the case they are the SoaC will have to send a command to the autopilot to avoid the obstacle. The objects locations can then be saved so that they can be avoided at a later stages of the flight.

Landing Target Recognition
The UAV needs to find an A2 sized Emergency-Landing-Target made up of four A4 papers located somewhere within 100 m of Joe's reported location. The target can have any pattern and colour of our choice on it. It then needs to identify its global coordinates, send them back to the ground station for approval and land autonomously on the target or within 10 m of it. All this requires computer vision and advanced algorithms. When the UAV reaches the 100 m radius circle around Joe's reported location, it starts flying a search pattern at loiter speed, covering the whole area. The SoaC will be triggered by the autopilot and uses the images of the down facing camera to try and identify the target. A preliminary analysis of the area around Dalby, Australia shows that a Blue or Red target would be beneficial, as these colours rarely appear in nature and are the inverted colours of the dominant green and brown tones there. The target pattern could be a bulls-eye or possibly something more rectangular, which might be easier to identify by camera. This will have to evaluated at a later stage and tested intensely. First, the camera images will be pre-processed to increase contrast and filter out colours that do not appear in the landing target. Then, edge detection can be performed. Again for this application, Canny edge detection is suitable and commonly used. A benefit here is that the shape of the target and pattern is known, which allows filtering potential targets by their shape. Once potential targets have been identified, pattern matching will be performed and a likelihood will be calculated. The relative position of the most likely target can then be calculated from the image as the field of view and the focal length of the camera are known. The relative position of the target can be combined with the location and attitude data provided by the autopilot, to obtain the global position of the target. In case of the competition, this position will then be sent to the ground station, where it can be confirmed by the judges and the UAV can begin landing. The SoaC will send the command to the autopilot to transfer to hover mode and it will then switch to the camera on the back of the UAV, which now is facing downwards. Once it has acquired the target, the SoaC will keep giving inputs to the autopilot to correct the position and try to stay above the target as close to the centre as possible. During the landing phase the LIDAR will also be utilised to determine the altitude above ground and allow for a smooth landing. The LIDAR has a large range of approximately 50 m, which is important as the UAV will be at about that altitude when it starts its landing manoeuvre. When the LIDAR detects an altitude of less than 20 cm, the SoaC gives the signal to the autopilot to turn off the motors and the UAV will have successfully landed. During all this, the SoaC will continuously analyse the camera images, perform edge detection and pattern matching not just to stay above the target but also to ensure that the area surrounding the target is suitable for landing, i.e. grass or earth and not composed of water or rocky terrain.

8.5.4. Others
Besides the autopilot, the FTS and SoaC other components also require software. This includes the power system, the communication system and the ground station. The power system comes with its own software. Commands can be sent to it and information be requested from it. The radio system has a modem with its own interface. The autopilot is connected to it and the GSM module is controlled by an Arduino communicating with the FTS. The ground station will be a laptop powered by a conventional operating system, preferably Linux with Paparazzi UAV installed on it. The laptop will require a custom program with a graphical output of the flight information and the video feed. Further software for the communication will have to be installed and then connected to Paparazzi UAV.

8.6. Conclusions & Recommendations

The electronics system consists of many components that have to work together to successfully complete the mission. The chosen components are of high quality and reliability. The designed system prioritises safety and offers many opportunities. Due to the high computational power available and the custom design, the UAV system is extendable and upgradeable and can be adjusted for other missions in the future. The system will consist of a power supply system, an autopilot, a flight termination system, a system on a chip, a communication system and a number of sensors and actuators. The autopilot and FTS will utilise Paparazzi UAV, while the SoaC will be using OpenCV. The final selection of components can be found in table 10.3.

For the next design stages it is recommended to purchase the components and perform thorough testing to ensure that the components work together well and as intended. It should be investigated whether getting custom made components offers a benefit compared to the selected off the shelf components. Not all the functions offered by the selected systems are needed and by designing and manufacturing a customer system mass, space and cost savings might be possible. The autopilot and FTS hardware is open source and can be adjusted for our specific needs. Equally the SoaC hardware motherboard is open source and can be adjusted. This way it can be made significantly lighter by removing unnecessary components. Additionally it has to be investigated whether the amount of computing power currently available is actually necessary. At this stage of the design it was not possible to determine how much computing power will be required. The components were chosen from reference missions such as the DelftaCopter and other UAVs that took part in the Outback Challenge before and are of equal computing power or better.

Additionally the lifetime and long-term availability of the selected components has to be investigated. Especially for the Royal Netherlands Navy a long life-time of the system and long-term availability of the components is important. NVIDIA is unfortunately not known for its long availability, therefore a replacement of the Jetson should be considered for this customer. However the Royal Netherlands also possesses their own Vision System already, which could potentially be used for the Landing Target Recognition.

Whether these improvements are made or not, the designed system will fulfil all requirements that were set and possibly exceed them. It can be said with confidence that the mission will be a success and future applications of the UAV system are possible.

9 Communication

The design of the communication system is presented in this chapter. The selection of communication equipment is given in section 9.3. The verification and validation data of the data link is given in section 9.4 using a link budget. An operational plan for the system is given in section 9.2. Conclusions and recommendations are given in section 9.5.

9.1. Applicable Requirements

The following requirements are relevant to the design of the communication subsystem:

- **MEUC-ACMA-01** The radio frequencies used shall comply with the Australian Communications and Media Authority (ACMA) regulations.
- **MEUC-ACMA-02** All relevant radio licenses shall be obtained before flight.
- **MEUC-UCTC-25** The UAV shall not take-off from the Remote Landing Site without active communications to the Ground Control Station.
- **MEUC-Sys-UCTC-12-01-Comm-04** The UAV shall be able to process the radar digital feed for the information handling of the DNFZ's size, position and velocity.
- **MEUC-Sys-UCTC-12-01-Comm-05** The UAV is required to have two-way communication with the ground station during the flight.
- **MEUC-Sys-UCTC-12-01-Comm-06** The received signal power at the receiver on both ground and UAV shall be at least as high as the sensitivity at the modems on the ground and UAV respectively.

9.2. Operational plan

Since continuous communication with the UAV is of key importance to ensure safety, two separate communication links (Radio and GSM) will be used for robustness of the data link. The required telemetry data to be send to the competition judges are the UAV's location, heading and speed. The crew and judges are allowed to enable the flight termination mode by sending a signal over the communication system. As the data rate of GSM communication is higher than for radio radio communication, a live video stream from the UAV can be transmitted over the GSM network. The required telemetry data will be send over radio as well as the GSM network at all times. There is a possibility that one of the communication systems fail during operation. Depending on the mission phase and the system that fails, an operational plan is established with the focus on reestablishing the communication link as fast as possible as is described below:

- Cruise:
  - **Loss of direct radio:** As the UAV is in line of sight during cruise, it is unlikely that radio signals gets lost, the drone operator will be warned.
  - **Loss of GSM:** As the GSM network is designed for modems at ground level, it may happen that there are periods of signal loss during cruise. In case of signal loss, the UAV can fly at a lower altitude to reestablish connection.
  - **Loss of all links:** The UAV must fly back to base in order to reestablish radio communication. In case the data link cannot be reestablished, the UAV must land at the base.
- Loiter / Landing:
  - **Loss of direct radio:** Due to the low altitude, a free line of sight for the direct radio cannot be guaranteed. The UAV will only communicate over the GSM network in case of radio loss.
  - **Loss of GSM:** The drone must fly higher in order to prevent the loss of the direct radio communication. The UAV can start loiter again when GSM communication is reestablished. The drone is not allowed to land without a working GSM communication as it is likely that a direct radio connection is not working as there is no direct line of sight.

- **Loss of all links:** The UAV must fly higher order to reestablish radio communication. In case the data link cannot be reestablished, the UAV must land at the base. The UAV not allowed to land at an remote landing site without communication.

- On ground
  - **Loss of direct radio:** Due to the low altitude, a free line of sight for the direct radio cannot be guaranteed. In case of radio loss the UAV will only communicate over the GSM network.
  - **Loss of GSM:** The UAV is only allowed to take-off if radio communication is working continuously.
  - **Loss of all links:** UAV is not allowed to take-off without continuous communication.

From the operational plan it can be concluded that it is vital that GSM communication is working prior to landing. Within a free line of sight, the GSM and radio communication will work simultaneous in order to make the data link robust.

9.3. Equipment Selection

Equipment is selected during the design of the communication system. In the midterm report [19] it was decided to combine a direct radio communication link with the usage of a GSM network. The equipment selection for the direct radio communication is given in section 9.3.1. The selection of GSM components is given in section 9.3.2.

9.3.1. Radio Equipment

The main restrictions on the radio system comes from the regulations. The Australian government restricts the available frequency bands along with the maximum equivalent isotropic radiated power (EIRP). The exact values of the standards in Australia are fixed and given in table 9.1.

Table 9.1: Frequency bands and power limits for spread spectrum and digital modulation devices[1]

Frequency band [MHz]	Maximum equivalent isotropic radiated power (EIRP)
915 to 928	1 watt (frequency hopping transmitters must use a minimum of 20 hopping frequencies)
2400 to 2483.5	500 milliwatts (a minimum of 15 hopping frequencies must be used)
2400 to 2483.5	4 watts (frequency hopping transmitters must use a minimum of 75 hopping frequencies)
5725 to 5850	4 watts (frequency hopping transmitters must use a minimum of 75 hopping frequencies)

The frequency bands from 915-928 MHz proved to be the most optimal for the specific use of the radio system. It appears that the lowest frequency results in the most favourable option. This finding is a conclusion of the subsequent different arguments:

- First of all, a lower frequency has better properties with respect to object propagation. As the low frequency means a long wavelength, which then results in better properties in propagating past obstacles. Waves with lower frequencies can pass through objects with less penetration that waves with higher frequencies.
- As can be seen in table 9.1, a higher frequency band means that the maximum EIRP can be higher. As the maximum EIRP at the lowest frequency band provides sufficient power at the receiver, this is not a limiting factor. Another downside of a higher frequency is that it will need a higher transmitter power to reach the same receiver power compared to lower frequencies. And as the lowest frequency is sufficient in terms of power, as will be proven in section 9.4.1, there is no rationale for using a higher frequency.
- Furthermore the cable losses are dependent on the frequency which goes through the cable. This trend can be seen in fig. 9.1, as the signal loss evidently increases with frequency.

[1] URL `https://goo.gl/I8jFZw` [cited 15 June 2017]

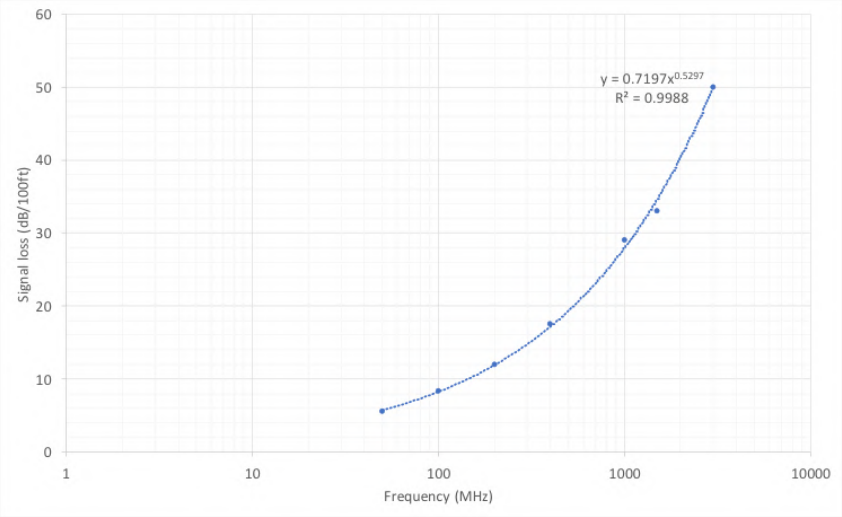

Figure 9.1: Signal Loss and Frequency relation for coaxial cable[2][3]

- And finally, as the equipment that is needed for frequencies at higher frequencies generally call for higher power, the equipment is also generally heavier to support this. Where the radio modems of the 915 to 928 MHz are generally about 10-20 times[4] lighter than the modems needed for 2400 to 2483.5 MHz.

Moving on, for both the UAV and the ground system, the final components for the radio system are chosen. The selected hardware is presented in section 10.2. Also, pictures of the chosen modems, ground antenna and UAV antenna is given in fig. 9.2, 9.3 and 9.4, respectively.

Figure 9.2: RFD 900x Modem[5]

Figure 9.3: Dipole Ground Antenna[6]

Figure 9.4: Dipole UAV Antenna[7]

As can be seen in section 10.2, the decision was made to use two PCB antennas on the UAV itself. This particular PCB antenna was chosen due to its omnidirectional radiation pattern. A general omnidirectional radiation pattern is shown in fig. 9.5. The weakness of this type of radiation pattern is at the top and bottom of the antenna. Therefore, it is chosen to use two antennas, at a 90 degrees angle with respect to each other attached in-plane with the wing. This way, the radiation pattern of the radio system on the UAV can be seen as almost spherical, as can be seen in fig. 9.6. A diversity mode on the radio modem regulates which antenna picks up the signal, which is the antenna that receives the highest signal power. Using this antenna setup, the probability that a signal is received at the UAV in its different configurations, is increased.

[2]URL http://www.l-com.com/content/Article.aspx?Type=N&ID=10336 [cited 15 June 2017]
[3]URL http://sonatechnologies.in/sona/tag/rf-cable-india/ [cited 15 June 2017]
[4]URL https://www.campbellsci.com/rf415 [cited 15 June 2017]
[5]URLhttp://store.rfdesign.com.au/rfd-900x-modem/ [cited 21 June 2017]
[6]URLhttp://store.rfdesign.com.au/antenna-900mhz-3dbi-dipole-rpsma/ [cited 21 June 2017]
[7]URLhttp://www.l-com.com/multimedia/datasheets/DS_HG902PU-UFL.PDF [cited 21 June 2017]

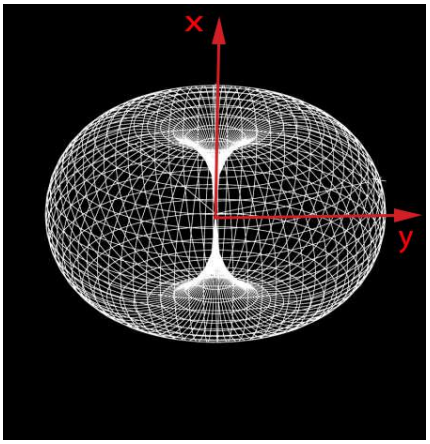

Figure 9.5: Omnidirectional Antenna Radiation Pattern

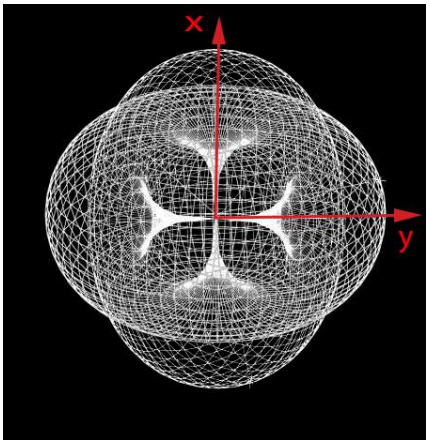

Figure 9.6: Radiation pattern of antennas in 90 degree orientation

9.3.2. GSM Equipment

In the midterm design phase [19] the usage of a GSM network was selected as a means of communication. In order to set up cellular communication the following set of equipment is required:

- Wireless module
- Antenna
- SIM card
- PCB
- Processor

There is already a 3G communication shield on the market that can be connected to an Arduino processor as can be seen in figure fig. 9.7. The shield consists of a SIM5216A[8] wireless module which is mounted on a PCB. An antenna must be connected to the wireless module. Because the 3G network operates at several frequency bands, a PCB antenna is selected that can operate at all 3G frequency bands as can be seen in fig. 9.8. A processor must be connected to the PCB in order to initialise and convert data to the wireless module. An Arduino UNO processor can be used for the ITEAD 3G shield as shown in fig. 9.9. Data on power, mass and volume of the selected equipment can be found in the budget given in section 10.2.3.

Figure 9.7: ITEAD Arduino 3G GSM Shield SIM5216A[9]

Figure 9.8: Laird Technologies 3G PCB antenna[10]

Figure 9.9: Arduino UNO processor[11]

The GSM communication system can be customised for the use on an UAV system by designing a small PCB which can be connected to a small processor. The selected equipment is compatible with the Australian cellular network and can be used for data transfer using a TCP/IP connection via the WCDMA and HCPDA networks (3G) of Telstra with a data rate of maximum 3.6 Mbps and 384 kbps respectively.

[8] URL `https://wirelessset.net/2011/12/` [cited 21 June 2017]
[8] URL `http://simcomm2m.com/En/module/detail.aspx?id=79` [cited 15 June 2017]
[10] URL `https://www.itead.cc/itead-3g-shield.html` [cited 15 June 2017]
[11] URL `https://www.digikey.com/product-detail/en/EPR8221A1-15UFL/994-1038-ND/2392217` [cited 24 June 2017]
[12] URL `http://www.arduino.org/products/boards/arduino-uno` [cited 24 June 2017]

9.3.3. Ground Equipment

For the ground station, a radio and a GSM modem is needed. The antenna's will be elevated using a telescopic rod in order to reduce propagation losses. The modems will be connected to a ground computer which will transfer location data to the competition jury. Data on Dynamic No Fly Zones will be fed to the ground computer by the jury.

9.4. Verification & Validation

The communication system is verified by means of a link budget which takes into account connector losses, cable losses and propagation losses. Connector losses[12] are given by the manufacturer of SMA connectors and increases with frequency. Cable losses are obtained from an interpolation of experimental data as is given in fig. 9.1. The verification for the direct radio communication is given in section 9.4.1. The verification and validation for the GSM communication is given in section 9.4.2.

9.4.1. Direct Radio Communication

The exact antenna pattern can be seen in fig. 9.10. Here, the red line represents the emission in vertical plane and the black line represents the horizontal plane. It can be seen that the radiation around the antenna is not ideal homogeneous, but has some irregularities as a dipole antenna is reconstructed in the PCB. The lowest gain of -13.5 dBi can be found at around -15 degrees in the vertical plane, while the highest gain of 5.40 dBi is found at -90 degrees in the horizontal plane or at 90 degrees in the vertical plane. The peak gain should be used to determine the maximum power allowed transmitting power of the UAV antenna, as the EIRP could not be higher than 1W (table 9.1). However, the lowest gain should be used to determine if the received power is higher than the sensitivity of the receiver at both ground and UAV. This particular power at the receivers can be determined with a link budget.

The link budgets for both the uplink and the downlink are represented in table 9.3. Here, the uplink is the link from the UAV to the ground station and the downlink is the link in the opposite direction. table 9.2 indicates the properties of the chosen antennas, which are used to create the link budgets. The link budget represents the worst case situation of the signal. The furthest distance that the UAV can be from the base station is 12km, which is used in the link budget. While the ground antenna will be held up by a telescopic rod of 7.2m[13], the height of the ground antenna is positioned at 4m in the link budget. Having to take a lower position, possible bad weather conditions and non optimal use of the telescopic rod, can be taken into account. With this position, the link budget indicates that the lowest altitude, where a link can still be established, is 20m. Below this altitude, the radio connection is likely to be unfeasible. For lower altitudes, the GSM network can be used.

The link budget is built-up as stated in the introduction of this section. For propagation loss, the radio link budget takes into account the flat earth loss. The flat earth loss consists of the ground bounce loss in combination with the free space loss[14]. The resulting link budget for the worst case situation is presented in fig. 9.11.

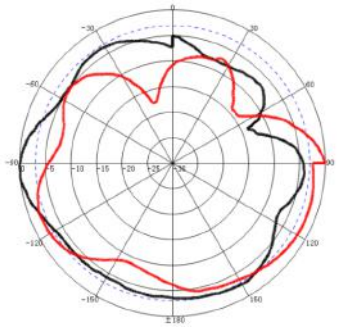

Figure 9.10: PCB Antenna Pattern[7]

[12] URL `https://www.amphenolrf.com/connectors/sma.html` [cited 22 June 2017]
[13] URL `https://goo.gl/2kV9g2` [cited 11May 2017]
[14] URL `https://www.maximintegrated.com/en/app-notes/index.mvp/id/5142` [cited 22 June 2017]

Table 9.2: Radio antenna details

Frequency [Mhz]	Uplink	Downlink
Antenna Height [m]	20	4
Transmitter EIRP [dBm]	11.1	30
Receiving antenna gain [dBi]	-13.5	3

Table 9.3: Link budget for radio connection

Frequency [MHz]	Uplink	Downlink
PA Power [dBm]	25.33	27.73
TX antenna gain [dBi]	-13.5	3
Connector loss [dB]	-0.0569	-0.0569
Cable loss [dB]	-0.676	-0.676
Flat earth loss [dB]	-128.65	-128.65
Ground bounce loss [dB]	-15.33	-15.21
Free space loss [dB]	-113.44	-113.44
RX antenna gain [dBi]	3	-13.5
RX Power [dBm]	-114.55	-112.15
RX sensitivity [dBm]	-116.79	-116.79
Excess signal strength [dBm]	2.24	4.64

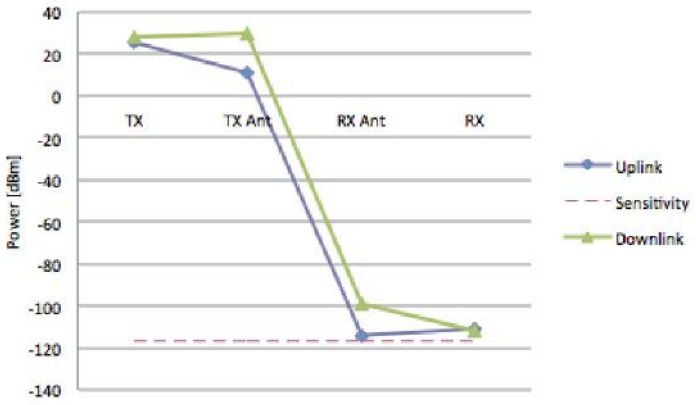

Figure 9.11: Radio Link Budget

Now that the verification of the direct radio link has been performed, validation needs to be done to fully ensure a proper radio system. Validation however will be a task that will be performed in the next phase of the project, when the equipment will actually be bought. A validation strategy that can be performed is testing the equipment by standing on top of a one story building at around 4m height whilst connecting with the UAV antenna at 12km at 20m height.

9.4.2. GSM communication

The mobile provider Telstra claims to cover the whole mission area with their 3G network as can be seen in fig. 9.12. The map is produced by the provider using network statistics.

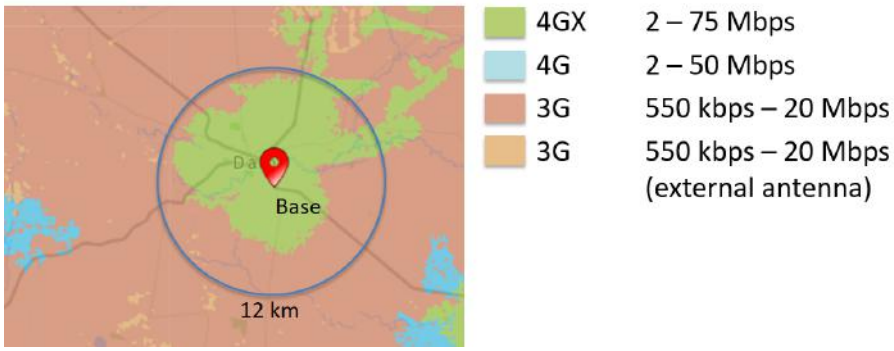

Figure 9.12: Coverage of the Telstra Network[15] within the mission area

The signal propagation of the 3G network of Telstra can be verified using (COST) Hata models for rural areas [33, p. 151-152]. The models are developed using statistical data and various experiments. The Hata model is valid for a frequency range of 150-1500 Mhz and the COST Hata model is an extension of the Hata model which is valid for a frequency range of 1500-2000 Mhz. The locations of any licensed radio equipment within Australia are listed in a register[16] by the Australian Communications and Media Authority. From the register it can be obtained that Telstra 3G antennas are located in the centre of Dalby transmitting at frequencies of 850 and 2100 MHz. The maximum distance between the 3G antenna and the UAV is 22 km at most during a mission. The 3G network coverage can be verified using the maximum link distance using the (COST) Hata models for 3G network frequencies of 850 and 2100 Mhz. The signal propagation loss for a 850 MHz signal is calculated using the Hata model. The signal propagation loss for 2100 MHz is calculated using the COST Hata model, the results can have an error due to the fact that the frequency to be investigated is 100 MHz outside the range of the model. A link budget is created for the worst case scenario when the UAV is at ground level at the maximum distance of 22 km from the 3G antenna located in Dalby. Specifications of this 3G antenna can be found in table 9.4. Uplink signals are send from the UAV to the 3G antenna. Downlink signals are send from the 3G antenna to the UAV.

Table 9.4: Details about the Telstra 3G antenna located in Dalby[16]

Frequency [Mhz]	**850 uplink**	**2100 uplink**	**850 downlink**	**2100 downlink**
Antenna Height [m]	70	70	53	70
Transmitter EIRP [dBm]	-	-	61.49	72.01
Receiving antenna gain [dBi]	18.2	19	-	-

A link budget is performed in case the UAV lands at a distance of 22 km from a 3G antenna. The result of the link budget is presented in table 9.5.

Table 9.5: Link budget for 3G GSM connection

Frequency [MHz]	**850 uplink**	**2100 uplink**	**850 downlink**	**2100 downlink**
PA Power [dBm]	24	24	61.49	72.01
TX antenna gain [dBi]	2.2	3.8		
Connector Loss [dB]	-0.06	-0.09	-0.06	-0.09
Cable Loss [dB]	-0.66	-1.06	-0.66	-1.06
Propagation loss [dB]	-139.74	-148.47	-142.47	-148.47
RX antenna gain [dBi]	18.2	19	2.2	3.8
RX Power [dBm]	-96.05	-102.81	-79.49	-73.80
RX sensitivity [dBm]	-126.2	-126.2	-106	-106
Excess signal strength [dBm]	30.15	23.39	26.51	32.20

From the table it can be seen that the excess signal power is positive for all investigated signals. A graphical presentation of the link budget is given in fig. 9.13. The signal power is given at the following stations: transmitter, transmitter antenna, receiver antenna and the receiver. The signal sensitivity for uplink and downlink are given as dotted lines.

[15] URL `https://www.telstra.com.au/coverage-networks/our-coverage` [cited 18 June 2017]
[16] URL `https://web.acma.gov.au/rrl/site_proximity.main_page` [cited 19 June 2017]

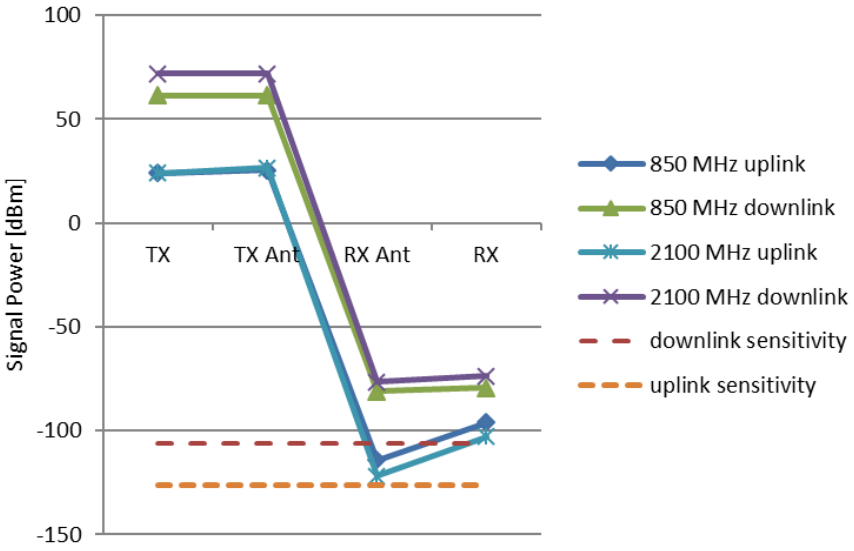

Figure 9.13: Link plot of 3G GSM network for a link distance of 22km

It can be concluded from the figure that the receiving power for all signals are bigger than the minimum required receiver sensitivity. Therefore the 3G GSM communication is verified to work within the mission area.

9.5. Conclusion and Recommendations

For communication, a direct radio connection will be used in combination with communication over a 3G GSM network. For radio communication, a 900 MHz modem will be used that transmits at a maximum isotropic radiated power of 1W in order to comply with Australian regulations. The selected radio equipment is verified to have an excess signal power of 2.24 dB at an altitude of 20 m and at a distance of 12 km from the base within a free line of sight. The 3G network coverage of Telstra is verified at the worst case distance from the provider's antenna located in Dalby. The excess signal power of the 3G network at the worst case distance from the 3G antenna is calculated to be 23.39 dB in case the UAV has landed.
During further design of the communication system, a PCB can be designed that is smaller than already existing 3G shields on the market. The usage of two 3G networks at the same time using two modems can be investigated as well, which will increase the data rate and robustness of the communication system.

10 System Integration

This chapter describes the method used to establish the final design of the UAV. The steps taken during design iterations are given in section 10.1. Performance parameters, visualisations and budgets of the final design are given in section 10.2. The robustness of the design is investigated by means of a sensitivity analysis in section 10.3. Requirements and their compliance are given in section 10.4. Finally the production plan and risk assessments are given in section 10.5 and section 10.6 respectively.

10.1. Iterations

In order to reach the final design, design steps often need to be repeated more than once, since the output from one design step may be an input of a previous design step. The design steps that need to be taken in order to reach the final design are indicated in a N^2-chart, which is represented in fig. 10.1. The arrows in the figure indicate the input and output direction of the subsystems that are indicated on the diagonal axis.

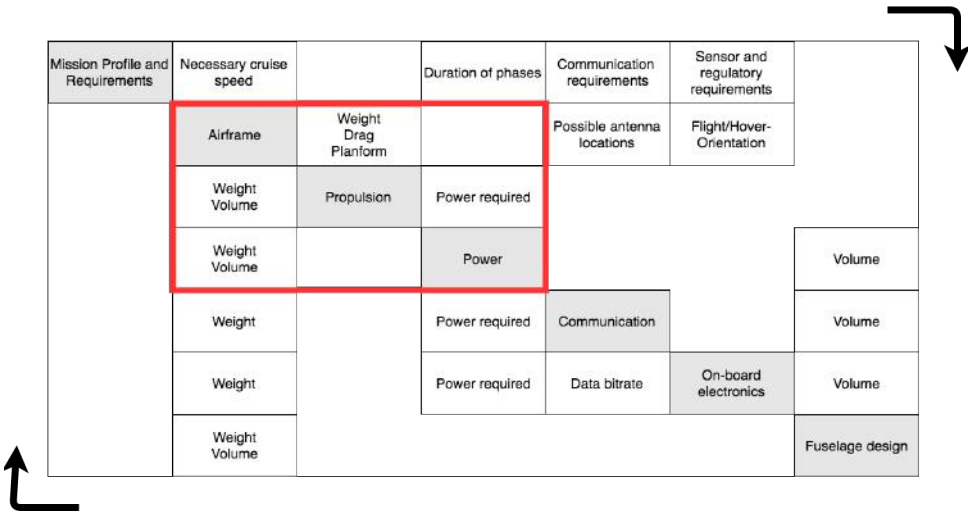

Figure 10.1: Design N^2-chart

The first inputs of the design process are extracted from the mission profile and the requirements, as can be seen in the upper horizontal row. With the use of these inputs, preliminary mass and volume budgets were made during the early phases of the design. The preliminary design budgets will be used as input for the first iteration. The red border around the air-frame, propulsion and power subsystems indicate the design section that is highly iterative. During this design phase, the iteration of this section will be executed first. After the iterations of that section are converged, the subsequent design steps are executed. After the design of all the subsystems, a final iteration has been executed. The design steps were performed once more to check whether or not the final design fully converged.

Parameter	Iteration				
	0	1	2	3	4
Fuel cell mass $m_{\text{fc.}}$	2234 g	2327.03 g	2327.03 g	2453.66 g	2453.66 g
UAV weight m	7.371 kg	7.679 kg	8.32 kg	8.454 kg	
Cruise drag $D_{\text{cr.}}$	7.857 N	7.918 N	8.32 N	8.403 N	
Max. drag D_{max}	9.096 N	9.298 N	9.511 N	9.578 N	
Cruise shaft power $P_{\text{cr.}}$	268 W	270 W	276 W	284 W	
Loiter shaft power P_{loiter}	252 W	234 W	252 W	258 W	
Max. shaft power P_{max}	480 W	434 W	498 W	488 W	
Take-off shaft power $P_{\text{to.}}$	848.69 W	841.69 W	913.42 W	957.41 W	
Landing shaft power P_{land}	506.32 W	524.40 W	567.49 W	568.12 W	

Table 10.1: Table showing the evolution of the important subsystem parameters. The 0'th iteration starts with an initial assumption of the fuel cell mass, from which the aerodynamic analysis is performed, and, consecutively, the propeller analysis. Finally, the iterations returns to the power system analysis. The iteration stops when one subsystems stagnate, seen in the 4th iteration.

Table 10.1 shows the evolution of the parameters throughout this iterative process. The iteration sequence started at zero with an initial guess of the fuel cell weight. This weight is then used as input for the next iteration, the iteration sequence stops when the results are within a small margin of change or no change at all. As shown in table 10.1 the final iteration process converged rather quickly. This is probably due to the fact that the guess of the fuel cell mass was already optimised for the planform. This caused that the initial guess was very close to the actual fuel cell weight already and it only needed to be adapted to the other subsystems within this iteration.

10.2. Final Configuration

The final configuration of the UAV is presented in this section. First performance parameters are discussed in section 10.2.1 followed by an visualisation of the final configuration, section 10.2.2. A budget breakdown is given in section 10.2.3.

10.2.1. Performance

After running through the iteration and optimising for performance at each iteration, the planform parameters, and accompanying aerodynamic characteristics are found, as displayed in table 10.2.

Table 10.2: Planform parameters and aerodynamic characteristics for the optimal (final) planform

Planform	
Surface area S	0.6645 m^2
Aspect ratio A	4.232
Taper ratio λ	0.8
Spanwidth b	1.452 m
Mean aero. chord $\bar{c}$	0.1989 m
Total mass m	8.454 kg
Systems m_{sys}	2.04 kg
Velocity V	27.7 m/s
Lift coef. C_L	0.3907
L/D	9.866
Drag D	8.403 N
Drag coef. C_D	0.027 91
Zero-lift drag coef. $C_{D,0}$	0.018 68
Fuselage $(C_{D,0})_{\text{fus.}}$	0.0079
Wing $(C_{D,0})_{\text{wing}}$	0.0084
Interference $(C_{D,0})_{\text{interf.}}$	5.0×10^{-5}
Other $(C_{D,0})_{\text{other}}$	0.0019
Induced drag coef. $C_{D,\text{i}}$	0.009 173
Planar Oswald factor e	0.902
Non-planar Oswald factor $e_{\text{np.}}$	1.25
Viscous drag coef. $C_{D,\text{v}}$	5.9×10^{-5}
Stall velocity	14.31 m/s
Stall lift coef.	1.032
Endurance velocity	19.61 m/s
Endurance drag	9.749 N
Range velocity	26.24 m/s
Range L/D	9.950
Range drag	8.3322 N
Maximum velocity	34.2 m/s
Maximum drag	9.578 N

Furthermore, the $(D-V)$-plot, indicating the variation of the drag with velocity, for the final planform is displayed in figure 10.2

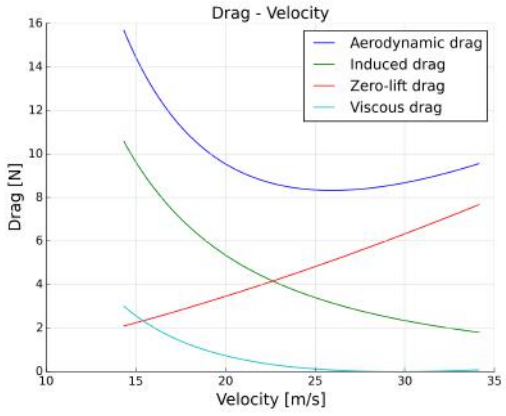

Figure 10.2: D-V plot for the final configuration

The variation between the lift coefficient C_L and the drag coefficient C_D for the final configuration is shown in fig. 10.3.

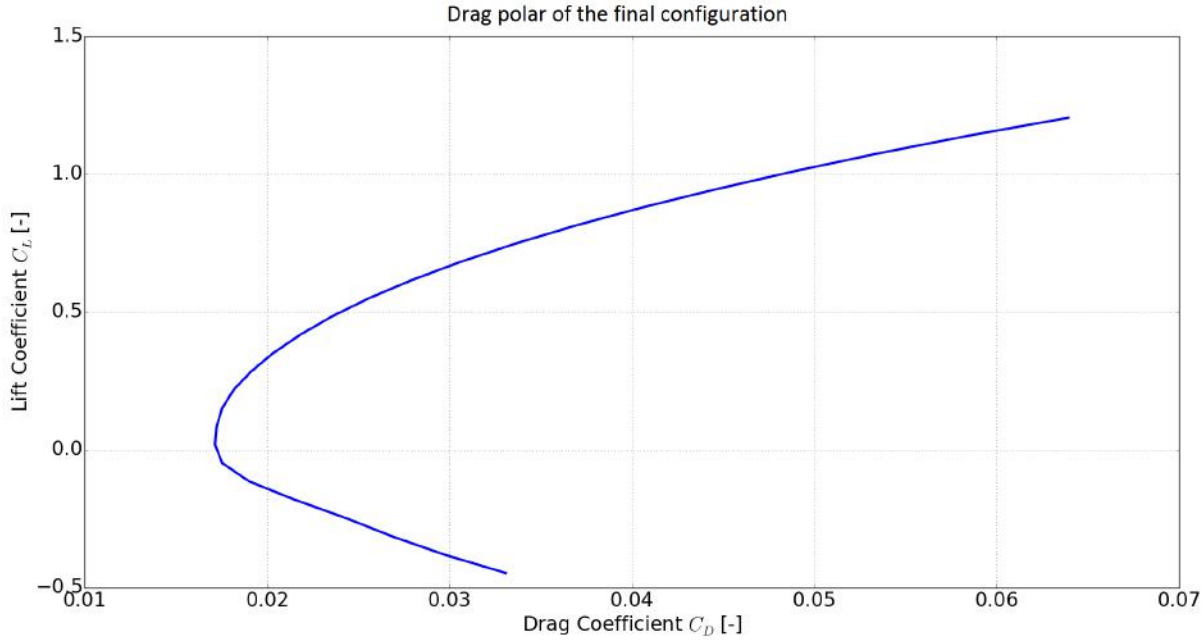

Figure 10.3: Drag polar for the final configuration

The $(C_L - \alpha)$-plot for the final configuration is shown in fig. 10.4.

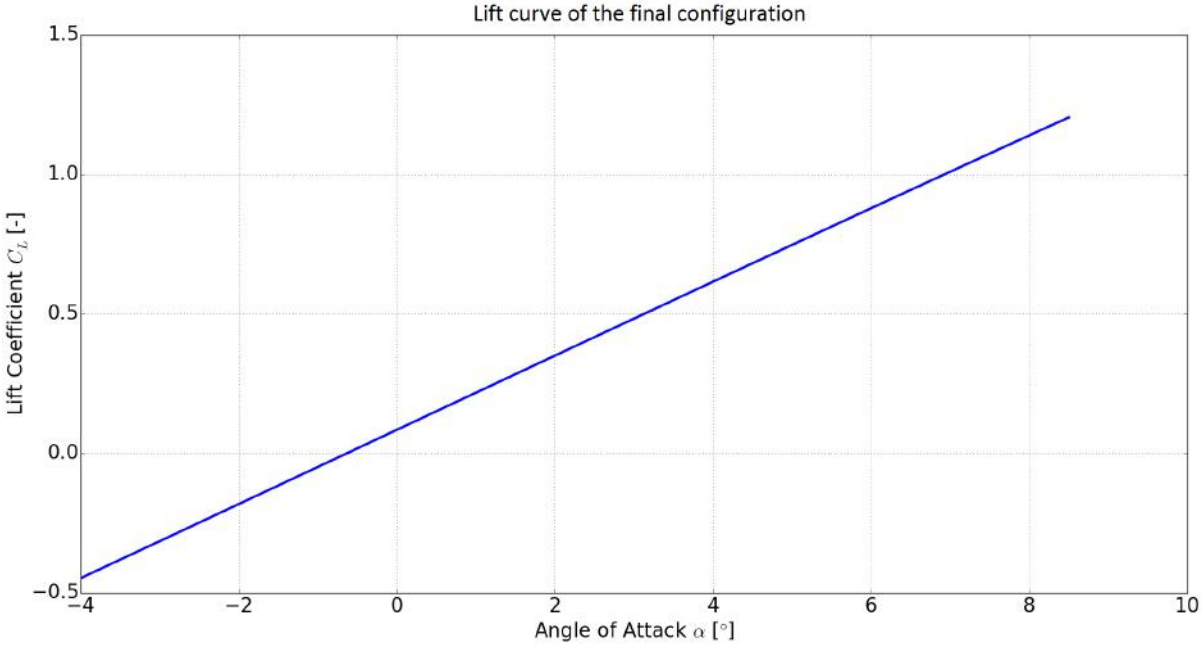

Figure 10.4: $(C_L - \alpha)$-plot for the final configuration

Finally, the $(C_m - \alpha)$-plot is shown in fig. 10.5.

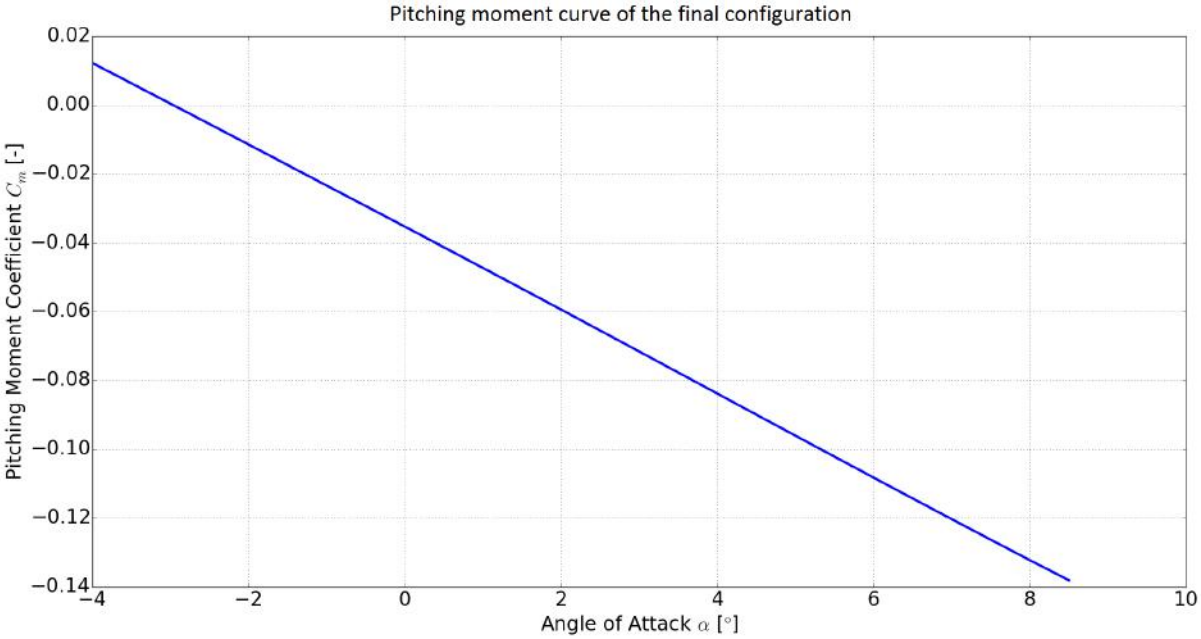

Figure 10.5: $(C_m - \alpha)$-plot for the final configuration

10.2.2. Layout

The layout and dimensions of the UAV system are presented in this section. First an overview of the assembled UAV is given. Secondly the internal design of the fuselage is presented.
An isometric view is given in fig. 10.6, a front view in fig. 10.7, a top view in fig. 10.8 and a left view in fig. 10.9.

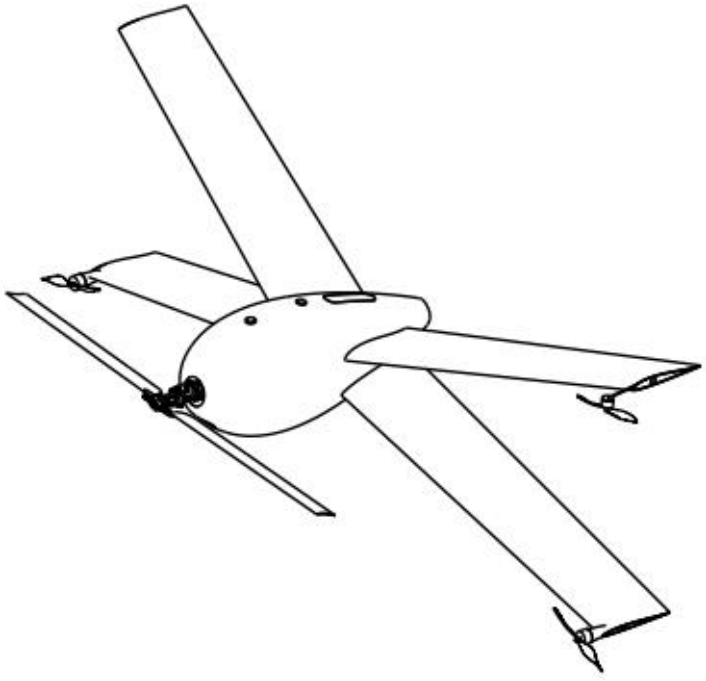

Figure 10.6: Assembly isometric view. Scale: 1:15

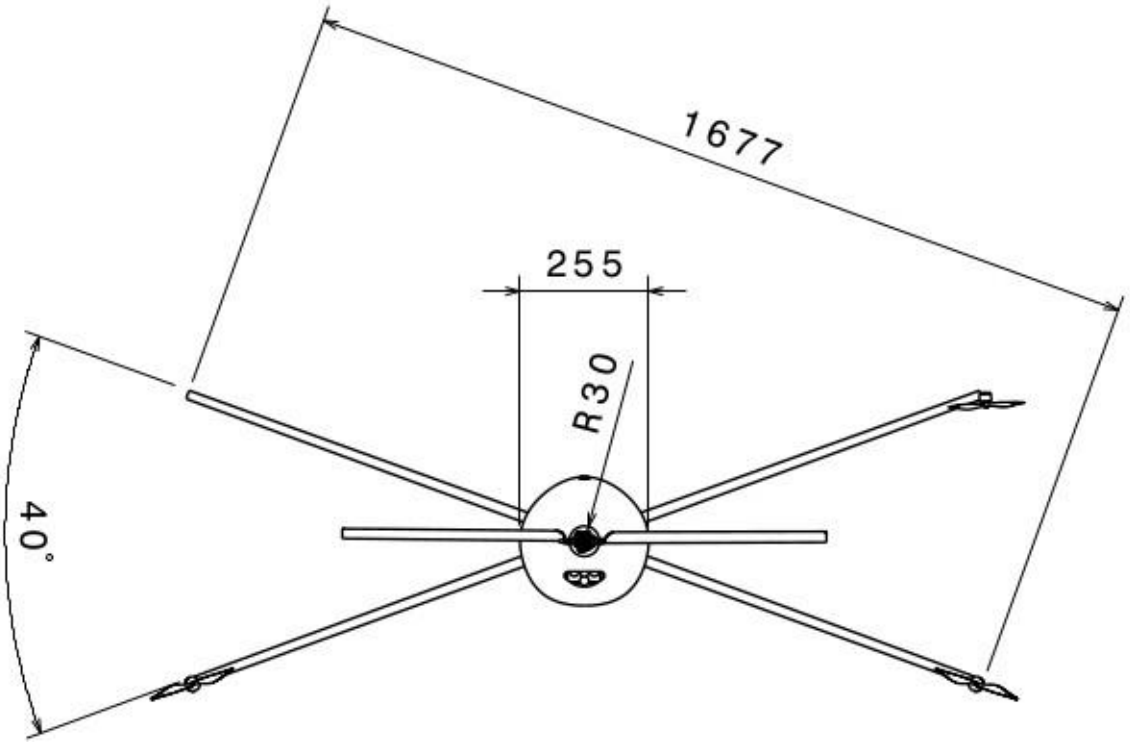

Figure 10.7: Assembly front view. Scale: 1:15

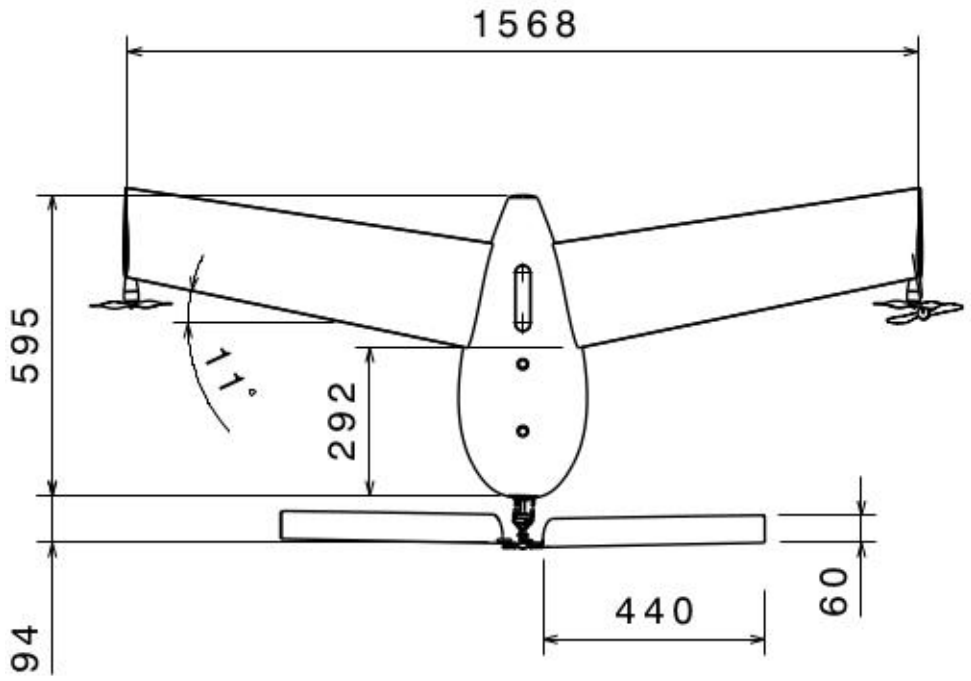

Figure 10.8: Assembly top view. Scale: 1:15

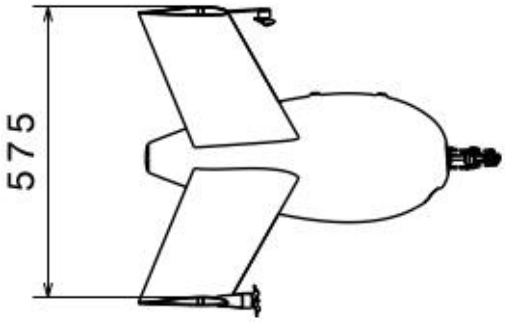

Figure 10.9: Assembly left view. Scale: 1:15

The internal layout of the fuselage is given in fig. 10.10. An isometric view of the internal fuselage design is given in fig. 10.11. The locations of all components in the fuselage are visualised in the drawings.

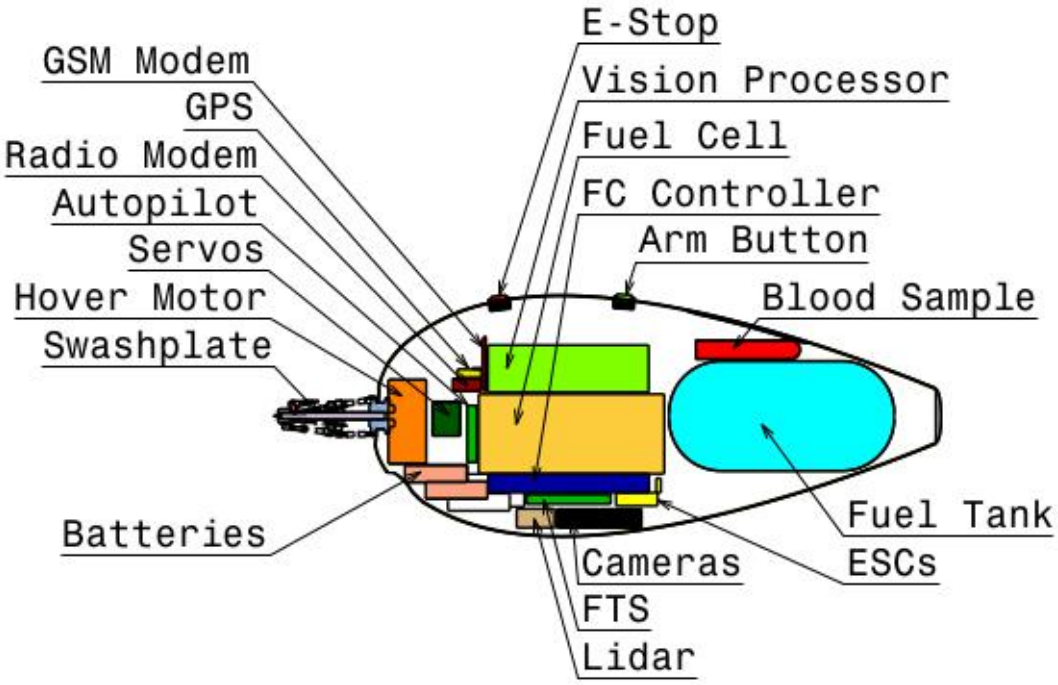

Figure 10.10: Internal fuselage design. Scale: 1:8

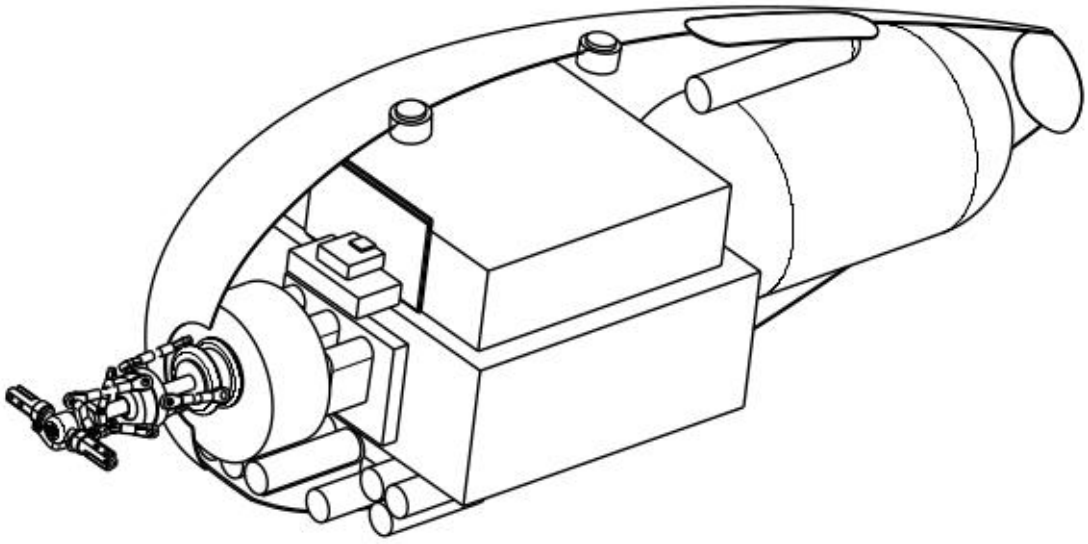

Figure 10.11: Isometric view of internal fuselage design. Scale: 1:4

10.2.3. Final Budget Breakdown

Table 10.3 lists all the components that were selected for the UAV and table 10.4 shows the budget for the ground station. At the bottom of the table a total budget for the number of components, mass, power and cost is compiled. A safety margin of 5% is applied to the mass and cost budget, except for the structural components as these are already conservative estimates. This is to account for missing components such as cables, connectors, switches, etc. The power is the maximum power consumption possible that will realistically never be reached as not all components can be active at the same time. As can be seen the system adheres to the requirements concerning the cost and mass of the system. The product names include hyperlinks leading to the websites, where the products can be purchased for easy production of the system at a later stage. A budget including materials to manufacture the UAV, labour and other costs can be found in table 11.1.

Table 10.3: UAV System Budget Table

Component	Type	QTY	Mass [g]	Voltage [V]	Power [W]	Dimensions [mm]	Cost [€]
Communication							
Huber and Suhner 22510079 Coax Cable	Cable	3	12	–	–	838.5 × ∅2.5	3.53
RP-SMA	Connector	2	9.9	–	–	10.9 × ∅7.67	2.99
Dipole Coaxial Feed Direct Connect Quarter Wave Antenna	Radio antenna	1	13	–	–	160 × 10 × 50	5.16
RFD900x Modem	Radio modem	1	14.5	5	4	57 × 30 × 12.8	119.50
IAS EPR8221A1-15UFL	GSM antenna	1	13	–	–	0.8 × 70 × 20	3.20
3G Shield	GSM modem	1	75	5	2.5	1.6 × 91.93 × 57.15	58.77
Arduino Uno Processor	GSM processor	1	25	5	0.25	1.6 × 91.93 × 53.4	23.00
Control System							
Chimera/v1.00	Autopilot & FTS	2	12	6 – 26	< 1	20 × 89 × 60	279.95
Pitot Tube	Pitot Tube	1	9	–	–	103 × ∅10	10.75
RGB LED	Status LED	1	2	5	< 1	8.7 × 5 × 5	2.00
SparkFun Venus GPS	GPS modem	1	3	3.3	0.03	1.3 × 10 × 10	44.71
Antenna GPS Embedded SMA	GPS antenna	1	18	3.3	0.004	8.7 × 25 × 25	10.70
LIDAR-Lite v3	Altitude sensor	1	15	5	0.065	48 × 40 × 20	134.26
NVIDIA Jetson TX2	SoaC	1	353.8	19	< 20	49.8 × 169.9 × 169.9	267.64
Chameleon3 3.2MP Color USB3 Vision	Camera	2	54.9	5	< 3	19.5 × 44 × 35	399.00
TI TPSB4259RKGT	DC/DC converter	2	0.9	4.5 – 40	5	11 × 9 × 3	13.12
Swash-Plate							
MKS HV9767 Servo	Swashplate servo	3	38.55	8.4	21.84	35.5 × 15 × 28.5	83.5
Swashplate (Custom made)	Swashplate	1	100	–	–	–	–
Turnigy Plush 60A Speed Controller w/ BEC	ESC	1	60	5.6 – 22.2	0.11	14 × 31 × 80	31.53
Motors and Propellers							
Motor Hover	Hover motor	1	511	24	2000	40 × ∅88.6	304.00
Motor Cruise	Cruise motor	2	42.1	22.2	1000	33.5 × ∅28.8	25.00
Motor Roll	Torque motor	1	18	11.1	125.43	26.7 × ∅23	11.15
ESC Cruise	Cruise ESC	2	6.6	22.2	0.11	30.5 × 14.9 × 5	15.00
ESC Roll	Roll ESC	1	3.7	14.8	0.074	23.5 × 11 × 5	11.00
Propeller Hover	Hover propeller	1	233	–	–	–	12.23
Propeller Cruise	Cruise propeller	2	3.5	–	–	–	1.37
Propeller Roll	Roll propeller	1	4.8	–	–	–	5.28
Power							
Fuel Cell	Fuel cell	1	550	–	650	84 × 196 × 198	18200.00
Controller	Controller	1	200	–	–	170 × 65 × 20	Included in FC
Tank	Tank	1	1010	–	–	238 × ∅116	Included in FC
Battery	Battery	12	44.6	3.7	84	65.3 × ∅18.3	8.00
FTS Battery	FTS Battery	2	19.7	3.7	< 6	51.2 × ∅14.3	4.50
Structure							
Foam	Wings	1	168	–	–	–	1.42
Carbon	Wings & Fuselage	1	1083.2	–	–	–	97.30
Glass Fibre	Wings & Fuselage	1	2900	–	–	–	16.41
Total UAV System excl. Power system	–	41	1977.41	–	6128.61	–	3049.16
Total UAV System incl. Power system	–	58	8463.21	–	–	–	22269.41

Table 10.4: Ground station budget table

Component	Type	QTY	Mass [g]	Voltage [V]	Power [W]	Dimensions [mm]	Cost [€]
Ground Communication							
RFD900x Modem	Radio modem	1	14.5	5	4	57 × 30 × 12.8	119.50
Antenna 900 MHz 3dBi dipole	Radio antenna	1	28	–	–	198 × ∅12	4.72
3G Shield	GSM modem	1	75	5	2.5	1.6 × 91.93 × 57.15	58.77
Arduino Uno Processor	GSM processor	1	25	5	0.25	1.6 × 91.93 × 53.4	23.00
IAS EPR8221A1-15UFL	GSM antenna	1	13	–	–	0.8 × 70 × 20	3.20
Antenna Elevation Rod	Telescopic rod	1	300	–	–	7200 × ∅100	38.44
Power							
Battery Charger	Battery Charger	1	50	6 – 26	< 720	–	20.00
Others							
Ground Station Computer	Computer	1	1800	110 – 220/19	< 100	400 × 250 × 25	1000.00
Total Ground system	–	8	2305.5	–	< 826.75	–	1267.63

10.3. Sensitivity Analysis

In this section, the sensitivity analysis of the global system design is performed. Technical parameters are analysed on their sensitivity on changes in the design. With such an analysis, the feasibility of the final design can be determined since there is the chance that calculations in the design are faulty. The analysis will be used to determine how other design parameters respond to change in the designed parameter. In this section, the major parameters of the design are analysed for its sensitivity, namely, the weight, stall speed/cruise speed, power and the drag. These particular parameters are chosen as they function as the core of the design iteration, as can be seen in fig. 10.1. Because the four parameters are the main drivers for the iterations, they highly

determine the final design. Therefore analysis of these parameters is essential.

10.3.1. Weight

The weight of the UAV can be estimated in the wrong way for several reasons. For example, the chosen material can be unavailable or inapplicable for an unforeseen reason or the fuel cell is heavier than expected. Such change in weight can have a significant impact on the entire design. As found in fig. 10.1, weight is an input for the airframe design as well as the propulsion design. The figure shows that for the airframe design, major output parameters are weight (including airframe weight) and drag. The drag and output weight are plotted as a function of input weight (weight of the UAV excluding airframe weight) in fig. 10.12 and fig. 10.13 respectively. The dot in the graphs indicate the value of the parameters of the final design.
A similar analysis is performed on the propulsion subsystem. In fig. 10.14 input weight is plotted against the climb power required for the hover propeller. The power required is specific for the hover propeller because the weight increase directly influences the hover power required, whereas drag has a direct relation with the cruise propeller. This relation will be discussed below in the drag parameter discussion. Focusing again on the weight parameter, it can be seen that all the relations have a positive relation. This is not surprising, as an increase in weight generally calls for a larger system.

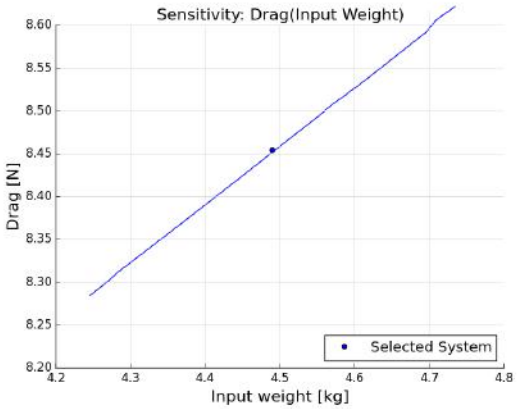

Figure 10.12: Airframe Input Weight to Drag Sensitivity

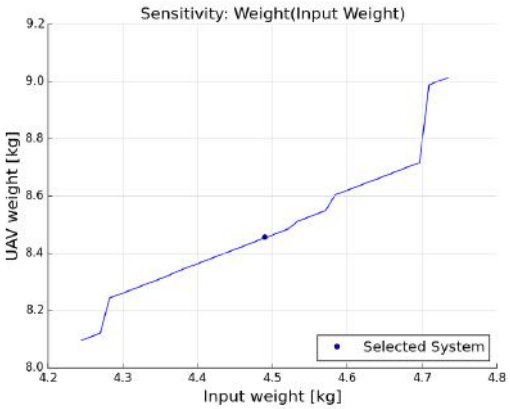

Figure 10.13: Airframe Input Weight to Output Weight Sensitivity

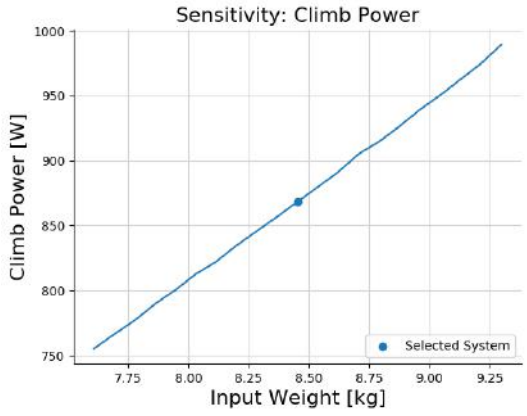

Figure 10.14: Propeller Input Weight to Output Climb Power Sensitivity

Table 10.5: Input Weight Sensitivity

Parameter	Underestimation	Current State	Overestimation
Input Weight	-10%	0%	+10%
Drag	-3.0%	0%	+3.0%
UAV Weight	-5.3%	0%	+8.3%
Climb Power	-13.8%	0%	+13.8%

Table 10.5 indicates what the result of 10% change in the input weight is for the other parameters. Here 0% is the final design weight. Firstly, it can be noted that the climb power is highly related to the input weight, as a change of 10% will result in a change of around 13.8%. This is due to the very close relation of both the parameters, as indeed, more power is needed to lift a system of higher weight. Furthermore, it is found that the relation between UAV weight and input weight is non-linear. The reason for this is that at a certain input weight, another planform design is more beneficial. This causes jumps in the relation. Finally, the drag has a less significant relation with weight, as an increase in weight does not directly implies an increase in drag. An increase in weight generally results in a bigger planform, which then results in an increment in drag.

10.3.2. Cruise Speed

As could be seen in fig. 10.1, cruise speed is one of the main input parameters of the airframe design. This parameter could potentially change due to changes in the requirements. The result of such change is that the UAV planform design will change to best tailor to the requirement. This planform change will then have an effect of both the drag of the UAV, as well as the UAV weight. These relations are given in fig. 10.15 and fig. 10.16 respectively.

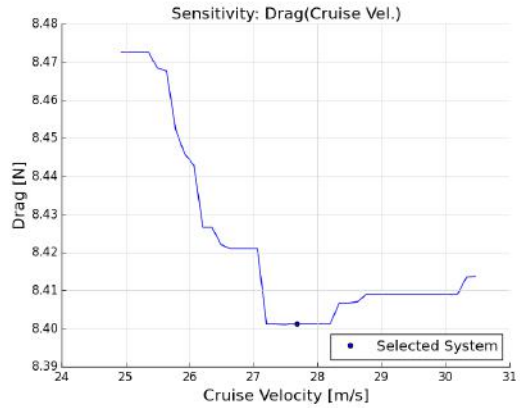

Figure 10.15: Airframe Cruise Speed to Drag Sensitivity

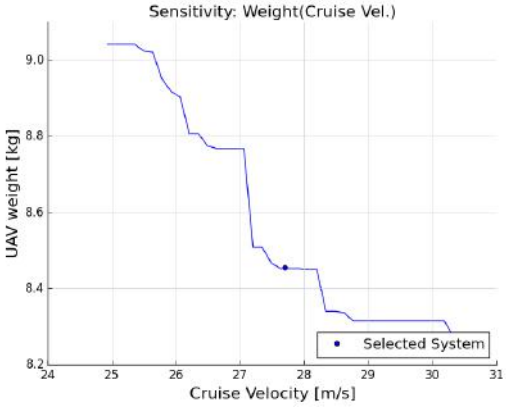

Figure 10.16: Airframe Cruise Speed to UAV Weight Sensitivity

Table 10.6: Cruise Sensitivity

Parameter	Underestimation	Current State	Overestimation
Cruise Velocity	-10%	0%	+10%
Drag	+0.9%	0%	+0.2%
UAV Weight	+7.0%	0%	-2.1%

As discussed in section 7.3.1, the structural components of the wing (i.e., the spar and skin) are sized such that a handling load of 270 N is sustained. The flight wing loading case was not found to be the most critical, hence indicating over-design for flight. Consequently, an increase in flight speed V_∞, see eq. (4.15), and thus an increase in flight wing loading would not require a heavier structure. Therefore, the increase in cruise velocity induces smaller optimal wings without an increase in specific structural weight per wing area. This is indicated in fig. 10.16.

The increase in drag for both an increase and decrease in cruise velocity, as indicated in fig. 10.15, is not as easily explained. The cruise velocity of 27.7 m/s seems to be optimal as far as drag concerned. As discussed in section 4.2, the drag is linked to airspeed through the Reynolds number *Re* and dynamic pressure. However, this differential may look out of proportion due to the scaling of the graph; the difference is actually a fraction of a percent, see table 10.6.

10.3.3. Power

The power that the power system needs to produce could be miscalculated as well. A result of needing a system that produces more power, would be an bigger power subsystem. The result is thus a higher weight. This trend can be clearly viewed in fig. 10.17. Here, the safety factor implemented in the calculations is plotted against the power system weight. This safety factor is an extra factor put upon the power required, that encapsulates the possible miscalculations. The current safety factor was chosen at 1.2. From table 10.7, it can be seen that

using no safety factor (SF=1.0), would result in a decrease of -10.2% in power system weight. Increasing the safety factor to 1.4 would result in increasing the weight by 10.2%. It is thus very evident that an increase in required power will strongly increase the power system weight.

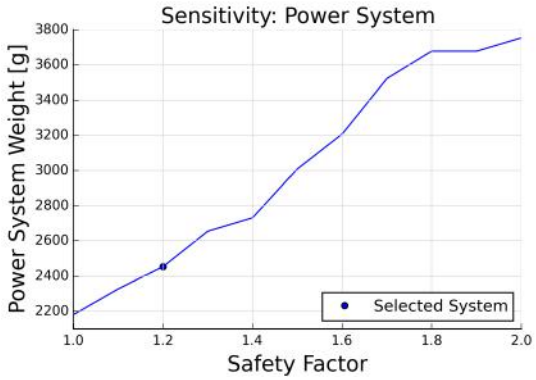

Figure 10.17: Power Safety Factor to Power System Weight Sensitivity

Table 10.7: Power Sensitivity

Parameter	Underestimation	Current State	Overestimation
Power Safety Factor	1.0	1.2	1.4
Power System Weight	-10.2%	0%	+10.2%

10.3.4. Drag

Finally, the drag parameter is discussed. Drag is a main input parameter for the propulsion design, and more specific for the cruise propeller design. Due to miscalculations, the drag could be higher or lower than first anticipated. The cruise propeller should be able to produce enough thrust to counter the drag. Thus an increase in drag would lead to a higher needed thrust for the cruise propeller and the opposite is true for a decrease in drag. When keeping all the other design parameters constant, this would mean that there is more power required to produce this thrust. This exact trend can be found in fig. 10.18, where a positive linear relation is found between input drag and cruise power. From table 10.8, it can be concluded that the cruise power is highly dependent on input drag, as 10% change in drag will result in about 11.6% change in cruise power.

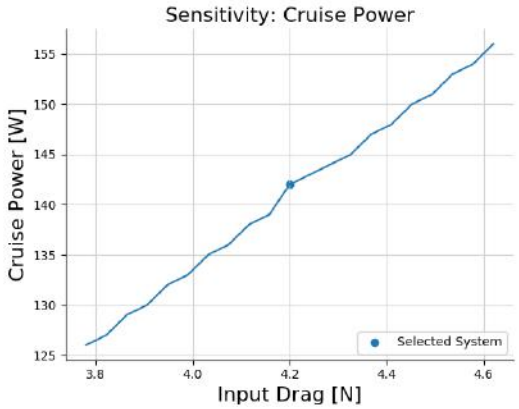

Figure 10.18: Propulsion Drag to Cruise Power Sensitivity

Table 10.8: Drag Sensitivity

Parameter	Underestimation	Current State	Overestimation
Input Drag	-10%	0%	+10%
Cruise Power	-11.6%	0%	+11.6%

10.4. Requirements Compliance Matrix & Feasibility Analysis

The requirements applying to the system design and mission can be found in the following tables. Further the compliance of the achieved design with the individual requirements is stated. The stakeholder requirements can be found in table 10.9. The Royal Netherlands Navy requirements can be found in table 10.10. The system requirements are listed in table 10.11 and the subsystem requirements are stated in table 10.12.
Some requirements had to be removed because they no longer applied to the mission or system, were duplicate or ill defined. Key requirements that have changed were discussed with the relevant Stakeholders prior to the change.

Table 10.9: Stakeholder Requirements Compliance Matrix

Requirement No.	Requirement	Value	Compliant	Comments
TU Delft:				
MEUC-TUD-01	The UAV shall be able to quickly and cost effectively deliver medical supplies to critically ill patients in the Australian Outback and return medical samples.	N/A	✓	Chapter 13
MEUC-TUD-02	The Medical Express UAV Challenge shall be completed in 50 min or less.	N/A	✓	Section 10.2
MEUC-TUD-03	The UAV shall have Type 2 Autonomy as defined by the Medical Express UAV Challenge 2018 rulebook.	N/A	✓	Section 8.5
MEUC-TUD-04	The UAV shall be able to perform vertical landings in unknown environments.	N/A	✓	Section 8.5
MEUC-TUD-05	The UAV system shall only use the open source software Paparazzi UAV for flight termination, real time re-planning and autopilot design.	N/A	✓	Section 8.5
MEUC-TUD-06	The UAV shall be fully electric only.	N/A	✓	Section 3.5
MEUC-TUD-07	The UAV shall have a range of 60 km.		✓	Section 10.2
MEUC-TUD-08	The UAV system shall be designed for end of life recuperation or recycling.	N/A	✓	Section 11.2.1
MEUC-TUD-09	The UAV system shall cost no more than €8000 (excluding fuel-cell system).	€4316.79	✓	Section 10.2
MEUC-TUD-10	The UAV system including fuel and payload shall not be heavier than 15 kg.	8.454 kg	✓	Section 10.2
MEUC-TUD-11	The maximum dimension of the UAV shall not be larger than 4 m.	1.452 m	✓	Section 10.2
MEUC-TUD-12	The UAV system shall be manufactured before the start date of the Medical Express UAV Challenge 2018.			
MEUC-TUD-14	The UAV system shall fit in a transportation box that fits in a standard car boot.	1.1 x 0.7 x 0.4 m	✓	Section 12.2
MEUC-TUD-15	The UAV system shall be capable of being transported from the Netherlands to Australia by a normal airline.	N/A	✓	Section 12.2
MEUC-TUD-16	The materials used shall be able to sustain normal usage during the operational lifetime.	~6000 h	✓	Section 11.2.3
MEUC-TUD-17	The UAV system shall not be a commercial off-the-shelf complete system (i.e., aircraft with all avionics, sensors and ground mapping processing systems that would result in completion of the mission already integrated).	N/A	✓	Section 8.3
MEUC-TUD-18	The UAV shall use a fuel-cell.	N/A	✓	Section 3.5
MEUC-TUD-19	The UAV main rotor shall use a swash plate design.	N/A	✓	Chapter 6, section 5.1, section 10.5.2
MEUC-TUD-20	The UAV shall be able to hover.	>40 min	✓	Section 6.5, section 3.3
MEUC-TUD-21	The UAV shall feature a fixed wing.	N/A	✓	Chapter 4
MEUC-TUD-22	The transition from forward flight to hover and vice versa shall be a soft transition.	N/A	✓	Section 5.2.4, section 5.2.3
CASA:				
MEUC-CASA-01	The UAV shall not come closer than 30 m in a straight line to any person during flight.	N/A	✓	Section 8.3, section 8.5
MEUC-CASA-03	The UAV shall remain within specified boundaries given by the Geofence coordinates (irregular 18 vertices' polygon).	N/A	✓	Section 8.3, section 8.5
MEUC-CASA-04	The UAV shall be able to avoid fixed No-Fly zones given by 4 coordinates.	N/A	✓	Section 8.3, section 8.5
MEUC-CASA-05	The UAV shall avoid Dynamic No Fly Zones (DNFZ) at all times.	N/A	✓	Section 8.3, section 8.5
MEUC-CASA-06	The UAV shall not fly over a building.	N/A	✓	Section 8.3, section 8.5
MEUC-CASA-07	The UAV shall not fly within 30 m of any building.	N/A	✓	Section 8.3, section 8.5
MEUC-CASA-08	When the UAV crosses a public roadway, it shall cross the roadway at right angles to minimise transit time.	N/A	✓	Section 8.3, section 8.5
MEUC-CASA-09	The UAV shall maintain a minimum altitude of 200 ft AGL when crossing a public roadway.	N/A	✓	Section 8.3, section 8.5
ATSB:				
MEUC-ATSB-01	The UAV shall not contaminate its operating environment.	N/A	✓	Section 11.2.1
MEUC-ATSB-02	All documents and operations shall comply with sections General 2.1.1 and General 2.1.3.1 of the Aeronautical Information Publication (AIP) Australia.	<tbd>	<tbd>	
UAV Chal. Comm.:				
MEUC-UCTC-01	The UAV shall not take off for one minute after arming.	N/A	✓	Section 8.5
MEUC-UCTC-02	The UAV system shall feature a Flight Termination System (FTS).	N/A	✓	Section 8.3, section 8.5
MEUC-UCTC-03	The UAV shall have an easily accessible E-stop which will break the electrical path to all motors and radios.	N/A	✓	Section 8.3
MEUC-UCTC-04	The UAV shall be free flying (not tethered).	N/A	✓	Chapter 4
MEUC-UCTC-05	The UAV shall not fly below 100 ft AGL while flying from base to remote landing site (Take-off and landing stages excluded).	N/A	✓	Section 8.3, section 8.5
MEUC-UCTC-06	The UAV shall fly through the first two waypoints in a specified order, the other waypoints can be flown in a random order.	N/A	✓	Section 8.5
MEUC-UCTC-07	The UAV shall pass a transit waypoint within 50 m to be considered as passed through that waypoint.	N/A	✓	Section 8.3, section 8.5
MEUC-UCTC-08	The UAV shall not fly to an area outside of the Geofence.	N/A	✓	Section 8.5
MEUC-UCTC-09	The UAV shall automatically detect on-board the crossing of a Geofence boundary.	N/A	✓	Section 8.3, section 8.5
MEUC-UCTC-10	The UAV shall automatically activate the FTS on crossing a Geofence boundary in all operating modes.	N/A	✓	Section 8.3, section 8.5
MEUC-UCTC-12	The UAV shall have a continuous datalink with the UAV controller at the base station.	N/A	✓	Section 9.5
MEUC-UCTC-14	The UAV shall have a loading place for a blood sample.	N/A	✓	
MEUC-UCTC-15	The whole system shall be set up at base and launched in a maximum time period of 15 minutes.	~9 min	✓	Section 12.2.2
MEUC-UCTC-16	The whole system shall be recovered and packed up at base in a maximum time period of 15 minutes.	~9 min	✓	Section 12.2.2
MEUC-UCTC-18	The retrieval aircraft shall have an Arming Switch in a readily visible, easily accessible location.	N/A	✓	Section 8.3
MEUC-UCTC-19	The UAV system shall be operable with a crew of maximum 6 people.	1 person	✓	Section 12.2
MEUC-UCTC-20	The ground control station shall produce a graphical display of waypoints and the UAV's current location.	N/A	✓	Section 9.5
MEUC-UCTC-21	The ground control station shall provide a data feed reporting the UAV's location, heading and speed to the range safety coordinator.	N/A	✓	Section 8.4
MEUC-UCTC-22	All altitudes concerning the UAV shall be given as Feet Above Mean Sea Level (AMSL) or Feet Above Ground Level (AGL).	N/A	✓	Section 8.4
MEUC-UCTC-23	The data format of the ground control station output shall be as follows: NMEA 0183 serial output, RS232, 4800 baud, 8 data bits, 1 stop bit, no parity, Male DB9 connector, GPGGA and GPRMC sentences, Update rate of 1 Hz.	N/A	✓	Section 8.4
MEUC-UCTC-24	If using 2 UAVs the ground control station shall have two data outputs, one for each UAV.	N/A	N/A	N/A
MEUC-UCTC-25	The UAV shall have an Arming Switch with LED signal.	N/A	✓	Section 8.3
MEUC-UCTC-26	The shall land no further than 10 m from the Emergency-Landing Target.	N/A	✓	Section 8.3, section 8.5
MEUC-UCTC-27	The Emergency-Landing Target shall be no larger than a piece of A2 paper.	N/A	✓	Section 8.3, section 8.5
MEUC-UCTC-28	The Emergency-Landing Target shall be made up from four pieces of A4 paper taped together.	N/A	✓	Section 8.3, section 8.5
Dep. of Health:				
MEUC-DoH-01	The transport of the blood sample shall adhere to the Therapeutic Goods Act 1989.	**X**	**X**	
MEUC-DoH-02	In case of an accident, the blood sample shall not be able to contaminate the surroundings.	**X**	**X**	
ACMA:				
MEUC-ACMA-01	The radio frequencies used shall comply with the Australian Communications and Media Authority regulations.	N/A	✓	Section 9.5
MEUC-ACMA-02	All relevant radio licenses shall be obtained before flight.	<tbd>	<tbd>	
Market Analysis:				
MEUC-MA-01	The UAV system shall not rely on the local infrastructure.	**X**	**X**	
MEUC-MA-02	The UAV system shall be used in different markets than the medical one as well.	N/A	✓	Section 11.1

Table 10.10: Royal Netherlands Navy Requirements Compliance Matrix

Requirement Number	Requirement	Value	Compliant	Comments
MEUC-NAVY-01	The UAV shall be able to fulfil its mission in wind conditions up to at least 7 bf.	30 kts	✓	Section 5.2.6
MEUC-NAVY-02	The UAV shall be able to fulfil its mission during snowfall with visibility of at maximum 1 km.	N/A	✓	
MEUC-NAVY-03	The UAV shall be able to fulfil its mission during fog with visibility of at maximum 500 m.	N/A	✓	
MEUC-NAVY-04	The UAV shall be able to fulfil its mission with a precipitation of at least 2.6 mm/h.	<tbd>	<tbd>	
MEUC-NAVY-05	The UAV shall be salt-water resistant.	<tbd>	<tbd>	
MEUC-NAVY-06	The UAV system shall be transportable by one person.	1 person	✓	Section 12.2
MEUC-NAVY-07	The UAV system shall weigh 20 kg maximum.	11.41 kg	✓	Section 10.2
MEUC-NAVY-08	The UAV shall weigh 10 kg maximum ideally less than 5 kg.	8.454 kg	✓	Section 10.2
MEUC-NAVY-09	The UAV system shall have an availability of at least twice a day.	> 2	✓	
MEUC-NAVY-10	The UAV shall be capable of VTOL.	N/A	✓	Section 6.5
MEUC-NAVY-11	The UAV shall be launched from aft deck measuring 10 m x 10 m.	N/A	✓	
MEUC-NAVY-12	The UAV shall identify the landing spot by a painted red dot.	N/A	✓	Section 8.3, section 8.5
MEUC-NAVY-13	The UAV shall be able to land while the base moves at a constant speed up to 15 kts relative to ground.	<tbd>	<tbd>	
MEUC-NAVY-14	The UAV shall be able to land while the base experiences a relative movement of maximum 10% roll.	<tbd>	<tbd>	
MEUC-NAVY-15	The UAV shall be able to land while the base experiences a relative movement of maximum 5% pitch.	<tbd>	<tbd>	
MEUC-NAVY-16	The UAV shall be able to launch and land fully autonomously.	N/A	✓	Section 8.3, section 8.5
MEUC-NAVY-17	The UAV shall have fast refuelling capabilities.	N/A	✓	
MEUC-NAVY-18	The UAV shall be able to land and launch again within 5 minutes.	<5	✓	
MEUC-NAVY-19	The UAV shall have an endurance of at least one hour.	>1.5 h	✓	Section 10.2
MEUC-NAVY-20	The UAV shall have a range of at least 30 km.	>145 km	✓	Section 10.2
MEUC-NAVY-21	The UAV shall cruise at an altitude of at least 500 ft.	1246 ft	✓	Chapter 4
MEUC-NAVY-22	At cruise, the UAV shall emit a maximum sound pressure of 61 dB(A).	<50 dB	✓	Section 6.7
MEUC-NAVY-23	The UAV shall have a cruise speed of at least 40 km/h.	99.72 km/h	✓	Chapter 4
MEUC-NAVY-24	The UAV shall have a top speed of at least 60 km/h.	123.12 km/h	✓	Chapter 4
MEUC-NAVY-25	The UAV shall be able to hover for at least 30 minutes at the destination while tracking a target.	>40 min	✓	Section 6.5, section 3.3
MEUC-NAVY-26	The UAV shall be fully autonomous.	N/A	✓	Section 8.3, section 8.5
MEUC-NAVY-27	The UAV shall have a function for direct control by a pilot.	N/A	✓	Section 8.3, section 8.4, section 8.5
MEUC-NAVY-28	The UAV shall navigate to any given GPS coordinates within range.	N/A	✓	Section 8.3, section 8.5
MEUC-NAVY-29	The UAV shall be able to navigate along waypoints.	N/A	✓	Section 8.3, section 8.5
MEUC-NAVY-30	The UAV shall be able to search predefined grids.	N/A	✓	Section 8.3, section 8.5
MEUC-NAVY-31	The UAV shall not rely solely on vision devices for navigation.	N/A	✓	Section 8.3
MEUC-NAVY-32	The UAV shall be capable of object avoidance.	N/A	✓	Section 8.3, section 8.5
MEUC-NAVY-33	The payload bay shall be modular.	<tbd>	<tbd>	
MEUC-NAVY-34	The swapping of the payloads shall be feasible by 1 person.	N/A	✓	Section 12.2
MEUC-NAVY-35	The payload shall feature a video system.	N/A	✓	Section 8.3
MEUC-NAVY-36	The payload shall record video in at least 720p/20fps resolution.	2048x1536/55fps	✓	Crefsec:hardware
MEUC-NAVY-37	The payload shall find objects in the water that are at least the size of a human body.	N/A	✓	Section 8.3, section 8.5
MEUC-NAVY-38	The UAV shall determine the size of the object with an accuracy of at least 20 cm.	N/A	✓	Section 8.3, section 8.5
MEUC-NAVY-39	The UAV shall determine the position of the object with an accuracy to at least 4.9 m.	<2.5 m	✓	Section 8.3, section 8.5
MEUC-NAVY-40	For ships, the UAV shall be able to distinguish between civilian and military vessels.	N/A	✓	Section 8.5
MEUC-NAVY-41	For military vessels, the UAV shall determine country of origin.	N/A	✓	Section 8.5
MEUC-NAVY-42	The communication system shall be modular.	<tbd>	<tbd>	
MEUC-NAVY-43	The communication system shall have a bandwidth of at least 8 Mbps.	<tbd>	<tbd>	
MEUC-NAVY-44	The communication system shall have a constant link with the base.	N/A	✓	Section 9.5
MEUC-NAVY-45	The communication system shall use a wide band radio transceiver with a range between 0.3 and 4 GHz.	<tbd>	<tbd>	
MEUC-NAVY-46	The communication system shall feature cognitive radio technology.	<tbd>	<tbd>	
MEUC-NAVY-47	The electronics shall be electromagnetically shielded.	<tbd>	<tbd>	
MEUC-NAVY-48	The electronics shall be shielded against laser fire.	<tbd>	<tbd>	
MEUC-NAVY-49	The structure of the UAV shall be manufactured out of titanium or carbon composites.	**X**	X	

Table 10.11: System Requirements Compliance Matrix

Requirement Number	Requirement	Value	Compliant	Comments
MEUC-Sys-UCTC-12-01	The UAV system shall guarantee continuous datalink throughout the mission.	N/A	✓	Section 9.5
MEUC-Sys-TUD-01-02	The UAV shall be able to fly in wind conditions of average wind speed up to 25 kts measured over a 10 minute time span.	30 kts	✓	Section 5.2.6
MEUC-Sys-TUD-03-03	The UAV shall have an on-board landing spot detection system.	N/A	✓	Section 8.3
MEUC-Sys-TUD-07-07	The UAV shall be able to fly at least 60 km in horizontal flight.	>145 km	✓	Section 10.2
MEUC-Sys-TUD-02-08	The UAV shall fly the shortest possible flight path through the waypoints from base to remote landing site and back.	N/A	✓	Section 8.5
MEUC-Sys-TUD-03-09	The UAV shall be able to re-plan the flight path/mission in real-time.	N/A	✓	Section 8.5
MEUC-Sys-TUD-03-10	The UAV shall have an on-board sense and avoidance system.	N/A	✓	Section 8.3
MEUC-Sys-TUD-03-11	The remote landing manoeuvre shall be fully autonomous.	N/A	✓	Section 8.5
MEUC-Sys-UCTC-25-13	The UAV shall have an external visual indication of state (armed, inert, disarmed).	N/A	✓	Section 8.3
MEUC-Sys-UCTC-03-14	The UAV shall be equipped with an Emergency-stop (E-stop) function.	N/A	✓	Section 8.3
MEUC-Sys-TUD-18-15	The UAV shall use a fuel-cell to provide the power.	N/A	✓	Section 3.5
MEUC-Sys-TUD-01-16	The UAV shall have a storage compartment for a blood sample.	N/A	✓	
MEUC-Sys-UCTC-02-17	The UAV shall have a Flight Termination System.	N/A	✓	Section 8.3
MEUC-Sys-TUD-19-18	The UAV shall be equipped with a propulsion system consisting of a rotor design.	N/A	✓	Section 6.11
MEUC-Sys-TUD-08-19	The UAV shall be designed for end-of-life recycling.	N/A	✓	Section 11.2.1
MEUC-Sys-UCTC-27-01	The UAV shall be able to locate the Emergency-Landing Target at the re-mote landing site.	N/A	✓	Section 8.3, section 8.5
MEUC-Sys-UCTC-27-02	The UAV shall be able to locate the Emergency-Landing Target in a circle of 100 m radius around Joe's reported location.	N/A	✓	Section 8.3, section 8.5

Table 10.12: Subsystem Requirements Compliance Matrix

Requirement Number	Requirement	Value	Compliant	Comments
Power:				
MEUC-Sys-TUD-18-15-Power-01	The fuel cell products shall not contaminate the environment.	N/A	✓	Section 11.2.1
MEUC-Sys-TUD-18-15-Power-02	The fuel cell shall be capable of providing power throughout the whole mission duration.	>1.5 h	✓	Section 10.2
MEUC-Sys-TUD-18-15-Power-03	The fuel cell shall have an efficiency of minimum 40 % between the temperature range of 50 - 200 °C.	N/A	✓	Section 3.5
MEUC-Sys-UCTC-03-14-Power-05	The FTS shall have a separate power supply in addition to the fuel cell.	2S Battery	✓	Section 8.3
Propulsion:				
MEUC-Sys-TUD-19-18-Propulsion-01	Upon landing, the UAV shall automatically remove power from any propellers making it safe for Joe to approach.	N/A	✓	Section 8.3, section 8.4
Flight Termination:				
MEUC-Sys-UCTC-02-17-FTS-01	The FTS shall be on-board the UAV.	N/A	✓	Section 8.3
MEUC-Sys-UCTC-02-17-FTS-02	The FTS shall not depend on the correct function of other on-board systems.	N/A	✓	Section 8.3, section 8.4
MEUC-Sys-UCTC-02-17-FTS-03	The FTS shall be able to override any other on-board system.	N/A	✓	Section 8.4
MEUC-Sys-UCTC-02-17-FTS-04	The FTS shall close the throttle on any propulsion system.	N/A	✓	Section 8.4
MEUC-Sys-UCTC-02-17-FTS-05	The FTS shall be able to set any control surfaces.	N/A	✓	Section 8.3, section 8.4
MEUC-Sys-UCTC-02-17-FTS-06	The FTS shall ensure a near vertical descend of the UAV to the ground.	N/A	✓	Section 8.5
MEUC-Sys-UCTC-02-17-FTS-07	The FTS shall be able to be activated from the ground by the UAV Controller at the command of the Judges or Range Safety Coordinator.	N/A	✓	Section 8.4, section 9.2
MEUC-Sys-UCTC-02-17-FTS-08	The FTS shall be activated in all instances (and control modes – Autonomous and Manual) when the flight termination criteria have been met, regardless of the previous or current state conditions of the aircraft.	N/A	✓	Section 8.5
MEUC-Sys-UCTC-02-17-FTS-09	Once the FTS has been activated, it shall not be stopped by any means under any circumstances.	N/A	✓	Section 8.3, section 8.4, section 8.5
MEUC-Sys-UCTC-02-17-FTS-10	For a pure fixed-wing UAV, the FTS shall deflect the elevator full up.	N/A	✓	Section 8.5
MEUC-Sys-UCTC-02-17-FTS-11	For a pure fixed-wing UAV, the FTS shall deflect the rudder full to the right.	N/A	N/A	N/A
MEUC-Sys-UCTC-02-17-FTS-12	For a pure fixed-wing UAV, the FTS shall deflect the right aileron full down.	N/A	✓	Section 8.5
MEUC-Sys-UCTC-02-17-FTS-13	For a pure fixed-wing UAV, the FTS shall deflect the left aileron full up.	N/A	✓	Section 8.5
MEUC-Sys-UCTC-02-17-FTS-14	For a pure fixed-wing UAV with flaps, the FTS shall extend the flaps full down.	N/A	N/A	N/A
MEUC-Sys-UCTC-02-17-FTS-16	Failure of communication to and from the UAV shall trigger the FTS.	N/A	✓	Section 8.5, section 9.2
MEUC-Sys-UCTC-02-17-FTS-17	Failure or "lock-up" of any processor or hardware related to the Geofence crossing detection shall trigger the FTS.	N/A	✓	Section 8.3, section 8.5
MEUC-Sys-UCTC-02-17-FTS-18	The FTS shall not be triggered in the event of breaching a DNFZ.	N/A	✓	Section 8.5
MEUC-Sys-UCTC-02-17-FTS-20	When under autopilot control, failure or “lock up” of the autopilot shall trigger the FTS.	N/A	✓	Section 8.3, section 8.5
MEUC-Sys-UCTC-02-17-FTS-21	If the GPS used by a Geofence system fails for more than 10 seconds, the FTS shall be triggered.	N/A	✓	Section 8.4, section 8.5
MEUC-Sys-UCTC-02-17-FTS-22	Failure of communication to and from the UAV during take-off at the remote landing site shall trigger the FTS.	N/A	✓	Section 8.4, section 9.2
Communication:				
MEUC-Sys-UCTC-12-01-Comm-04	The UAV shall be able to process the radar digital feed for the information handling of the DNFZ's size, position and velocity.	N/A	✓	Section 8.5
MEUC-Sys-UCTC-12-01-Comm-05	The UAV is required to have two-way communication with the ground station during the flight.	N/A	✓	Section 9.5
MEUC-Sys-UCTC-12-01-Comm-06	The received signal power at the receiver on both ground and UAV shall be at least as high as the sensitivity at the modems on the ground and UAV respectively.	N/A	✓	Section 9.5
Safety:				
MEUC-Sys-UCTC-25-13-Safety-01	The aircraft shall be equipped with an arming switch.	N/A	✓	Section 8.3
MEUC-Sys-UCTC-25-13-Safety-02	The activation of the arming switch shall indicate that the aircraft may autonomously takeoff no earlier than one minute from arming.	N/A	✓	Section 8.5
MEUC-Sys-UCTC-25-13-Safety-03	The colour red shall always indicate the system is armed.	N/A	✓	Section 8.5
MEUC-Sys-UCTC-25-13-Safety-04	The colour green shall always indicate the system is disarmed.	N/A	✓	Section 8.5
MEUC-Sys-UCTC-25-13-Safety-05	No colour shall indicate that the system is inactive.	N/A	✓	Section 8.5
MEUC-Sys-UCTC-03-14-Safety-06	The E-stop shall be external.	N/A	✓	Section 8.3
MEUC-Sys-UCTC-03-14-Safety-07	The E-stop shall be easily accessible.	N/A	✓	Section 8.3
MEUC-Sys-UCTC-03-14-Safety-08	The E-stop shall be easily understandable.	N/A	✓	Section 8.3
MEUC-Sys-UCTC-03-14-Safety-09	The E-stop shall function without requiring the correct operation of any other system in the UAV.	N/A	✓	Section 8.3
MEUC-Sys-UCTC-03-14-Safety-10	The E-stop shall not utilise any software.	N/A	✓	Section 8.3
Structural:				
MEUC-Sys-TUD-10-18-Structure-03	The integrity of the structure of the UAV shall be easily assessed.	N/A	✓	
MEUC-Sys-TUD-08-19-Structure-05	The structure of the UAV shall use sustainable materials.	N/A		Section 11.2.1
MEUC-Sys-TUD-08-19-Structure-06	The structure of the UAV shall use recyclable materials.	N/A		Section 11.2.1
MEUC-Sys-TUD-08-19-Structure-07	The structure of the UAV shall not hinder the maintenance operations.	N/A	✓	
MEUC-Sys-TUD-12-17-Structure-08	The structure of the UAV shall be easy to manufacture.	N/A	✓	
Payload Support:				
MEUC-Sys-TUD-01-16-Storage-01	The UAV shall have an easily accessible storage compartment that is easy to open and close.	N/A	✓	
MEUC-Sys-TUD-01-16-Storage-02	The storage compartment shall allow storage of a cylindrical vial that is no greater than 20 mm in diameter, 110 mm in length.	20 x 110 mm	✓	Section 10.2.2
MEUC-Sys-TUD-01-16-Storage-03	The storage compartment shall be able to carry a sample with a weight of no more than 25 g.		✓	
MEUC-Sys-TUD-01-16-Storage-04	The payload shall be contained within the payload bay at all stages.	N/A	✓	Section 10.2.2
MEUC-Sys-DoH-01-17-Storage-05	The payload shall not be damaged during transport.	N/A	✓	
MEUC-Sys-DoH-02-17-Storage-06	The payload shall not leak into the operational environment especially during a crash.	<tbd>	<tbd>	
MEUC-Sys-DoH-01-17-Storage-07	The payload shall have all accommodations needed to be able to transport blood samples of Outback Joe according to the rules set by the Australian Red Cross Blood Service.	**X**	**X**	
Control & Software:				
MEUC-Sys-UCTC-13-04-Control-01	The UAV software shall be able to read a single KMZ file containing all the coordinates of waypoints, fixed No-Fly zones, Joe's reported location and Geofence data.	N/A	✓	Section 8.5
MEUC-Sys-UCTC-13-04-Control-02	The UAV software shall map a flying route after data readin.	N/A	✓	Section 8.5
MEUC-Sys-TUD-03-09-Control-03	The UAV shall be a real-time system capable of recalculating its flight path taking into account the dynamic No-Fly zones.	N/A	✓	Section 8.5
MEUC-Sys-TUD-03-11-Control-04	The UAV shall take-off autonomously from base after arming it.	N/A	✓	Section 8.5
MEUC-Sys-MA-02-Control-05	The UAV system's software shall be expandable to be applied for different functions.	N/A	✓	Section 8.5
Pointing System:				
MEUC-Sys-UCTC-13-05-Pointing-01	The UAV shall have a positioning accuracy of better than +/- 25 meters at 1500 ft AGL.	< 2.5 m	✓	Section 8.3

Unfortunately not all requirements could be fulfilled due to a number of reasons. A number of requirements are still open as certain parts of the design are still incomplete. While the design processes these features will be added and the requirements will be fulfilled. On the other hand some requirements cannot be fulfilled in general. This applies specifically to MEUC-NAVY-49, which could not be fulfilled due to sustainability concerns and because titanium and carbon composites do not allow radio signals to be transmitted easily. Another requirement not currently fulfilled is EUC-Sys-DoH-01-17-Storage-07, applying to the transport of the blood sample. For the UAV Medical Express Challenge this requirement does not have to be fulfilled, therefore it has been ignored in the current design. However this requirement can be fulfilled in the future, when alterations are made to the design for potential clients. The majority of requirements have been fulfilled or will be fulfilled in the next stages. It is expected that our customers will be content with the result.

10.5. Production Plan

When producing the UAV system several subsystems will be integrated together. To structure this process this chapter will be divided into a few different processes each discussed in their own section. First the wings, fuselage and structural part of the UAV will be produced. This is followed by the production of a payload bay which is situated inside the fuselage in section 10.5.1. Section 10.5.2 will discuss the production of the hover and cruise propellers. The chapter finishes off with section 10.5.3, which includes the production of the ground system and flight case.

10.5.1. Core Structure

Since an X-wing design is not conventional, clever thinking in the production phase is necessary. First a mould will be produced in which the fuselage can be laminated. The mould can easily be 3D printed from hard foam. The laminating process will be done by hand with the use of bleeder material, rollers and vacuum bags. Care should be taken that protection is always worn by the team members during this process. In the mould the place for the hatches will be marked by thin grooves. These hatches will be laminated before the rest of the fuselage such that they will somewhat overlap after production. After the lamination process the hatches and fuselage will be made to fit flush by the use of rotary tools. When both halves of the fuselage are finished, a slot as is shown in fig. 10.19 is made with a rotary tool so that the entire fuselage is flush. Note that they will not be permanently attached at this point.

After the fuselage is finished the wings will be produced. Four foam cores will be cut with a hot wire, they will serve as a positive mould for the lamination of the wings. From the foam core a tubes of material will be removed in order to make space for the wing spars and cables. The lamination of the wings will use the same materials as the fuselage. After lamination the surface will be smoothed in order to polish away any imperfections.

Now the challenge for the production of the structural part comes in. The wing spars will consist out of four spars which run through the fuselage and will be connected to the payload bay in such a way that they can easily be detached for transport. The spars will be composed of carbon and will be ordered off-the-shelf. The payload bay will fit the fuselage precisely by making dents in the skin where the structure will be unable to move from when the two halves are permanently connected.

The payload bay is a simple lightweight box construction which is designed to fit all subsystems. Not only the inside of the payload bay can be used to carry systems also the outside can be used to attach smaller subsystems which optimises the entire use of the fuselage. The payload bay will be constructed from carbon beams and then fit in the fuselage. When all components are fit inside the fuselage shells they will be permanently attached by the use of resin. After hardening, the surface around the connection will be smoothed again.

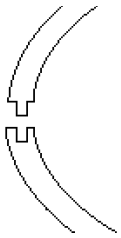

Figure 10.19: Fuselage Shell Connection

10.5.2. Propeller and Swash Plate

To make an optimal propeller for hover the propeller blades will be custom made following the design discussed in chapter 6. These blades are produced from a foam core surrounded by a composite. The production method will be the same as for the wings as mentioned in section 10.5.1. The swash plate system will be a modified version of the old DelftaCopter swash plate (see section 6.10). The pins in the system will be made longer such that they can make at least a 90° and preferably 100° turn. The cruise propeller blades will be custom made as well, these can however be cast with a 3D printed mould. The blades will be attached to the off-the-shelf motors selected in chapter 6

10.5.3. Other Structures

For the ground system a casing is needed which fits a laptop, battery pack, telescopic rod, radio transceiver and a GSM transceiver. An off-the-shelf laptop operating Linux can be used as ground computer. A battery pack or generator is used to power the ground computer and the communication equipment. The transceivers of the communication system will be placed on top of a telescoping rod, which will be secured to the ground by guy-ropes and pegs. Power and signal cables will run through this rod in order to connect the transceivers to

the battery and the ground computer. A cable must be connected from the ground computer to the challenge jury providing telemetry data in serial format. The flight case for the entire system should be lightweight as well as safe. In order to achieve this a custom made flight case will be ordered which will include a hard case and foam inside in which all components of the UAV system can be placed.

10.6. Risk Assessment

This section describes the risk analysis that was performed for the system. In the Baseline and Midterm Review [18], [19], a previous risk analysis was performed. Here, the risk assessment has been updated to include more specific subsystem-related risks together with proposed mitigation plans. The categories taken into account are: Business Plan, Legal, Payload Transportation, Operational, Health, Safety and Environment (HSE), Autopilot (Paparazzi), Structural, Electronics and Sensors, Production, Aerodynamic performance and Communication.

At this stage of the design phase, in total, roughly 100 risks were identified. The extensive list can be seen in appendix A. The purpose of this chapter is to discuss the most important risks that require close monitoring and mitigation, which is substantial for project success.

The result of the risk analysis is the risk map, which can be found in fig. 10.20. This figure represents the risks visualised on a map with likelihood on one axis and severity on the other one. The product of these two represents the risk priority. The colour coding is as follows: light blue = risk acceptable, dark blue = review, orange = high priority risk and red = risk not permissible. The top map represents the risks before mitigation has been applied. Several risks are within the red region which directly result in mission/system failure. This emphasises the need for mitigation plans to get the risk priorities down to acceptable levels. The lower risk map shows the risk after mitigation. The indexes as shown in the risk maps correspond to a specific risk that is explained in detail in the above mentioned list.

Risk Priority = Severity x Likelihood		Severity				
		Negligible (1)	Mariginal (2)	Serious (3)	Very serious (4)	Critical (5)
Likelihood	Frequent (5)			HSE-8, Pro-2		
	Moderate (4)		Ele-7, Bus-9, Str-11	Bus-4, HSE-5, Pap-7, Pro-4	Op-2, Op-3, Pap-1, Pap-2, Pro-1	Leg-1, Op-1, FC-1, Str-1, Com-1
	Occasional (3)		Pay-4, Pap-9, Str-12	Bus-6, Bus-7, Op-9, HSE-3, HSE-4, Ele-3, Ele-4, Ele-5, Ele-6, Str-10, Pro-5	Bus-3, Bus-5, Pay-1, Pay-2, HSE-9, HSE-10, Ele-1, Ele-2, Ele-11, Ele-12, FC-5, Str-5, Str-6, Str-7, Pro-3, Aer-1, Aer-2	Bus-1, Bus-2, HSE-1, HSE-2, Pap-3, Pap-4, Pap-5, Pap-6, Ele-9, Ele-10, FC-2, FC-3, FC-4, Str-2, Str-3, Str-4, Com-2, Com-3
	Remote (2)		Pap-10, Pap-11	Pay-3, HSE-6, Pap-8, Com-7, Com-8	Bus-8, Leg-3, Pro-6, Aer-3, Com-6, Com-9	Leg-2, Op-4, Op-5, Op-6, Op-7, Op-8, HSE-7, FC-6, Str-8, Str-9, Com-4, Com-5
	Unlikely (1)			Ele-8	Aer-4, Aer-5	

AFTER MITIGATION

Risk Priority = Severity x Likelihood		Severity				
		Negligible (1)	Mariginal (2)	Serious (3)	Very serious (4)	Critical (5)
Likelihood	Frequent (5)					
	Moderate (4)	Ele-7	Com-3			
	Occasional (3)	Op-9	Com-1, Pap-1, Pap-2, Pro-4, Bus-9, Str-11,	Pap-3, Pro-2, Bus-4, HSE-1	FC-1	Leg-1, HSE-2
	Remote (2)	HSE-5, Pap-11	Op-7, Pro-5, Pay-4	Str-2, HSE-8, Ele-1, Ele-2, Pap-7, Leg-2, Bus-7, HSE-3, HSE-4, Str-10	Op-2, Op-3, Pro-1, Bus-1, Pap-6, FC-2, FC-3, FC-4, Bus-3, Bus-5, Ele-11, Str-7	Op-1, Bus-2, Ele-9, Com-2
	Unlikely (1)	Aer-4	Aer-3, Pap-9, Str-12, Aer-5, Pap-10	Aer-1, Aer-2, Bus-6, Ele-3, Ele-4, Ele-5, Ele-6, Pay-3, HSE-6, Pap-8, Com-7, Com-8, Ele-8	Pay-1, Pay-2, HSE-9, HSE-10, Ele-12, FC-5, Str-5, Str-6, Pro-3, FC-6, Bus-8, Leg-3, Pro-6, Com-6, Com-9	Str-1, Pap-4, Pap-5, Ele-10, Str-3, Str-4, Op-4, Op-5, Op-6, Op-8, HSE-7, Str-8, Str-9, Com-4, Com-5

Figure 10.20: Risk map showing the identified risk and their priority before and after mitigation

The most critical risks are related to legal, operational and HSE issues which are difficult to eliminate completely as they contain an influence of the human factor, the operator or other external parties. These risks are the following:

- **Op-1** Damage in transport
- **Op-2** Crash landing
- **Op-3** Crash at take-off
- **Leg-1** Air worthiness/safety regulations not met
- **HSE-1** UAV collision with private property
- **HSE-2** Collision with operator, user or other people
- **HSE-5** Debris entering the environment
- **HSE-8** Polluting gasses released to the environment
- **HSE-9** Radiation damage to the environment
- **HSE-10** Blood contaminates the environment

After mitigation **HSE-2**, **Leg-1** and **FC-1** are the only risks remaining with a "High Priority" and no more risks are identified as not permissible. **HSE-2** should be monitored and avoided as much as possible, because safety is of utmost importance both during the competition and commercial use of the UAV. Further **Leg-1** should be monitored frequently, because it concerns air-safety regulations and permission for commercial use, which are often changing for UAVs. The risk **FC-1** is related to the UAV running out of fuel which will lead to fuel shortage. One has to take margins on the fuel taken aboard for the mission and monitor it during flight in order to prevent this risk of occur.
There were several other risks (different than the operational, legal and HSE ones) identified as not permissible. Their mitigation plans however bring the respective priorities down to a level of review/acceptable risk. Those risks are explained below. There is one important structural risk:

- **Str-1** In-flight partial disassembly

This risk is partially related to operator mistake in pre-flight assembly/check, thus it will be mitigated during the detailed structural design by implementing a robust and fail-proof system of locks and overlaps. Misalignment and hence loss of water sealing is a danger that should be paid special attention to during production, which is indicated by the following risk:

- **Pro-1** Misalignment of the parts

More product specific risks are related to the communication subsystem, namely:

- **Com-1** Signal is blocked

As loss of signal may result in flight termination or collision it should be avoided by any chance. Proposed mitigation is to use statistical data of the mission environment to account for obstacles prior to flight and also to design a redundant communication system.
Finally, essential for completing the mission is proper functioning of the UAV software. High priority autopilot risks are indicated by:

- **Pap-1** Failure to locate the target
- **Pap-2** Failure to locate landing spot

These risks underline the importance of correctly functioning target location algorithms. A UAV lacking this functionality will loose its autonomy and hence will not be able to fulfil its mission. For the mitigation outside of the competition an alerting system is proposed, such that when a problem with localising the target (or landing spot) emerges, an operator gets informed and can make a decision about how to proceed further.

10.7. Conclusion

After initial analysis of the mission, setting up requirements and detailed design, it was possible to perform iterations between the different subsystems and obtain a final design. The final UAV has a mass ob 8.463 kg and will cost approximately €3050.00 excluding the power system and ground station. Including the ground station and power system the component and material cost result to approximately €23540.00. With the design, layout and system design completed a sensitivity analysis could be performed. Changes in the input parameters would result in gradual changes in the final design, however the resulting system turned out to be consistent and stable in its design point. As the design is mostly completed a production plan was developed that outlines how the system can actually be manufactured. Lastly a risk analysis has been performed one again and risk mitigation strategies were developed for severe risks.

11

Market Analysis & Sustainability

A market analysis and sustainability development plan are created in order to investigate the interaction of the product with its environment. The market analysis given in section 11.1 explains the interaction of the product with the economic environment. The sustainability development plan given in section 11.2 explains how sustainability is implemented in the design.

11.1. Market Analysis

A market analysis is performed for the UAV system. First an analysis of the meso-environment is performed using Porter's model as described in section 11.1.1, followed by a SWOT analysis of the system in section 11.1.2. The competitive costs are analysed in section 11.1.3. The strategy plan and the return on investment is discussed in section 11.1.4 and section 11.1.5. The chapter is concluded by the sustainability plan discussed in section 11.2.

11.1.1. Porter Model

The meso-environment of the UAV system is analysed using Porter's model. The Porter model identifies and analyses five competitive forces that shape the industry. The forces analysed by the model are: competition within the industry, power of suppliers, potential of new entrants, power of customers and the threat of substitute products. To be able to identify the profitability of the UAV system, the threats of each force are identified. A graphical representation of the Porter model is given in fig. 11.1.

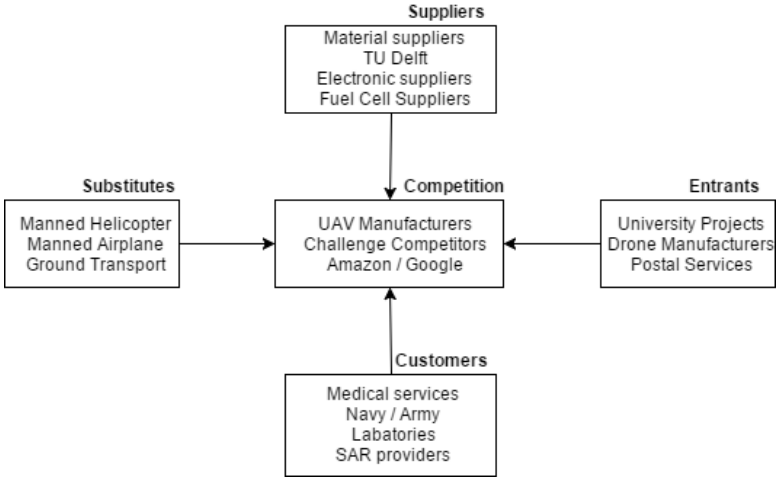

Figure 11.1: Porter's model of analysed market

The threat of each force represented by the Porter model is described below.

Competitive Analysis

The main direct competitors for the UAV system are the ones who base their system on the same set of top level requirements. Teams that compete in the same contest are for example Canberra UAV[1] who won the 2016 contest using a UAV using a combustion engine as main power source. The threat of these competitors is high. Amazon[2] and Google[3] designed drones in order to deliver small post packages. Because these drones are able to fly autonomous, they create a big threat. But the main competitors are mainly playing on the postal market, the threat of these competitors is categorised as moderate.

[1] URL `http://canberrauav.org.au/` [cited 9 June 2017]
[2] URL `https://www.amazon.com/Amazon-Prime-Air/b?node=8037720011` [cited 9 June 2017]
[3] URL `http://www.businessinsider.com/google-project-wing-drone-service-2016-8?international=true&r=US&IR=T` [cited 9 June 2017]

Suppliers
The main suppliers for the UAV system are material suppliers, electronic suppliers and TU Delft. Because in general there are a lot of structural material suppliers, the threat coming from these suppliers is categorised as low. Because specific electronic components are required for the fuel cell, the threat of fuel cell suppliers is categorised as high because there are only two suppliers who can easily set their price. TU Delft is willing to make the UAV system a success and tries to provide the project team with as many supplies as needed. Therefore the threat of TU Delft is categorised as low.

Entrants
As the drone market is a growing market, the revenues earned at this market are growing at a fast rate as depicted in fig. 11.2. New entrants will enter growing markets in order to take advantage of the growing revenues on this market. The main players that enter the market are university projects, drone manufacturers and postal services. The threat of entrants is limited by legal barriers defined by governments like EASA[4] in Europe and CASA [5] in Australia. Therefore the threat of new entrants is categorised as moderate.

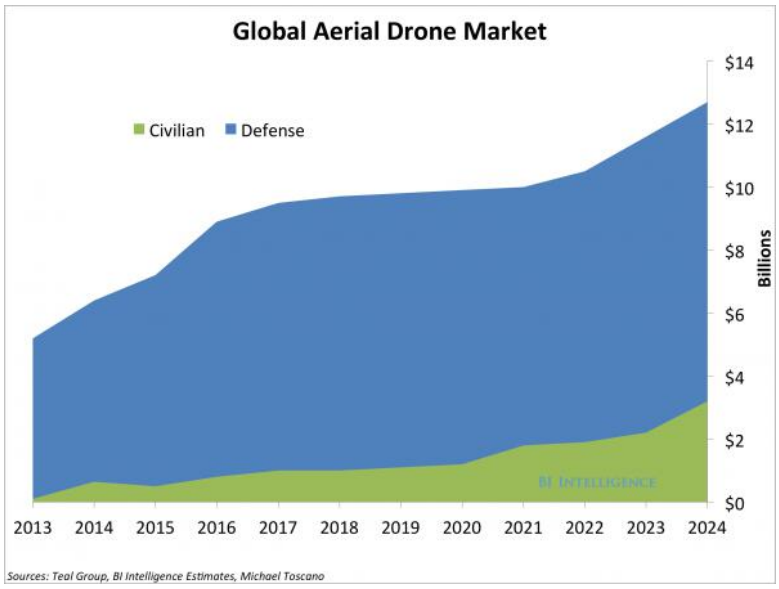

Figure 11.2: Drone market forecast [29]

Customers
The UAV system will be mainly designed for medical services transporting their goods to and from remote areas. Other potential customers are laboratories, delivery services for small parcels and the Dutch Navy. From fig. 11.2 it can be seen that the drone market is predicted to grow for civilians as well as for military usage during the coming decade. Because of the growing market, customers are offered with a wider choice of UAV products. Because of the fact that drone market is growing and the applicability of drones is increasing, the threat of customers is categorised as moderate.

Substitutes
The main substitutes for the UAV system are the usage of manned aerial vehicles and ground transport vehicles. The use of manned aerial vehicles is expensive compared to the use of drones. Ground transport is not always possible and is not as fast as drone transport. Therefore, the new market created by the introduction of drones is difficult to substitute by other markets. The threat of substitutes is thus categorised as low.

Conclusion of Porter analysis
From the Porter model it can be concluded that the main threat comes from the suppliers of fuel cells. The only manufacturers that can provide feasible fuel cells are HES Energy[6] and Intelligent Energy[7]. In order to lower the cost of fuel cell technology it is favourable to work close together with fuel cell experts within the TU Delft in order to obtain test data and order the fuel cells within a batch.

[4] URL `https://www.easa.europa.eu` [cited 9 June 2017]
[5] URL `https://www.casa.gov.au` [cited 9 June 2017]
[6] URL `https://www.hes.sg/` [cited 9 June 2017]
[7] URL `http://www.intelligent-energy.com/` [cited 9 June 2017]

11.1.2. SWOT Analysis

A SWOT analysis consists of four parts which represent the internal and external risks and opportunities for a system or organisation. In this SWOT analysis the strengths, weaknesses, opportunities and threats of the UAV system with respect to the UAV market will be analysed as can be seen in fig. 11.3.

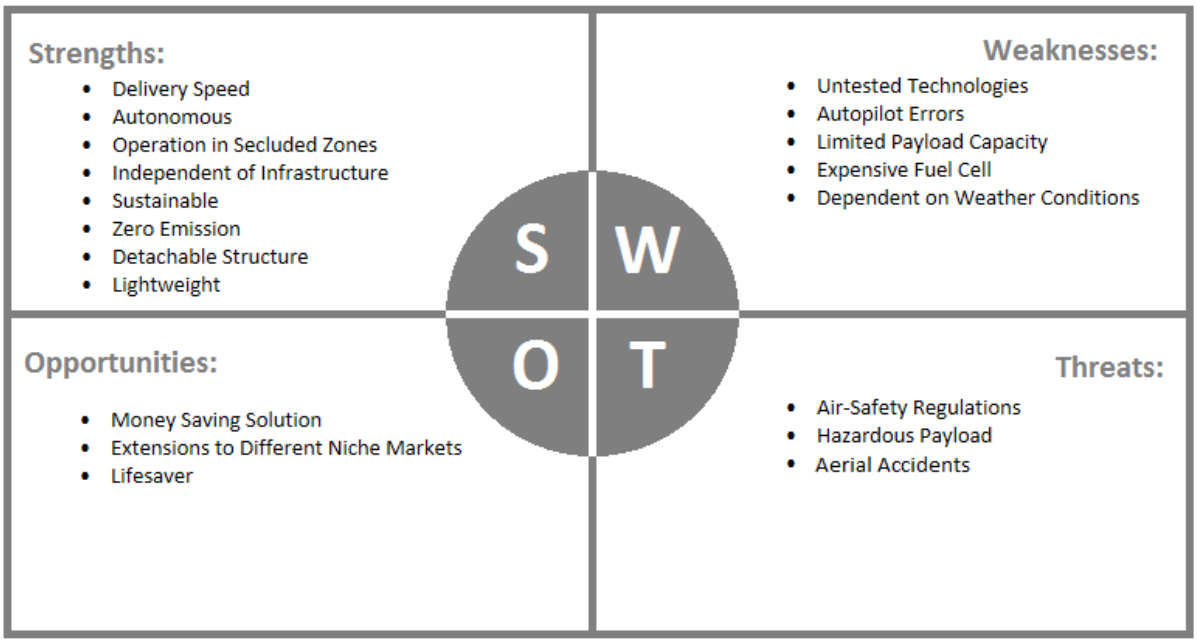

Figure 11.3: Porter's model of analysed market

Strengths

When defining the strengths of the UAV system on the market, one can look at the advantages the use of this system are and what makes it unique on the market. Since the UAV system will be used for missions which involve a certain time frame and inaccessible terrains, the speed and operation in secluded zones are crucial. Because the drone is autonomous, no specialised crew is required to travel to a base to take off. One press of the button is enough for the mission to start, which saves time. The autonomous UAV system is programmed to land on any kind of terrain, which gives it a great advantage with respect to other forms of transportation which might not have access to all areas or are too large to land in forest or mountainous terrains. This independence of any form of infrastructure makes the UAV system a versatile product that can be used for a wide range of transportation missions, ranging from medical assistance to deliveries on navy carriers. Another advantage of the UAV system is its lightweight and detachable design, meaning that it can be easily transported by car if needed and no more than two persons will be needed to set the device up. The last point in which the UAV system stands out from the rest of the market is the fact that it is the only product in this market niche having zero CO_2 emissions during operation and is produced with a minimal carbon footprint.

Weaknesses

The UAV system is a brand new design and therefore comes with a few weaknesses that should be kept in mind during design, production and service. First of all, the technologies used in the UAV systems are mostly new and untested. This could bring along some unexpected problems and inconvenience in the first use of the product. As previous experiences with the UAV challenge medical express have shown, the autonomous system might have some errors concerning terrain which have not been accounted for, such as variable height of trees and terrain. Another disadvantage of the system is its limited payload capacity which makes that only small and lightweight samples can be transported. The use of the fuel cell comes with some inconveniences in terms of budget since it is an expensive part of the UAV system and if it breaks down, it will be very costly to replace. Dependency on weather conditions is the last point in which the UAV system will have a weakness since it cannot fly during storms or heavy rain because this could bring fatal damage to the fuel cell system.

Opportunities

The UAV system brings a lot of opportunities for the external market with it. Because of the small design, sustainable design and autonomous flight capability, the operation of the UAV is much cheaper than that of a

helicopter. This money saving solution is therefore a great business opportunity. Steps can be made in other markets such as postal services and search and rescue missions which makes the business market broader and more attractive. Since the system can contribute to saving lives there is expected to be a big market and therefore need for further development which is a good opportunity for the UAV system developers.

Threats
There are external factors which can be a threat to the UAV system which should be carefully taken into consideration during the design phase. Air safety regulations on drones are quite strict and vary per country[5]. This could bring extra costs to the customers if they do not operate in a target area. Since the UAV will be carrying payloads that are often labelled as hazardous, the loss of payload or damage to it could not only bring financial damage but is a bio-hazard or could cause leakage of personal information. This threat will have to be treated with the utmost care because if such an event will take place it damages the goodwill and integrity of the UAV system mission. Another threat is aerial accidents such as collisions or bird strikes which could jeopardise the task of the UAV, ultimately making it unable to complete its mission.

11.1.3. Competitive Costs and Cost Estimation
In this section, first the competitors in the drone delivery industry will be discussed in terms of their flight costs and what their missions look like. Following this, an estimation of operation costs and its variables will be discussed.

Competitors
When looking at competitor costs, first the largest competitors on the market should be defined. When looking at the delivery of medical supplies only a few companies share a link with the niche market of the UAV system since it is a very new market. Among these companies is Flirtey[8] an American business which focuses on a broad delivery market with quadcopters which can carry up to 5.5 pounds of payload with a range of 20 miles. The delivery costs at the moment are however huge according to Aerotas, a drone consultancy office. They even state that the delivery via drone can cost up to 10,000 times as much as normal truck delivery at the moment as is shown in fig. 11.4.
Amazon wants to focus on the delivery of small packages which weigh less than five pounds that will be transported over relatively small distances. It seems to have a similar price prospect to Flirtey according to ARK Invest research[9]. As can be seen in fig. 11.5, the manner in which ARK Invest predicts the flight costs is based on assumptions which only bring along small deviations in price. Mostly the low price of delivery is determined by their lightweight and short distance strategy, however since the project is not up and running yet this is only a preliminary price point.
The company of Zipline[10] is based in Rwanda and works together with the government to deliver blood, costs are not specified but will expected to be high since every route has to be checked by the government before flying, since the drone has to be launched by hand this also brings extra labour costs to the flight. Another disadvantage for the market is that it can only drop goods, but not retrieve samples. This company is however included in this analysis since it is the only one focusing on blood delivery which comes close to the objective of the Medical Express UAV Challenge.

[8] URL `http://flirtey.com/about/` [cited 9 June 2017]
[9] URL `https://ark-invest.com/research/drone-delivery-amazon#fn-7141-13` [cited 9 June 2017]
[10] URL `http://flyzipline.com/product/` [cited 9 June 2017]

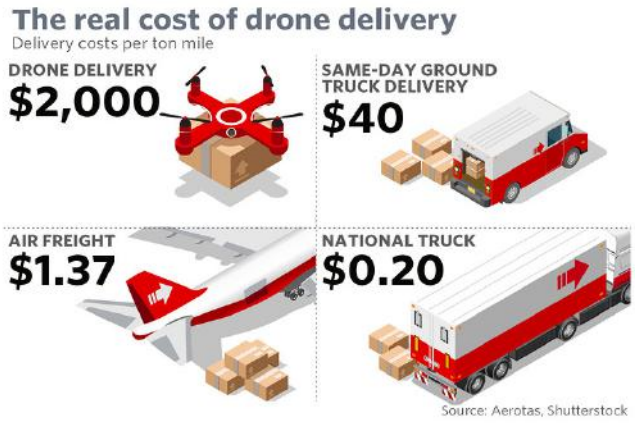

Figure 11.4: Flirtey drone delivery costs[11]

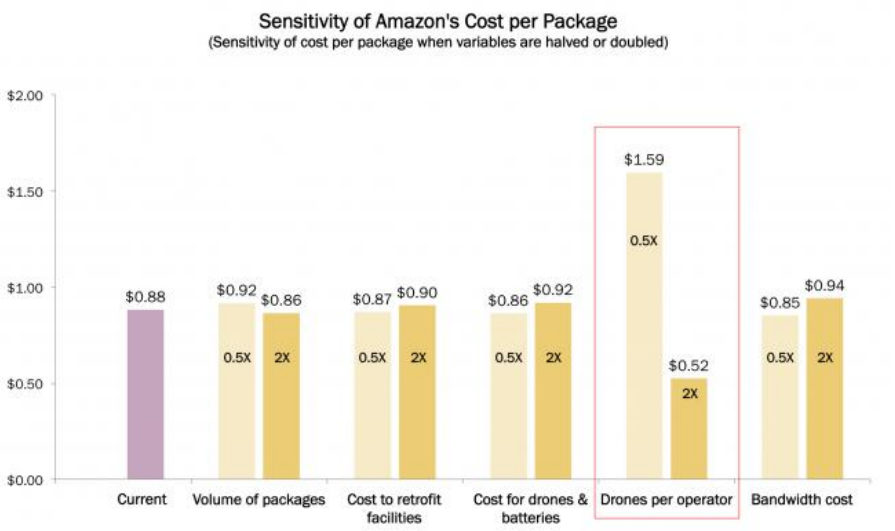

Figure 11.5: Amazon drone delivery costs[9]

Cost Estimation

When comparing the goal of the MEUC with these of Flirtey, Amazon and Zipline, some similarities and differences can be spotted. For instance none of the companies have a goal to return goods which is the case for the MEUC, this brings along some extra costs for extra energy storage which is needed. Another important difference is the distance to be travelled, since Amazon and Flirtey focus on short distances, their costs are not to be compared to those of Zipline which is able to cover the same range as that of the to be designed UAV for the Medical Express UAV Challenge. Another variable on the cost is of course the amount of payload which is very small in the Medical Express UAV Challenge, making cheaper flight possible with respect to five pound packages. The only component which will cause an increase in price with respect to the other companies is the fuel cell which is a costly item to replace. In conclusion, it can be said that the operational costs of the Medical Express UAV Challenge will exceed those of most competitors, the high pricing for customers is however not expected to be a big problem since the focus of the UAV is very specialised and can save lives.

11.1.4. Strategy plan

In this section the strategies of the current and future markets for the UAV system will be discussed. This section will also contain concluding notes to the market analysis.

Market Opportunities

For customers and investors, it is important to know what the concrete business opportunities are for the drone designed for the Medical Express UAV Challenge. As already stated in section 11.1.1 the only big competitors in

[11] URL `https://goo.gl/g6r9bg` [cited 2 May 2017]

this market are the other contestants of the challenge. Since other companies like Google and Amazon aim at direct delivery of any kind of parcel they are only a mild competitor on the market. The way in which the UAV will differentiate itself from other players on the market comes from the different gaps in the market which it closes. First of all, the range of delivery and the fact that the UAV will be able to land on almost any kind of terrain is of great value. The inclusion of fuel cell also has added market value since no fossil fuels have to be used to power the UAV and energy conversion is efficient. Having a long range and sustainable UAV is quite unique on the market since most of the competitors in the Medical Express UAV Challenge do not use a sustainable strategy. Closing two big gaps in the market while saving lives means that the UAV system is a very valuable asset to the current market.

New Markets
Since the introduction of drones for military purposes, it became popular on the civilian market during the last century as the cost of hardware decreased to an acceptable level. Nowadays, civilian drones are used in the following work areas: agriculture, construction, real estate, applied sciences, law enforcement, media, mining, private security, search & rescue and wildlife conservation. In the early stages, the hardware price and size was a key driver for the breakthrough for commercial drones. In order to become a player on the market today, a UAV system must be developed to allow new functionality in a niche space by means of software and vehicle configuration[7]. As the UAV system will be designed mainly for medical purpose, its functionality can be easily expanded by customising its software. As the UAV system will be mainly designed for blood transport from remote areas, the system can be used as well for transport of small payloads for medical purpose, humanitarian aid and laboratories. As the UAV system is equipped with state of the art sensors for autonomous take-off and landing, the functionality of the system can be easily extended for observation missions using these sensors. In order to attract new markets, two stakeholder requirements are derived from the market analysis. The MEUC-MA-01 requirement ensures that the drone's communication system is modular such that it can be operated in different areas with different infrastructure. The MEUC-MA-02 requirement ensures that the drone is able to operate in multiple market areas.

Packages
In order to attract customers in different market segments, three purchase packages are defined dependent on the drone usage and customer's preferences. The purchase packages ensure to make the customer loyal to the product such that the threat described in Porter's model stay at a low level.

Owner Package The owner package is meant for customers that operate multiple drones on a daily basis. Technical training and documentation of the UAV system will be provided in this package such that the operators can perform repair and maintenance tasks themselves. Potential customers for this package are the Navy or the Army who want to operate multiple drones on a regular basis for observation missions. Customers can get discount on a revised power system if they send it back at end of life.

Power Lease Package Within the power lease package, the drone will be purchased by the customer except for the power system. The power system will be leased by the customer such that the purchase price of the drone is acceptable. The Power Lease Package can be purchased by customers operating one to several drones on a regular basis. Maintenance and repairs can be done by the manufacturer or by the operator based on the customer's preference. If the power system is at its end of life, a revised system will be provided within this package.

SOS Package The SOS Package will be mainly used by humanitarian aid organisations in case of a disaster. As it is unpredictable when disaster strikes, the manufacturer has some standby drones ready for rent. Within this package, the manufacturer will take care of repairs and maintenance.

11.1.5. Return on Investment
Return on investment is calculated using eq. (11.1). To determine this rate all costs are listed in table 11.1. These costs have to be covered as well as that some profit will have to be made in order to accommodate further research and development and build up capital for the company.

$$\text{RoI} = \frac{\text{Gain from Investment} - \text{Costs}}{\text{Costs}} \tag{11.1}$$

Table 11.1: Component and Material Costs

Component	Cost [€]	Materials	Cost [€]	Other	Cost [€]
Power	18,200	Foam	1.42	Labour	45,488.88
Ground Communication	2,305.5	Carbon	97.3	Office	12,000
Communication	226.2	S-glass fibre	16.41	Equipment	6,000
Swash Plate	282.0				
Propellers and Motor	426.4				
Total	21,440.1	Total	115.13	Total	63,488.88

In table 11.1 the labour and office costs are calculated for a year of full time work with ten people who earn thirteen euros an hour after taxes. Also the rent of machining tools are incorporated under the section equipment. The basic cost of one drone will be € 21,555.23. This cost will be raised by 10 % in order to account for material loss and varying market prices, putting it at € 23,710,75. The 'other' costs will be divided over the annual amount of ordered UAV systems. When the case is taken that the Navy would want to buy ten UAV's the total cost of one UAV system will be € 30,059.64. After this a thirty percent margin is added to account for the building of capital and research and development. The later causes the sales price to be € 39,077.53 per UAV system, which is rounded to € 39,000. The return on investment for the system will therefore be 30%.

11.2. Sustainable Development Plan

In this section the consideration taken with respect to a sustainable design are discussed. The design phase section 11.2.1, production section 11.2.2 and end of life recuperation section 11.2.3 are discussed in the respective sections.

11.2.1. Design

During the design process of the UAV system the sustainability engineer has been keeping track of all subsystems and their considerations with respect to sustainable design. Each subsystem department justified their choices with a sustainable design in the following list.

- Power
  - Battery: LiMn, the Lithium Mangan batteries are made out of an earth abundant material and are non toxic. The batteries have a long lifetime and are better recyclable than the average lithium ion battery.
  - Fuel: Hydrogen, no carbon-dioxide emissions, pure water is the waste product. Unfortunately, energy is required to produce hydrogen which has to be renewable as well.
  - Fuel Cell: The membrane electrode assembly (MEA) comprises of materials that can be rare and environmentally harmful to mine. The fuel cell is made of platinum coating supported by porous carbon for the cathodes and anodes and the membrane material is based on perfluorosulfonic acid. The casing is aluminium, whose mining can have severe environmental effects. At the end of the life-time, MEAs can be refurbished several times. This includes significant costs but is in most cases cheaper or on par with a new fuel cell. When this is not possible anymore, aluminium can be easily recycled, most other materials with some more effort as well.
- Electronics
  - Metals and Silicon: Silicon is abundant however not all metals are. While buying parts or materials care should be taken in order to support sustainable mining and working conditions. Further recycling should take place in certified facilities.
  - Durability: Electrical components should be durable so they will not have to be replaced during the life-time of the UAV.
  - Energy Consumption: electric components are energy and weight efficient due to miniaturisation (i.e., transistors approaching 7 nm in size) — inversely following Moore's law. This allows reduced power consumption, which reduces the carbon footprint of the UAV.
  - Signals: The signals emitted and received by the radio, mobile and A-GPS system are in the radio frequency spectrum and of the same strength as the mobile phone and radio signals. Many studies have been done on their effect and none were so far able to conclude that they would be harmful.
  - LiDAR: The lasers used in LiDARs are categorised as Class 1, which means they are not harmful to humans and other organisms and they usually utilise infrared light, which can not be seen by humans and most animals.

- Propeller
  - Efficiency: The propeller is designed as efficient as possible in order to have a low power consumption.
  - Material: At the moment carbon fibre which is only down-gradable. The carbon can be retrieved by burning the resin however this is an energy intensive process.

11.2.2. Production

In the production phase it is important to keep sustainability in mind as a baseline. The spars and fuselage internal skeleton are made with a carbon fibre composite which are only down-cyclable. At the moment, S-glass fibre with an epoxy resin is used for production which unfortunately can also only be down-cycled as well. However, research is going on in order to use Kenaf fibre with PLA resin in the future. This material is biodegradable but the material properties could not be verified at this point. The potential of this material has been shown by TU Eindhoven producing a car made of the material [5]. All known properties of the material are shown in table 11.2. If these values are indeed valid, then this could potentially represent a large weight saving if assuming that the skin thickness will remain at 1 mm since the density of the Kenaf composite is nearly a quarter of the density of the S Glass fibre composite that is currently used. An added benefit of using this material would be that it is fully bio degradable.

Table 11.2: Kenaf composite properties [28]

Property	**Kenaf fiber + PLA resin**
Density [kg/m^3]	440
Young's modulus [GPA]	13
Poisson's ratio [-]	0.1
Tensile strength [MPa]	130

Not only is the material choice important in production, also the way tools and conditions are handled is of utmost importance. The tools used during production should be long lasting, thus reuse-able moulds and brushes would be used. When using tools which can be re-used it is important to keep tools clean and in good shape to prolong their lifetime. When production begins, rules should be communicated with the production team to ensure this happens. In terms of production conditions the team has to ensure that all processes take place in a secure place so that small dust or leaking materials will not pollute the environment. In table 11.3 a list of $C0_2$ pollution during production is included, it is recommended to compensate for this pollution trough the planting of trees or using other materials in the future.

Table 11.3: CO_2 exhausted during production

Material	CO_2 **Output [kg]**
PE-LD Foam	0.26
PEEK + Carbon Fibre	22
S-Glass Fibre	16.41

11.2.3. Lifetime and End of Life

During the lifetime of the UAV system a package system will make sure that sustainability and end of life re-cuperation is ensured. As stated in section 11.1.4 three packages will come available to costumers which also come with their own sustainability strategies. The expected lifetime of the system depends on the fuel cell, which is expected to fail first after 6000 hours of operating time[19]. After failure it can possible be replaced and the system further used.

Owner Package As states in section 11.1.4 the customer is the owner of the drone. In order to keep control over the product during end of life stages of subsystems, attractive deals such as discounts when returning a subsystem to the company will be used. In this way fuel cells can be revised and reused. The discount is of course dependent on how critical the specific recycle method for that subsystem is.

Power Lease Package As the power system is leased by the customer revision and eventually recycling of the fuel cell is covered for. This method is also used by Renault [12] for its electrical cars and is both beneficial for the costumer and the company in terms of recycling effort. The main drone which is property of the costumer a

[12] URL `https://electrek.co/2017/03/30/renault-electric-vehicles-lease-battery-upgrade/` [cited 9-6-2017]

recycle manual shall be included as well as discount options on new purchases if old components are handed in for end of life recuperation by the company.

SOS Package Since the company is the owner of the product, end of life recuperation is guaranteed to be handled by the company. Fuel cells can be revised or recycled, and all drone components can be disassembled in order to make sure each part is reused or disposed of properly.

11.3. Conclusion and Recommendations

From the Porter model and SWOT analysis can be concluded that the business potential of the UAV system is quite large. The market niche is very new and therefore the company will have a lot of room to grow. To be as versatile as possible in this market three packages are offered namely the owner, power lease and SOS packages. The sales price for the owner package will be about € 54852.90. Furthermore a good end of life plan for the system has been put up. It is recommended to look out for new sustainable materials and ways to reduce the CO_2 pollution during production.

12
Post Design Phase

In this chapter the phase after the design process, the current stage of the project, is discussed. The post design phase includes activities regarding safety analyses, logistics and future planning. Safety analyses are done in section 12.1, where the Reliability, Availability, Maintainability and Safety (RAMS) analysis is done. After that, the operations and logistics are discussed in section 12.2. Finally, the post design phase is discussed in section 12.3.

12.1. Reliability, Availability, Maintainability and Safety

In the first section, the reliability and safety of the UAV system is determined and ensured. This is done with the use of Failure Mode Effect Analysis (FMEA), Fault Tree Analysis (FTA) and a health and environment risk analysis. Furthermore a maintenance policy is determined and the availability of the system is discussed.

12.1.1. Reliability and Safety

In order to analyse the safety and reliability of the UAV system, a FMEA is performed for its main functions and can be found in table 12.1. The first column presents the ID number assigned to a functional Failure Mode (FM) followed by a Fault Tree (FT) ID presenting the reference number to the hardware fulfilling the described function as presented in the Fault Tree in fig. 12.1. For the FMEA, the following four functional failure modes are considered: total loss, partial loss, inadvertent operation and erratic / misleading operation. The cause and end effects of potential failure modes are indicated in the FMEA as well as the severity levels which are classified as follows [14]:

1. **NO EFFECT** no safety effects
2. **MINOR** no injury, property damage, or system damage, unscheduled, maintenance or repair necessary
3. **MARGINAL** minor injury, minor property damage, minor system damage, delay or loss of availability or system degradation
4. **CRITICAL** severe injury, major property damage, major system damage, mission loss
5. **CATASTROPHIC** death or system loss

Table 12.1: Qualitative Functional Failure Mode Effect Analysis

#	FT ID	Function	Potential FM	End Effect of failure	Severity	Cause
1	1.1.1	Provide UAV communication	total loss	Link loss / not able to take-off	4	Loss of main and redundant communication system
2	1.1.1	Provide UAV communication	partial loss	Partial loss of transmitted data	3	Radio signal jamming / GSM provider not available
3	1.1.1	Provide UAV communication	erratic/misleading op.	Wrong data packages received	3	Radio signal jamming
4	1.1.2	Provide structural integrity	total loss	Crash of the UAV	5	Overloading up to ultimate load
5	1.1.2	Provide structural integrity	partial loss	Reduced manoeuvring / handling loads	3	Overloading up to limit load
6	1.1.4.1	Provide flight termination funct.	total loss	Immediate execution of landing	4	Power source loss / hardware error
7	1.1.4.1	Provide flight termination funct.	inadvertent op.	Immediate activation of flight termination	4	Navigation error / software error
8	1.1.4.2.2	Control UAV attitude	total loss	Crash of the UAV	5	Attitude sensor loss
9	1.1.4.2.2	Control UAV attitude	partial loss	Activation of flight termination system	4	Partly loss of attitude sensors
10	1.1.4.2.2	Control UAV attitude	erratic/misleading op.	Temporary loss of stability	3	Magnetic interaction
11	1.1.4.2.1	Identify obstacles / person	total loss	Obstacle / person collision	5	Hardware / software error
12	1.1.4.2.1	Identify obstacles / person	partial loss	Obstacle / person collision	4	Hardware / software error
13	1.1.4.2.1	Identify obstacles / person	erratic/misleading op.	Reduced efficiency due to false detection	2	software error
14	1.1.5	Provide UAV Power	total loss	Crash of the UAV	5	Failure of power electronics / overheating
15	1.1.5	Provide UAV Power	partial loss	Immediate emergency landing	4	Failure of fuel cell, tank or battery
16	1.2.1	Provide ground communication	total loss	Link loss / not able to take-off	4	Loss of main and redundant communication system
17	1.2.1	Provide ground communication	partial loss	Partly loss of transmitted data	3	Radio signal jamming / GSM provider not available
18	1.2.1	Provide ground communication	erratic/misleading op.	Wrong data packages received	3	Radio signal jamming
19	1.2.2	Provide ground power	total loss	Direct activation of landing mode	4	Failure of power electronics / empty ground battery
20	1.2.4	Monitoring mission	total loss	Direct activation of landing mode	4	Ground computer failure

The reliability of the total system can be determined with the use of a FTA. This tool is used to identify failure modes. The branches of the tree all represent a mode which leads to mission failure. The branches can be connected to a top level with either an or- or and-gate. The or-gate indicates that top level failure is caused by failure of one of the branches. With an and-gate, all branches must fail in order to cause top-level failure. The

FTA of the Medical Express Challenge mission is given in fig. 12.1. This FTA does not include quantitative values for the probability of failure of the events since this can not yet be determined. It cannot be done as the failure probabilities of each mode cannot be evaluated thoroughly in this stage of the design. As for the next stage, reliability's of each component can be analysed more thoroughly. With the reliabilities of a quantitative FTA, a proper redundancy policy can be set up. When the FTA indicates a low probability on certain branches of the tree, redundancy should be applied to the parts of the system. The quantitative FTA is especially valuable for commercial use of the UAV, as the system will then be use regularly which requires a higher degree of reliability.

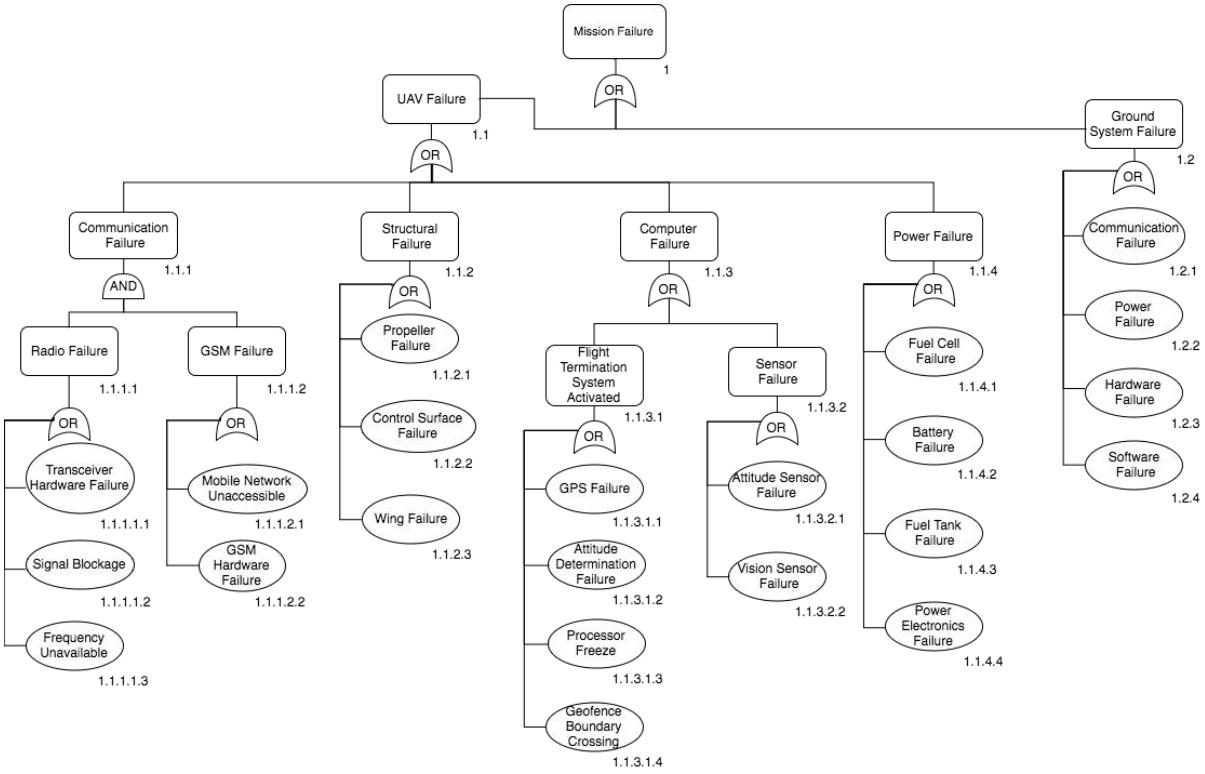

Figure 12.1: Qualitative Fault Tree Analysis

As the safety of third parties and surrounding environment should be taken into account during the design of the UAV, a risk analysis is performed on this area as well. For this risk analysis, a focus is laid upon risks for parties other than the UAV engineers. Also, a mitigation plan needs to be enforced to ensure a safe and environmentally friendly design. The risk analysis and mitigation plan is presented in table 12.2. The table severity and likelihood of the risks are scaled from 1 to 5 and elaboration is given in table 12.3.

Table 12.2: Health and Environment Risk Analysis

Index	Cat.	Cause	Event	Consequence	Severity	Likelihood	Risk Priority		Mitigation	Sev. after mitigation	Lik. after mitigation	Risk Priority after mitigation	
THIRD PARTY RISKS													
HSE-2	Health & Environment	Object detection failure or propulsion failure	Collision with operator, user or other people	Person harmed or killed resulting in legal issues	5	5	25	Not permissible	Emergency procedures for safety should be implemented, such as a flight termination system during potentially dangerous situations.	5	3	15	High priority
HSE-8	Health & Environment	The use of pollutant gasses in the system	Pollutanting gasses released to the environment	Environment pollution	3	5	15	High priority	Minimise the use of polluting gasses in the design.	3	2	6	Risk acceptable
HSE-5	Health & Environment	Breakdown of the system	Debris entering the environment	Environment pollution	3	4	12	High priority	Perform a accurate load case study including a safety margin, and ensure structural integrity. Use biodegredable materials for the UAV design.	1	2	2	Risk acceptable
HSE-9	Health & Environment	High radiation of the communication system	Radiation damage to the environment	Harm to objects, animals or people in vicinity of the UAV	4	3	12	High priority	Minimise the radiation strength of communication system design.	4	1	4	Risk acceptable
HSE-7	Health & Environment	Fuel tank overheating	Fuel tank explosion	Permanent damage to surrounding environment	5	2	10	Review	Determine the maximum temperature, including safety margin, of the fuel tank during operation at apply cooling measures if necessary.	5	1	5	Risk acceptable
HSE-1	Health & Environment	Object detection failure or propulsion failure	UAV collision with private property	Property damage resulting in legal issues	3	3	9	Review	Emergency procedures for safety should be implemented, such as a flight termination system during potentially dangerous situations.	5	1	5	Risk acceptable
HSE-3	Health & Environment	Object detection failure or propulsion failure	UAV collision with a bird or other animal	Animal harmed or killed	3	3	9	Review	Emergency procedures for safety should be implemented, such as a flight termination system during potentially dangerous situations.	3	2	6	Risk acceptable
HSE-4	Health & Environment	Object detection failure or propulsion failure	UAV collision with vegatation	Nature permamently damaged	3	3	9	Review	Emergency procedures for safety should be implemented, such as a flight termination system during potentially dangerous situations.	3	2	6	Risk acceptable
HSE-6	Health & Environment	Fuel tank failure	Fuel leakage	Environment pollution	3	2	6	Risk acceptable	Determine the load bearing capabilities of the fuel tank to the maximum loads of the UAV.	3	1	3	Risk acceptable
HE-10	Health and Environment	Leakage of the payload blood	Blood contaminates the environment	Harm to animals or people that come in contact with the blood	4	3	12	High priority	Design a payload case that can resist the loads on the UAV and include a safety factor.	4	1	4	Risk acceptable

Table 12.3: Risk Analysis Scales

No.	Severity	Likelihood
1	No Effect	Extremely Unlikely
2	Minor	Unlikely
3	Marginal	Neutral
4	Critical	Likely
5	Catastrophic	Extremely Likely

12.1.2. Maintainability and Availability

As a part of the RAMS Engineering approach, maintainability describes the ease at which the product can be sustained in a good, operative condition and range of required actions to maximise its lifetime. This is especially important for the long-term usage Navy applications, which will be a long-term purpose of the UAV. For the Medical Express Challenge on the other hand, the number of flights is limited to competition and testing. Nevertheless, it is desired that an operator is able to carry out the most of repairs and replacements when needed. This also includes emergency repairs that in case of accidents (crash, damage in transport) can be carried out and still enable participation in the challenge.

The maintenance policy will highly depend on the power subsystem, as the components of the fuel system need regular replacement. Integrated automatic system checks will provide the necessary information about power levels and battery lifetime status. The secondary battery needs replacement every 200 flights and the solid storage fuel tank every 100 flights. As the Navy is planning to use the UAV around twice a day (MEUC-NAVY-09)[11], the secondary battery needs replacement around every 100 days and the fuel tank every 50 days as determined by the chosen power subsystem. The Navy operator should be able to easily replace these components themselves, and these components should be easily accessible and available. The battery will most likely be an off-the-shelf component available for large batch commercial purchase, the fuel storage can be a unique product in order to meet the specific requirements. In that case, the storage tank producer shall be enclosed in the contract as one of the key stakeholders to ensure supply chain continuity and replacement parts meet quality standards. The replacement procedure will not require specific tools (details depend on detailed structural design to be determined in later stages of design process), both battery and fuel tank slot will be made easily accessible after opening the fuselage lid.

Furthermore, it is recommended to perform a visual inspection before using the UAV to increase the detectability of possible faults. Dirt particles, dead insects, bird guano, salt and any other contamination should be removed, especially from the camera lens, sensors and pitot tube to ensure undisturbed functioning of the UAV. Other components of the system are assumed to maintain their operative condition throughout the whole lifetime of the system, without need for manual repairs or adjustments. The sensors will be automatically re-calibrated before every launch, as a part of automatic flight preparation procedure. Also, mechanical

flight controls: flaps and servos will be tested before flight. In case system check will detect a mismatch with expected component response it will inform the operator by printing a suitable error statement. In case repairs need to be carried out, the UAV unit shall be sent back to the production site, where delegated specialists will be able to diagnose and fix the fault. The conditions of repair will be enclosed in the proper maintenance (DBM based) contract. The lifetime of the UAV system will be dictated by the power subsystem. It has been estimated that the fuel cell will not be able to produce required power levels above 6000 hours of operation. Being the most expensive component of the whole system, its replacement is not cost-effective, as for a similar price a new system can be delivered. Still, refurbishment of some of the UAV sub-components is planned.
Finally, the availability of the system is discussed. Availability is the degree in which the system is available when required for use and is a function of its reliability and maintainability [14]. When reliability is increased, the availability is increased as well. Also increased maintainability leads to an increased availability. As reliability has yet to be quantified, no numbers can be given to the availability of the UAV.

12.2. Operations and Logistics

After production, the UAV system relies on a number of support equipment and actions during operation and later in its life-time. A typical operation cycle is given in fig. 12.2. Here the distinction is made between the one-time use of the UAV Medical Express challenge and a repetitive application like the naval reconnaissance mission that it will be used for. The overall system will be operable by just one person as it is lightweight and simple enough to be transported, assembled and operated alone.

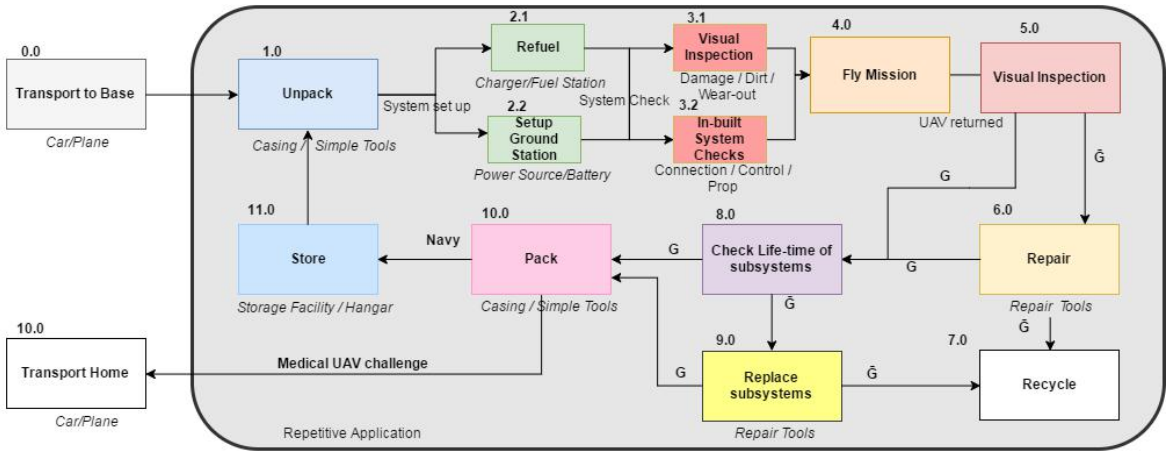

Figure 12.2: Logistics and Operation Flow Block Diagram

12.2.1. Transport

As requirement MEUC-TUD-15 states, the system shall be transportable by a regular airline. Taking KLM airlines as an example, it is possible to transport baggage up to 3m combined length (length + width + height) and 32 kg weight[1]. The UAV also has to be able to fit in a car boot and should be easily transportable by one person. Thus, weight is not the driving factor, but the size. The UAV system has to fit in a casing that fulfils this requirement. In this state the UAV system will be transported in block 0.0 and 11.0. After developing the whole system, a transport casing was designed as well according to aforementioned regulations. The closed casing has the following dimensions: 1.1x0.7x0.4m and can contain a disassembled UAV together with a computer and a telescopic rod used for the ground station. The size enables transportation in a regular car trunk. Fitting of the UAV inside the casing is presented on the drawings in fig. 12.3 and fig. 12.4.

[1] URL `https://goo.gl/rZm5Mr` [cited 22 May 2017]

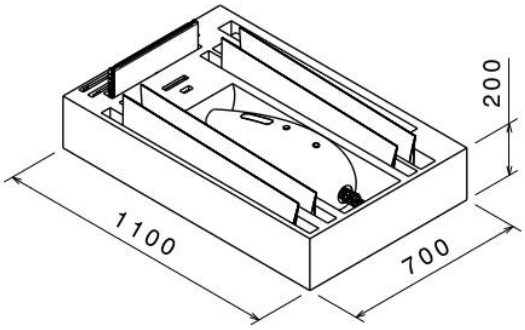

Figure 12.3: UAV casing dimensions.

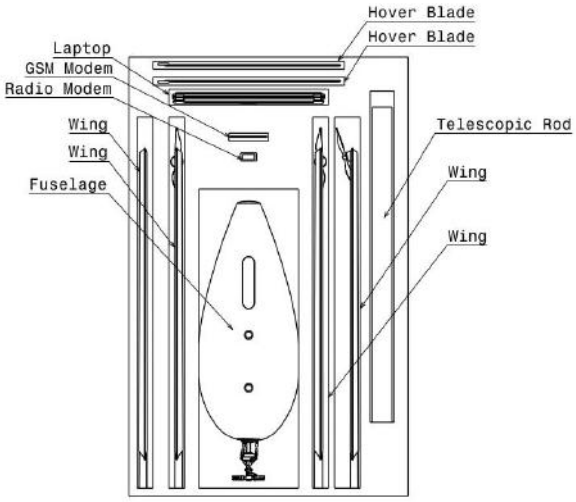

Figure 12.4: Disassembled UAV ready for transport.

Together with a casing, isolating foam and ground station the whole packed up system weight will not exceed 15 kg.

12.2.2. Assembly

As the UAV will be split in several parts, it has to be assembled in block 1.0 and the reverse in block 10.0. The parts to be disassembled are: four wings, fuselage and hover propeller blades from the swashplate. The wings will be attached to the payload box with screws and additional pins to avoid moving in horizontal plane. The bolts will join wing spars, made a bit longer than skin around them to enable sliding the into the fuselage. Analogically, propeller blades can be attached with screws going through the hub section and attached to the swashplate rotating cam shafts. The whole assembly is estimated to take up to 10 minutes and should be possible using only simple tools. The need of support and needed equipment for block 2.1, refuelling, highly depends on the chosen hydrogen storage solution and should be minimised for the participation in the UAV challenge but can be more complex for later applications. For the ground station to be set (block 2.2) a computer has to be turned on with reliable power connection to avoid unpredicted system shutdown. Also, the antenna, which is an integral part of the ground station has to be unfold and connected to the ground station.

12.2.3. Pre-flight system check

The UAV shall be ready to operate after assembly and refuelling. Before launch automatic system checks will be performed to assure operational readiness. A series of subsystem check will test if control surfaces are working, if required secondary battery and fuel cell energy levels can be delivered. Also navigation system and sensors, data uplink and downlink will be tested. After that the system will report of its readiness to flight. A visual inspection made by the operator should be performed as well, to ensure that no physical damage was done to the UAV during storage and assembly. Special attention should be paid to the dirt and other constituents had not gathered on the control surfaces, camera, pitot tubes and propellers of the UAV.

12.2.4. Maintenance

Repair for the structure and subsystems in blocks 6.0 and 9.0 respectively, can involve more complex tools, as it is not intended to be performed at all after the UAV challenge and it is assumed that navy ships are equipped with a full workshop where these repairs can be handled. If reparation is not possible post-life procedures should be performed to utilise the system and recycle materials and components.

12.3. Project Design & Development Logic

All the activities that are to be performed after the DSE are shown in fig. 12.5 in a logical order. In the diagram, the three deliverables which are to be handed to participate in the MEUC are shown at the relevant phases. The diagram describes the extensive validation process that has to be performed to guarantee that the UAV system meets all the requirements set by the MEUC board. Continuous adjustments have to be made to the design until all the requirements are complied with. Finally, the diagram takes into account the end of life strategy which has to be performed when the lifetime of the UAV has been reached to ensure that the least amount of damage is done to the environment. The colour structure is as follows; Orange blocks indicate deadlines that have to be met for successful participation in the MEUC. The light blue blocks indicate non technical

tasks. The blue blocks indicate the technical tasks to be performed. The yellow blocks indicate validation tasks that will be performed and the red block indicates the end of life strategy. The green blocks represent tasks that have a high chance of happening but don't yet have a guarantee. For this reason, they have not been elaborated upon in detail however they were still considered to be worth showing. To gain a clear overview of the activities to be performed after the DSE, the activities are chronologically ordered with the use of a Gantt chart. The post DSE Gantt chart is given in appendix B.

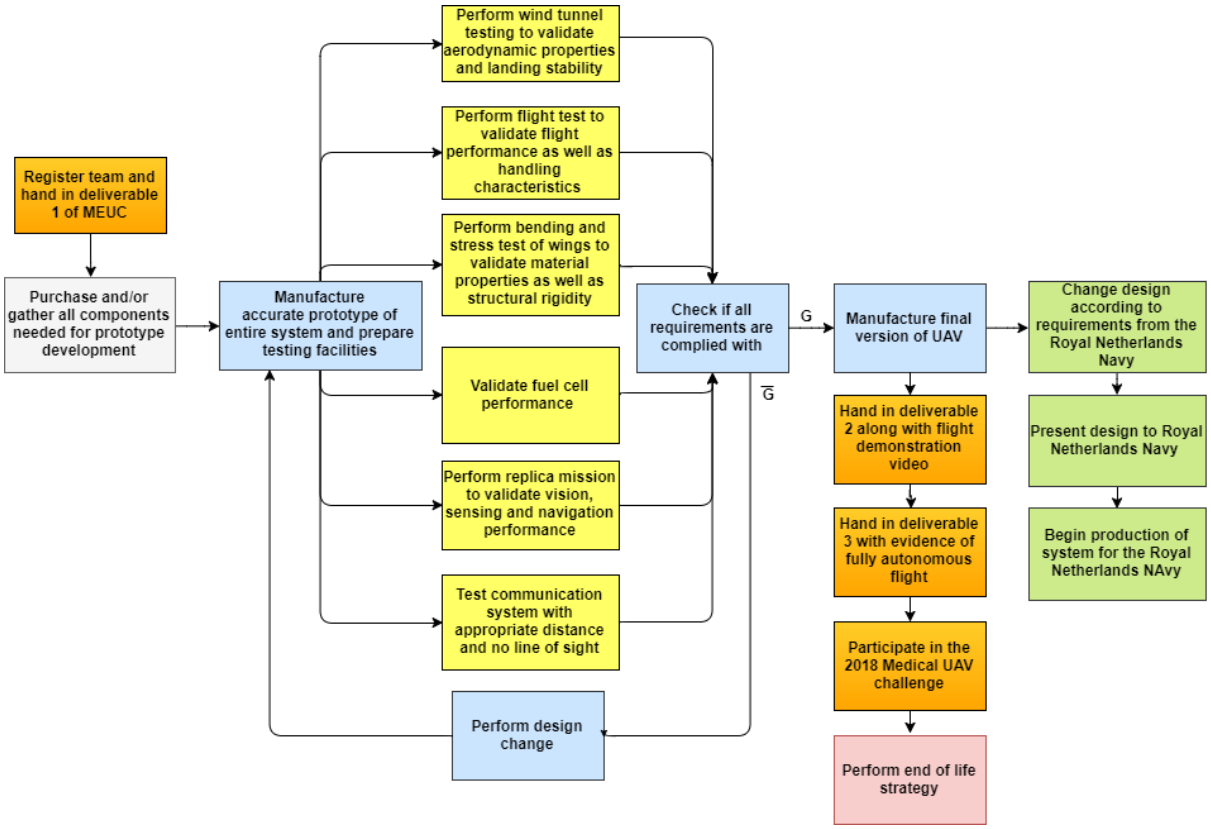

Figure 12.5: Project Design & Development logic diagram

12.4. Conclusions and Recommendations

An operational and logistics plan is established which describes the activities to be performed to operate the UAV system. In order to be able to transport the system within a car trunk or by an airliner, a casing is designed with the following dimension: 1.1 x 0.7 x 0.4 m. The UAV fits inside the casing with the wings and main rotor blades detached. The casing also includes space for communication equipment, a telescopic rod for the antennas and a laptop used for the ground station. Visual checks must be performed before and after every flight in order to decide if repairs are necessary.

During further design phases, tests have to be performed on a prototype in order to validate the design. Furthermore, the design can be optimised for the usage on Navy ships.

13

Conclusion and Recommendations

Conclusion

The aim of this report is to give an overview of the design process of a UAV system capable of winning the Medical Express UAV Challenge 2018. Firstly, a mission overview is given, after which the design reasoning of each subsystem is presented. Subsequently, the entire subsystem analysis is presented. Not only was focus laid on the design of the system itself, attention was also paid to the market feasibility of the design. Finally, thought was given to the future steps that need to be taken to turn this project into a success.

The first and most vital subsystem that was required for the design was the power subsystem. The required cruise shaft power is 284 W and peak shaft power is 957 W. A PEM fuel cell, together with a pressurised gas tank and a supporting lithium-ion battery, is chosen to provide this power to the system. In addition, a separate battery is used to power the flight termination system.
For the aerodynamic design configuration of the UAV, an X-wing configuration is chosen. The aerodynamic configuration results in a statically stable but dynamically unstable UAV. The dynamic instability can however be compensated by the autopilot. The transitions can be achieved but cause considerable changes of altitude (up to 45 m). Regarding the propulsion, one centred hover propeller is chosen with two cruise propellers on the lower wing tips. Finally, a fourth propeller is added on the top left wing to counteract the torque in hover and provide yaw stability. This propeller is left inactive in feather position during cruise.
Moving on, electronics were chosen. For the computer vision subsystem, two high-resolution global shutter colour cameras are chosen. For the location determination system, a LiDAR sensor, in combination with a GPS module, is used. To determine the attitude, a 9 degrees-of-freedom IMU is used. Lastly, a pitot tube is picked for speed determination, hence completing the sensing subsystem.
Next, the design of the communication subsystem is presented. The UAV will have both a radio and a GSM connection, ensuring redundancy.
Finally, to integrate all of these modules into the aerodynamic configuration, a fuselage is designed in which the components are integrated. The fuselage will have a 'rain drop'-shape on account of the aerodynamic benefits.
The final costs of the UAV system is estimated to be €23710,75, and, once the system will go on the market, the sales price of one system will be approximately €92000.

It was not possible to design a system that complies with both the Medical Express UAV Challenge and the Dutch Netherlands Navy requirements. Therefore it was chosen to optimise the design for the Medical Express UAV Challenge and alter this design in the future to suit the requirements of the Navy.

Recommendations

When actually building the UAV next year, it is recommended to spend additional time analysing the characteristics of the UAV. As many analyses were performed during this phase, refinement of these analyses is recommended. More accurate analyses would result in lower safety factors necessary and, consequently, potentially a more efficient system. Furthermore, taking a broader selection of choices for the various design trade-offs could also be considered. The trade-offs that were performed during this design have been done with a narrow selection of design choices, due to time limitations. A broader selection could lead to carefully assessed improvements.
In this design phase, all the necessary verification was performed. Performance of physical tests could alleviate the design of the lack of validity, and would close the gap between theoretically possible and physically possible. The main reason for the lack of validation activities is that physical tests costs resources, which were not available during the DSE. However, in the upcoming year, when the actual UAV will be build, these tests can be executed. It is highly recommended to assure the validity of the design by such tests.
Furthermore, components that currently bought off-the-shelf could be self-developed in improved versions. Due to time limitation and convenience, for some sub-components of the UAV, off-the-shelf products were chosen. These however could be designed to be tailored for this specific project. When doing this, a more optimal sub-component could be created, potentially meaning more compact, lightweight and cheaper components with less power consumption. Furthermore, complete specifications were not always available for

some components such as the fuel cell and the motors. Testing of these components might result in component changes if their performances turn out to be poor.
Another important factor that needs to be considered before the UAV can be launched is the adjustment of the Paparazzi Autopilot software for the specific configuration chosen. Due to originality of aerodynamic configuration, it is expected to see some issues in control of the aircraft and the software may require a lot of careful testing. The flight model should also be improved and fed with experimental data in order to provide more accurate simulations. This might result in shorter and less altitude-hungry transitions.
Moreover, the design of several subsystems can be brought to an lower level. For the structural subsystem, a skeleton could be designed for the fuselage. Also, the detachable connection between the fuselage and wing should be designed such that it is capable of withstanding the loads on the UAV. Furthermore, the payload bay for the medical sample could be designed more thoroughly to include for example a payload bay. And lastly, the open-source PaparazziUAV project can be used to design the autopilot operation, ensuring mission completion.
Finally, a design should be created specifically aimed to be most optimal for fitting the requirements for the Dutch Netherlands Navy. Especially attention should be paid to the design of the fuel cell, however, the other subsystem should be optimised as well for these purposes.

Bibliography

[1] Federal Aviation Administration. *Helicopter Flying Handbook*. U.S. department of Transportation, 2012. URL https://goo.gl/TDx9hX.

[2] Rutkay B.D. *A Process for the Design and Manufacture of Propellers for Small Unmanned Aerial Vehicles*. Carleton University, 2014.

[3] Marilena Bos-Pavel. Guidelines for first dimensioning of a helicopter rotor, 2016.

[4] UAV Challenge Technical Committee. Uav challenge medical express 2018 - competition rules. https://uavchallenge.org/medical-express/, 2017.

[5] W De Jong. *'Vlasbak': eerste auto ter wereld die volledig afbreekbaar is*. NOS.nl, 2016.

[6] TU Delft. Dined anthropedic database. http://dined.io.tudelft.nl/en/database/tool, 2017.

[7] J. Desjardins. Here's how commercial drones grew out of the battlefield. *Business Insider*, 2016. URL https://goo.gl/9s4g5y. [cited 2 May 2017].

[8] Robert W. Deters. Static testing of micro propellers. *Applied Aerodynamics Conference 18 - 21 August 2008, Honolulu, Hawaii*, 2008.

[9] R.W. Deters, G.K. Ananda, and M.S. Selig. *Reynolds Number Effects on the Performance of Small-Scale Propellers*. University of Illinois at Urbana-Champaign, 2014.

[10] M. Drela. Xrotor v7.55 [computer software]. URL: http://web.mit.edu/drela/Public/web/xrotor/xrotor_doc.txt, 2009.

[11] A. Imbrechts et al. *Stakeholder Requirements imposed by the Royal Netherlands Navy*. Faculty of Aerospace Engineering, TU Delft, 2017.

[12] E. Gill, G. LaRocca, W. Verhagen, and A. Cervone. *AE3211-I Systems Engineering and Aerospace Design - Slides*. TU Delft, 2016.

[13] Granta. Ces edupack 2017 [computer software]. https://www.grantadesign.com/education/edupack/index.htm, 2017.

[14] R.J. Hamman and M.J.L. van Tooren. *SYSTEMS ENGINEERING & TECHNICAL MANAGEMENT TECHNIQUES PART II lecture notes*. TU Delft, 2006.

[15] Martin Hepperle. Basic design of flying wing models. http://www.mh-aerotools.de/airfoils/flywing1.htm, 2002.

[16] R.C. Hibbeler and Kai Beng Yap. *Mechanics for Engineers - Statics*. Pearson, 13 edition, 2013.

[17] Dr.Ing. S. F. Hoerner. *Fluid Dynamic Drag*. Dr.Ing. S. F. Hoerner, 1965.

[18] A. Imbrechts et al. *Baseline Report - Medical Express UAV*. TU Delft, April 2017.

[19] A. Imbrechts et al. *Midterm Report - Medical Express UAV*. TU Delft, May 2017.

[20] Itseez Intel Corporation, Willow Garage. Opencv (open source computer vision library) 3.2 [computer software]. URL: http://opencv.org/, 2016.

[21] M. Kaltschmitt et al. *Renewable Energy: Technology, Economics and Environment*. Springer, 2017.

[22] I. Kroo. Nonplanar wing concepts for increased aircraft efficiency, 2005. URL http://aero.stanford.edu/reports/vki_nonplanar_kroo.pdf.

[23] J. Larminie and A. Dicks. *Fuel Cell Systems Explained*. Wiley, 2003.

[24] J.G. Leishman. *Principles of Helicopter Aerodynamics*. Cambridge University Press, 2 edition, 2006.

[25] S.A. Ning. A simple solution method for the blade element momentum equations with guaranteed convergence. *Wind Energy*, June 2013.

[26] M. Nita and D. Scholz. Estimating the oswald factor from basic aircraft geometrical parameters, 2012. URL http://www.fzt.haw-hamburg.de/pers/Scholz/OPerA/OPerA_PUB_DLRK_12-09-10.pdf.

[27] Purdue University College of Engineering. Xflr5: Analysis of foils and wings operating at low reynolds numbers - guidelines. URL: goo.gl/sbtnyg, 2009.

[28] Q Oostvogel. Duurzaam composiet. Email, 2017.

[29] S. Peasgood and M. Valentin. *DRONES: A RISING MARKET*. Sophic Capital, 2015. URL http://sophiccapital.com/wp-content/uploads/2015/09/Download-Sophic-Capitals-Aerial-Drone-Report-Here.pdf.

[30] Paparazzi Project. Paparazzi uav v5.10 [computer software]. URL: http://wiki.paparazziuav.org/wiki/Main_Page, 2017.

[31] M. Sadraey. *Aircraft design : a systems engineering approach*. John Wiley Sons, 2012. ISBN 9781119953401. URL https://ebookcentral-proquest-com.tudelft.idm.oclc.org/lib/delft/detail.action?docID=1078755.

[32] Mohammad H. Sadraey. *Aircraft Performance*. VDM Publishing, 2009. ISBN 9783639200133. URL https://books.google.nl/books?id=7m8LQgAACAAJ.

[33] J.S. Seybold. *Introduction to RF Propagation*. Wiley Interscience, 2005.

[34] Techwinder. Xflr5 v.6.38 [computer software]. URL: http://www.xflr5.com/xflr5.htm, 2017.

[35] J.S. Touma. Dependence of the wind profile power law on stability for various locations. *Journal of the Air Pollution Control Association*, 27, 1977.

[36] I.P. Tracy. Propeller design and analysis for a small, autonomous uav. *DSpace*, 2011.

[37] Dr. Murat Vural. *Estimating R/C model aerodynamics and performance*. Illinois Institute of Technology, 2014. URL https://mypages.iit.edu/~vural/RC%20Airplane%20Design.pdf.

[38] C. Wagter et al. *Design, Control and Visual Navigation of the DelftaCopter*. TU Delft, 2016.

[39] A.D. Young. *The Calculation of the Total and Skin Friction Drags of Bodies of Revolution a Zero Incidence*. AIR MINISTRY, 1939.

A

Appendix A: Risk Assessment & Mitigation

This appendix contains the extensive list of risks related to the system. It describes the risk events and gives the respective priorities and mitigation plans.

DSE Medical Express UAV Challenge 2018 - Risk Assessment & Mitigation													
Index	**Cat.**	**Cause**	**Event**	**Consequence**	**Severity**	**Likelihood**	**Risk Priority**		**Mitigation**	**Sev. after mitigation**	**Lik. after mitigation**	**Risk Priority after mitigation**	
BUSINESS PLAN RISKS													
Bus-1	Business	Client's needs were not met, low reliability of the product	UAV cannot be applied in commercial use, outside competition	Project financial failure	**5**	**3**	**15**	**High priority**	Market analysis, identification of stakeholder requirements	**4**	**2**	**8**	**Review**
Bus-2	Business	Underestimation of costs	Budget overrun	Bankruptcy	**5**	**3**	**15**	**High priority**	FED, contingency, risk analysis, market analysis, supply chain assurance, good management	**5**	**2**	**10**	**Review**
Bus-3	Business	High price makes the product inattractive	Low sales	Financial failure	**4**	**3**	**12**	**High priority**	Make cost one of the important design cirterion, budget analysis, FED	**4**	**2**	**8**	**Review**
Bus-4	Business	Subcontractor fails to deliver in time	Delay in the production of the UAV	Delayed delivery time, financial loss	**3**	**4**	**12**	**High priority**	Establish clear deadlines and communication lines with subcontractor; shared responsibilities; critical path investigation	**3**	**3**	**9**	**Review**
Bus-5	Business	General safety requirements not met	The product does not comply with safety regulations	The product can not be sold and used in some countries	**4**	**3**	**12**	**High priority**	Make sure that product meets safety requirements of countries in the targeted market	**4**	**2**	**8**	**Review**
Bus-6	Business	Bad marketing	Not enough clients buy the product	Product is not profitable	**3**	**3**	**9**	**Review**	Pay attention to commercial applications; incolve PR and marketing specialists	**3**	**1**	**3**	**Risk acceptable**
Bus-7	Business	PR and marketing not sufficient, not enough information about the project shared to the media	Lack of sponsorship	Less ressources available	**3**	**3**	**9**	**Review**	Contact potential sponsors individually; make a use of social media and university representation	**3**	**2**	**6**	**Risk acceptable**
Bus-8	Business	Party pulls out of project	Change in stakeholder requirement	Potential need for redesign	**4**	**2**	**8**	**Review**	Involve all stakeholders on early stage of development and fit the project for the purpose based on their needs	**4**	**1**	**4**	**Risk acceptable**
Bus-9	Business	Mission failure/better competitor	Competition not won	50k€ not won, main goal of the project failure	**2**	**4**	**8**	**Review**	Design UAV able to complete the mission, review competition solutions	**2**	**3**	**6**	**Risk acceptable**
LEGAL RISKS													
Leg-1	Legal	Different laws in different countries	Air worthiness/safety regulations not met	UAV not allowed to operate in some areas	**5**	**4**	**20**	**Not permissible**	Involve air safety representatives in project revision on en early stage of development	**5**	**3**	**15**	**High priority**
Leg-2	Legal	Crash or collision	No money to cover damage to the system	Project terminated	**5**	**2**	**10**	**Review**	Proper insurance planning, contingency budget	**3**	**2**	**6**	**Risk acceptable**
Leg-3	Legal	Fuel cell not allowed to transport in some conditions (on a plane)	Transportation not possible due to safety reasons	The transportation by plane is banned	**4**	**2**	**8**	**Review**	Ensure secure transportation casing for the fuel cell	**4**	**1**	**4**	**Risk acceptable**
PAYLOAD TRANSPORTATION RISKS													
Pay-1	Payload	Loosely secured sample falls off on the way back to the base	Sample dropped	Loss of sample	**4**	**3**	**12**	**High priority**	Simple, foolproof loading casing; lock to secure the payload	**4**	**1**	**4**	**Risk acceptable**
Pay-2	Payload	Sample does not fit the container	Sample can not be loaded	Loss of sample	**4**	**3**	**12**	**High priority**	Communicate container size to the target; ask customer to use standard sampling container	**4**	**1**	**4**	**Risk acceptable**
Pay-3	Payload	Improperly sealed sample starts leaking	Sample leak	(Partial) loss of sample; Contamination of environment/UAV.	**3**	**2**	**6**	**Risk acceptable**	Remind target to verify that the payload is well sealed	**3**	**1**	**3**	**Risk acceptable**
Pay-4	Payload	Vibrations/acceleration of the UAV deteriorates the quality of the blood sample	In flight deterioration of the sample	Sample quality decreased	**2**	**3**	**6**	**Risk acceptable**	Payload protection and damping mechanism (e.g. spring or insulation)	**2**	**2**	**4**	**Risk acceptable**
OPERATIONAL RISKS													
Op-1	Operations	Packaging for transport not securing the payload	Damage in transport	UAV damaged permamently	**5**	**4**	**20**	**Not permissible**	Transport container has to secure the payload, whithstand air/ground transportation	**5**	**2**	**10**	**Review**
Op-2	Operations	Power setting for propulsion too low	Crash landing	UAV damaged permamently	**4**	**4**	**16**	**Not permissible**	Ensure enough landing space to land with high power setting for controllability	**4**	**2**	**8**	**Review**
Op-3	Operations	Power setting for propulsion too low	Crash at take-off	UAV damaged permamently	**4**	**4**	**16**	**Not permissible**	Ensure enough take-off space to land with high power setting for controllability	**4**	**2**	**8**	**Review**
Op-4	Operations	Storage not secure or UAV left without supervision	Theft	UAV stolen	**5**	**2**	**10**	**Review**	Locked transport container, UAV cannot be left in public open areas without supervision	**5**	**1**	**5**	**Risk acceptable**

Op-5	Operations	Criminal act	Hijacking	UAV misuse, act of terror, theft	**5**	**2**	**10**	**Review**	Safety switch incorporated that can kill the drone at request of the operator	**5**	**1**	**5**	**Risk acceptable**
Op-6	Operations	Flight altitude too low in heavy traffic areas	Road traffic interference	UAV and private property damage, legal issues	**5**	**2**	**10**	**Review**	Include public roads and heavy traffic areas into no-fly zones	**5**	**1**	**5**	**Risk acceptable**
Op-7	Operations	Emergency landing	Landing in no-go zone	Need to recover the drone	**5**	**2**	**10**	**Review**	Keep the position tracking on until drone is localized and recovered	**2**	**2**	**4**	**Risk acceptable**
Op-8	Operations	Flight in weather conditions not allowed for the considered design	Crash in flight due to bad weather	Wetting of the electronics, crash due to gust, ligthning strike, etc.	**5**	**2**	**10**	**Review**	State the range of weather and gust wind conditions allowed for flight	**5**	**1**	**5**	**Risk acceptable**
Op-9	Operations	Swash plate/control surfaces failure	VTOL transition failure	Not possible to transfer to horizontal flight	**3**	**3**	**9**	**Review**	If in the base - land immediately, if not - calculate if there is enough fuel to return in vertical position	**1**	**3**	**3**	**Risk acceptable**
HEALTH AND ENVIRONMENTAL RISKS													
HSE-1	Health and Environment	Object detection failure	UAV collision with private property	Property damage resulting in legal issues	**5**	**3**	**15**	**High priority**	Emergency procedures for safety should be implemented, such as a flight termination system during potentially dangerous situations.	**3**	**3**	**9**	**Review**
HSE-2	Health and Environment	Object detection failure	Collision with operator, user or other people	Person harmed or killed resulting in legal issues	**5**	**3**	**15**	**High priority**	Emergency procedures for safety should be implemented, such as a flight termination system during potentially dangerous situations.	**5**	**3**	**15**	**High priority**
HSE-3	Health and Environment	Object detection failure	UAV collision with a bird or other animal	Animal harmed or killed	**3**	**3**	**9**	**Review**	Emergency procedures for safety should be implemented, such as a flight termination system during potentially dangerous situations.	**3**	**2**	**6**	**Risk acceptable**
HSE-4	Health and Environment	Object detection failure	UAV collision with vegatation	Nature permamently damaged	**3**	**3**	**9**	**Review**	Emergency procedures for safety should be implemented, such as a flight termination system during potentially dangerous situations.	**3**	**2**	**6**	**Risk acceptable**
HSE-5	Health and Environment	Breakdown of the system	Debris entering the environment	Environment pollution	**3**	**4**	**12**	**High priority**	Perform a accurate load case study including a safety margin, and ensure structural integrity. Use biodegredable materials for the UAV design.	**1**	**2**	**2**	**Risk acceptable**
HSE-6	Health and Environment	Fuel tank failure	Fuel leakage	Environment pollution	**3**	**2**	**6**	**Risk acceptable**	Determine the load bearing capabilities of the fuel tank to the maximum loads of the UAV.	**3**	**1**	**3**	**Risk acceptable**
HSE-7	Health and Environment	Fuel tank overheating	Fuel tank explosion	Permanent damage to surrounding environment	**5**	**2**	**10**	**Review**	Determine the maximum temperature, including safety margin, of the fuel tank during operation at apply cooling measures if necessary.	**5**	**1**	**5**	**Risk acceptable**
HSE-8	Health and Environment	The use of pollutant gasses in the system	Pollutanting gasses released to the environment	Environment pollution	**3**	**5**	**15**	**High priority**	Minimise the use of polluting gasses in the design.	**3**	**2**	**6**	**Risk acceptable**
HSE-9	Health and Environment	High radiation of the communication system	Radiation damage to the environment	Harm to objects, animals or people in vicinity of the UAV	**4**	**3**	**12**	**High priority**	Minimise the radiation strength of communication system design.	**4**	**1**	**4**	**Risk acceptable**
HSE-10	Health and Environment	Leakage of the payload blood	Blood contaminates the environment	Harm to animals or people that come in cc	**4**	**3**	**12**	**High priority**	Design a payload case that can resist the loads on the UAV and include a safety factor.	4	1	**4**	**Risk acceptable**
AUTOPILOT (PAPARAZZI) RISKS													
Pap-1	Autopilot	Image recognition algorithm cannot localize the target	Failure to locate the target	Mission cannot be completed	**4**	**4**	**16**	**Not permissible**	Loiter around target area, image improvement algorithm, message operator (not in competition)	**2**	**3**	**6**	**Risk acceptable**
Pap-2	Autopilot	Image recognition algorithm cannot estimate good location to land the UAV	Failure to locate landing spot	Landing in vicinity of target is impossible; mission failed	**4**	**4**	**16**	**Not permissible**	Loiter around target area, image improvement algorithm, message operator (not in competition)	**2**	**3**	**6**	**Risk acceptable**
Pap-3	Autopilot	Feedback data transfer failure	System does not report system status	No information on system status	**5**	**3**	**15**	**High priority**	Reset the system; blackout not allowed due to safety reasons	**3**	**3**	**9**	**Review**
Pap-4	Autopilot	Paparazzi not incorporating safety/emergency protocols	Emergency landing cannot be performed	Crash	**5**	**3**	**15**	**High priority**	Include gliding/one-engine/propeller loss landing procedures in autopilot design	**5**	**1**	**5**	**Risk acceptable**
Pap-5	Autopilot	Paparazzi not incorporating safety/emergency killswitch	Emergency takedown cannot be performed	Crash or damage caused to people or private property	**5**	**3**	**15**	**High priority**	Include a "kill switch" command to instantenously shut down the system	**5**	**1**	**5**	**Risk acceptable**
Pap-6	Autopilot	Code errors: floating point, overflow, etc.	System crash	System shut-down	**5**	**3**	**15**	**High priority**	Code verification, continuous system updates	**4**	**2**	**8**	**Review**
Pap-7	Autopilot	Mistake of image recognition algorithm	Landing spot located on water	Possible damage, drowning a drone	**3**	**4**	**12**	**High priority**	Check for reflectivity of the landing surface	**3**	**2**	**6**	**Risk acceptable**

Pap-8	Autopilot	Routing algorithm fails or no no-fly zones interfere with flight range	Failure to locate the safe route (outside no fly-zones)	Cannot perform a flight or UAV flies into no-fly zone	**3**	**2**	**6**	**Risk acceptable**	Range big enough to fly around no-fly zones, route review by an operator (not in competition)	**3**	**1**	**3**	**Risk acceptable**
Pap-9	Autopilot	Paparazzi not taking into account CG shift due to mass change	Autopilot stability error due to mass change	Iduced oscillation, instabillity	**2**	**3**	**6**	**Risk acceptable**	Consider CG shifting in autopilot design	**2**	**1**	**2**	**Risk acceptable**
Pap-10	Autopilot	Loss of coordinates data	Failure to return autonomously, system cannot locate the base	UAV stuck mid-air or cannot perform a flight back to base	**2**	**2**	**4**	**Risk acceptable**	Data backup with base coordinates to ensure UAV can retum	**2**	**1**	**2**	**Risk acceptable**
Pap-11	Autopilot	Root locus of the feedback controller	Autopilot stability error (system not damped correctly)	Induced oscillation, instabillity	**2**	**2**	**4**	**Risk acceptable**	Backup feedback controller settings	**1**	**2**	**2**	**Risk acceptable**
ELECTRONICS & SENSORS RISKS													
Ele-1	Electronics	GPS failure	No auto-location	Loss of control over the system	**4**	**3**	**12**	**High priority**	Hover, if reset of GPS unsuccessful - perform emergency landing	**3**	**2**	**6**	**Risk acceptable**
Ele-2	Electronics	Software/Hardware failure	Transmitter/receiver failure	No data link, loss of control over the system	**4**	**3**	**12**	**High priority**	Hover, if reset of data link unsuccessful - perform emergency landing	**3**	**2**	**6**	**Risk acceptable**
Ele-3	Electronics	Manufacturing flaws or faulty solder	Short circuit/connection failure	System shut-down	**3**	**3**	**9**	**Review**	Use redundant electronic components and connections, check manufacturing quality	**3**	**1**	**3**	**Risk acceptable**
Ele-4	Electronics	Water/dust getting on electronics	Short circuit	System shut-down	**3**	**3**	**9**	**Review**	Use waterproof/dust sealing	**3**	**1**	**3**	**Risk acceptable**
Ele-5	Electronics	Interference	Electronic devices inaccuracy, malfunction, etc.	Inaccuracy, errors, offset	**3**	**3**	**9**	**Review**	Check electronic systems integrity, ensure no magnetic/electric interference	**3**	**1**	**3**	**Risk acceptable**
Ele-6	Electronics	Unexpected shut off	Sensor failure	Autonomous control system may become dysfunctional	**3**	**3**	**9**	**Review**	Use redundant sensors	**3**	**1**	**3**	**Risk acceptable**
Ele-7	Electronics	Spots and flaws on the lens	Camera image quality drops	Image recognition system effectiveness drops	**2**	**4**	**8**	**Review**	Protect the lens from environmental conditions with a filter, use STEREO vision	**1**	**4**	**4**	**Risk acceptable**
Ele-8	Electronics	Vibration or forces acting in flight	Cable disconnected	System shut-down	**3**	**1**	**3**	**Risk acceptable**	Use solid connections, clamps and soldering	**3**	**1**	**3**	**Risk acceptable**
Ele-9	Electronics	Hover motor overheats	Hover motor failure	Loss of thrust and crash	5	3	**15**	**High priority**	Selection of motor that can handle load; Proper cooling of the motor	5	2	**10**	**Review**
Ele-10	Electronics	Too much torque is applied on the motor	Motor stalls	Loss of thrust and crash	5	3	**15**	**High priority**	Selection of motor that can handle load	5	1	**5**	**Risk acceptable**
Ele-11	Electronics	Cruise motor overheats	Cruise motor failure	Emergency landing must be performed	4	3	**12**	**High priority**	Selection of motor that can handle load; Proper cooling of the motor	4	2	**8**	**Review**
Ele-12	Electronics	Too much torque is applied on the motor	Motor stalls	Emergency landing must be performed	4	3	**12**	**High priority**	Selection of motor that can handle load	4	1	**4**	**Risk acceptable**
FUEL CELL & POWER RISKS													
FC-1	Fuel Cell & Power	UAV runs out of fuel	Fuel shortage	Loss of power	**5**	**4**	**20**	**Not permissible**	Use of safety margins for fuel consumption; development of accurate mission fuel consumption model; constant measurements of remaining fuel to avoid unexpected power loss; implementation of fuel shortage emergency landing procedure; display warnings to the operator GUI	**4**	**3**	**12**	**High priority**
FC-2	Fuel Cell & Power	Mechanical failure, overheating, leaking, perforation	Fuel cell failure	Loss of power	**5**	**3**	**15**	**High priority**	On board battery to avoid crash landing and communicate the problem to the ground station; use of reliable fuel cells; extensive testing of the fuel cells	**4**	**2**	**8**	**Review**
FC-3	Fuel Cell & Power	Fuel cell humidifier failure	Dry out of the fuel cell membrane	Partial/Full loss of power; Potential permanent damage of the fuel cell	**5**	**3**	**15**	**High priority**	Redundancy; extensive testing of the humidifier; implementation of dry out procedure to avoid permanent damage of the fuel cells	**4**	**2**	**8**	**Review**

FC-4	Fuel Cell & Power	Loss of cooling	Overheating of the fuel cell	Partial/Full loss of power; Potential permanent damage of the fuel cell	**5**	**3**	**15**	**High priority**	Passive cooling or redundant cooling system; implementation of overheating procedure to avoid permanent damage of the fuel cells	**4**	**2**	**8**	**Review**
FC-5	Fuel Cell & Power	Type of fuel used results in overly complicated supply or loading procedures	UAV can not be refueled	Mission can not be carried out	**4**	**3**	**12**	**High priority**	Use easily accessible, easy to load fuel within safe pressure range	**4**	**1**	**4**	**Risk acceptable**
FC-6	Fuel Cell & Power	Tank/Fuel cell sealing failure	Loss of fuel	Loss of power; Release of potentially harmful and dangerous fuel into the environment	**5**	**2**	**10**	**Review**	Extensive testing of the sealing; multiple layered sealing; on board battery to avoid crash landing and communicate the problem to the ground station; use of safe and non toxic fuels	**4**	**1**	**4**	**Risk acceptable**
STRUCTURAL RISKS													
Str-1	Structure	Mistake done during assembly by customer	In-flight partial dissassembly	Structural failure	**5**	**4**	**20**	**Not permissible**	Simple, foolproof re-assembly procedures; use of checklists; use click locks; no spare parts/bolts/screws/specialised tools in the assembly	**5**	**1**	**5**	**Risk acceptable**
Str-2	Structure	Propeller blade/shaft fails	Propeller failure	Loss of thrust	**5**	**3**	**15**	**High priority**	Extensively tested propeller blade/shaft; implementation of an emergency zero-thrust landing (e.g. belly landing, autorotation landing); multiple propellers	**3**	**2**	**6**	**Risk acceptable**
Str-3	Structure	Vibration loads exceed max structural loads	Structural failure	Repair necessary	**5**	**3**	**15**	**High priority**	Make sure resonance can not happen (especially ground resonance during landing); use material with good dynamics load properties; usage of "low-vibration" propeller	**5**	**1**	**5**	**Risk acceptable**
Str-4	Structure	Extreme weather condition (warm or cold) cause structure to melt/become brittle	Structural failure	Replacement or repair necessary	**5**	**3**	**15**	**High priority**	Use materials that can survive temperature range (-30°C->100°C)	**5**	**1**	**5**	**Risk acceptable**
Str-5	Structure	One of the control surface fails	Control surface failure	Partial/Full loss of control	**4**	**3**	**12**	**High priority**	Implementaion of procedures for every control surface to minimize the effect of a failure; extensive testing of the control surfaces; simple mechanisms	**4**	**1**	**4**	**Risk acceptable**
Str-6	Structure	Some disturbance (e.g. gust, uneven ground, animal, etc.) causes the UAV to tip over	Tip over	Take-off impossible	**4**	**3**	**12**	**High priority**	Stable landing gear, well-tought weight balance; landing on uneven groud not permissible by autopilot	**4**	**1**	**4**	**Risk acceptable**
Str-7	Structure	UAV left under influence of extreme weather condtitions; improper storage	Wear out of structural parts	Creep, cracking, weathering of plastic parts	**4**	**3**	**12**	**High priority**	Inform the customer about proper storage, use durable materials	**4**	**2**	**8**	**Review**
Str-8	Structure	Material fails	Structural failure	Repair necessary	**5**	**2**	**10**	**Review**	Inspect material regularly; use tested materials; extensive testing; investigate fatigue life of the structure	**5**	**1**	**5**	**Risk acceptable**
Str-9	Structure	Too high load results in failure of the structure	Structure fails	Repair necessary	**5**	**2**	**10**	**Review**	Prevent (with the autopilot) the aircraft from flying outside its flight envelope; safety marigins for gust conditions; flight simulation in critical conditions	**5**	**1**	**5**	**Risk acceptable**
Str-10	Structure	Failure of water seal	Water enters system	Water damage of the system	**3**	**3**	**9**	**Review**	Regular inspection of the seal; use insulating washers; add "verify that the system is properly sealed" in the pre-flight checklist	**3**	**2**	**6**	**Risk acceptable**
Str-11	Structure	Dust/insects accumulate on the structure	Structure is dirty	Higher weight and drag	**2**	**4**	**8**	**Review**	Regularly clean the UAV, easiness of maintanance, avoid crevices in the outer shell	**2**	**3**	**6**	**Risk acceptable**
Str-12	Structure	Rusting of the structure	Rust on some parts of the structure	Weakening of the structure	**2**	**3**	**6**	**Risk acceptable**	Use of non rusting alloys or polymers; avoid galvanic corrosion at connections, limit amount of metallic parts, regular inspections, coating	**2**	**1**	**2**	**Risk acceptable**

PRODUCTION RISKS													
Pro-1	Production	Tolerances do not meet the expectations	Misalign of the parts	Loss of waterproof sealing	**4**	**4**	**16**	**Not permissible**	Design fail-safe connections between parts, use overlaps	**4**	**2**	**8**	**Review**
Pro-2	Production	Not a mass production, innovative method	Production costs kills the budget	Budget overrun, lack of resource	**3**	**5**	**15**	**High priority**	FED, production planning, careful choice of the methods; use re-usable molds	**3**	**3**	**9**	**Review**
Pro-3	Production	Innovative production method	Unforseen production errors	Production delays, possible critical failures	**4**	**3**	**12**	**High priority**	Contract experienced stakeholders for production; use non-destructive & material testing for quality tests	**4**	**1**	**4**	**Risk acceptable**
Pro-4	Production	Unskilled construction team, unique product	Low quality production	Value of the product decreases	**3**	**4**	**12**	**High priority**	Contract experienced stakeholders for production; use non-destructive & material testing for quality tests	**2**	**3**	**6**	**Risk acceptable**
Pro-5	Production	Material was not treated properly	Production defect in internal structure	Crack growth, fatigue failure	**3**	**3**	**9**	**Review**	Investigate internal structure, i.e. X-ray	**2**	**2**	**4**	**Risk acceptable**
Pro-6	Production	Material unavailability	Production delay	Drone not ready for the competition	**4**	**2**	**8**	**Review**	Use off-shelf products and materials	**4**	**1**	**4**	**Risk acceptable**
AERODYNAMIC PERFORMANCE RISKS													
Aer-1	Aerodynamics	Cl design underestimated	Power consumption grows	UAV unable to finish mission	**4**	**3**	**12**	**High priority**	Have a margin for the amount of fuel in the tank	**3**	**1**	**3**	**Risk acceptable**
Aer-2	Aerodynamics	Not enough control actuators	Aircraft uncontrollable	UAV unable to fly	**4**	**3**	**12**	**High priority**	Perform a scenario analysis to ensure that the UAV will be controllable in all scenarios	**3**	**1**	**3**	**Risk acceptable**
Aer-3	Aerodynamics	Aircraft unbalanced	Aircraft uncontrollable	UAV unable to fly	**4**	**2**	**8**	**Review**	Perform accuratte stability analysis to ensure that the aircrraft will be balanced	**2**	**1**	**2**	**Risk acceptable**
Aer-4	Aerodynamics	Underestimate drag	Insufficient top speed	Not complete the mission in the time limit	**4**	**1**	**4**	**Risk acceptable**	Perform CFD analysis for final design to get accurate values for drag	**1**	**1**	**1**	**Risk acceptable**
Aer-5	Aerodynamics	Transition not smooth	Fall out of sky	UAV unable to take off or land	**4**	**1**	**4**	**Risk acceptable**	Design CL stall to be high enough that the transition can happen at a low enough speed	**2**	**1**	**2**	**Risk acceptable**
COMMUNICATION RISKS													
Com-1	Communication	Unexpected obstacle	Signal is blocked	DNFZ and Telemetry cannot be send back and forth	**5**	**4**	**20**	**Not permissible**	Establish a statistical tool that accounts for obstacles and use a redundant communication system	**2**	**3**	**6**	**Risk acceptable**
Com-2	Communication	Bad research about available frequencies at the competition location	Planned frequency not available during operation	DNFZ and Telemetry cannot be send back and forth	**5**	**3**	**15**	**High priority**	Perform thorough research on which frequencies are available for use in the competition location	**5**	**2**	**10**	**Review**
Com-3	Communication	Mobile Provider outage	Mobile network is unavailable	DNFZ and Telemetry cannot be send back and forth	**5**	**3**	**15**	**High priority**	Use a redundant communication system	**2**	**4**	**8**	**Review**
Com-4	Communication	Transceiver hardware failure	Transceiver does not work	DNFZ and Telemetry cannot be send back and forth	**5**	**2**	**10**	**Review**	Test the hardware and, if the budget allows, choose a higher quality transceiver	**5**	**1**	**5**	**Risk acceptable**
Com-5	Communication	GSM runs out of prepaid credit	Mobile network is unaccessible	DNFZ and Telemetry cannot be send back and forth	**5**	**2**	**10**	**Review**	Buy sufficient prepaid credit beforehand	**5**	**1**	**5**	**Risk acceptable**
Com-6	Communication	Signal jaming	A frequency range gets jammed by other electronic hardware	Received signal Power is decreased	**4**	**2**	**8**	**Review**	Use different frequency bands for two communication systems onboard	**4**	**1**	**4**	**Risk acceptable**
Com-7	Communication	Poor telescopic rod quality	Telescopic rod breaks off at ground station	Signal power is weaker	**3**	**2**	**6**	**Risk acceptable**	Determine the maximum loads on the rod and choose a rod that can withstand these loads	**3**	**1**	**3**	**Risk acceptable**
Com-8	Communication	Hardware failure of direct radio	Loss of direct radio signal during cruise	No redundant communication system	**3**	**2**	**6**	**Risk acceptable**	Test radio communication before and use 2 sets of antenna's in dversity mode	**3**	**1**	**3**	**Risk acceptable**
Com-9	Communication	Out of range of mobile network	Loss of GSM communication during landing	No communication possible at landing site	**4**	**2**	**8**	**Review**	Review and test network before mission within the area	**4**	**1**	**4**	**Risk acceptable**

B

Appendix B: Gantt Chart

In order to reach the final design, many steps need to be performed. To ensure a smooth project progression, it is essential to properly plan each and every task. A Gantt chart is a remarkable tool to neatly plan these tasks and establish a clear overview over the tasks ahead. The Gantt chart for the final phase of the DSE is illustrated in fig. B.1. Also, a Gantt chart is created to organise the activities that need to be performed after the DSE in order to continue the project. The chart is indicated in fig. B.2 and illustrates the activities for the upcoming two years. In these charts, the green tasks represent completed tasks, red overdue tasks and blue to-be-finished tasks. For each tasks, a responsible team member is assigned. This however does not mean that the entire task is executed by that person alone.

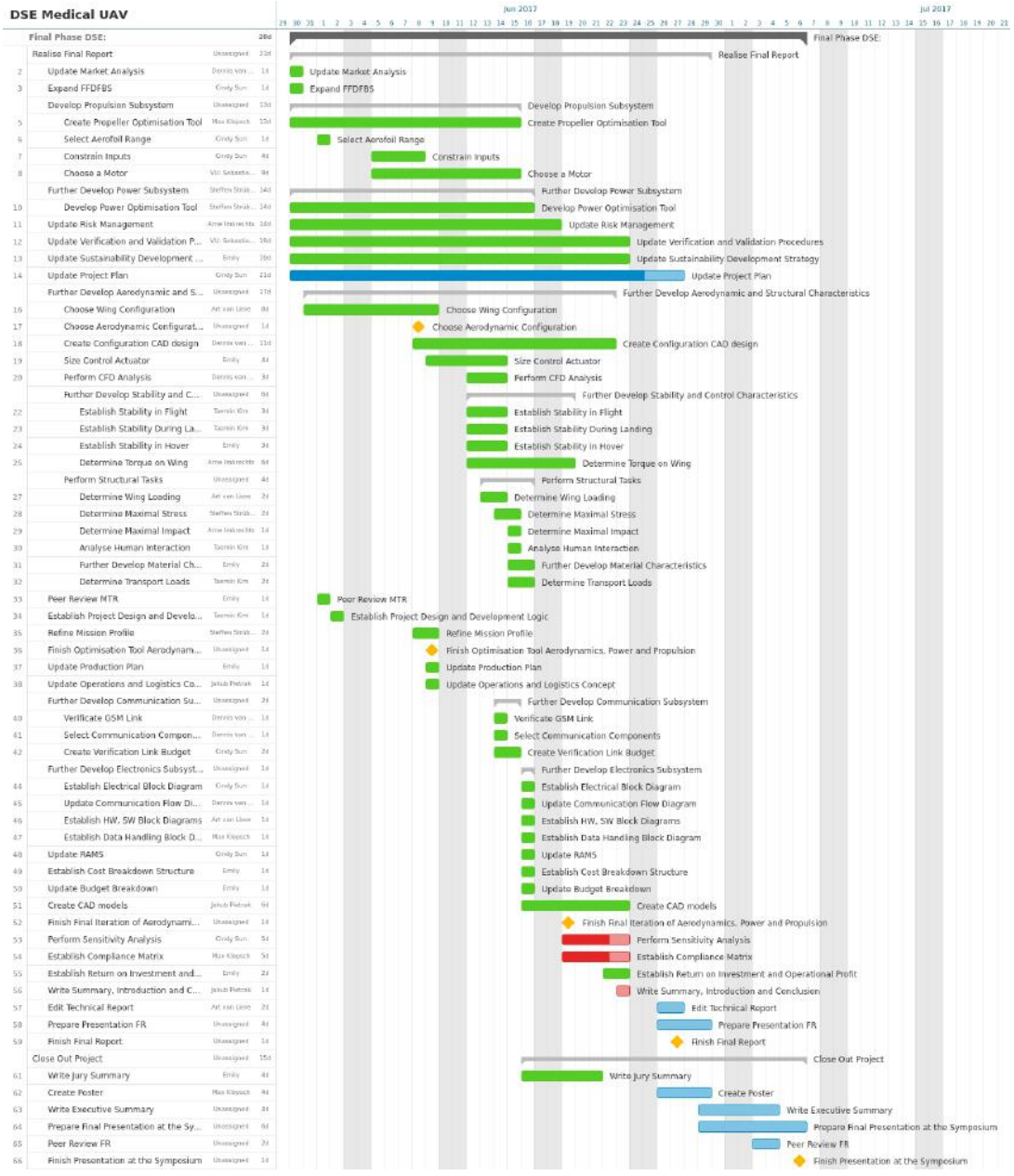

Figure B.1: Project Gantt Chart [24-06-2017]

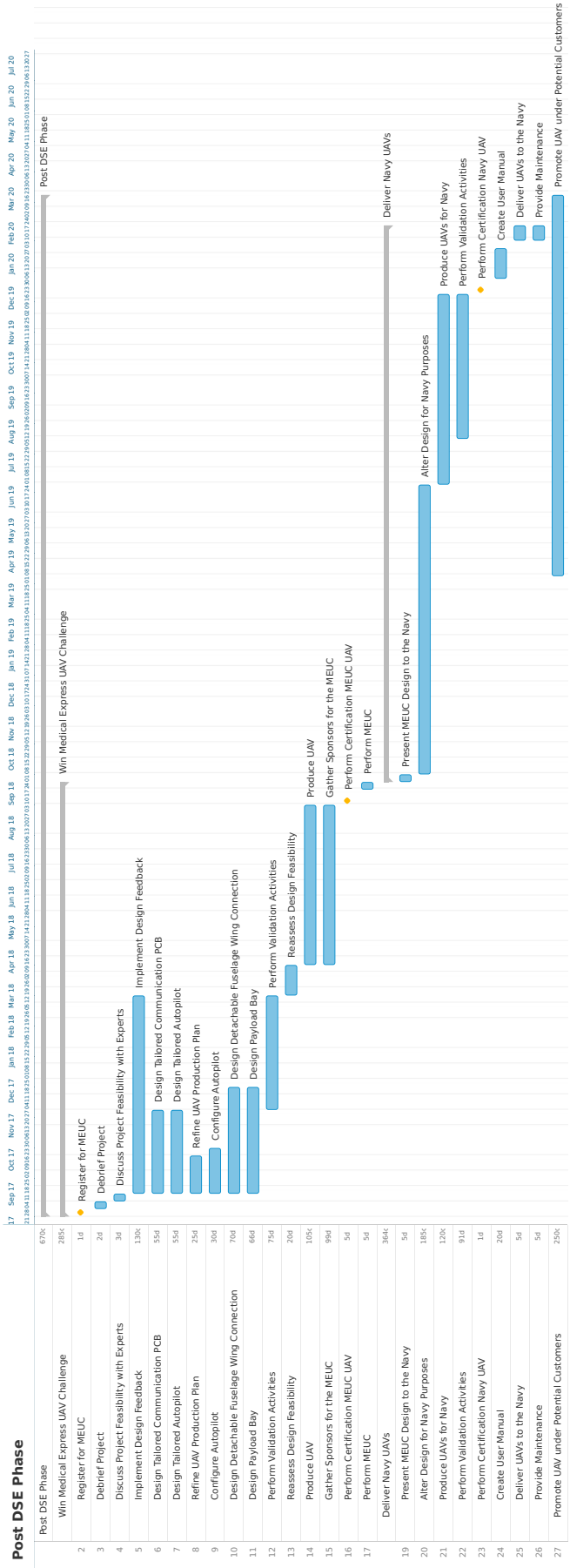

Figure B.2: Post DSE Gantt Chart [04-07-2017]